UNIVERSITÉ DE SHERBROOKE
Faculté de génie
Département de génie civil

# ANALYSE ET PRÉVISION DES CARACTÉRISTIQUES DU POMPAGE DU BÉTON AUTO-PLAÇANT À HAUTE RÉSISTANCE

Thèse de doctorat Spécialité: génie civil

Rami Khatib

Jury: Kamal Henri Khayat (directeur)
Dimitri Feys
Ammar Yahia
Jay Lacey
Marwan Al Kazzaz

Sherbrooke (Québec) Canada

Rami Khatib

*Your file Votre référence*
*ISBN: 978-0-499-00401-7*

*Our file Notre référence*
*ISBN: 978-0-499-00401-7*

# ANALYSIS AND PREDICTION OF PUMPING CHARACTERISTICS OF HIGH-STRENGTH SELF-CONSOLIDATING CONCRETE

By

RAMI KHATIB

A THESIS SUBMITTED IN PARTIAL FULFILLMENT OF THE
REQUIREMENTS FOR THE DEGREE OF
DOCTOR OF PHILOSOPHY
IN
CIVIL ENGINEERING

DEPARTMENT OF CIVIL ENGINEERING
UNIVERSITÉ DE SHERBROOKE

SUPERVISOR: KAMAL HENRI KHAYAT

SHERBROOKE
CANADA

OCTOBER 2013

# Acknowledgment

The pages of this dissertation hold far more than the culmination of four years of research. They reflect my memories of the moments I shared with many generous and inspiring people whom I had the occasion to meet and with whom I built solid relationships throughout these years. The list is long, but I cherish each person, for he or she has contributed to my development on both a professional and personal level.

The enthusiastic advice, support, and friendship of my supervisor, Prof. Kamal Henri Khayat was invaluable on both academic and personal levels, and I am extremely grateful to him.

I am indebted to Prof. Dimitri Feys for his precious advice, discussions, and comments on my work while he was a postdoctoral researcher at the Research Group on Cement and Concrete Infrastructure at the Université de Sherbrooke. I send you my best wishes as you start your career at Missouri University of Science and Technology.

I would like to express my appreciation to the thesis committee members: Kamal Henri Khayat, Dimitri Feys, Ammar Yahia, Jay Lacey, and Marwan Al-Kazzaz, for their time and precious feedback.

I am especially grateful to Aurelian Perez-Schell for his valuable scientific contribution to this research project and for his help during the pumping tests at the laboratory of the Université de Sherbrooke. I am also very thankful to Demix Béton in Sherbrooke for providing the ready mix and for being helpful throughout the pumping tests.

My sincere gratitude goes to my colleagues, research assistants, faculty members, technical staff, and graduate students at the Research Group on Cement and Concrete Infrastructure at the department of Civil Engineering; your continued encouragement and interest in my work helped make this project a joy to work on.

I gratefully acknowledge the funding received toward my PhD research from Sodamco Inc., in collaboration with The Natural Sciences and Engineering Research Council of Canada, and The Industrial Research Chair on High-Performance Flowable Concrete with Adapted Rheology, as well as the 17 Industrial Partners of our research group. The generous support and technical help of the sponsors were critical to the success of this project.

I owe my deepest thanks to my friend Mario-Tomas Coimbra for his priceless advice and for having spent his time providing me with distinct feedback. I look forward to the time when I can help others as you have helped me. Thank you, Mario.

I extend genuine gratitude to my friend Stephane Leahy. His constructive advice and insightful engineering comments made enormous contribution to this work. I will miss our jokes and arguments in the kitchen. Thank you very much, Stephane.

Many appreciations to my friends: Jason Duguay, Mohammad Hamouch, Ali Mikael, Magali Suc, Fatima Awwad, Nacéra Grini, Ghadie El Rahy, and Sarah Hachem. Thank you for your support during the hard times and for cheering me up when I really needed it.

To all my other friends that I could not list here, your support and warm encouragement were invaluable over the last years. I am very fortunate to have friends like you.

To my dear brothers, thank you for always having hope in me when I did not have it in myself. Your love and unending faith have given me a beautiful site to see.

To my parents, I pride myself on having words for everything, but they truly fail to describe how much I appreciate your efforts to allow me be where I am in my life. It is thanks to you that I first became interested in science when I was a great deal less large, and it is to you that this thesis is dedicated.

*Rami Khatib*
*Université de Sherbrooke*
*October, 2013*

# Abstract

Modern construction practices require proper knowledge to predict concrete pumping pressure, especially in high-volume and high-rise applications. Despite the progress made over the last decades, the spread of concrete pumping to high-rise construction has been hampered by the lack of standardized operating procedures and performance criteria. By and large, the guidelines available today focus predominantly on pumping Conventional Vibrated Concrete (CVC), while ambiguity still surrounds pumping Self-Consolidating Concrete (SCC) and other types of Highly-Workable Concrete (HWC). This PhD dissertation focuses on the fundamental principles relevant to the flow of high-strength SCC in pumping pipes, and it aims to develop methods to predict and reduce the required pumping pressure.

The flow pattern of SCC in pipes is analytically investigated, providing a numerical approach to predict the pumping pressure based on the properties of both concrete and the lubrication layer, the pipe diameter, and the flow rate.

The analytical results are further validated through full-scale pumping tests executed at the laboratory of the Université de Sherbrooke. Through this phase 26 optimal concrete mixtures were pumped in a 30-m pumping circuit to investigate the interactions between the concrete properties and pressure loss. The same tests are also employed to empirically correlate pressure loss with rheological and tribological properties of concrete at different flow rates. The resulting correlations furnish instrumental models capable of computing pressure loss for a wide range of concrete properties. In another application, the experimental results are analyzed to identify the influence of pumping on concrete properties with time.

Full-scale pumping results are statistically analyzed in order to establish a quantitative description of the most influential parameters governing the concrete flow in pipes. As a result, concrete pipe flow is statically modeled, allowing the computation of pressure loss at different flow rates based on the the rheological and tribological properties of the concrete and the pipe diameter. Another statistical model is derived to calculate the pressure loss as a function of the V-funnel flow time, granting the advantage of predicting the pressure loss on job sites without the need for complex rheological and tribological measurements. In light of the research findings of the previous phases, a new simple test method called the pipe flow test (PFT) is developed in the context of this research, specifically for predicting pipe flow pressure loss.

With preceding research phases as insights, the final stage of this project is directed toward mix design optimization faced with the challenge of reducing the pumping pressure and meeting the strength requirements of high-strength SCC.

Ultimately, the research findings emanating from this investigation provide practical guidelines and conclusive models to predict and reduce pumping pressure for a wide scope of concrete mixtures and pipe diameters.

**Key-words**: flow resistance, high-rise construction, high-strength, lubrication layer, pipe flow, pressure loss, pumping, rheology, SCC, tribology.

# Résumé

Les pratiques modernes de construction ont encouragé des efforts de recherche concernant la prédiction de la pression de pompage des bétons, plus particulièrement dans des applications à grande hauteur et grand volume. Malgré les progrès réalisés au cours de la dernière décennie, le pratique du pompage de béton pour les constructions de grande hauteur a été freinée par l'absence de procédures d'exploitation normalisées et de critères de performance. En général, la plupart des directives concernant le pompage du Béton Conventionnel (BC), tandis que le pompage de Bétons Auto-Plaçants (BAP) et autres types des bétons fluides reste encore négligé. Cette thèse se concentre sur les principes fondamentaux applicables à l'écoulement des bétons auto-plaçants dans les conduites, et vise à développer de nouvelles méthodes pour prédire précisément la pression de pompage et des moyens pour réduire la pression.

Sous pression d'écoulement des BAPs dans des conduites a été étudié analytiquement, fournissant ainsi une approche numérique pour prédire la pression de pompage basée à la fois sur les propriétés du béton et de la couche limite, et du diamètre de la conduite. En outre, les propriétés de la couche lubrifiante et son influence unique sur les pertes de pression ont été décrites dans cette thèse.

Les résultats analytiques sont ensuite validés par des essais de pompage à grande échelle exécutés au laboratoire de l'Université de Sherbrooke. Les mêmes esais sont également utilisés pour analyser l'influence de plusieurs propriétés du béton sur les pertes de pression à différents débits. Les corrélations résultantes ont fourni des modèles instrumentaux capables d'évaluer les pertes de pression pour une grande portée de propriétés du béton. Une autre application a permis d'analyser les résultats expérimentaux afin de comprendre l'influence du pompage sur les propriétés rhéologiques du béton en question.

Finalement, les résultats de pompage à grande échelle ont été analysés statistiquement visant à fournir une description quantitative des paramètres les plus influents sur l'écoulement du béton dans des conduites. En conséquence, l'écoulement du béton dans les conduites est statistiquement modélisé, permettant ainsi le calcul des pertes de pression pour différents débits à partir des propriétés rhéologiques et tribologiques du béton et du diamètre des conduites. Un autre modèle statistique a été conçu pour calculer la perte de charge en fonction du temps d'écoulement au V-funnel, ce qui permet de prédire les pertes de pression sur chantier sans recours à des mesures rhéologiques ou tribologiques complexes.

Le test de débit en conduite (TDC) est une nouvelle méthode développée dans le cadre de cette recherche et plus particulièrement afin de prédire les pertes de pression d'écoulement dans les conduites. Suite à la recherche décrite précédemment, la phase finale de ce projet a été orientée vers l'optimisation des mélanges afin de réduire la pression et répondre aux exigences de résistance du béton auto-plaçants (BAP) .

Finalement, les résultats de recherche issus de cette étude fourniront des directives pratiques pour réduire la pression de pompage ainsi que plusieurs modèles, pour une large gamme de propriétés du béton et de diamètres de conduite.

**Mots-clés**: BAP, couche de lubrification, débit de conduite, grande hauteur, pression de pompage, haute résistance, résistance à l'écoulement, tribologie, viscosité.

# Contents

# List of Figures

# List of Tables

# Chapter 1

# Introduction

## 1.1 Research context

Despite the significant progress made over the last decade, the spread of pumping concrete to high-rise applications has been hampered by the lack of standardized operating procedures and performance criteria. Practical guidelines, mainly based on field experience, for pumping equipment and concrete properties do exist and are available through pump companies and research institutes [1, 2]. By and large, these guidelines and studies focus on pumping Conventional Vibrated Concrete (CVC) [3–5], much to the neglect of Self-Consolidating Concrete (SCC) and other types of Highly-Workable Concrete (HWC). In practice, the rules derived for CVC are still applied to SCC and altered based on the experience of the pumping operator [6]. Because of the unique flow pattern of SCC, applying the CVC guidelines to SCC will fail to take into account the rheological and tribological properties governing SCC's flow behavior, and thus can lead to unrealistic prescriptions.

Although much has been learned about pumping of SCC, modern construction technologies have stimulated the substantial need for research efforts to accurately predict its required pumping pressure. Unfortunately, the absence of such research limits the applicability of pumping SCC in modern concrete practices, especially for high-volume and high-rise applications. This opens the door for more comprehensive studies that link pumping pressure to the fundamental rheological properties governing the flow of SCC in pipes.

## 1.2 Scope

This PhD dissertation focuses on the fundamental principles of the flow of High-Strength SCC and HWC in pumping pipes, aiming to reduce pumping pressure and develop empirical and analytical models to predict it. The investigation is founded on a solid understanding of the rheological properties of SCC and HWC, established by the Research Group on Cement and Concrete Infrastructure at the Université de Sherbrooke. Corresponding to its research goals, the project is divided into two main parts: the first part represents the literature review (Chapters 2-4) dealing with rheology and indispensable basics of pumping concrete. The second part (Chapters 5-7) covers the analytical characterization of SCC's pipe flow, the full-scale pumping tests, and the mix design optimization to reduce pumping pressure.

Through the literature review, the theoretical aspects of rheology and the fundamental properties of materials are outlined. Rheological behaviors of different types of suspensions are described on the basis of the particles' dimension ranges. Focus is set on the rheological behavior of concrete in the steady state and on various time-dependent phenomena. The state of the current understanding and challenges of pumping concrete, factors affecting pumping pressure, and different changes in concrete properties due to pumping are addressed.

The second part undertakes a critical analysis of the flow of SCC in pipes based on two key aspects. The first is the analytical characterization of the different flow zones of concrete formed across the pipe section during flow. The second is the quantitative description of the most influential parameters governing the concrete pipe flow, including

the properties of both concrete and the lubrication layer, and the geometrical characteristics of the pumping circuit. Both aspects involve deep understanding of concrete-steel interface boundary conditions and the influence of the lubrication layer properties on overall pipe flow. Together, the two aspects combine to numerically predict the pumping pressure based on the properties of both concrete and the lubrication layer, the geometry of the conveying pipes, and flow rate.

Full-scale pumping tests are undertaken to validate the results obtained from the analytical analysis and to empirically correlate pressure loss with various rheological properties of the concrete. By incorporating different mix design parameters in the tested mixtures, their effects on pressure loss are disclosed. Also, in virtue of a prolonged pumping testing procedure, the different changes in properties of various types of concrete during pumping are revealed. Based on the knowledge gained through the previous phases, a new simple test method (PFT) is developed to assess the concrete flow in pumping pipes. A correlation is established between the concrete flow time in the testing pipe and the rheological and tribological properties of concrete. Based on this correlation, a future validation of this test is planned to link between the concrete flow time in the testing pipe and the pressure loss in the field.

The empirical results of the full-scale pumping tests serve as a base for statistical analyses directed toward modeling both pressure loss and the parameters proven most influential throughout the experimental program. As a result of the statistical analyses, a quantitative description of the effects of certain rheological and tribological properties on the pressure loss is established. Additional statistical analysis is performed for the V-funnel results, granting a very practical approach to accurately predict pressure loss on job sites. At this point, the flow of SCC in pumping pipes is understood and can be predicted by means of analytical, statistical, and empirical models.

In light of the research findings of the previous phases, the last experimental phase focuses on optimizing mix design parameters with the goal of reducing pumping pressure. Faced with the challenge of reducing pumping pressure, the work is proceeded using Concrete Equivalent Mortar (CEM) and concrete in order to examine the different effects of mix design parameters on pressure loss reduction.

Ultimately, research findings emanating from this investigation, put into practice conclusive guidelines and insights to reduce pumping pressure, and several models to predict it for a wide range of flowable concrete and pipe diameters.

## 1.3 Thesis outline

This study is divided into eight chapters. A general presentation of the investigation and its main objectives are detailed in Chapter 1. Introductions to rheology and tribology are presented in Chapter 2, followed by a more detailed scan on rheology of suspensions and concrete in Chapter 3. Chapter 4, establishes briefly the historical context and current knowledge of pumping concrete. Chapter 5 is devoted to analytical analyses determining the properties of the lubrication layer and characterizing the flow of concrete in pipes. In this chapter interactions between the properties of concrete and lubrication layer in relation to the pressure loss are highlighted. Chapter 6 discusses the experimental results of the full-scale pumping tests intended to validate the analytical findings of Chapter 5.

These results are also used as bases for empirical and statistical correlations that are established between the rheological and tribological properties of concrete and pressure loss. The effect of changes in concrete rheological properties with pumping duration on pumping characteristics is examined. Finally, the PFT test, a new test method to estimate the pressure loss on job sites is introduced. Chapter 7 is dedicated to optimizing mix design parameters to reduce pumping pressure and meet the strength requirements of HS-SCC. Chapter 8 presents the conclusions and highlights the most significant findings of the investigation. Future research perspectives relevant to the investigation is also presented.

Three appendices are attached; Appendix A includes the properties of the constituent materials used through the different phases of the investigation. Appendix B presents the mix design parameters and proportions, fresh properties, temperature changes, rheological and tribological properties, a selection of hardened properties of the tested mixtures, and the pressure loss data measured during the full-scale pumping tests. Appendix BC presents the results of the pumping tests in graphical form.

## 1.4 References

[1] Eckardstein K., Ernst V., "Concrete and concrete pumps; a concrete placing manual", Schwing, Tech. Rep., 1983, p. 133.

[2] ACI 304.2R, "Placing concrete by pumping methods", *ACI Material Journal*, vol. 92, no. 4, pp. 441–464, 1995.

[3] Kaplan D., "Pumping of concretes", Ph.D. dissertation, Laboratoire Central des Ponts et Chausées, Paris, 2001.

[4] Chapdelaine F., "Fundamental study and practice on concrete pumpability", Ph.D. dissertation, University of Laval, 2007.

[5] Ngo T.T., "Influence of concrete compositions on the pumpability parameters", Ph.D. dissertation, Cergy Pontoise, France, 2009.

[6] Feys D., "Interactions between rheological properties and pumping of self-compacting concrete", Ph.D. dissertation, Ghent University, 2009.

# Chapter 2

# Rheology

# 2.1 Introduction

In this chapter, the theoretical aspects of rheology and the fundamental properties of materials are outlined. Different ways to determine the rheological properties of materials and their responses to an applied force are detailed. In addition, several types of rheometers and their working principles are described.

# 2.2 Definitions

## 2.2.1 Stress and strain

In the elastic domain, stress is simply defined as the force divided by the area over which it is applied. When a stress is applied to a material, a deformation will occur and the strain can be defined as the relative deformation caused by the stress (see Figure 2.1).

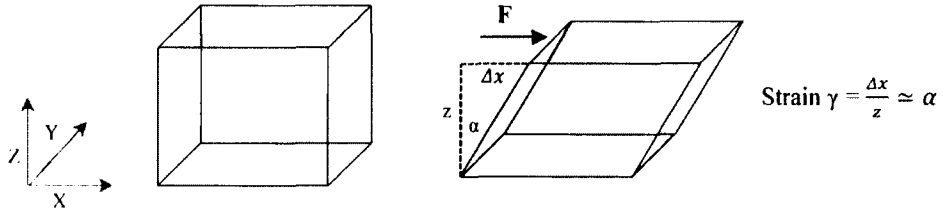


***Figure 2.1:*** *Shear deformation induced by shear stress.*

## 2.2.2 The rate of strain and flow

When a fluid system is deformed by an applied stress, the motion continuous until the stress is removed. Consider two surfaces separated by a small gap containing a liquid, as shown in Figure 2.2, a constant shear stress must be applied on the upper surface to maintain the movement at constant velocity, u. Assuming there is no slip between the surfaces and the liquid, the velocity gradient is constant across the small gap and the velocity reaches zero at the lower surface. Considering the displacement x produced in every second, then the strain becomes:

$$\gamma = \frac{x}{z} \tag{2.1}$$

and as

$$u = \frac{dx}{dt} \tag{2.2}$$

the rate of strain can be written as:

$$\dot{\gamma} = \frac{d\gamma}{dt} = \frac{u}{z} \tag{2.3}$$

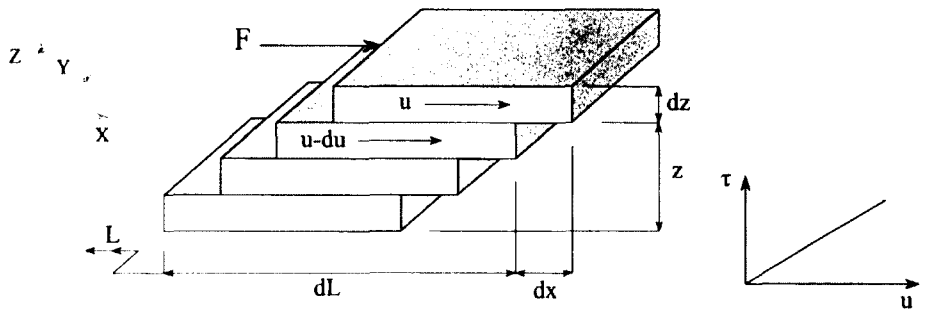


***Figure 2.2:*** *Velocity gradient produced when a fluid is sheared.*

The terms rate of strain, velocity gradient and shear rate are all used synonymously and Newton's dot is normally used to indicate the differential operator with respect to time. For large gaps the rate of strain will vary across the gap since velocity is not constant, hence

$$\dot{\gamma} = \frac{du}{dz} \tag{2.4}$$

### 2.2.3 Viscosity and rheology

The measure of the internal resistance of a fluid being deformed by shear stresses is called viscosity. In this context, the less viscous a fluid is, the easier it flows. In fact, all fluids have some resistance to flow; it can be very low, such as it is for air ($1.81 \times 10^{-5}$) or very high as it is for oil (0.250 Pa s).

The term rheology is frequently used synonymously with rheometry. This rheometry generally refers to the experimental techniques used to determine the rheological properties of materials; these properties express themselves in terms of quantitative and qualitative relationships between deformations, stresses and their derivatives. The theoretical aspects of rheology are explained by the deformation behavior and the internal structure of a material.

## 2.3 Materials behavior

### 2.3.1 Elastic (Hookian) behavior: for solids

The law of elasticity was established by the English scientist Robert Hooke in 1678. It states that for relatively small deformations of an object, the displacement or size of the deformation is directly proportional to the deforming force or load and the object reverts back to its original shape and size upon removal of the load [1]. Elastic behavior has no dependency on time, thus any kind of strain is completely and instantaneously recoverable. Materials for which Hooke's law is valid are known as linear-elastic. In fact, there is no perfect elastic material because any material will yield some permanent deformations when applied loads are removed, but within limits Hooke's law is still valid [2].

Hooke's law is better known under the form of equations 2.5 and 2.6.

$$\sigma = E\varepsilon \tag{2.5}$$

$$\tau = G\gamma \tag{2.6}$$

where

$\sigma$: axial stress (Pa)
$E$: Young's modulus (Pa)
$\varepsilon$: strain (-)
$\tau$: shear stress (Pa)
$G$: shear modulus (Pa)
$\gamma$: angle of deformation (-)

Equation 2.5 describes an axial deformation in an elastic material while equation 2.6 describes an angular displacement resulted by an angular force. In fact, for many materials (such as many types of polymers), the stress-strain relationship is not linear and their behaviors are then described by neo-Hookean models [3].

### 2.3.2 Plastic (St.Venant) behavior

Plasticity generally refers to the material's ability to be shaped, and more specifically, plasticity describes the deformation of a material undergoing non-reversible changes of shape in response to applied forces. For the vast majority of materials, a material has some inherent strength (called yield strength) such that below a certain value of stress (called yield stress) there is no permanent deformation. When a plastic substance is stressed above the yield stress, it deforms yielding a permanent strain. Once plastic deformation begins, it continues as long as the stress is applied. Most materials that approach plastic behavior exhibit elastic characteristic below the yield point and beyond the yield point the strain becomes permanent. This behavior, described by the elasto-plastic behavior, can be found in many types of materials (especially plastic products), and is considered the most common among materials under stress.

### 2.3.3 Viscous behavior: fluids

Viscosity describes the resistance of a fluid to flow. In everyday terms (and for fluids only), viscosity is "thickness", thus, water is "thin", having a lower viscosity, while honey is "thick", having a higher viscosity. The difference between a perfectly elastic and a perfectly viscous material is illustrated in Figure 2.3. For a constant stress the angle of deformation is constant for the elastic material, whereas the angle of deformation changes at a constant rate for the viscous material. Once the stress is removed, the elastic material returns to its original condition, while the viscous material stays in its final deformed shape. The elastic material is said to have a perfect memory, whereas the viscous material does not have any memory [4].

As mentioned previously, the velocity gradient when stress is applied can be expressed as the time variation of the angle of deformation referring to the shear or strain

rate. Hence, depending on the change of strain rate versus stress inside a fluid, the viscosity can be categorized as having a linear or a non-linear response. When a fluid exhibits a linear response it is considered as a Newtonian fluid and the relation between the shear stress and the shear rate is linear, passing through the origin. Fluids with flow properties differ in any way from those of Newtonian fluids are characterized as non-Newtonian fluids.

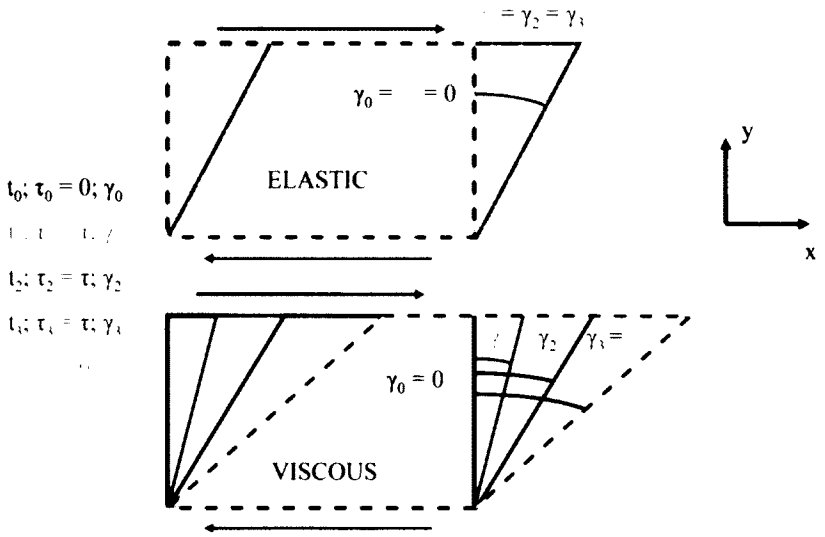


***Figure 2.3:*** *Description of the elastic and viscous behaviors under angular deformations [5].*

### Newtonian and non-Newtonian fluids

A Newtonian fluid [named after Isaac Newton (1687)] is a fluid whose stress versus strain rate curve is linear and passes through the origin. The constant of proportionality is the viscosity, as indicated in equation 2.7. The Newtonian fluid starts moving instantly when stress is applied and the best known example of a Newtonian fluid is water.

$$\tau = \eta \frac{du}{dz} = \eta \dot{\gamma} \tag{2.7}$$

where

$\tau$: shear stress (Pa)

$\eta$: viscosity (Pa s)

$du/dz$: velocity gradient perpendicular to the direction of shear or shear rate ($d\gamma/dt$)

In a non-Newtonian fluid, the relationship between the shear stress and the strain rate can be linear, or nonlinear, or even time-dependent. Therefore, a single constant coefficient of viscosity could be inadequate to describe the flow behavior of a non-Newtonian substance. Most fluids are non-Newtonian; many polymer solutions and molten polymers are non-Newtonian fluids. They are best studied through other rheological properties that

relate the stress and strain rate tensors under different flow conditions, such as oscillatory shear or extensional flow, which are measured using different devices or rheometers.

### Bingham visco-plastic fluid

A Bingham fluid is a non-Newtonian visco-plastic material that behaves as an elastic material at low stress and flows as a viscous fluid at high stress. A Newtonian fluid flows and gives a shear rate (or strain) for any finite value of shear stress, while the Bingham fluid does not exhibit any flow until a yield stress is exceeded; beyond this point the flow rate increases constantly with the shear stress. In contrast to the Newtonian fluid for which only one parameter is needed to describe its flow, the Bingham fluid requires two identifying parameters, the yield stress and the plastic viscosity, as shown in equation 2.8.

$$\tau = \tau_0 + \mu_p \dot{\gamma} \tag{2.8}$$

where

$\mu_p$: plastic viscosity (Pa s)
$\tau_0$: yield stress (Pa)

### Shear thinning and shear thickening

One possibility of the non-Newtonian behavior is a non-linear relationship between the shear stress and the shear rate. In this case, viscosity is no longer constant for all shear rates. Two different types of behavior can be highlighted at this point; when viscosity decreases with increasing shear rate, the behavior is called shear thinning (or pseudo-plastic) and the flow curve of shear stress-shear rate bends downward, as illustrated in Figure 2.4. When viscosity increases with the shear rate, the behavior is shear thickening, or dilatants, and the flow curve bends upward. The shear thinning and thickening behaviors can be observed in many materials undergoing a shear effect, such as certain types of cement grout, mortar, and concrete. Equation 2.9, known as the power-law model, is one of the most applied models in rheology to describe shear thinning and shear thickening behavior.

$$\tau = m\dot{\gamma}^n \tag{2.9}$$

where

$m$: consistency factor (Pa $s^n$)
$n$: consistency index (-)

The distinction between shear thinning and shear thickening is made by the consistency index "$n$". For $n < 1$, the material is shear thinning, whereas it is shear thickening for $n > 1$. If $n = 1$, the linear Newtonian behavior is obtained.

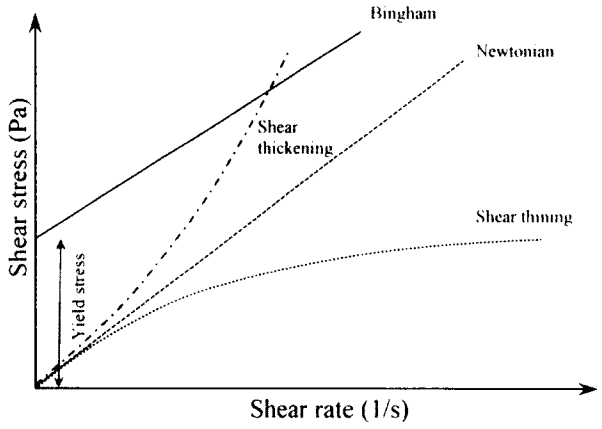


***Figure 2.4:*** *Flow curves for a Newtonian, shear thinning, shear thickening, and Bingham materials.*

### Different kinds of viscosity

Different types of viscosity can be used to identify the rheological behaviors of fluids. The choice of each type depends on the rheological model in use and its fitting to the real material's behavior. As shown in Figure 2.5, the tangential (or differential) viscosity at a certain shear rate is the slope of the flow curve at that shear rate, while the apparent viscosity at a specific shear rate is calculated by dividing the shear stress by that shear rate. The plastic viscosity, is presented by the slope of the flow line when the flow curve is a straight line obeying Bingham's model. For a Newtonian liquid, the three different types of viscosity are all equal since the flow curve is a straight line.

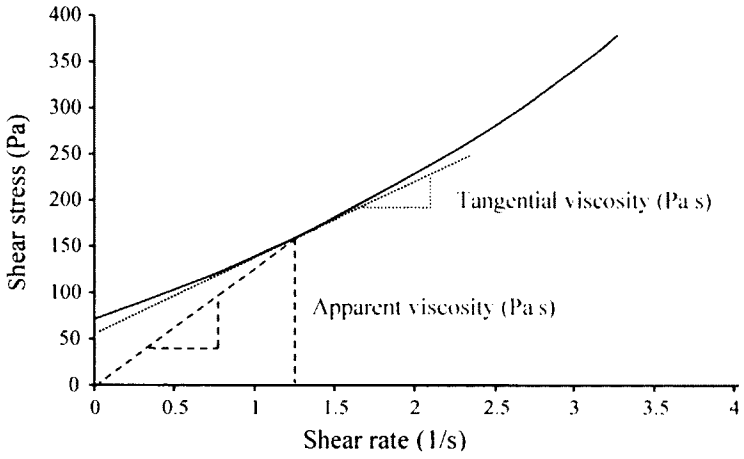


***Figure 2.5:*** *Determining different types of viscosity from a flow curve. Adapted from [5].*

## 2.4 Tribology

Tribology is the science dealing with interacting surfaces in relative motion, including properties at interfaces such as friction, abrasion, and lubrication. Any product, where one material slides or rubs over another, is affected by complex tribological interactions. The study of tribology is commonly applied in bearing design and extends into almost all other aspects of modern technologies.

More specifically applied to concrete science, tribology is the study of the flow behavior of fresh concrete when it is in direct contact with a solid surface such as a form work or a pumping pipe. Tribological interactions in concrete are more complex since it does not remain a homogeneous material in relative motion. Some mixture constituents can migrate from the concrete mixture toward the interacting surface forming a thin layer (called the lubrication layer) which possesses different rheological properties than those of concrete. Because of this particular migration phenomenon, determining the tribological interactions of concrete is not a straightforward procedure. Additional analysis takes into account properties of the lubrication layer and the properties of concrete itself is needed. Further information concerning the tribological analyses and measurements for concrete are detailed in section 5.7.

## 2.5 References

[1] Encyclopidia Britannica, *http://www.britannica.com/EBchecked/topic/271336/Hookes-law.*

[2] Rivlin R.S., "Large elastic deformations of isotropic materials. IV. Further developments of the general theory", *Philosophical Transactions of the Royal Society A Mathematical Physical and Engineering Sciences*, vol. 241, no. 835, pp. 379–397, 1948.

[3] Treloar L.R.G., *The physics of rubber elasticity*, 3rd ed. London, 1975.

[4] Macosko C.W., *Rheology principles, measurements and applications*, 10. Vch New-York, 1994.

[5] Feys D., "Interactions between rheological properties and pumping of self-compacting concrete", Ph.D. dissertation, Ghent University, 2009.

# Chapter 3

# Rheology of Suspensions and Cement-Based Materials

## 3.1 Introduction

In the first part of this chapter, a clear distinction between colloidal and non-colloidal suspensions is made. Rheological behavior of both types of suspensions are described on the basis of the particle's size. In the second part, light is shed on the rheological behavior of concrete in steady state as well as various time-dependent phenomena. Two rheometers which have been used in this investigation are described in the third part of this chapter in terms of functionality, testing procedures, and data treatment. A new tribometer developed in the context of this research, in addition to other types of tribometers which have been used in previous studies to determine the tribological properties of concrete are also outlined in the third part.

## 3.2 General

A suspension is any system in which small solid particles are more or less dispersed in a liquid medium [1]. In any suspension undergoing a shear effect, or flow, different types of mutual interactions between the basic materials' elements can lead to different rheological behavior. Overall, the interactions occurring during shear may be classified into two main categories: hydrodynamic interactions and solid interactions [2]. Hydrodynamic interactions result from a disturbance induced in the liquid phase, which in turn exerts a force on the suspended particles. Hydrodynamic interactions dominate the rheological behavior in a liquid system, while in a granular system the solid interactions (like collision, friction, slippage, etc.) are more important. Therefore, the rheological behavior in the latter becomes more dependent on the configuration of the spatial distribution of particles and their direct contacts.

In a granular-paste medium, such as concrete, both hydrodynamic and solid interactions take place through the interstitial paste and by direct contact between particles. The magnitude of the solid and hydrodynamic interactions is greatly affected by ($\phi$) the solid volume concentration (defined by the ratio of the volume of solid elements to the total volume of the sample). In this context, different $\phi$ and particle' size ranges can result in different regimes and rheological characteristics of granular systems, as discussed in the following sections.

## 3.3 Distinction between colloidal and non-colloidal suspensions

The rheological behavior of a suspension is a complex function of the interactions that occur at the scale of the suspended particles [3]. The maximum size of particles is a determining factor of the interactions between the particles and the interstitial medium. Two main regimes can be distinguished based on the maximum size of the particles: the non-colloidal, and the colloidal. In the case of non-colloidal systems, the particles volume fraction, shape, and the spatial arrangement, are dominant parameters influencing the behavior of the suspension [3]. In the colloidal regime, the upper limit of the particle size is commonly taken at 1 μm [4, 5]. Within this size range, the total surface area of the

particles is much greater than their total volume. Consequently, volume fraction, particle shape, distribution, and inter-particle forces (e.g. electrostatic effects) become the main parameters influencing the rheological behavior of colloidal systems.

## 3.4 Rheology of non-colloidal suspensions

Based on the solid concentration (expressed by the particle volume fraction $\phi$) three regimes can be highlighted [6, 7]: (i) a dilute regime, restricted to $\phi < 0.02$ where the relative apparent viscosity ($\eta_r$, see section 3.4.1) is a linear function of $\phi$; (ii) a semi-dilute regime with $\phi < 0.25$, where the relative apparent viscosity shows a higher order dependency on the volume fraction; (iii) a concentrated regime, starting near $\phi = 0.25$, characterized by rapid growth of the relative apparent viscosity and of the non-Newtonian behavior with increasing particle volume fraction. The three regimes and their anticipated rheological behavior due to solid concentration changes are detailed in the following sections.

### 3.4.1 Dilute suspensions

The behavior of a suspension within the dilute limit was first addressed theoretically by Einstein (1906, corrected 1911) who derived an analytical solution for the relative apparent viscosity:

$$\eta_r = \frac{\eta_s}{\eta_m} = 1 + B\phi \tag{3.1}$$

where

$\eta_r$: relative apparent viscosity (-)
$\eta_s$: apparent viscosity of the suspension (Pa s)
$\eta_m$: apparent viscosity of the suspending medium (Pa s)
$\phi$: volume fraction (-)
$B$: Einstein's coefficient or the 'intrinsic viscosity'; B equals to 2.5 for spherical particles [8]

As can be deduced from equation 3.1, the relative apparent viscosity increases linearly with the volume fraction. The value of Einstein's coefficient (B) has not been incontrovertibly validated, with different researchers favoring values covering the range [1.5 < B <5] [9–11]. Quite a few researchers agree on applying Einstein's equation with B = 2.5 when specific conditions are fulfilled such as: spherical particles, no interaction between particles, no slip at the particle surface [5, 12].

### 3.4.2 Semi-dilute suspensions

As the volume fraction increases, the relative apparent viscosity shows higher dependency on the volume fraction, especially when it approaches 0.25. On the microstructure scale, the particles show some mutual interactions, and the distribution of the particles' orbits remains close to random over time. Their random distribution indicates rotary diffusion

of the particles' orientations created by the hydrodynamic interactions between particles [3]. Scientific work in the semi-dilute regime has been focused on finding coefficients for the higher order terms of the volume fraction; sometimes neglected by Einstein. As a result, an extension of Einstein's equation was derived with a second order term of the volume fraction [13 15]:

$$\eta_r = 1 + B\phi + B_1\phi^2 + .... \tag{3.2}$$

where

$B$: Einstein's coefficient equals to 2.5 for spheres

$B_1$: factor depends on the type of flow and the particle shape, $7.35 < B_1 < 14.1$

In this polynomial model, viscosity reaches infinity only when $\phi$ reaches 1, while infinity can be practically reached when $\phi$ approaches its maximum value ($\phi_m = 0.64$) for a suspension of monosized spheres. In order to overcome this inconvenience, the maximum volume fraction should be involved as a parameter in the model to describe the materials behaviors in the vicinity of the maximum volume fraction.

### 3.4.3 Concentrated suspensions

Increasing the solid concentration increases the particle volume fraction resulting in a rapid growth in the relative apparent viscosity, as a result, equation 3.2 becomes no longer valid. Theoretical models are not available for this case and the relative viscosity instead is described by means of semi-empirical equations or numerical simulations. One of the most successful experimental models in the concentrated regime is the Krieger&Dougherty model (1972) (termed the "functional equation" approach by Pabst 2004) [11]. It comprises the maximum volume fraction ($\phi_m$) as a parameter, and considers the contribution of successive packets of suspension to the total particle volume fraction and to the viscosity of the suspension:

$$\eta_r = \left(1 - \frac{\phi}{\phi_m}\right)^{-[\eta]\phi_m} \tag{3.3}$$

$$[\eta] = \lim \phi_{\phi \to 0} \left[\frac{\frac{\eta}{\eta_s} - 1}{\phi}\right] \tag{3.4}$$

where

$\eta_r$: relative apparent viscosity (-)

$\phi_m$: maximum volume fraction (-)

$[\eta]$: intrinsic viscosity equals to 2.5 for spheres and higher for other particle shapes

As can be inferred from equation 3.3, increasing the maximum volume fraction $\phi_m$ decreases the relative viscosity for a given volume fraction. On the other hand, for a given maximum volume fraction, the relative viscosity increases with the volume fraction and

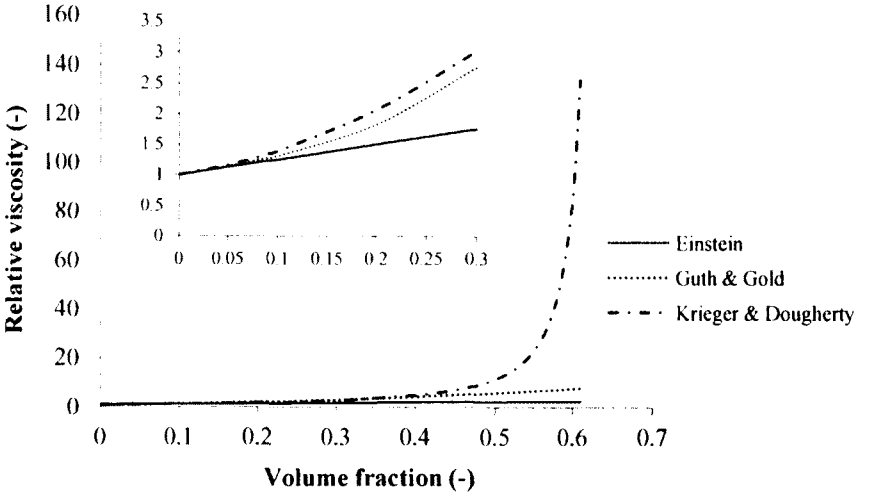


***Figure 3.1:*** *Relative viscosity plotted against particle volume fraction according to the Einstein equation (black), the Guth and Gold equation (to the second order in $\phi$, $B$ =2.5, $B_1$ =14) (dotted line), and the Krieger-Dougherty model (dashed line) with a maximum volume reaction of 0.64. The inset shows the same data focusing on the semi-dilute and dilute regimes. Adapted from [16].*

it becomes infinite when the volume fraction approaches its maximum value. The advantage of the Krieger-Dougherty equation is that, no matter the particle size, shape, or distribution, the equation scales all data on a master curve where the relative viscosity is plotted versus the ratio of the volume fraction to the maximum volume fraction [17, 18].

A comparison between the relative viscosity plotted and volume fraction according to Einstein's, Guth&Gold's, and Krieger-Dougherty's models are sketched in Figure 3.1. As demonstrated, for all three models, the relative apparent viscosity increases with the volume fraction for a given $\phi_m$. This increase is more pronounced in the Krieger-Dougherty model, particularly when the volume fraction is close to its maximum value. On the other hand, Einstein's and Guth&Gold's models underestimate the relative viscosity (compared to Krieger&Dougherty model) starting from a volume fraction of around 5%.

## 3.5 Rheology of colloidal suspensions

In a colloidal regime, the surface area of the particles is much greater than their volume, therefore, the inter-particle forces at the surface of the particles are central to its rheological properties. The fundamental characteristic of these forces is that they act at distance between the elements through the liquid, even when at rest. Depending on the distance between the colloidal particles within a particle's range of interaction, different attraction and repulsion forces can act to stabilize, or destabilize, the colloidal suspension. At a very short distance, two adjacent particles repel each other because of the impossibility of overlapping the electronic clouds [2]. At a larger distance, the particles interact via Van der Waals forces which (at a certain distance between the particles) appears as an attraction force caused by the interaction between the dipoles. In addition to the Van der Waals forces, the particles interact through electrostatic forces induced by the ions

adsorbed at the surfaces of the particles. The magnitude of the attraction or repulsion forces between two electric charges depends on the product of their charges and separation distance. Summing the repulsion and attraction forces between every two adjacent particles delivers a net force. The net forces then determine the stability of the colloidal suspension and consequently the total potential energy of the system.

In the absence of other forces, colloidal particles can undergo a random motion called the Brownian motion which is caused by thermal agitation of the liquid medium. The Brownian motion is believed to enhance restructuration at the origin of thixotropy since it allows particles to explore different positions in the medium, each with different potential energies [2].

The interactions in colloidal suspensions are complex functions of the particles size, shape, concentration, and distribution. The stability of a colloidal system is determined by the net forces resulted from summing the repulsion and attraction forces between particles. These net forces determine the energy of the colloidal suspension, and therefore the force needed to break the connections between the particles in order to introduce a change or a flow to the system.

## 3.6 Rheological measurements

Rheological measurements are commonly presented by the flow curve and yield stress, that are discussed in the following sections.

### 3.6.1 Flow curve

The flow curve is the plot of shear stress as a function of shear rate. Shear rate can be applied in either descending or ascending order. In certain materials, the ascending and descending flow curves are identical and the flow curve is said to be reversible. However, decreasing the shear rate, is considered a safer procedure to measure intense shear thickening behavior [16]. Non-reversibility can be characterized by different ascending and descending flow curves. This difference can be attributed to particles alignment or to time dependent phenomena in the material like thixotropy [16]. Because of the immense diversity in rheological behavior of materials, knowing the range of shear rate that the material will undergo in practice is of prime importance to avoid unrealistic flow curves [19].

### 3.6.2 Static and dynamic yield stress

It is often difficult to accurately define yield stress because of the wide variety of stress-strain curves exhibited by materials. From a practical standpoint, yield stress is defined as "the maximal stress at which no flow is observed during a reasonable time frame" [20].

In a suspension of spheres, the suspension shows a yield stress at particle volume fractions greater than 50%. This pheneomenon is attributed to the particles' networks formation that act to prevent flow [21]. In this high volume fraction state, the particle network deforms elastically in response to an applied stress transmitted via direct particle-particle contact. The yield stress is reached at a point when the applied stress is sufficient

to bring the network to the point of break up. Beyond this point, the suspension flows viscously in responce to the applied force. From this perspective, the yield stress can be well described by a modified form of the Maron-Pierce relationship:

$$\tau_0 = \tau^* \left[ \left( 1 - \frac{\phi}{\phi_m} \right)^{-2} - 1 \right] \tag{3.5}$$

where

$\tau_0$: yield stress (Pa)

$\tau^*$: a fitting parameter; the value of the yield stress at $\phi = \phi_m$ (1-$\sqrt{2}$/2)

$\phi$: volume fraction (-)

$\phi_m$: maximum volume fraction (-)

From equation 3.5, it can be deduced that yield stress increases with the solid concentration (or volume fraction). This finding is further validated through Figure 3.2 that also demonstrates that yield stress increases with the particle size for a given volume fraction [22]. Equation 3.5 is one possible description of yield stress; other interpretations of yield stress based on established physical principles can be found in literature.

In practice there exist two different ways of measuring the yield stress that each deliver different types of values. The first is a dynamic method yielding a value known as the dynamic yield stress, the second is the static method delivering the static yield stress. The question that arises here is, which yield stress should be used? A good starting point is to identify the flow process of interest. In the case of flow stopping after shear, then the dynamic yield stress is the key determinant. On the other hand, if the interest is the energy needed to initiate movement in the first place (for example pumping start-up) then the static yield stress will prove the key parameter. The most common method used for obtaining the dynamic yield stress is to shear the sample over a range of shear rates, plot the shear stress as a function of the shear rate, and finally fit a curve through the data points by means of a rheological model (see Figure 3.3a). The intercept of the fit line with the stress axis is considered the dynamic yield stress, which is used to describe the material behavior in motion (i.e. under shear). Theoretically, any stress below this value should be insufficient to create flow. Another approach to measure the yield stress is to start shearing the sample from its at-rest state and incrementally increase the stress until the value at which it starts to flow (see Figure 3.3b). This value is called the static

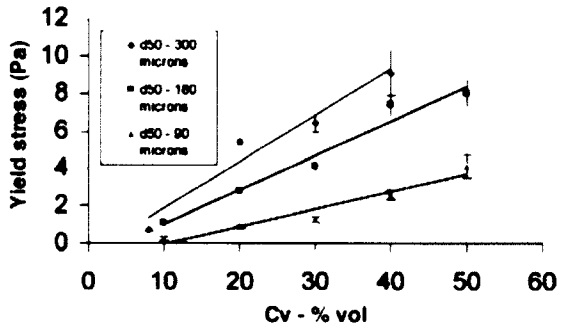


***Figure 3.2:*** *Effect of particle size and solid concentration on yield stress [22].*

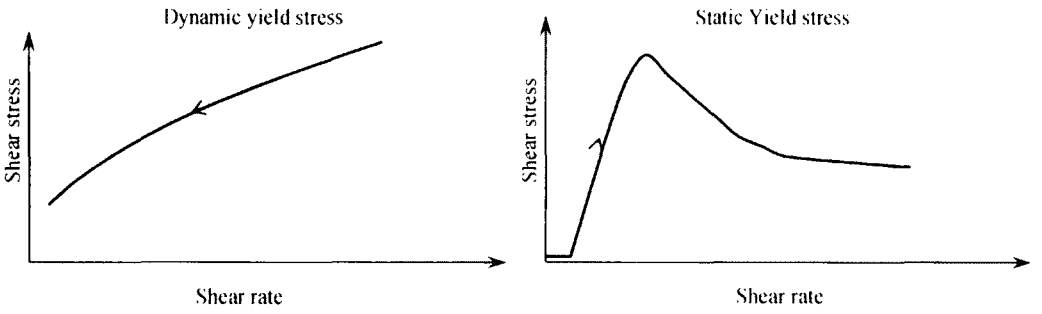


***Figure 3.3:*** *Shear rate ramp reveals dynamic and static yield stress. For the static yield stress the test starts at rest-state (zero shear rate).*

yield stress and is usually higher (or equal) than its dynamic counterpart for a given material. When tested below the static yield stress, the sample is not completely moving but rather undergoing elastic deformation. For the majority of practical purposes, the flow rates during elastic deformation are so low that it can be assumed as static.

It should be noted here that the testing procedure of the dynamic yield stress is easier to perform, but it is more sensitive to variations and errors [4, 20]. The choice of the minimal shear rate significantly influences the value of the dynamic yield stress, even if the same rhelogical model is applied [16]. Different values of the yield stress, even illogical ones, can be obtained with one measurement, especially when low yield stress is expected; making yield stress a difficult parameter to measure.

### 3.6.3 Thixotropy

Thixotropy can be defined as a decrease of viscosity over time under a constant shear stress or shear rate, followed by a gradual recovery when the stress or shear rate is removed [5] (see Figure 3.4). This time-dependent phenomenon can be attributed to the formation of "physical" connections caused by the attracting forces between the colloidal particles [23–25]. These forces create a coagulation effect between the particles leading to an increase in viscosity of the suspension. If a sufficient amount of energy is introduced to the medium, the particles will break their connection and de-flocculate leading to lower viscosity. Although many assumptions have been made to explain thixotropic behavior, characterizing thixotrpy by means of a microstructural approach is very challenging.

For the last fifty years the dominant method to measure thixotropy has been by measuring the area of what is called the "thixotropic loop", or a area related to the thixotropic loop [26, 27]. The method is based on successively measuring the loop throughout increasing and decreasing sequences of applied shear rates (see Figure 3.5). The surface between the descending and ascending curves is measured and considered as representative of the work done to break some of the connections per unit time and unit volume of the material. Despite its wide use, this measurement approach suffers from a couple flaws. Firstly, it is very dependent on the test apparatus and procedures [29], and secondly it does not consider intrinsic value of any physical rheological parameter since flocculation and de-flocculation cannot be separated [28]. The argument is that the measured surface can be the same for a mixture displaying fast flocculation and fast de-flocculation and a mixture displaying slow flocculation and slow de-flocculation, although the two mixtures

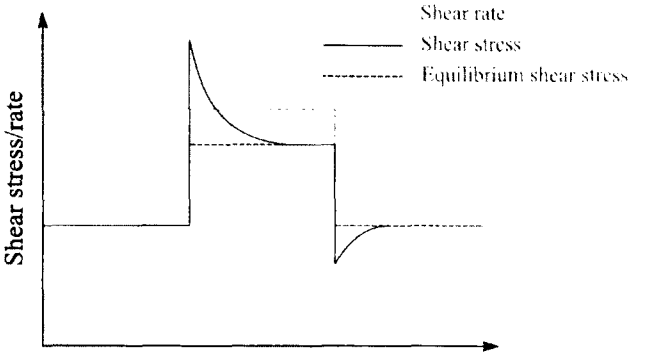


***Figure 3.4:*** *Response of a thixotropic material (solid black line) and non-thixotropic material (dashed line) to sudden changes in shear rate (solid grey line). Adapted from [16].*

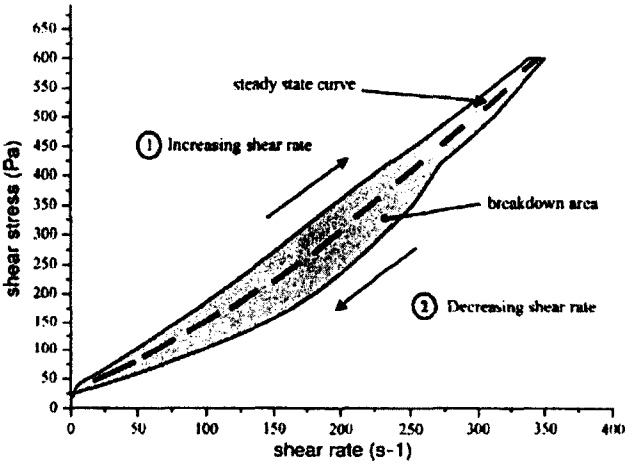


***Figure 3.5:*** *Example of thixotropic loop for a cement paste. The hashed area shows the surface confined by the increasing and decreasing shear rate ramps [28].*

will behave very differently in practice. To overcome the inconveniences of the traditional method, new analytical models have been recently developed introducing a new structure (or flocculation) parameter $\lambda$. The parameter describes the apparent rheological properties of the material and better interprets the macroscopic thixtropical behavior of concrete. Useful in this connection is the constitutive mathematical form proposed by Cheng and Evans [30], explaining thixotropy by linking the shear stress to the shear rate and the flocculation parameter ($\lambda$):

$$\tau = \eta(\dot{\gamma}, \lambda)\,\dot{\gamma} \tag{3.6}$$

$$\frac{d\lambda}{dt} = f(\dot{\gamma}, \lambda) \tag{3.7}$$

where

$\tau$: shear stress (Pa)

$\dot{\gamma}$: shear rate (1/s)

$\lambda$: structure parameter, varying from 0 (no structure) to 1 or $\infty$
$\eta(\dot{\gamma}, \lambda)\dot{\gamma}$: viscosity as a function of the shear rate and structure parameter (Pa s) (full structure) (-)
$f(\dot{\gamma}, \lambda)$: function describing the rate of change of the structure parameter, as a function of shear rate and the structure parameter itself.

Recently, less general models have given more importance to the flocculation phenomenon [28] with the goal of describing the thixotropic behavior. A good example of these models is the one developed by Mewis et. al [5], interpreting thixotropy in deference to the change of the structure with time:

$$\tau(\dot{\gamma}, t) = \lambda\tau_0 + \lambda K_{st}\dot{\gamma}^n + K_\infty\dot{\gamma}^n \tag{3.8}$$

$$\frac{d\lambda}{dt} = -K_1\dot{\gamma}\lambda + K_2\dot{\gamma}^m(1-\lambda) + K_3(1-\lambda) \tag{3.9}$$

where
$\tau_0$: yield stress (Pa)
$K_{st}$: consistency factor due to the structure (Pa $s^n$)
$K_\infty$: consistency factor at $\lambda$= 0 (Pa $s^n$)
$K_1, K_2, K_3$, $m$: factors describing change of structure in time
$t$: elapsed time (s)

The first term ($\lambda\tau_0$) in equation 3.8 represents the yield stress influenced by the structure, while the second one ($\lambda K_{st}\dot{\gamma}^n$) represents the contribution of the structure to the flow resistance, and the last term ($K_\infty\dot{\gamma}^n$) is the power-law of shear rate when the structural is broken down completely. The changes in the structure with time are described in equation 3.9. They include breakdown changes (first term), shear-induced build-up changes (second term), and build-up at rest due to Brownian motion changes (last term). Other models describing the thixotropic behavior of concrete and cement paste materials are discussed in section 3.7.2.

## 3.7 Rheology of Concrete

The following sections outline the rheological behavior of concrete in steady-flow state and explain various time-dependent phenomena including, thixotropy, structural break down, and loss of workability.

### 3.7.1 Rheological models for the steady state

Most of the available rheological models describe the concrete behavior in the steady state, which is achieved by eliminating all time-dependent properties in concrete [31]. In practice this means subjecting the concrete to a sufficient shear effect over a certain period of time, that varies with each mixture.

There exist numerous models to describe the rheological behavior of concrete in steady state, however it is difficult to capture with sufficient accuracy all possible trends using a single model [32]. Rheological analysis involving a single model is only possible with careful model selection. In this respect, finding the appropriate model is a crucial step in the analysis phase, involving consideration of the intrinsic properties of the tested concrete, the range of the testing shear rate, and each model's specific advantages and disadvantages. The most used models to describe the rheological properties of cement-based materials are presented in Table 3.1.

***Table 3.1:*** *Rheological models for cement-based materials. Adapted from [33].*

| Model | Equation | Number |
|---|---|---|
| Newtonian | $\tau = \mu\dot{\gamma}$ | 1 |
| Bingham | $\tau = \tau_0 + \mu_p\dot{\gamma}$ | 2 |
| Herschel and Bulkley | $\tau = \tau_0 + K\dot{\gamma}^n$ | 3 |
| Casson model | $\sqrt{\tau} = \sqrt{\tau_0} + \sqrt{\mu_p}\sqrt{\dot{\gamma}}$ | 4 |
| Modified Bingham model | $\tau = \tau_0 + \mu\dot{\gamma} + c\dot{\gamma}^2$ | 5 |
| Sisko model | $\eta = \mu_\infty + K\dot{\gamma}^{n-1}$ | 6 |

where

$\tau$:shear stress (Pa)
$\mu$: viscosity (Pa s)
$\dot{\gamma}$: shear rate (1/s)
$\tau_0$: yield stress (Pa)
$\mu_p$: plastic viscosity (Pa s)
$K$: consistency factor in Hershel-Bulkley model (Pa $s^n$)
$n$: flow index in Hershel-Bulkley model (-)
$c$: regression constant in the modified Bingham model (Pa $s^2$)
$\eta$: apparent viscosity (Pa s)
$\mu_\infty$: viscosity at infinite shear rate (Pa s)

As listed in Table 3.1, all models, excluding Newton's, use at least two parameters to describe the flow. The Herschel-Bulkley model contains three parameters, one of which, n (the flow index) does not represent any physical property, but defines the degree of

non-Newtonian behavior (shear thickening for n > 1, and shear-thinning for n < 1); K represents the consistency factor, which is not a physical entity neither. Characterizing a liquid in terms of these three parameters gives a much richer description of its rheology than is possible with a single value of apparent viscosity [3]. The Bingham model (2) has been commonly used for rheological investigations on cement pastes [34], while the Hershel-Bulkely model (3), the Casson model (4), and the modified Bingham model (5) have been used in comparative studies of rheological models [35 37]. Sisko's model (6) has the advantage of calculating viscosity at a theoretically infinite shear rate ($\mu_\infty$) [33, 37].

In general, many researchers approve on using the Bingham model to describe the rheological behavior of conventional concrete when a linear shear stress-shear rate relationship is expected. In some cases with SCC where non-linear behavior is anticipated, applying the Bingham model may lead to negative values of yield stress, which is physically impossible [38]. To avoid this problem, rheologists suggest a non-linear rheological model such as the Herschel-Bulkley model; considered one of the most appropriate non-linear model, particularly in the case of shear thickening [39]. Although the Herschel-Bulkley model is most frequently applied for non-linear concrete rheology, it has several downsides. Firstly, difficulties arise when determining the physical meaning of the consistency factor (K) which takes the dimension of $Pa\ s^n$ indicating its dependency on the material properties [16]. Secondly, the slope of the Hershel-Bulkley curve tends to zero (equation 3.10) for very low shear rates, resulting in an overestimation of the yield stress [38].

$$\frac{d\tau}{d\dot{\gamma}} = nK\dot{\gamma}^{n-1} \tag{3.10}$$

Another model describing the non-linear behavior of concrete was recently developed by Yahia and Khayat [32] as the modified Bingham model (5), by extending the Bingham model with a second order term. The shear thickening in the modified Bingham model is identified for c > 0, while the shear thickening for c < 0. The drawback in the modified Bingham model is that no physical meaning of the second order term (c) has been found yet [16], but there is still a possibility due to its fixed dimension.

In conclusion, the Bingham model is most applicable in cases of linear rheological behavior (such as for CVC), and the modified Bingham and Hershel-Bulkley are most applicable in the case of non-linear behavior. Despite the fact that the Hershel-Bulkley and modified Bingham models show adequate ability to describe nonlinearity in concrete behavior, many doubts still surround the physical meaning of some of their parameters. Presently, one of the most commonly used models in concrete research is the Bingham model. Applying the Bingham model to slight non-linear behavior may result in an acceptable measurement error. On the other hand, applying the Bingham model in the case of strong nonlinearity may result in negative yield stress [38]. At this point, the choice then between the modified Bingham and the Hershel-Bulkley model remains in question depending on the real rheological behavior of the mixture during testing. Specifically, in this investigation, it was found that the Bingham and the modified Bingham models describe fairly well the rheological behavior of the vast majority of the tested concrete in cases of linearity and nonlinearity. Both models will, therefore, be applied to all the results through the different phases of the experimental program, unless otherwise stated.

### 3.7.2 Transient behavior

For any concrete there exists a transient phase between two successive steady states, during which a yield stress model is not sufficient to describe the rheological behavior [31]. The interactions between the particles in this phase lead to some rheological time-dependent properties such as: thixotropy, structural break down, and loss of workability. These phenomena and their anticipated causes are described in the following sections.

#### Thixotropy

Thixotropy has been primarily described in section 3.6.3. Because thixotropic behavior is reversible, the major complication in determining thixotropic properties consists of the influence of the shear history. The shear history of the material influences the behavior at the moment the measurements are performed [40–42]. From this perspective, a reference point is needed in order to evaluate the thixotropic behavior accurately. Two states can be proposed at this stage, the completely flocculated state, or the completely de-flocculated state [28]. In practice, however, none of these states can ever be reached [28]. Several researchers agree on that the most suitable reference state is the most de-flocculated state of the concrete flow history measured immediately after mixing [28].

Different test methods to determine thixotropy are available in literature. The loop curve method (previously described in section 3.6.3) can be considered one of the easiest. Thixotropy can also be practically characterized by determining its effect on the increase in static yield stress with time. This can be easily determined by performing static yield stress measurements on a material, which has been kept at rest in the rheometer for a certain period of time [43–45]. Comparing the results obtained at different resting times gives information on the thixotropic build-up. Besides the above discussed approaches, a number of microstructural models have been developed with the goal of characterizing thixotropy from a practical viewpoint. Although these models seem very logical, it is not evident which of the different parameters of the equations need to be adjusted through experiments, calculations or simulations [16]. A good example of these models is the simplified model of Roussel [28]. Assuming that concrete follows Bingham behavior and the yield stress at rest increases linearly with time (equations 3.11, and 3.12), the Roussel model determines the influence of thixotropy on the static yield stress. On the other hand, the influence of thixotropy on the plastic viscosity is not relevant (as indicated in equation 3.11), since it may be neglected in practice in short time applications (not more than 30 min [28]).

$$\tau = \left(1 + \lambda_0 e^{-\alpha\dot{\gamma}t}\right)\tau_0 + \mu_p\dot{\gamma} \tag{3.11}$$

$$\lambda = \lambda_0{}^{-\alpha\dot{\gamma}t} \tag{3.12}$$

where

$\tau$: shear stress (Pa)

$\lambda_0$: initial structural state (-)

$\lambda$: flocculation state of the material (0 = fully dispersed, $\infty$ = fully coagulated) (-)

$\alpha$: thixotropy parameter (-)

$t$: time (s)
$\mu_p$: plastic viscosity of cement paste or concrete (Pa s)
$\dot{\gamma}$: shear rate (1/s)

The flocculation state $\lambda$ depends on the flow history, if the mixing phase is considered the reference point (the phase when the maximum shear rate is applied), then $\lambda$ is equal to zero. This implies that the contribution of thixotropy to the yield stress is also equal to zero. Over time, $\lambda$ will evolve from its initial zero value to a positive value according to equation 3.12. The structural build up at rest is then described by equation 3.13, assuming that the shear rate at rest equals zero, the apparent yield stress then becomes:

$$\tau_0(t) = (1+\lambda)\tau_0 = \tau_0 + \tau_0\frac{t}{T} = \tau_0 + A_{th}t \tag{3.13}$$

where

$$A_{th} = \frac{\tau_0}{T} \tag{3.14}$$

As shown in equation 3.14, $A_{th}$ is a material constant representing the flocculating rate (Pa/s) and indicating the linear increase of yield stress with the rest time (t). From equation 3.13 it is evident that thixotropy is an significant parameter to determine the energy needed to de-flocculate a concrete kept at rest for a certain period of time, which is a significant parameter involved in many concrete applications on job sites.

### Structural breakdown

The term "structural breakdown" was first introduced by Tattersall in 1954 [46]. The mechanisms of this phenomenon are attributed to the processes of breaking certain chemical linkages between the cement particles formed by the hydration process [25]. The breaking of linkages is considered to be an irreversible structural breakdown thus non-thixotropic. This has been justified by the theory considering that when concrete undergoes a shear effect, the groups of cement particles that share a single hydrant breakdown and a new membrane rapidly forms around the dispersed cement particles, partially inhibiting further agglomeration [47, 48]. The formation of these membranes has been practically validated using environmental scanning electron microscopy [48].

In 1954, Tattersall characterized the structural breakdown in cement pastes using a coaxial viscometer and equation 3.15 [46]:

$$T = T_E + (T_0 - T_E)\exp(-Bt)_0\frac{t}{T} \tag{3.15}$$

Where T is the torque at time t, while the suffixes 0 and E refer to the initial and equilibrium states; B in this case could be considered as the inverse of the de-flocculation characteristic.

Another method has been widely used to assess the structural breakdown in cement paste through evaluation of the hysteresis loop area and plastic viscosity, as depicted in Figure 3.6. Despite its wide use, the method suffers from major inconveniences because

of its high dependency on the testing procedures and equipment, as previously outlined in section 3.6.3.

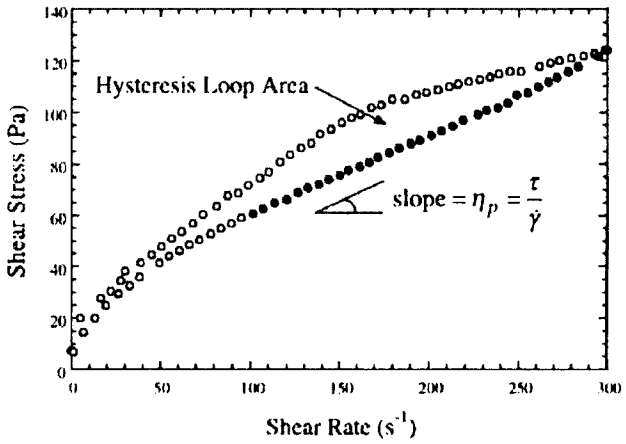


***Figure 3.6:*** *Typical hysteresis loop to calculate structural breakdown for hand-mixed paste presheared at 100 1/s. The plastic viscosity is calculated using the slope of the hysteresis down curve from 300 to 100 1/s (filled black circles) [49].*

### Loss of workability

The term "loss of workability" refers to the reduction of concrete workability with time, which is considered a major problem in the concrete industry. The loss of workability is explained by the formation of permanent connections due to coagulations or chemical reactions between cement particles able to resist a certain amount of applied work [23–25]. Concrete technologists have adopted various methods for managing the inevitable loss of workability over time. The most common practices range from retempering concrete with water at the job site to adding High-Range Water Reducing Admixtures (HRWRA) during mixing. Retempering concrete is probably one of the most common solutions to loss of workability, because it is the most intuitive to workers. Such a solution can degrade the quality of the concrete by disturbing the intended of water-to-cement ration ($w/cm$), which may exceed the target value $w/cm$. In the case of SCC, because of its sensitivity to water fluctuations and strict stability requirements, the practice of adding water is more avoided.

Due to the inherent inadequacies of the first method, adding retarding admixtures is probably the most practical way of fighting against workability loss. Also, hydration-controlling and retarding admixtures have a successful history of improving workability retention. The advance in Viscosity-Modifying Admixtures (VMA) has also helped to overcome the loss of workability [50]. Many VMAs are widely used nowadays to maintain workability over different periods of time depending on the required application.

The downside of using HRWRAs and VMAs is they are highly sensitive to changes in the mix proportion, mixing procedures, and ambient temperature. Because of their sensitivity, VMAs or HRWRAs if used in adequate dosages may result in undesired properties especially in hot-weather conditions.

## 3.8 Concrete rheometers

The ConTec and ICAR rheometers, used in the experimental program of this investigation, are described in terms of operating systems, testing procedures, and data interpretation processes.

### 3.8.1 The ConTec Rheometer

#### Description

The ConTec Viscometer is a coaxial cylinder rheometer in which a stationary inner cylinder measures the torque and an outer cylinder rotates at variable angular velocities to create the shear effect [46]. Several versions have been designed from the basic apparatus and can be used depending on the maximum aggregate size in the suspension. Each measuring system is related to the diameter of the inner cylinder. Figure 3.7 shows ConTec Viscometer 5, the best known version, and the Viscometer 4, a smaller model designed mainly for mortar and highly fluid concrete [51]. The entire apparatus is user-friendly, fully-automated, and controlled by a computer software installed and operated via a touch screen monitor located at the head of the machine.

***Figure 3.7:*** *The ConTec rheometers at the Université de Sherbrooke. The ConTec 5 for conventional concrete and SCC (left), ConTec 4 for SCC and mortar (middle), and ConTec 6 for micro mortar and paste (right).*

As presented in Figure 3.7, both inner and outer cylinders contain ribs parallel to their axis to reduce the risk of slippage. The inner cylinder consists of two parts, the upper measuring unit and the impeller. The upper part is stationary and connected to a sensor to measure the torque, while the lower impeller is used to minimize the effect of any potential 3D flow, ensuring that only two-dimensional shearing of the testing material will occur [16].

Personal experience with the ConTec rheometer reveals that depending on the mix design, some water droplets can migrate from the concrete toward the highest shear rate

zone located in the vicinity of the inner cylinder. This migration can result in some inhomogeneous material distribution in the tested sample, leading to inaccurate measurements. Hence, the appropriate choice of the pre-shearing period and the maximum shear rate are of outmost importance to avoid any segregation or particles separation during testing.

### Data treatment

Average torque and rotational velocity at each time step are calculated by default via the operating software and plotted in a torque-rotational velocity diagram. After each test, the raw data are temporarily available for separate analysis. This can be useful in order to investigate if the data points have been obtained in equilibrium conditions and no large fluctuations in the torque measurements occurred. By applying the Reiner-Riwlin equations (3.20 and 3.21), the data points can be transformed into a flow curve expressing the relationship between shear stress and shear rate [33, 52, 53]. The advantage of using the Reiner-Riwlin equations is that the transformed values are independent of the geometry, as long as it is a concentric cylinder geometry [16]. Nevertheless, the transformation by Reiner-Riwlin's equations requires a preliminary choice of the rheological model; changing the rheological model will change the transformation equations. In the absence of a presumed model, approximation can be made using equations 3.16 and 3.17, to transform the data points into a flow curve expressing the shear stress-shear rate relationship [16].

$$\tau = \frac{T_i}{2\pi R_i^2 h} \tag{3.16}$$

$$\dot{\gamma}_i = \frac{2\Omega_i}{n\left[1 - \left(\frac{R_i}{R_o}\right)^n\right]} \tag{3.17}$$

$$n = \frac{d\ln(T_i)}{d\ln(\Omega_i)} \tag{3.18}$$

The developers of the ConTec Viscometers have chosen to impose the Bingham model on all results so that fundamental rheological units may be obtained [16]. The transformation of the torque versus rotational velocity is a two-step process. Firstly, the linear relationship of torque as a function of rotational velocity is determined according to equation 3.19:

$$T = G + HN \tag{3.19}$$

where

$T$: torque (N m)
$G$: intercept of the relationship with the T-axis, for N = 0 (N m)
$H$: slope of relationship between T and N (N m s)
$N$: rotational velocity (rotation/s)

Secondly, the values of G and H are transformed into yield stress ($\tau_0$) and plastic viscosity

($\mu_p$), the two parameters of the Bingham model, by means of equations 3.20 and 3.21 (Reiner-Riwlin equations).

$$\tau_0 = \frac{G\left(\frac{1}{R_i^2} - \frac{1}{R_o^2}\right)}{4\pi h \ln\left(\frac{R_o}{R_i}\right)} \tag{3.20}$$

$$\mu_p = \frac{H\left(\frac{1}{R_i^2} - \frac{1}{R_o^2}\right)}{8\pi^2 h} \tag{3.21}$$

where

$\tau_0$: yield stress (Pa)
$G$: G from equation 3.19
$R_i$: radius of inner cylinder (m)
$R_o$: radius of outer cylinder (m)
$h$: height of inner cylinder submerged into concrete (m)
$\mu_p$: plastic viscosity (Pa s)
$H$: H from equation 3.19 (N m s)

Note that the Reiner-Riwlin equation does not transform data points from the T-N graph to a shear stress-shear rate diagram, but a pre-defined relationship between T and N is transformed into a shear stress-shear rate relationship. Equations 3.20 and 3.21 are only valid if the material between the two cylinders is entirely sheared. If the shear stress at a certain radius in the rheometer is lower than local yield stress, the material is not sheared and plug flow is obtained. In this case, the equations need slight modifications, as described in [52].

In case the Bingham model is not valid (due to non-linear behavior of concrete for example), equations 3.20 and 3.21 need to be changed by incorporating a non-linear model (such as the Hershel-Bulkley or the modified Bingham models). This is exemplified in equations 3.22-3.25 where a "new Reiner-Riwlin" equation has been derived in [54, 55] based on the Herschel-Bulkley relationship incorporating a third parameter that needs to be determined and transformed. As indicated in equations 3.23 and 3.24, the relationship between T and N from equation 3.22 is transformed into a Herschel-Bulkley relationship.

$$T = G + K_{HB}.N^m \tag{3.22}$$

$$\tau_0 = \frac{G_{HB}}{4\pi h}\left(\frac{1}{R_i^2} - \frac{1}{R_o^2}\right)\frac{1}{\ln\left(\frac{R_o}{R_i}\right)} \tag{3.23}$$

$$K = \frac{K_{HB}}{2^{2n+1}\pi^{n+1}h}.n^n\left(\frac{1}{R_i^{2/n}} - \frac{1}{R_o^{2/n}}\right)^n \tag{3.24}$$

$$n = m \tag{3.25}$$

where

$G_{HB}$, $K_{HB}$, m: Herschel-Bulkley parameters of the T-N relationship

$\tau_0$, $K$, $n$ : Herschel-Bulkley parameters of the shear stress-shear rate relationship

Similar to equations 3.22-3.25, an extension of the Reiner-Riwlin equation using the modified Bingham model was derived, as presented in equations 3.26-3.28 [56]:

$$\tau_0 = \frac{G\left(\frac{1}{R_i^2} - \frac{1}{R_o^2}\right)}{4\pi h \ln\left(\frac{R_o}{R_i}\right)} \tag{3.26}$$

$$\mu = \frac{H\left(\frac{1}{R_i^2} - \frac{1}{R_o^2}\right)}{8\pi^2 h} \tag{3.27}$$

$$c = \frac{C\left(\frac{1}{R_i^2} - \frac{1}{R_o^2}\right)}{8\pi^3 h}\frac{(R_o - R_i)}{(R_o + R_i)} \tag{3.28}$$

Where the relationship between the torque (T) and rotational velocity (N) for the modified Bingham model is defined by equation 3.29.

$$T = G + HN + CN^2 \tag{3.29}$$

where

$\tau_0$: yield stress (Pa)

$G$: G from equation 3.29

$R_i$: radius of inner cylinder (m)

$R_o$: radius of outer cylinder (m)

$h$: height of inner cylinder submerged into concrete (m)

$\mu$: viscosity (Pa s)

$H$: H from equation 3.29 (N m s)

$c$: regression constant in the modified Bingham model (Pa $s^2$)

$C$: C from equation 3.29

One can use the raw data file in order to apply equations which are not (yet) incorporated in the software [16] such as equations 3.23 and 3.24 for the Herschel-Bulkley model, or equations 3.26-3.28 for the modified Bingham model .

## 3.8.2 The ICAR Rheometer

### Description

The ICAR rheometer is a portable coaxial cylinder rheometer developed at the International Center for Aggregate Research (ICAR) at the University of Texas. The ICAR rheometer provides a low-cost, rugged, and simple instrument that can be used on job sites to characterize the flow behavior of concrete. As shown in Figure 3.8, the ICAR rheometer is composed of a container, a driver head with an electric motor, a torque meter, a four-blade vane that is held by the chuck on the driver, a frame to attach the driver (or vane assembly) to the top of the container, and a laptop. The laptop is used to operate the driver and record the torque and velocity during testing. The container serves to hold the concrete and it contains a series of vertical ribs around the perimeter to prevent concrete slippage along the wall during testing (Figure 3.8). The size of the container and length of the vane shaft are selected based on the nominal maximum size of the aggregate. For the purpose of this investigation, a vane with a diameter and a height of 127 mm was used.

### Testing procedure and data treatment

The testing procedures of both the ICAR and ConTec rheometers are similar to each other. Simply put, a set of velocities is applied to the concrete and the corresponding torques are measured. The number of data points and velocity steps can be adjusted easily. During each step, the velocity is held constant and the average velocity and torque are recorded. The ICAR rheometer software performs all the necessary functions (operates the driver, records the torque, computes test results, and stores data). The data are available for custom analysis and can be transformed into a flow curve expressing the relationship between shear stress and shear rate (as discussed in the previous section). In case of plug flow, the equations need slight modifications as described in [52]. Despite that the ICAR is a convenient tool to measure rheological properties of concrete on job

***Figure 3.8:*** *The ICAR rheometer [57].*

sites, the practical experience with the ICAR (of the Université de Sherbrooke) showed that it can deliver different results than the ConTec rheometer. A comparison between the measurements of both rheometers and further details concerning this matter are presented in the following section.

## 3.9 Comparison between the ConTec and ICAR rheometers

Encountering inaccurate test measurements is quite normal in any scientific research; the deficiency in the measurements can be related to several causes such as the operator error, defects in the testing equipment, data treatment process, etc. Throughout this investigation and for some uncertain reasons, the rheological measurements obtained with the ICAR and ConTec rheometers (of the Université de Sherbrooke) were not identical. A special campaign was carried out in order to compare the results and find a correlation between the measurements of both rheometers.

The comparative study covered a wide scope of SCC and HWC mixtures with viscosities between 20 and 150 Pa s (measured with the ConTec), and yield stress up to 650 Pa. All mixtures were tested simultaneously in both rehometers to avoid any aside effect of time on the results. Also, in both rheometers, the concrete sample was pre-sheared for 20 seconds to eliminate any possible effect of thixotropy on the measurements. Afterward, the rotational velocity was decreased in both rheometers through 10 steps (5 seconds each) from the maximum rotational velocity (0.5 rps) to the minimum velocity (0.03 rps). The measured torque (T) and rotational velocity (N) were averaged and registered during the last 4 seconds of each step. From the T-N relationship, the slope (H) and intercept with the T-axis (G) were calculated for both rheometers and transformed into yield stress and plastic viscosity, respectively, by means of the Reiner-Riwlin equation [53]. Plug flow was verified by comparing the shear stress applied at the most outer point (at $R_o$) with the measured yield stress. If a shear stress value lower than the yield stress was obtained, plug flow was considered and the yield stress and plastic viscosity were recalculated (by replacing $R_o$ by $R_p$ in the Reiner-Riwlin equation) through an iterative process in order to eliminate this influence.

The test results of the concrete mixtures including viscosity and yield stress measured in both rheometers are illustrated in Figure 3.9. As indicated in Figure 3.9a, the ICAR underestimates viscosity and, in some cases, overestimates yield stress compared to the ConTec. This could be due to some malfunctions in the machine or the accuracy of its measuring system. It could also be attributed to the test geometry; for example the full-plate vane in the ICAR may somewhat affect the homogeneity of the tested sample, especially when testing mixtures with low viscosity. This phenomenon was witnessed throughout several experiments as segregation problems within the tested sample. This could be explained by the dynamic collision occurring between the driven aggregate and the full-plate vane which urges the aggregates to sink down the reservoir. Consequently, the concentration of aggregate becomes higher at the bottom of the tested sample, whereas the concentration of paste becomes higher at the top.

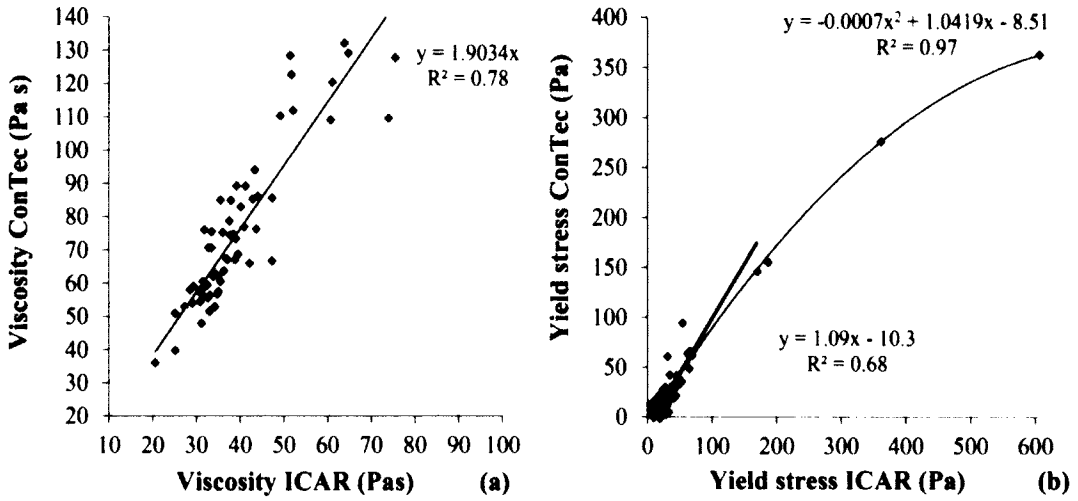


***Figure 3.9:*** *Relationship between (a) viscosity and (b) yield stress of concrete mixtures tested simultaneously in the ICAR and ConTec. Feys D. et al. (2012), unpublished raw data.*

As shown in Figure 3.9, the correlations between the viscosities and yield stresses measured in both rheometers can be described as follows:

- Plastic viscosity
  - Plastic viscosity < 150 Pa s (measured with the ConTec rheometer)

$$\mu_{ConTec} = 1.9\,\mu_{ICAR} \tag{3.30}$$

- Yield stress:
  - Plastic viscosity < 100 Pa s (ConTec) and yield stress < 100 Pa:

$$\mu_{ConTec} = 1.09\,\mu_{ICAR} - 10.32 \tag{3.31}$$

  - Plastic Viscosity > 100 Pa s (ConTec) or yield stress > 100 Pa:

$$\mu_{ConTec} = -0.00071\,\mu_{ICAR}^2 + 1.04\,\mu_{ICAR} - 8.51 \tag{3.32}$$

As an overall evaluation, it is believed that the ConTec rheometer is more reliable than the ICAR by virtue of its stable and accurate measuring system. Unfortunately, transferring the ConTec rheometer to the job site was not possible. Therefore, throughout several phases of the experimental program the ICAR was used. In these instances, the rheological properties were converted to the equivalent rheological properties obtained by the ConTec rheometer, using the relationships established above.

## 3.10 Concrete tribometers

Tribology in its narrow sense has been previously defined in section 2.4. When the concrete is in relative motion with a steel interface (a pumping pipe for example), the steel-concrete interface plays an important role in determining the flow behavior of the

concrete. Different attempts, using various types of tribometers, have been made in literature to determine the tribological properties of concrete. Several kinds of these tribometers as well as the one developed at the Université de Sherbrooke (UdS) are described in the following sections.

### 3.10.1 Best and Lane tribometer (1960)

Best and Lane (1960) developed and validated a tribological test on a pumping circuit, using pipes with an inner diameter of 150 mm [58]. The test consists of pushing the concrete via hydraulic piston in a 250 mm pipe at a controlled velocity. At the end of the pipe, the concrete must pass through an elliptical reducer, decreasing the initial cross-section by 16%. The energy used to force the concrete to pass through the reduction is measured and used to assess the pumpbility of the tested concrete. Even though measuring the force needed to make the concrete pass the reduction does not permit the measurement of its tribological behavior, the following conclusions obtained from this experiment can still be highlighted:

- The high water content favors the development of segregation during pumping, and low water content below a certain limit will hinder pumping and abundant resistance can be expected.
- For a fixed granular distribution, a minimum amount of mortar is required to make the concrete pumpable.
- The shape of coarse aggregate strongly influences the pumping pressure, especially if the mortar content is relatively low.
- The maximum aggregate size has a minor influence on the pumping pressure as long as the mortar is sufficient to provide proper lubrication for the coarse aggregate.
- The presence of fly ash increases the granular compactness, thus for a fixed water content, concrete shows a better deformability and pumpability with increasing the fly ash content.

### 3.10.2 Tribometer developed by Morinaga (1973)

Morinaga's tribometer was developed to suit actual pumping conditions [59]. It consists of a 2-m long pipe with a diameter of 50 mm placed on wheels. A special set connected to a load cell is used to apply a balancing force in order to hold the pipe in place during testing. Concrete is placed inside the pipe and pushed using pressurized air. The load cell measures the force necessary to hold the pipe in place and thus gives the stress generated between the concrete and the pipe wall, which can be related to the pumping pressure.

### 3.10.3 Modified BTRheom (Kaplan, 2001)

Kaplan developed his tribometer using the frame of the BTRheom [60]. The outer wall of the BTRheom, employed to contain the concrete between the parallel plates, is used as outer cylinder. The radii of the inner and outer cylinders are 75 and 175 mm, while

the height is 200 mm. Kaplan's tribometer is a practical tool that can be easily used in the field, but the sealing between the stationary bottom plate and the rotating inner cylinder is problematic. The sealing is provided by a rubber strap and causes parasitic friction, and consequently a bias in the measurements. The testing procedure for the Kaplan tribometer is similar to that for the cylindrical rheometers: a set of rotational velocities is applied, and the resulting torque is measured. The relationship between the measured torque and the applied rotational velocities is used to determine the tribological properties of concrete. Further details concerning the data treatment for this tribometer are discussed in section 5.7.

### 3.10.4 Modified Tattersall Mk-III rheometer (Chapdelaine, 2007)

Chapdelaine developed a concrete tribometer to measure the interaction between concrete and a steel or rubber wall [61]. A bowl of the same size as the IBB rheometer (360 mm in diameter and 250 in height) is used. Fixed blades of 12 mm wide are placed on the inside walls of the bowl, at the bottom and in the center, to prevent concrete slipping, while a clearance between the edge of the cylinder and the bottom of the bowl of 50 mm is maintained. A sketch of the bowl and the moving part of Chapdelaine's tribometer are depicted in Figure 3.10.

As the open cylinder is rotated in the bowl, a lubrication layer is formed on both sides of the rotating cylinder. This simple design has allowed the testing of different materials as rotating cylinder. In theory, the modified Tattersall Mk-III tribometer can be applied on HWC and SCC, but only with a lot of precautions. The main complexity is caused by the double-sided flow in the tribometer [62]; the concrete undergoes different flow conditions on both sides as the outside has a lower shear rate than the concrete on the inside.

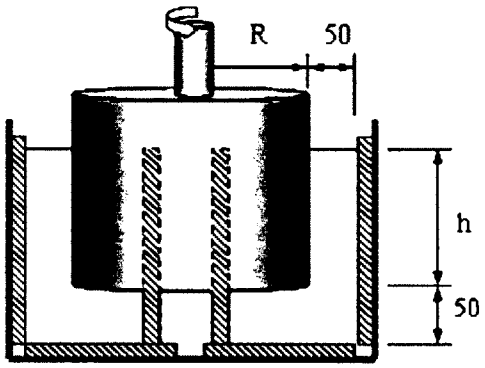


***Figure 3.10:*** *Sketch of the tribometer developed by Chapdelaine (2006), all dimensions in mm.*

### 3.10.5 Portable tribometer developed by Ngo (2009)

Ngo's tribometer can be considered as an accurate, stable tool of reasonable cost to measure the interaction at the concrete-steel interface in the case of CVC [63]. This

tribometer consists of a cylinder with a radius of 54 cm and a height of 100 mm that can rotate in a stationary cylindrical reservoir with a radius of 150 mm. The testing procedure includes two consecutive series of measurements. The first set is performed on the concrete with the 50-mm deep reservoir half full to determine the effect of the concrete bottom layer on the measurements. The second set is performed with the rotating cylinder entirely immersed in concrete. In both cases, the rotational velocity is imposed in a loop order and the resulting torque is measured. The properties of the lubrication layer of CVC can thus easily be determined when subtracting step 1 from step 2. With a typical high yield stress of CVC, the concrete is not sheared in the tribometer's gab. As a result, the properties of the lubrication layer can be determined from the torque-velocity relationship. When defining G as the intercept of the line (in the torque-velocity relationship) and H as the slope of the line, the yield stress and viscous constant (expressed in Pa s/m) can be calculated using equations 3.33 and 3.34.

$$\eta_i = \frac{H_i}{8\pi^2 R^3 h} \tag{3.33}$$

$$\tau_{0i} = \frac{G_i}{2.2\pi R^2 h} \tag{3.34}$$

The above equations are only applicable when the concrete is not sheared. In the case of SCC, this condition is not likely to be fulfilled due to its low yield stress. The registered torque in the tribological test then includes both effect of the sheared concrete and the lubrication layer. As a result, another approach to interpret the tribological measurements in the case of SCC is required (described in section 5.7). Despite that Ngo's tribometer is an instrumental tool to determine the tribological properties of CVC, using this tribometer in the case of SCC (or HWC) can result in inaccurate measurements. For example, in the first step of the testing procedure, the concrete would rather flow like in a parallel plate rheometer, while it is confined by vertical walls. In the second step, the concrete underneath the inner cylinder is sheared as in a parallel plate rheometer, whereas the concrete next to the inner cylinder is sheared like in a coaxial cylinder rheometer, but the other part of the concrete undergoes a complex 3D shearing pattern [62]. These problem were avoided in the design of the UdS tribometer by extending the height of the inner cylinder in such way that the effect of the bottom can be quantified [62].

### 3.10.6 Development of the UdS tribometer (2012)

A new tribometer was developed at the Université de Sherbrooke in the context of this research. Certain inconveniences found in the previously presented tribometers were avoided in the design of the UdS tribometer. The new tribometer is based on the Tattersall Mk-III rheometer as a modified version of the Ngo tribometer [63] (see Figure 3.11). The planetary motion of the impeller is removed and the H-impeller is replaced by a smooth steel cylinder that can rotate centrally at different velocities in a cylindrical reservoir. The diameters of the outer and inner cylinders are 237 mm and 125 mm, respectively, while their heights are 200 mm and 260 mm, respectively. The head of the inner cylinder is cone-shaped (with a height of 50 mm and an angle of 38.7°) to facilitate

the penetration into the concrete. The clearance between the cone and the bottom of the reservoir is 5 mm, which is very low. A measuring cell is connected to the inner cylinder to measure the corresponding torque. The tribometer is connected to a computer through which the testing velocities and other testing parameters can be defined.

The main advantages of the design of the UdS tribometer is that, there is no sealing problem (between the stationary bottom plate and the rotating inner cylinder) as in the case of the modified BTRheom. Also, in the new design there is only one gap between the inner and outer cylinder filled with concrete, consequently no double-sided flow will be generated as in the tribometer of Chapdelaine (2007).

The testing procedure in the UdS tribometer is similar to that in the cylindrical rheometers. A predefined set of rotational velocities is applied, and the resulting torque is measured. The measured data including the imposed velocities (N) and the corresponding torques (T) are registered by the tribometer's computer for further data analysis. The T-N relationship is then established and used to determine different tribological parameters that describe the tribological properties of concrete. Further details concerning the data treatment and the mathematical derivation of the tribological parameters are discussed in sections 6.8.2 and 5.7.

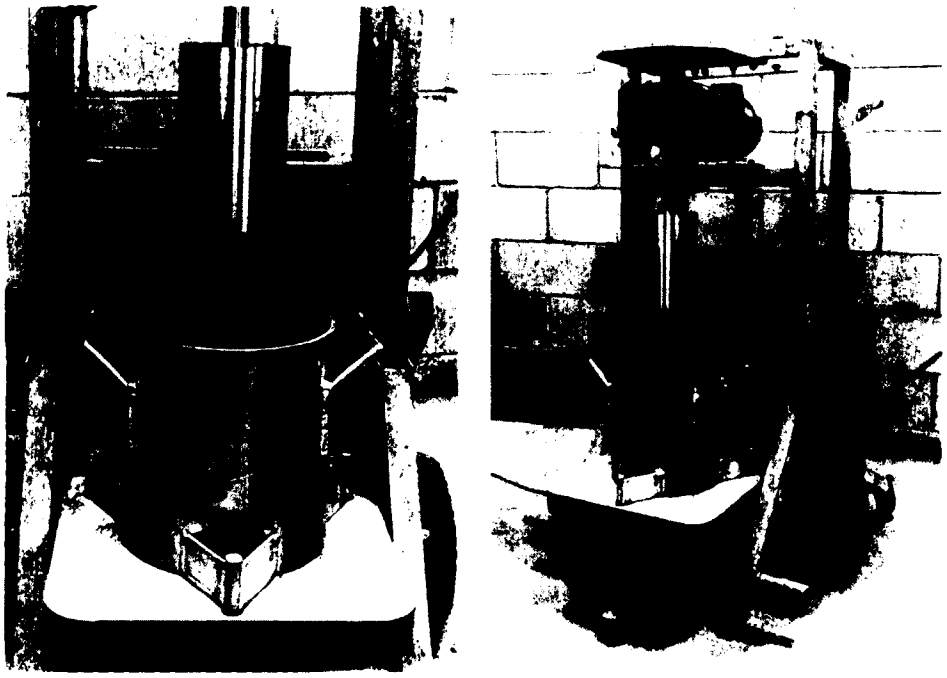

***Figure 3.11:*** *Tribometer developed at the Université de Sherbrooke (2012).*

## 3.11 References

[1] Morris C.G., *Academic Press dictionary of science and technology*, E. Book. 1992, p. 2432.

[2] Coussot P., *Rheometry of pastes, suspensions, and granular materials: applications in industry and environment*, 2. New Jersey: John Wiley & Sons, Inc., Hoboken, 2005, pp. 317–318.

[3] Mueller S., Llewellin E.W., Mader H.M., "The effect of particle shape on suspension viscosity and implications for magmatic flows", *Geophysical Research Letters*, vol. 38, no. L13316, 2011.

[4] Macosko C.W., *Rheology principles, measurements and applications*, 10. Vch New-York, 1994.

[5] Mewis J., Wagner N.J., "Thixotropy, advances in colloid and interface science", *Colloids, polymers and surfactants. Special Issue in honour of Brian Vincent.*, 2009.

[6] Rutger I.R., "Relative viscosity of suspensions of rigid spheres in Newtonian liquids", *Rheologica Acta*, vol. 2, no. 3, pp. 202–210, 1962.

[7] Thomas D.G., "Transport characteristics of suspension: VIII. A note on the viscosity of Newtonian suspensions of uniform spherical particles", *Journal Of Colloid Science*, vol. 20, no. 3, pp. 267–277, 1965.

[8] Brenner H., "Rheology of two-phase systems", *Annual Review of Fluid Mechanics*, vol. 2, pp. 137–176, 1970.

[9] Happel J., "Viscosity of suspensions of uniform spheres", *Journal of Applied Physics*, vol. 28, pp. 1288–1292, 1957.

[10] Jeffre D.J., Acrivos A., "The rheological properties of suspensions of rigid particles", *ACI Journal*, vol. 22, no. 3, pp. 417–432, 1976.

[11] Pabst W., Gregorova E., Berthold C., "Particle shape and suspension rheology of short-fiber systems", *Journal of the European Ceramic Society*, vol. 26, no. 1-2, pp. 149–160, 2006.

[12] Einstein A., "Eine neue bestimmung der moleküldimensionen", *Annalen der Physik*, vol. 324, no. 2, pp. 289–306, 1906.

[13] Guth E., Gold O., "On the hydrodynamical theory of the viscosity of suspensions", *Physical Review*, vol. 53, pp. 22–322, 1938.

[14] Vand V., "Viscosity of solutions and suspensions", *Journal of Physical and Colloid Chemistry*, vol. 52, pp. 277–299, 1948.

[15] Manley R.St.J., Mason S.G., "Further observations on collisions of spheres. Particle motions in sheared suspensions.", Montreal, 1955.

[16] Feys D., "Interactions between rheological properties and pumping of self-compacting concrete", Ph.D. dissertation, Ghent University, 2009.

[17] Krieger I.M., Elrod H., "Direct determination of the flow curves of non-Newtonian Fluids. II. Shearing rate in the concentric cylinder Viscometer", *Journal of Applied Physics*, vol. 24, p. 134, 1953.

[18] Sierou A., Brady J.F., "Accelerated stokesian dynamics simulations", *Journal of Fluid Mechanics*, vol. 448, no. -1, pp. 115–146, 2001.

[19] Geiker M.R., Wallevik O.H., "Rheology of cement based materials", in *DTU-RILEM Doctoral course*, Lyngby, 2007.

[20] Barnes H.A., "The yield stress-a review or everything flows?", *Journal of Non-Newtonian Fluid Mechanics*, pp. 133–178, 1999.

[21] Heymann L., Peukert S., Aksel N., "On the solid-liquid transition of concentrated suspensions in transient shear flow", *Rheologica Acta*, vol. 41, pp. 307–315, 2002.

[22] Mangesana N., Chikuku R.S., Mainza A.N., Govender I., Westhuizen A.P., Narashima M., "The effect of particle sizes and solids concentration on the rheology of silica sand based suspensions", *Journal of The Southern African Institute of Metallurgy*, vol. 108, 2008.

[23] Hattori K., "Electrokinetics and rheological behaviour of cement suspensions", Department of Civil Engineering, Chuo University, Tokyo, Tech. Rep.

[24] Hattori K., Izumi K., "A new viscosity equation for non-newtonian suspensions and its application in Rheology of Fresh Cement and Concrete", in *Int. Conf. Organized by the British Society of Rheology.*

[25] Wallevik J.E., "Rheological properties of cement paste: Thixotropic behavior and structural breakdown", *Cement and Concrete Research*, vol. 39, pp. 14–29, 2009.

[26] Lapasin R., Longo V., Rajgelj S., "Thixotropic behavior of cement pastes", *Cement and Concrete Research*, vol. 9, no. 3, pp. 309–318, 2006.

[27] Assaad J., Khayat K.H., Mesbah H., "Variation of formwork pressure with thixotropy of self-consolidating concrete", *ACI Materials Journal*, vol. 102, no. 1, pp. 215–223, 2003.

[28] Roussel N., "A thixotropy model for fresh fluid concretes: Theory, validation and applications", *Cement and Concrete Research*, vol. 36, pp. 14–29, 2006.

[29] Banfill P.F.G., Saunders D.C., "On the viscosimetric examination of cement pastes", *Cement and Concrete Research*, vol. 11, no. 3, pp. 363–370, 1981.

[30] Cheng D.H., Evans F., "Phenomenological characterization of the rheological behaviour of inelastic reversible thixotropic and antithixotropic fluids", *British Journal of Applied Physics*, vol. 16, no. 11, pp. 1599–1617, 1965.

[31] Roussel N., "Steady and transient flow behaviour of fresh cement pastes", *Cement and Concrete Research*, vol. 35, no. 9, pp. 1656–1664, 2005.

[32] Yahia A., Khayat K.H., "Analytical models for estimating yield stress of high-performance pseudoplastic grout", *Cement and Concrete Research*, vol. 31, no. 5, pp. 731–738, 2001.

[33] Nehdi M., Rahman M.A., "Effect of geometry and surface friction of test accessory on oscillatory rheological properties of cement pastes", *ACI Materials Journal*, vol. 101, no. 5, pp. 416–424, 2004.

[34] Ferraris C.F., Obla K.H., Hill R., "The influence of mineral admixtures on the rheology of cement paste and concrete", *Cement and Concrete Research*, vol. 31, no. 2, pp. 245 255, 2001.

[35] Atzeni C., Sanna U., "Comparison between rheological models for portland cement pastes", *Cement and Concrete Research*, vol. 15, no. 3, pp. 511 519, 1985.

[36] Chen C.-T., Struble L.J., Zhang H., "Using dynamic rheology to measure cement admixture interactions", *Journal of ASTM International*, vol. 3, no. 3, pp. 1–13, 2006.

[37] Papo A., "Rheological models for cement paste", *Materials and Structures*, vol. 21, no. 121, pp. 41 46, 1988.

[38] Feys D., Verhoeven R., Schutter D.G., "Evaluation of time independent rheological models applicable to fresh self-compacting concrete", *Applied Rheology*, vol. 17, no. 5, 2007.

[39] Herschel W.H., Bulkley R., *Konsistenzmessungen von Gummi-Benzol-Lösungen*, Kolloid Z. 1926, pp. 291–300.

[40] Cheng D.C.-H., "Hysteresis loop experiments and the determination of thixotropic properties", *Nature*, no. 216, pp. 1099 1100, 1967.

[41] Mewis J., Spaull A.J.B., Helsen J., "Structural hysteresis", *Nature*, no. 253, 1975.

[42] Barnes H.A., "Thixotropy - a review", *Joural of Non-Newtonian Fluid Mechanics*, vol. 70, pp. 1 33, 1997.

[43] Mahaut F., Chateau X., Coussot P., Ovarlez G., "Yield stress and elastic modulus of suspensions of noncolloidal particles in yield stress fluids", *Journal of Rheology*, vol. 52, pp. 287 313, 2008.

[44] Mahaut F., Mokéddem S., Chateau X., Roussel N., Ovarlez G., "Effect of coarse particle volume fraction on the yield stress and thixotropy of cementitious materials", *Cement and Concrete Research*, vol. 38, pp. 1276 1285, 2008.

[45] Billberg P., Österberg T., "Thixotropy of self-compacting concrete", in *the second International RILEM Symposium on SCC*, Tokyo, 2001, pp. 99–108.

[46] Tattersall G.H., "The rheology of Portland cement pastes", *British Journal of Applied Physics*, vol. 6, pp. 165–167, 1955.

[47] Tattersall G.H., Banfill P.F.G., *The rheology of fresh concrete*. Great Britain: Pitman Books Limited, 1983.

[48] Yang T.M.T., Krieger I.M., "Comparison of methods for calculating shear rates in coaxial viscometers", *Journal of Rheology*, vol. 22, pp. 413 421, 1978.

[49] Boger D.V., Walters K., Webster M.F., Williams R.P., "Yield stress", in *The XVth Int. Cong. On Rheology*, Monterey, 2008.

[50] The European Associations of Concrete Admixtures, "Guidelines for viscosity modifying admixtures for concrete", The European Associations of Concrete Admixtures, Tech. Rep., 2006.

[51] Ferraris C.F., Brower L.E., Beaupré D., Chapdelaine F., Domone P., Koehler E., Shen L., Sonebi M., Struble L., Tepke D., Wallevik O., Wallevik J.E., "Comparison of concrete rheometers: International tests at MB (Cleveland OH, USA) in May, 2003", *NIST report 7154, Gaithersburg*, 2004.

[52] Wallevik J.E., "Rheology of particle suspensions of fresh concrete, mortar and cement paste with various types of lignosulfonates", Ph.D. The Norwegian University of Science and Technology, 2003.

[53] Reiner M., *Deformation and flow: An elementary Introduction to Theoretical Rheology*. Great Britain: H.K. Lewis & Co. Limited, 1949, p. 348.

[54] Heirman G., Vandewalle L., Van Gemert D., Wallevik O., Cauberg N., "Contribution to the solution of the Couette inverse problem for Herschel-Bulkley fluids by means of the integration method", in *The 2nd International Symposium on Advances in Concrete through Science and Engineering*, Quebec-City, 2006.

[55] Heirman G., Vandewalle L., Gemert D.V., Wallevik O., "Integration approach of the Couette inverse problem of powder type self-compacting concrete in a wide-gap concentric cylinder rheometer", *Journal of Non-Newtonian Fluid Mechanics*, vol. 150, no. 2-3, pp. 93 103, 2008.

[56] Feys D., Wallevik J.E., Yahia A., Khayat K.H., Wallevik O.H., "Extension of the Reiner-Riwlin equation to determine modified Bingham parameters measured in coaxial cylinders rheometers", *Materials and Structures*, vol. 46, no. 1-2, pp. 289–311, 2013.

[57] German Instruments, "NDT Systems, Catalog NDT 2010", *NDT Systems, Catalog NDT 2010*,

[58] Best J., Lane R., "Testing for optimum pumpability of concrete", *Concrete International*, pp. 9–17, 1960.

[59] Morinaga M., "Pumpability of concrete and pumping pressure in pipelines, Fresh Concrete: important propeties and their peasurement", in *RILEM, Seminar*, Leeds, 1973, pp. .1–39.

[60] Kaplan D., "Pumping of concretes", Ph.D. dissertation, Laboratoire Central des Ponts et Chausées, Paris, 2001.

[61] Chapdelaine F., "Fundamental study and practice on concrete pumpability", Ph.D. dissertation, University of Laval, 2007.

[62] Feys D., Khayat K.H., Perez-Schell A., Khatib R., "Relation between rheological and tribological properties of Highly-Workable Concrete, in view of estimating pumping pressures", in *The Fifth North American Conference on the Design and Use of Self-Consolidating Concrete*, Chicago, 2013.

[63] Ngo T.T., "Influence of concrete compositions on the pumpability parameters", Ph.D. dissertation, Cergy Pontoise, France, 2009.

# Chapter 4

# Pumping Concrete

## 4.1 Introduction

This chapter is divided into three main parts. The first one provides a brief review on some commonly used pumps in the concrete industry. The second part discusses practical approaches to assess concrete pumpability and several pumping issues. The third part details the factors affecting pumping pressure and the changes in concrete properties associated with prolonged pumping.

## 4.2 Concrete pumps

The first concrete pump was developed in the U.S. in 1913 [1]. The pump operated on the principle of a piston pushed by a mechanical force that would then advance the concrete. After the Second World War, dual piston pumps were introduced to increase the pumping speed. Presently, piston pumps dominate the concrete pumping industry due to their high capacity [2] and lack of a better alternatives. Figure 4.1 shows an example of a dual piston pump working by filling one piston while emptying the other one. This is accomplished via a valve shifting its opening toward the feeder and shutting it toward the pipe. Piston pumps can be typically mounted on a truck or on a trailer to facilitate transportation. Truck-piston pumps are more often used for intensive pumping projects, while trailer-mounted pumps are used more for shotcrete works or where access is difficult.

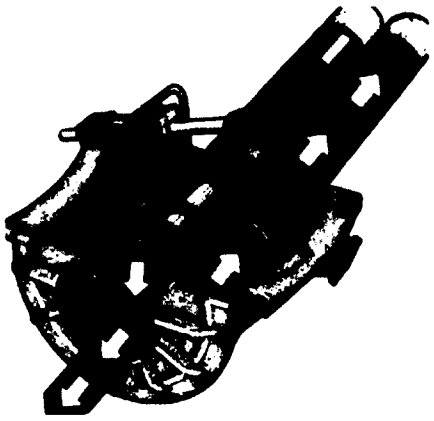

***Figure 4.1:*** *Mechanism of a hydraulic pump with two pistons [3].*

When using piston pumps, the pressure within the concrete shifts with the frequency of the pump strokes. As depicted in Figure 4.2, the maximum concrete pressure can become quite high. On the other hand, the minimum pressure, coinciding with the closing of the valve can create the effect of a pressure wave that for certain types of concrete results in a considerable negative value (Figure 4.2).

The screw- (or worm-) pump is another type of widely used concrete pump. Its working principle is moving the concrete forward by means of a steel screw inside a rubber stator, with conveying chambers between the steel and the rubber. As sketched in Figure 4.3, the screw at the bottom of the feeder moves the concrete toward the entrance of the stator, and the concrete consequently flows into the pump through the suction effect

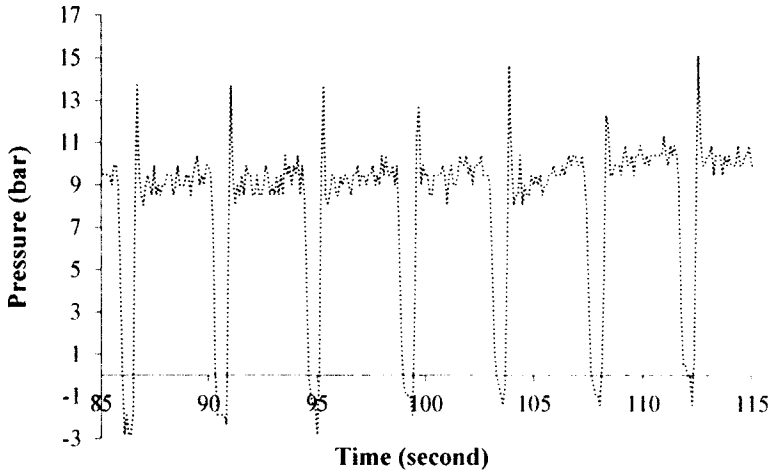


***Figure 4.2:*** *Changes in concrete pressure during pumping. The pressure alters according to the frequency of the pump; a negative pressure can be observed at the turn off of the piston. 1 bar = 100 kPa.*

created by the forward movement of the conveying chambers. The inconvenience of this design is that the hydrostatic pressure created by the self-weight of the pumped concrete still in the pipes applies a cumulative negative pressure on the feeder and conveying chambers. This pressure limits, unfortunately, the capacity of screw pumps to certain heights [2]. Instead, due to their light weight and easy manipulation, screw pumps specialize in smaller short-distance pumping jobs.

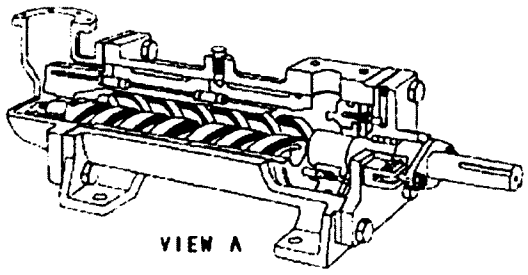


***Figure 4.3:*** *Schematic representation of a screw pump [4].*

## 4.3 Pumpability guidlines

Several pumping companies and research institutes provide practical guidelines for pumping concrete based on simple test methods and field experience. Most of these test methods, if not all, are established for CVC. For example, the slump test (ASTM C143 / C143M - 12) has been considered the simplest experiment to describe concrete pumpability [5, 6]; one early recommendation was that slump $< 50$ mm gives unpumpable concrete, a slump range of 50-100 mm can ensure pumpable concrete, whereas a slump $> 100$ mm can lead to unpredictable pumpability response [5]. Another empirical correlation presented in Figure 4.4 was developed as a guide to relate the pressure loss per

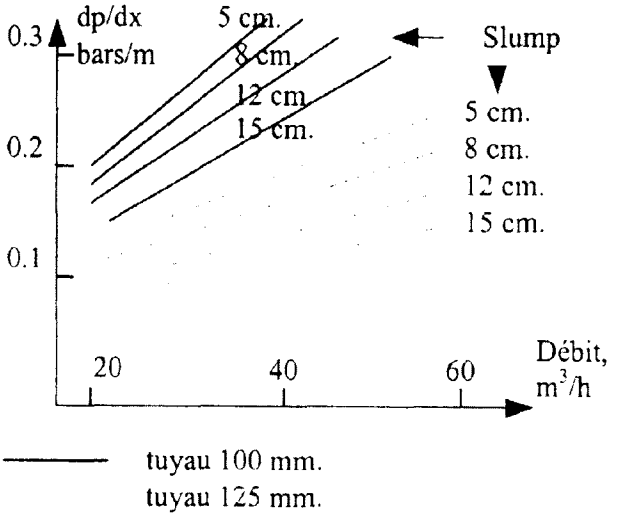


***Figure 4.4:*** *Effect of slump on pressure loss per meter (dp/dx) as a function of flow rate for different pipe diameter (tuyau). Adapted from [7].*

unit length (dp/dx) to the discharge rate for concrete of different slump values and pipe sizes [7]. The results indicated in Figure 4.4 show that for a given discharge rate and pipe size, pressure loss decreases with increasing the slump of the concrete. For a given slump and discharge rate, pressure loss increases with decreasing the pipe (tuyau) size, as presented in Figure 4.4.

A similar approach, covering a wide range of pumping power and using slump to

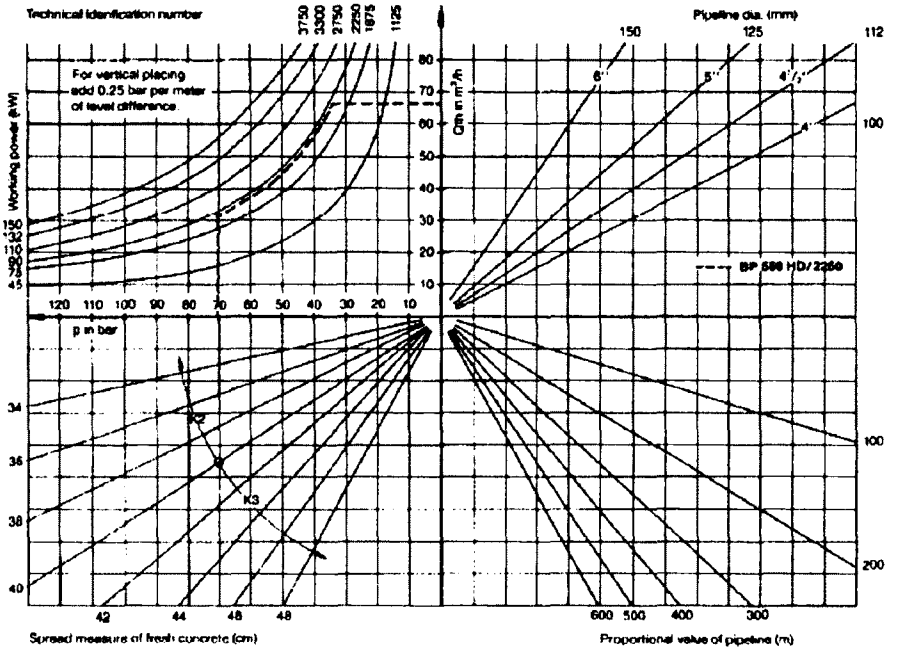


***Figure 4.5:*** *Nomograph to calculate the pumping pressure at different discharge rates based on slump, pipe length, and pipe diameter [8].*

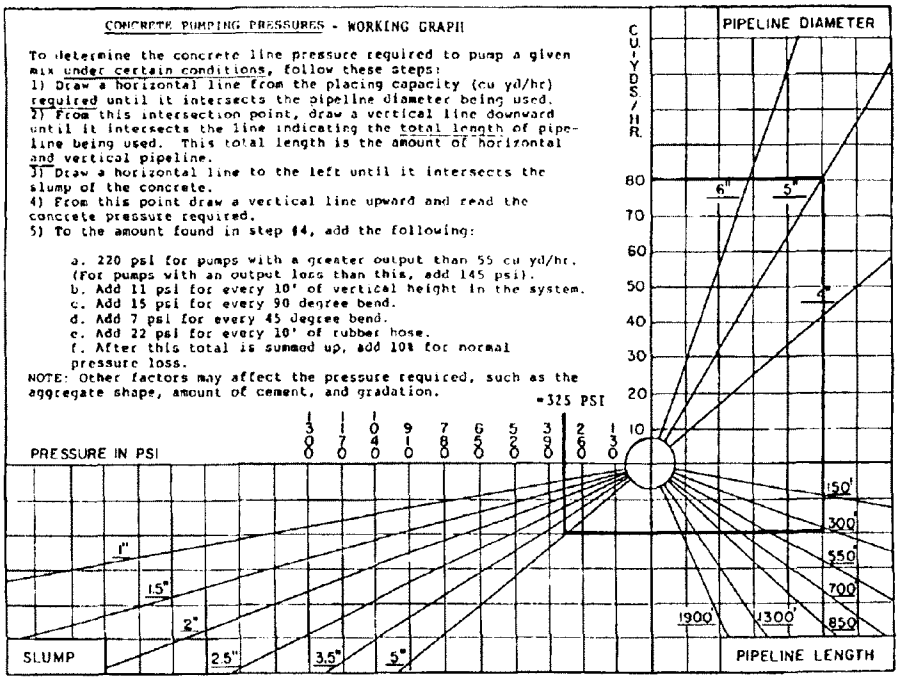


***Figure 4.6:*** *Diagram to determine pumping pressure for a given pump capacity, pipe length, and concrete slump, ACI Committee 304.2R-96 (from Morgen Manufacturing Co., Yankton, SD).*

calculate the required pumping pressure is illustrated by Figure 4.5. A more detailed working graph developed by ACI Committee 304.2R-96 (Figure 4.6) calculates the required pumping pressure based on the slump of concrete, the geometrical configuration of the circuit including elbows, reducers, and pipe diameter, etc. If applied to SCC, the recommendations offered by ACI 304 can underestimate pressure loss in the case of SCC due to its high slump flow, as indicated in Figure 4.6. Furthermore, practice has shown that the flow pattern of SCC in pipes is dictated by its viscosity [6], which has not (yet) been included in the ACI recommendations.

Reflecting on the above discussed approaches, it is apparent that the research efforts and field experience on the subject of pumping concrete have established a variety of methods to assess pumpability. Despite the wide spread use of these approaches, they remain inadequate when applied to HWC or SCC. The main argument is that the flow patterns of SCC and CVC show different dependencies on viscosity and yield stress, which is translated into different flow behaviors in pumping pipes. Viscosity is a key parameter affecting the flow of SCC in pipes, while yield stress becomes the most influential parameter in the case of CVC. Most, if not all, of the available pumping guidelines and recommendations were developed for CVC. These recommendations, if applied to SCC, will not account for the rheological and tribological properties governing SCC's flow behavior, which may result in unrealistic prescriptions. A more comprehensive study linking pumping pressure to the fundamental rheological and tribological properties of SCC is warranted.

## 4.4 Today's pumping challenges

A new concrete pumping world record was attained during the construction of the Burj Khalifa in 2008. Highly flowable concrete was delivered to a height of 611 m with a pump output of 30 $m^3/h$. Despite this significant milestone, many challenges are still associated with pumping operations on job sites today. The majority of these challenges can be related to three main causes: deficient mix design, problematic pipeline setup, and operator error [7]. Other challenges not falling in these categories can be attributed to the delay in concrete placing (due to traffic or job site mismanagement) causing the concrete to lose workability. Because this work concerns engineering and not job site management, only the challenges facing the mix design will be addressed in the following sections.

### 4.4.1 Blockage

Blockage refers to a delay or stop in the flow due to a formation of a plug, hindering the continued movement of concrete (see Figure 4.7). Blockages, usually accompanied with elevated pumping pressure, can occur at any phase of the pumping operation. However, blockages that occur during pumping are rare and are mainly due to errors in pipe configuration or concrete composition [6].

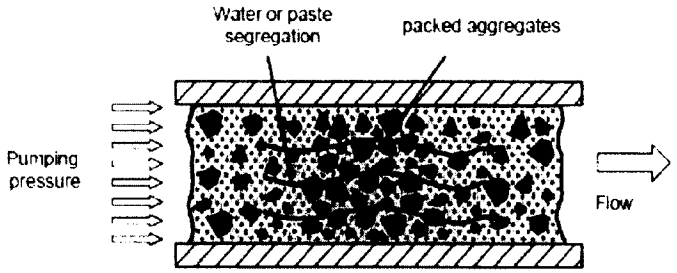


***Figure 4.7:*** *Mechanism of concrete plug formation in a pumping pipe [9].*

Blockage at start-up is much more common during pumping operations. The mechanism of this type of blockage is explained by the accumulation of aggregate. During start-up, each pump stroke causes the aggregate to move forward in the grout under inertia effect, blockage occurs once the coarse aggregate accumulated in front of the grout reaches a critical concentration. A major cause of the start-up blockage can be related to a significant increase in the rate of pumping since it directly increases the risk of segregation. It is, therefore, recommended to start with low pumping rates during the priming phase to reduce the risk of start-up blockage [10].

Similar to start-up blockage in name but very different in behavior, the restart blockage is due to abnormally high friction along the pipe wall. When the flow is stopped, the aggregate settles in the pipes and comes into contact with the pipe wall. Consequently, the lubrication layer will be damaged and the flow behavior will be altered to friction [10].

The last type of blockage occurs during the cleaning process. When cleaning the circuit, a separation plug in the form of sponge ball is inserted into the pipe, behind

which water is pumped. If the plug is not watertight, water can pass through it and wash out the front concrete, resulting in the accumulation of aggregates, which can consequently clog the pipe. Cleaning can also be done with compressed air, thus rarely resulting in blockage; however, this can cause safety problems [10].

Deficiency in the granular system is considered a principal cause of blockage. Therefore, concrete mixtures that are prone to segregate can more than likely cause blocking problems. To avoid this, sand and aggregate should be carefully selected to guarantee their proper suspension in the cement paste and prevent any separation under high pumping pressure. Further details concerning the effect of aggregate on the pumpability and stability of concrete under pressure are discussed in section 4.5.1.

### 4.4.2 Phase-separation

One of the most common mix design problems is the poor ability of the concrete to retain its mixing water. Concrete can then bleed under pressure through the small channels formed in the poorly graded sand resulting in phase-separation and blockage. Phase-separation can also occur when the coarse aggregate particles start to interlock because of either insufficient or excessive cement paste. This phenomenon occurs when the pump pressure forces the lubricating mortar to separate from the mixture, usually at a bend or other slight obstruction, leaving a plug of coarse aggregate which eventually blocks the stream. Besides the problems it causes during pumping, concrete phase-separation can seriously impair its workability and in certain cases increase and localize its air content resulting in low mechanical properties.

There exist different strategies to promote concrete resistance to phase-separation under pressure. Well-graded aggregate should be used. Adequate paste content is also needed to lubricate the aggregate being pumped [11]. The use of rounded aggregate can also improve concrete stability under pressure. Certain types of cementitious materials are proven to enhance the resistance to bleeding and phase-separation. For example, bleeding resistance noticeably augments with increasing fly ash content [12]. For concrete mixtures with a slump range of 45-55 mm, and $w/cm$, fly ash replacement levels of 30% to 40% gave the most stable concrete mixtures [12].

In conclusion, blockage and phase-separation present very important challenges to pumping concrete operation. These problems are primarily caused by mix design parameters among which the aggregate and paste volumes are of prime importance. Since both parameters are interrelated, a balance between them must exist to improve flowability while maintaining proper stability. Several practical measures for selecting aggregate and paste volume to enhance pumpability and avoid blockage are presented in the following section.

## 4.5 Avoiding pumping problems

### 4.5.1 Recommendations for aggregate selection

Aggregates have a profound influence on the flow behavior of concrete because they inadvertently determine the paste volume needed to fill the voids created in the granular

skeleton [13]. The effect of aggregate is defined by its shape, texture, mineral composition, and size distribution. Based on the size distribution, the aggregate can be divided into three main categories [14]:

- Coarse aggregate: material retained by sieve No. 4 (4.76 mm).
- Fine aggregate (sand): material passing sieve No. 4 and retained on sieve No. 200 (0.074 mm).
- Microfines: material passing sieve No. 200 (0.074 mm).

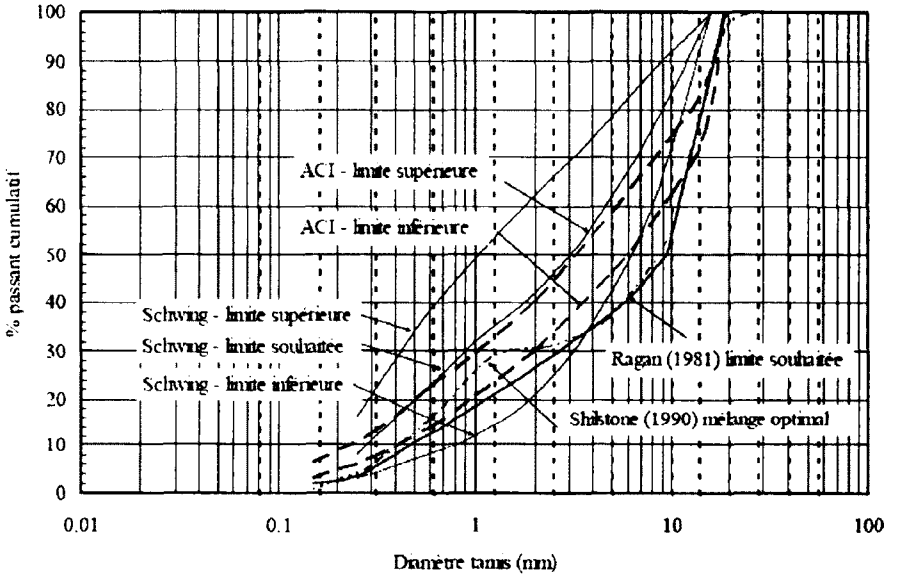


***Figure 4.8:*** *Recommended grain-size distributions for pumpable concrete [8, 15, 16].*

For the coarse aggregate, the effect of the size distribution is more prevalent than the shape and surface texture [17]. In general, the greater the maximum aggregate size, the less paste volume is needed in the mixture. It also follows that, the more the fine particles in the mixture, the more paste is needed [14].

Apart from aggregate proportioning, it is recommended to limit the maximum aggregate size of crushed aggregate to $(D_{pipe}/4)$ to reduce the inertia effect of the aggregate, and avoid segregation problems during steady state pumping [18]. When rounded aggregate is used, this limit can be considered 40% of the smallest inner diameter of the pipe [19]. Experience shows that when using rounded aggregate as opposed to crushed aggregate, lower mortar content is necessary to effectively pump concrete, as rounded aggregate can facilitate the movement of concrete in pipes. Furthermore, the use of rounded aggregate can significantly reduce water demand, and reduces the risk of bleeding and separation, thus improving the stability of the mixture under pressure.

When designing pumpable concrete mixtures, the properties of the fine aggregate (a.k.a sand) are more critical than those of coarse aggregate [19]. A sand that is too coarse will lead to harshness, bleeding, and segregation, whereas a sand that is too fine

will result in high water demand and higher viscosity [20]. Practice has it that sand graded to ASTM C 33 requirements (CRD-C 133) can lead to problem-free pumping operations. It is also recommended, when pumping concrete in 6-in. (152 mm) pipes or smaller, 15% to 30% of the sand should pass the 300-$\mu m$ (No. 50) sieve and 5% to 10% should pass the 150-$\mu m$ (No. 100) sieve. Sands that are deficient in either of these two sizes should be blended with finer sand selected to produce the required grading [19]. Previous studies have found that correcting the sand to grading spans comprised between 0.1 mm and 0.7 mm improves the stability of the mixture and its resistance to bleeding [10].

Another strategy embraces decreasing the fineness modulus of sand to improve pumpability [19]. Sands with fineness moduli between 2.4 and 3.0 are generally satisfactory but, fineness moduli alone without specific grading stipulations may not produce satisfactory results [19]. However, it is always possible to combine aggregate (or sand) of different sizes to reduce the void ratio created by the voids between the larger aggregate and increase the packing density [17, 20]. Additional recommendations and limitations of various grain-size distributions to design pumpable concrete mixtures are presented in Figure 4.8 [2, 15].

### 4.5.2 Optimum paste volume

For any given granular system, there exists an optimal range of paste volumes that can simultaneously properly lubricate the coarse aggregate and provide sufficient suspension to prevent segregation. Paste volumes below the optimal range can increase the inter-particle friction between the aggregate that can lead to higher viscosity and blockage problems. Low paste volumes can also prevent the lubrication layer from forming, and make pumping difficult or even impossible as a result of the abnormally excessive friction. Contrarily, using high paste volume can reduce the stability of the mixture, and increase the risk of segregation and blockage. The optimal paste volume for pumpable concrete is therefore a delicate compromise between the flowability and stability of the mixture. One of the main objectives of this research is to investigate the effect of paste volume on the concrete pipe flow to find optimal ranges of paste volume that can ensure proper balance between flowability and stability.

## 4.6 Factors affecting pumping pressure

### 4.6.1 The lubrication layer

When concrete is pumped, fine materials and water droplets migrate under the shear effect to the high shear zone near the pipe wall, forming the lubrication layer. This layer is a central parameter for successful pumping as it is believed to impede the coarse aggregate to enter in solid-solid contact with the pipe wall. Failure to build a proper lubrication layer will eliminate the lubrication effect at the pipe wall and drastically increase friction and pumping pressure. Because of its particular materials composition, the lubrication layer exhibits different rheological properties than those found in the pumped concrete.

The properties of the lubrication layer are difficult to measure physically and the real parameters affecting these properties are not yet well known. It is believed that rheological properties of the lubrication layer are related to those of concrete, therefore, it follows that all properties affecting the rheology of the concrete are prone to influence the lubrication layer properties. A recent study concluded that the thickness of the lubrication layer increases with the volume of the cement paste, $w/c$, and the HRWRA content, and decreases with the increase of the fine sand content [21].

Although different attempts have been made to conclusively establish the importance of the lubrication layer, its real contribution to the total flow rate in pumping pipes is not yet well established. Kaplan (2000) [7] evaluated the influence of the lubrication layer on concrete flow in pipes. This influence was expressed by the viscous constant (in Pa s/m) of the lubrication layer, as indicated in equation 4.1.

$$\tau_l = \tau_{0,l} + \eta_l V \tag{4.1}$$

where

$\tau_l$: shear stress in the lubrication layer (Pa)
$\tau_{0,l}$: yield stress of the lubrication layer (Pa)
$\eta_l$: viscous constant (Pa s/m)
$V$: linear velocity (m/s), determined from the rotational velocity of the tribometer cylinder

The viscous constant of the lubrication layer calculated from the discharge-pressure relationship and the tribometer were well correlated, as can be seen in Figure 4.9 [7]. In spite of this cogent correlation, the exact importance of the lubrication layer on pumping pressure remains questionable since its rheological properties and thickness could not be understood individually.

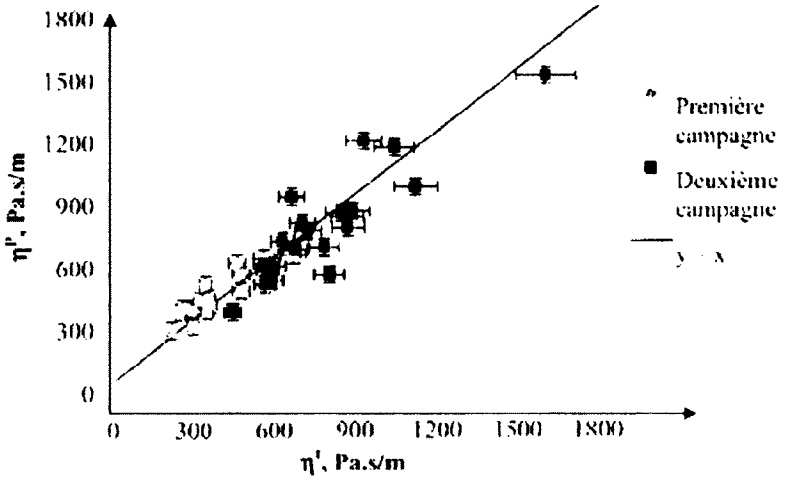


***Figure 4.9:*** *Relationship between the viscous constant (expressed in Pa s/m) of the lubrication layer measured by the tribometer (horizontal axis) and the viscosity obtained from the discharge-pressure relationship (vertical axis) [7].*

In the investigation undertaken in this thesis, using rheological and tribological measurements, the effect of thickness and viscosity of the lubrication layer on pumping pressure will be determined. Their correlations with rheological properties of concrete in relation to the pumping pressure loss will also be investigated.

### 4.6.2 Viscosity and yield stress

The quantity and depth of information concerning the effect of the rheological properties of concrete on pumping pressure is limited. Most of the available literature on pumping neglects rheological properties of concrete when determining the required pumping pressure. Research efforts directed toward CVC have firmly established that yield stress to be crucial parameter determining CVC pressure loss, and viscosity to be insignificant [7]. The strong rheological dependency of CVC on yield stress is a well established fact and widely used to predict pressure loss for most pumping operations [5, 7].

Recent studies conducted by Feys (2007) [6] showed that viscosity and not the yield stress (as it is the case for CVC) is the key parameter affecting the pumping pressure of SCC (see Figure 4.10). The pressure loss is also, to a certain extent, correlated with the yield stress, indicating that yield stress and viscosity are not independent of each other [6] (see Figure 4.11). Nevertheless, pressure loss is still shown to be much more sensitive to variations in viscosity than to an equivalent variations in yield stress [6].

As a result, SCC and CVC show different dependencies on viscosity and yield stress, which is translated into different flow behaviors in pumping pipes. Investigating their behaviors in response to pumping pressure is one of the main intentions of this study.

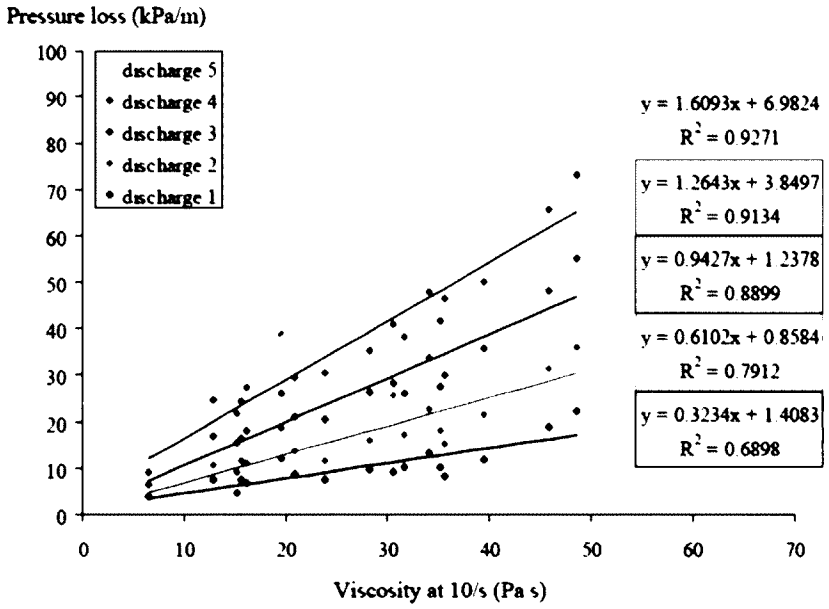


***Figure 4.10:*** *Pressure loss per unit length in 4-in. (102 mm) pipes correlated with the tangential viscosity at a shear rate of 10 1/s [6]. Discharge rates 1-5 = 5-20 L/s.*

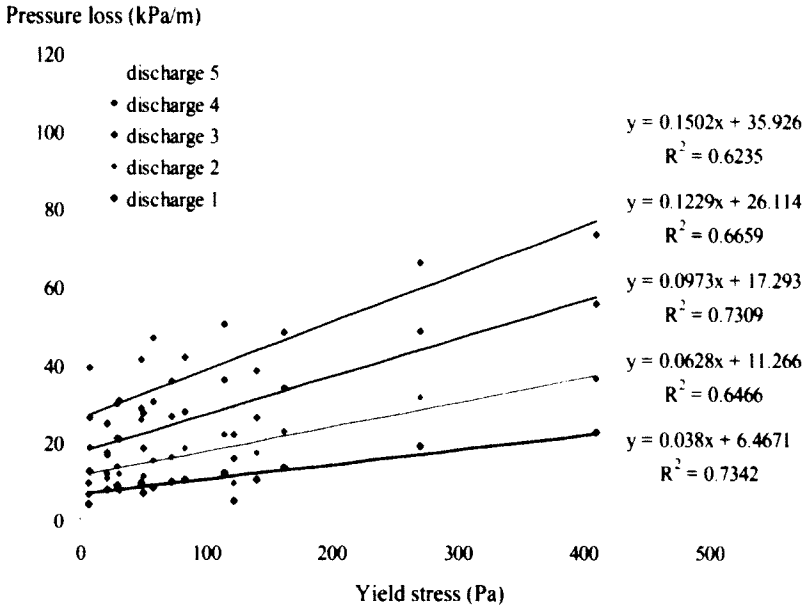


***Figure 4.11:*** *Pressure loss per unit length in 4-in pipes related to yield stress of SCC [6].*

### 4.6.3 Energy conservation principle

For pumping to be successful, the power of the pump must overcome the various forms of pressure losses along the streamline and the self-weight of the concrete in the pipes. The required pumping energy is described by the principle of energy conservation using Bernoulli's equation. The following equation is a common form of Bernoulli's equation valid at any arbitrary point along a streamline:

$$h + \frac{v^2}{2g} + \frac{p}{\rho g} = Constant \tag{4.2}$$

where

$h$: elevation above reference height (m)
$v$: fluid flow velocity (m/s)
$g$: gravitational constant (m/s$^2$)
$p$: absolute pressure (Pa)
$\rho$: fluid density (kg/m$^3$)

Multiplying both sides of equation 4.2 by $\rho g$ yields:

$$h\rho g + \frac{v^2\rho}{2} + p = Constant \times \rho g \tag{4.3}$$

The first term ($h\rho g$) in equation 4.3 refers to the hydrostatic energy, the second term ($v^2\rho/2$) is the kinetic energy, which is considered constant if there is no change in the pipe diameter. Applying equation 4.2 to two points along a streamline delivers equation 4.4 that can be used to calculate the pressure between two points from the energies available at points 1 and 2:

$$h_1 + \frac{v_1^2}{2g} + \frac{p_1}{\rho_1 g} = h_2 + \frac{v_2^2}{2g} + \frac{p_2}{\rho_2 g} = Constant \tag{4.4}$$

where

$h_{1,2}$: elevation above reference level (m)

$v_{1,2}$: fluid flow velocity on the streamline (m/s)

$g$: gravitational constant (m/s$^2$)

$p_{1,2}$: absolute pressure (Pa)

$\rho_{1,2}$: fluid density (kg/m$^3$)

In pipe flow, different types of pressure loss and energy exchange are involved along the stream. The Bernoulli derivation does not account for possible energy exchange due to shaft work or heat exchange in pipe flow [22]. Bernoulli's equation (4.4) then may be extended by such an energy exchange, giving the steady flow energy equation:

$$\left(h_1 + \frac{v_1^2}{2g} + \frac{p_1}{\rho_1 g}\right)_{in} = \left(h_2 + \frac{v_2^2}{2g} + \frac{p_2}{\rho_2 g}\right)_{out} + \Delta F - h_{pump} \tag{4.5}$$

where

$\Delta F$: pressure loss along a pipeline (m)

$h_{pump}$: head of the pump (m)

Equation 4.5 is a common form of the energy equation, in which every term is a length (or head). The terms in parentheses are the upstream (1) and downstream (2) values of the available (or total) head. The term $p_1/\rho_1 g$ is called pressure head and term $v_1^2/2g$ is denoted as velocity head, while $h_{pump}$ is the pump head input, and $\Delta F$ the friction head losses. Additional terms can be involved in the energy equation when several pumps or turbines are included in the pipe system. From equation 4.5, it can be deduced that the applied pumping pressure must balance for different effects: the pressure change, the elevation, the kinetic energy, and the friction and minor losses ($\Delta F$). Therefore, decreasing the friction loss or the hydrostatic pressure results in a decrease in the necessary pumping pressure. The self weight of the concrete in the pipes can be considerably reduced by employing light-weight aggregate concrete (LWA). However, problems may arise because of LWA's relative high compressibility. This small particularity can affect the air content, and the concrete's ability to retain water, leading to phase-separation and blockage problems. Moreover, the ability of LWA to absorb large quantity of the mixing water can lead to sharp and undue increases in viscosity and pressure loss.

The pumping pressure (in equation 4.5) can also be effectively decreased by reducing the pressure loss. This can be achieved by reducing the viscosity of the concrete or adjusting the properties of the lubrication layer. Finding new approaches to reduce the pumping pressure loss on the basis of the rheological and tribological properties of concrete and lubrication layer is one of the primary objectives of this investigation.

### 4.6.4 Minor losses: effect of elbows

An elbow is a fitting used for changing the direction of the stream. There are many types of elbows available on the market with bending angles varying from 45° to 180°. Characterizing the concrete flow in elbows is complicated, and determining the pressure loss in elbows is even more complicated. For the sake of simplicity, most common practice for pipe flow suggests theoretically replacing the elbow effect by a certain corresponding length of the straight section to calculate an equivalent pressure loss.

Kaplan (2000) concluded from his pumping tests that the pressure drop in a 90°-elbow having a radius of 0.28 m is equal to the pressure drop in a straight pipe section with the same length of the elbow [7]. The Schwing guide indicates that the pressure drop in a 90°-elbow with a radius of 0.25 m is equivalent to the pressure drop in a 1-m straight pipe section, while the pressure is equivalent to the pressure drop in a 3-m straight pipe section if the pipe curving radius is 1 m [8]. A more recent study on SCC concluded that by means of an amplification factor, indicating how many meters of straight pipes correspond with one meter of the elbow, the total pressure loss over a certain elbow could be calculated at a given discharge [6]. This can be performed by multiplying the amplification factor with the pressure loss per unit of length in a straight pipe and the distance along the center line of the elbow [6]. Figure 4.12 presents an example of the amplification factor for a 90°-elbow.

It should be noted that the applicability of the above discussed results to different circuits is limited due to the complexity of the flow in these parts of the circuit. Depending on the type of concrete and bend, the influence of an elbow can vary from minimal to extreme. Many models have attempted to diagnose the pressure loss in elbows, but unfortunately most of them deliver different results when reapplied in the field limiting their practical applicability.

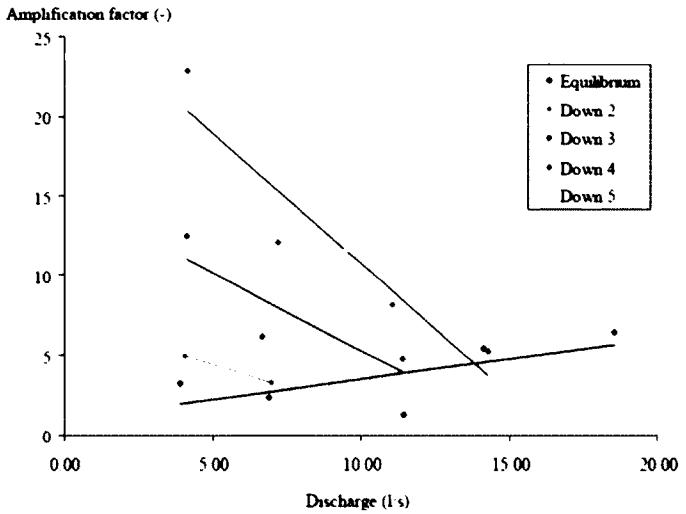


***Figure 4.12:*** *Example of the amplification factor for one SCC (LM-17) mixture in a 90°-bend [6].*

## 4.7 Effect of pumping on concrete properties

### 4.7.1 Rheological properties

The high shear effect (shear rates on the order of 20-40 1/s) that is produced in pumping pipes can cause significant changes in the concrete properties with time. In practice, pumping process acts as a kind of remixing that keeps the material workable up to approximately 45 minutes of age [2, 7, 23]. This enhanced workability was measured with improved slump, T-50 flow, yield stress, and viscosity after pumping [2]. Feys (2009) concluded that continuous pumping increases the yield stress and decreases viscosity due to the effects of structural breakdown and increases in air content. The increase in air content due to pumping results in an increase in yield stress and a decrease in viscosity, while structural breakdown causes the yield stress and viscosity to both decrease [6]. Since the two phenomena can occur simultaneously, the final change in concrete will depend on the dominating effect.

The changes in rheological properties due to pumping increase in importance with pumping velocity. Therefore, high-speed pumping should be avoided, especially in the case of long-distance pumping. As a negative consequence of these changes is segregation that can appear when viscosity decreases and yield stress does not significantly increase [6].

In addition to the phenomena explained above, it is believed that pumping duration is an important factor in determining the variation of concrete properties. A more inclusive study is needed to reveal the influence of pumping on concrete properties with time.

### 4.7.2 Temperature

A part of the mechanical energy applied to maintain the flow in pipes is consumed by friction and converted into heat, resulting in temperature increases during pumping. One source of friction can be attributed to the interactions between the solid particles within the concrete matrix. In this respect, the constituent materials, particularly sand and aggregate, play a key role in the thermal changes occurring during pumping. Previous research findings demonstrate that aggregate rich mixtures produce larger temperature increase, for a certain pressure loss [6]. It is also common in pumping applications that segregated mixtures show larger increase in temperature compared to stable ones.

As indicated in Figure 4.13, the temperature is shown to increase as a function of the pumping time. The rate of temperature increase is linearly related to the pressure loss per unit length for each concrete at different discharge rates, as demonstrated in Figure 4.14. A faster increase in temperature is the result of higher pressure loss [6]. At low pressure losses (or discharge rate), the temperature flux can be equal to zero or even be negative; however, this is probably due to the lower ambient temperature of the testing environment [6].

The relationship between the temperature increase per unit of time and pressure loss per unit length seems to be a constant material property [6]. Up until this point, no clear relationship has been found between the temperature increase and any other pumping parameter [6]. It should be noted here that the temperature increase due to pumping can significantly affect the yield stress and viscosity of concrete. This relationship is a

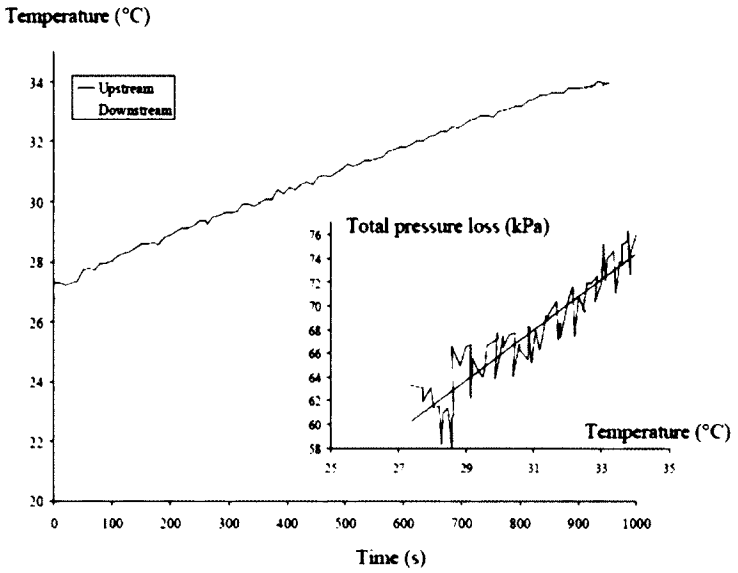


***Figure 4.13:*** *Temperature evolution with time and pressure loss for a SCC mixture pumped at 12 L/s for 15 minutes [6].*

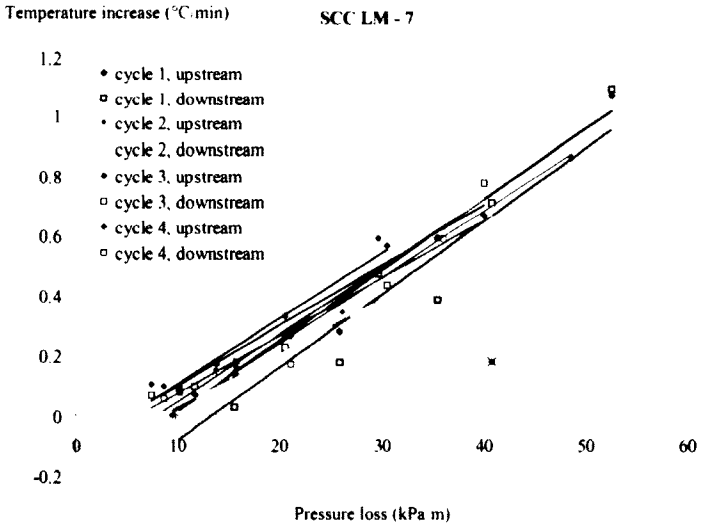


***Figure 4.14:*** *Relationship between pressure loss and rate of temperature increase due to pumping for a SCC mixture measured throughout 4 different testing cycles [6].*

function of the magnitude of the applied pressure and the mixture composition. Finding the governing correlations between these parameters can further the understanding of the underlying causes of rheological changes during pumping.

### 4.7.3 Air content and distribution

Concrete undergoes a pressurized flow during pumping that can cause 1% to 3% change in the air content [24]. At present, no theory exists that can conclusively explain this phenomenon. Instead, there are several causal hypotheses that use suction, dissolving and pressure to explain the change in the air content. One theory attributes the change to negative pressure (suction) causing expulsion or swelling of the air bubbles in the concrete [25]. This suction mechanism may occur at two locations in the pumping circuit: in the pump when the piston draws the concrete from the reservoir, and when concrete falls into the pipe at a vertical section of the pumping circuit [25].

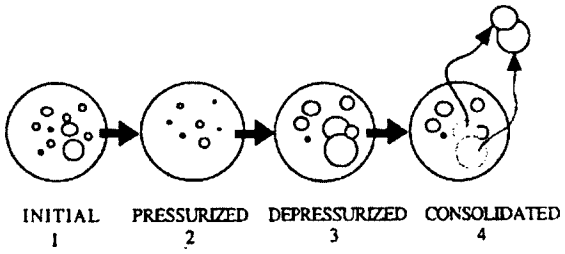


***Figure 4.15:*** *Hypothesis explains the air loss in concrete due to pumping [26].*

According to Dyer (1991) the dissolution process of air bubbles is a result of the high pressure environment created in the pipes during pumping. When concrete is pumped and pressure is applied, the small bubbles are dissolved in the mixing water droplets, as demonstrated in Figure 4.15 [26]. Later on, close to the exit of the pipe when the pressure becomes lower, the pressurized small air bubbles that have not been fully dissolved reappear, but mainly in larger bubbles (Figure 4.15). Charles et al. [27] further expanded on Dyer's model. Their research attributed changes in air content to the dissolution of air voids by high pressure, the bursting of air bubbles by vacuum pressure, and the mechanical rupture of bubbles by impact forces. Strategies to control these detrimental actions include limiting the pumping pressure, and slowing the rate of flow through the use of reducers and elbows, and avoiding steep downward slopes along the pipeline [27].

More recent empirical studies have reported different changes in air content due to pumping based on the type of concrete. One study noted that traditional concrete displays an increase in air content due to pumping [28], whereas superplasticized high performance concrete displays a reduction [29]. The same study also demonstrated that the air void structure may not necessarily be destroyed by pumping [29], rather a large part of the lost in the air content consists of dissolved and/or gashed large bubbles.

Presented above is the state of the current understanding of pumping induced air content variation. At this point, researchers are able to identify several mechanisms through which this phenomenon can possibly act, but unifying through empirical investigations has proved difficult. This leaves open avenues for further research into the subject, while in the framework of this study other subjects are prioritized.

## 4.8 References


[1] Weber R., "The transport of concrete by pipeline", *Cement and Concrete Association Library*, p. 85, 1963.

[2] Jacobsen S., Mork J.H., Lee S.F., Haugan L., "Pumping of concrete and mortar, state of the art, COIN Project report 5", Tech. Rep., 2008.

[3] S. pumps, *Www.schwing.de.*

[4] Maxit Group company, *www.maxit-Group.com.*

[5] Stephenson T.O., "Concrete pumping, pumpable concrete", *Australian civil Engineering*, pp. 24–27, 1968.

[6] Feys D., "Interactions between rheological properties and pumping of self-compacting concrete", Ph.D. dissertation, Ghent University, 2009.

[7] Kaplan D., "Pumping of concretes", Ph.D. dissertation, Laboratoire Central des Ponts et Chausées, Paris, 2001.

[8] Eckardstein K., Ernst V., "Concrete and concrete pumps; a concrete placing manual", Schwing, Tech. Rep., 1983, p. 133.

[9] Browne R.D., Bamforth P.B., "Tests to establish concrete pumpability", *ACI Journal*, vol. 74, pp. 193–203, 1977.

[10] Kaplan D., de Larrard F., Sedran T., "Avoidance of Blockages in Concrete Pumping Process", *ACI Materials Journal, technical paper*, vol. 102, no. 3, pp. 183–191, 2005.

[11] The European Associations of Concrete Admixtures, "Guidelines for viscosity modifying admixtures for concrete", The European Associations of Concrete Admixtures, Tech. Rep., 2006.

[12] Ravindrarajah R.S., "Bleeding of fresh concrete containing cement supplementary materials", in *The Ninth east Asia-Pacific Conference on Structural Engineering and Construction*, Bali, 2003.

[13] Kempster E., "Measuring void content: new apparatus for aggregates, sands, and fillers", *Contract Journal*, vol. 228, p. 409, 1969.

[14] Quiroga P.N., Fowler D.W., "Guidelines for proportioning optimized concrete mixtures with high microfines", *International Center for Aggregates Research*, no. Report 104-2,

[15] Ragan S.A., *Evaluation of tests for determining the pumpability of concrete mixtures.* Vicksburg, Miss.: U.S. Army Engineer Waterways Experiment Station, miscellaneous paper SL-81-29, 1981, p. 36.

[16] ACI 304.2R, "Placing concrete by pumping methods", *ACI Material Journal*, vol. 92, no. 4, pp. 441–464, 1995.

[17] Rached M., De Moya M., Fowler D.W., "Utilizing aggregates characteristics to minimize cement content in portland cement concrete. Report ICAR 401.", The University of Texas at Austin Construction Materials Research Group, Tech. Rep.

[18] Coussot P., *Rheometry of pastes, suspensions, and granular materials: applications in industry and environment*, 2. New Jersey: John Wiley & Sons, Inc., Hoboken, 2005, pp. 317–318.

[19] Department of the Army U.S. Army Corps of Engineers Washington, DC, "Engineering and design - standard practice for concrete for civil works structures proponent. Engineer Manual CECW-EG", Washington, Tech. Rep., pp. 20 314–1000.

[20] Lamond J.F., Pielert J.H., "Significance of tests and properties of concrete and concrete-making materials. Report FHWA/IN/JTRP-98/11.", Indiana Department of Transportation and Purdue University, Indiana, Tech. Rep., 2006, p. 645.

[21] Ngo T.T., "Influence of concrete compositions on the pumpability parameters", Ph.D. dissertation, Cergy Pontoise, France, 2009.

[22] White Frank M., *Fluid Mechanics*, Sixth. New York: McGraw-Hill, 2008.

[23] Hu C., De Larrard F., Sedran T., "A new rheometer for high performance concrete, 4th", in *International symposium on high strength/high performance concrete, presses de LCPC*, 1996, pp. 179–186.

[24] Boulet D., "Influence of pumping on the characteristics of the network of air bubbles in concrete", Master's thesis, University of Laval, 1997, p. 172.

[25] Chapdelaine F., "Fundamental study and practice on concrete pumpability", Ph.D. dissertation, University of Laval, 2007.

[26] Dyer R.M, "An investigation of concrete pumping and effects of pressure on the air void systeme of concrete", Master thesis, university of Washington, 1991, p. 222.

[27] Scholer C.F., Grossman J., "Controlling Air Content in Concrete that is Being Pumped. A Synthesis Study.", Joint Transportation Research Program Technical, Purdue University, Tech. Rep., 1998.

[28] Johansson A., Tuutti K., "Pumpbetong och betongpumpning (Del 1), Betongmassas strömning i rör (Del 2)", Stockholm, 1976.

[29] Pleau R., Boulet D., Aïtcin P.C., "Influence of pumping on the air-void system of HPC", in *Proc Consec 98, Gjørv, Banthia (Eds.)*, Sakai: E&FN Spon, 1998, pp. 2047–2056.

# Chapter 5

# Concrete Flow in Pipes

## 5.1 Introduction

When concrete is pumped, shear effect takes place within the concrete resulting in different flow zones across the pipe section. The shear effect causes some fine particles and water droplets to migrate from the concrete matrix toward the high shear zone near the pipe wall, where they accumulate and form the lubrication layer. This layer possesses different rheological properties than concrete, and thus it flows differently.

The boundaries of the flow zones and their contribution to the total flow rate in relation to the concrete and lubrication layer properties are new concepts in concrete science and technology.

This chapter presents an analytical model that can be employed to determine the properties of the lubrication layer by means of rheological and tribological measurements. It also discusses the different flow zones across the pipe section and their velocity profiles and flow rates. Various parameters influencing pressure loss, including the properties of the lubrication layer and those of concrete, and the pipe diameter are highlighted in this chapter. In addition, a critical analysis is undertaken to disclose the interactions between properties of the lubrication layer and concrete, in relation to pressure loss. The resulting relationships between the affecting parameters are used in a pressure prediction model that can be employed to estimate the required pumping pressure for a wide range of concrete and lubrication layer properties.

## 5.2 Conservation of momentum

Consider a uniform flow in a pipe section of radius $R$ and length $L$, as shown in Figure 5.1. Assuming a constant density and the pressures on the left and right sides are $p_1$ and $p_2$, respectively, the pressure difference between $p_1$ and $p_2$ is balanced by the shear stress acting at the pipe wall, hence

$$p_1 \pi R^2 - p_2 \pi R^2 - 2\pi R \tau_w L = 0 \tag{5.1}$$

By rearranging equation 5.1, the shear stress at the pipe wall is obtained:

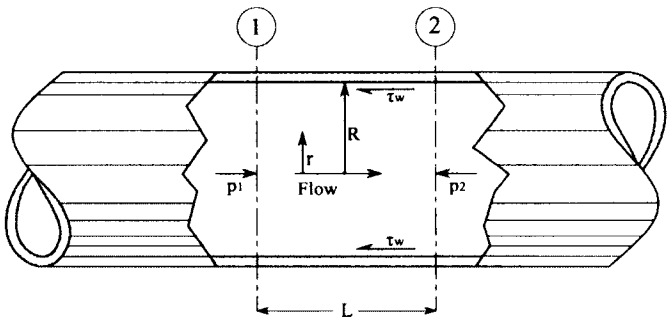


***Figure 5.1:*** *Force analysis in pipe flow.*

$$\tau_w = \frac{p_1 - p_2}{L}\frac{R}{2} = \frac{\Delta p_{tot}}{L}\frac{R}{2} = \Delta p\frac{R}{2} \tag{5.2}$$

where

$\tau_w$: shear stress at the wall (Pa)
$\Delta p_{tot}$: total pressure loss over the length L of the pipe (Pa)
$R$: radius of the pipe (m)
$L$: length of the pipe section (m) (over which the total pressure loss is measured)
$\Delta p$: pressure loss per unit length of the pipe (Pa/m)

As can be inferred from equation 5.2, the pressure loss is a function of the shear stress at the pipe wall and pipe radius regardless of the properties of the pumped concrete.

## 5.3 Flow regimes

In the design or operation of any flow system it is indispensable to determine the flow regime which will influence the amount of energy required to maintain a desired flow. All fluid flows can be classified under three regimes: laminar, turbulent, and transitional flow. In laminar flow, layers of a substance flow over one another at different velocities in definite paths or streamlines with no mixing between layers. Turbulent flow is described by the irregular movement of (imaginary) fluid particles with no fixed pattern. In this case, the particles travel in irregular paths and exhibit additional transverse motion leading to higher pressure loss and heat transfer. Transitional flow is considered an intermediate phase between laminar and turbulence. Characterization of the flow pattern is more specifically determined by the Reynolds number ($Re$) given by equation 5.3.

$$Re = \frac{\rho V L}{\mu} \tag{5.3}$$

where

$\rho$: fluid density (kg/m$^3$)
$V$: mean fluid velocity (m/s)
$L$: characteristic linear dimension, (traveled length of fluid, or hydraulic diameter when dealing with pipe systems) (m)
$\mu$: viscosity of the fluid (Pa s)

If $Re$ is less than approximately 2000 for a fluid in a pipe, the flow can be considered laminar. If $Re$ is greater than 4000, turbulence occurs, and in between these values, the flow is in the transition zone.

Assuming the concrete a homogenous material, concrete flow in pumping pipes is considered to be laminar, as it yields far lower Reynold numbers than those for conventional flow, as demonstrated in the following example.

Consider concrete with a density of 2400 kg/m$^3$ and viscosity of 30 Pa s, flowing through 15-cm pipe at a velocity of 1.5 m/s. The actual value of the Reynolds number becomes:

$$Re = \frac{2400 \times 1.5 \times 0.15}{30} = 18 \tag{5.4}$$

From this example, it is evident that the Reynolds number in pumping concrete is considerably lower than the conventional limits for laminar flow, and even in extreme applications $Re$ will rarely exceed 100. It may therefore be safely assumed that the concrete flow in pumping pipes is always laminar.

## 5.4 Concrete pipe flow

The flow of concrete in pipes is dictated by the shear stress, which varies linearly with the distance from the pipe center, resulting in different flow zones across the pipe section. As shown in Figure 5.2, three different flow zones can be distinguished across the pipe section. Near the pipe center, the shear stress applied on the concrete is insufficient to overcome its intrinsic yield stress, and as a result, the concrete remains unsheared in this zone (referred to as the plug). As the shear stress increases with distance from the pipe center, at a certain distance ($rp$) it becomes high enough to overcome the yield stress, and consequently, the concrete is sheared beyond this point. The shear effect extends to the lubrication layer, formed by fine particles and water droplets. Because the lubrication layer exhibits different rheological properties than the sheared concrete, the flow behavior within the lubrication layer is also different.

To summarize, in concrete pipe flow, three zones with distinctive flow characteristics can be defined across the pipe section. In the first zone, the plug, the concrete moves along the pipe without being sheared. In the second zone, concrete is sheared as it moves. The third zone, the lubrication layer, displays unique flow characteristics compared to the other two zones. A schematic representation of the different flow zones formed across the pipe section are pictured in Figure 5.2. It is important to note that the case of the three flow zones is the general one, and it applies to concrete with relatively low yield stress. In special cases of concrete with relatively high yield stress (like CVC), the pumping pressure is insufficient to overcome its yield stress, and consequently, the concrete section

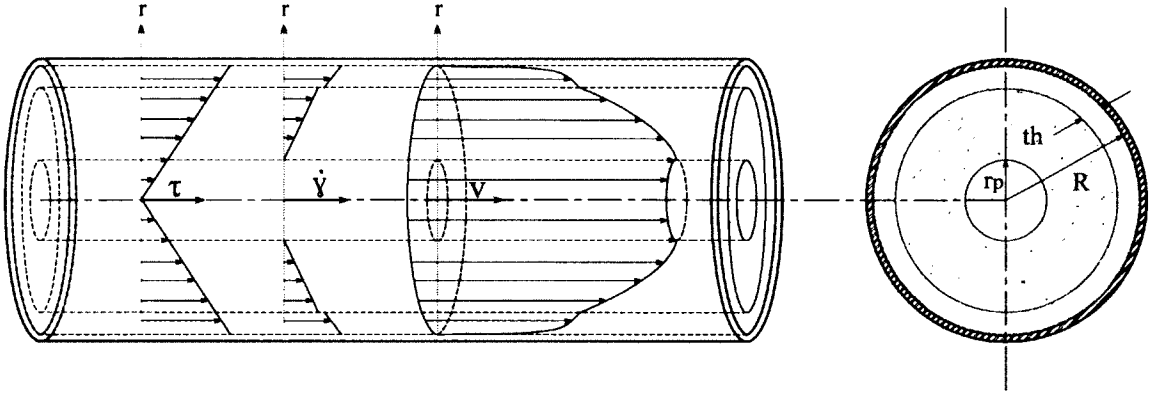


***Figure 5.2:*** *The flow zones and their velocity profiles formed across the pipe section in concrete pipe flow.*

is not entirely sheared. In this case of plug flow, the sheared concrete zone disappears and only two zones: the lubrication layer and the unsheared concrete can be distinguished across the pipe section.

## 5.5 Boundary conditions

Different pipe flow behaviors can be highlighted depending on the steel pipe-concrete interface boundary conditions. The assumption of the no-slip condition is very common in fluid mechanics and can be used to describe concrete flow in pipes, especially in the case of highly-flowable concrete. This theory has been approved on a smaller scale of particles lying in the range of 10 $nm$ to 1 $\mu m$ [1]. In the no-slip condition, the wall friction is considered constant and independent of the applied pressure, and the flow velocity and pressure loss are determined by only the geometry of pipe line, the rheological properties of the concrete [2, 3] and those of the lubrication layer. As a result, the extended version of the Poiseuille formula (Buckingham-Reiner) for laminar flow in circular pipes may be used to describe the velocity profile within both the lubrication layer and the concrete section [4].

When the interaction between the concrete and the pipe wall is of a solid-solid type of behavior, the pipe friction becomes dependent on the local pressure. Hence, the no-slip condition is invalid and the Coulombs friction law governs. It follows that the local pressure no longer evolves linearly with the pipe length; rather a decreasing exponential curve is obtained that can be very disadvantageous in the case of long-distance pumping [5, 6]. This type of behavior is more likely to happen when the magnitude of the stress transfer in the liquid is minor (for example in aggregate-rich concrete), and where solid friction prevails [5, 6].

In this research, the no-slip condition is assumed to be met, and thus the concrete flow behavior is only a function of the pipe radius and the properties of both concrete and the lubrication layer.

## 5.6 Determination of the lubrication layer properties

The lubrication layer is a product of the uneven shear effect exerted on the concrete by the pumping pressure. It follows that the concrete properties and the shear magnitude are key factors in determining the properties of the lubrication layer.

The properties of the lubrication layer are difficult to measure physically, particularly in complex flow conditions like pipe flow. Fortunately, the lubrication layer can be reproduced in the tribometer where a rotating inner cylinder and a stationary outer cylinder generate a relative motion between the concrete-steel interface. As in concrete pumping pipes, fine particles and water droplets under the shear effect are drawn toward the inner cylinder where they assemble and form the lubrication layer (Figure 5.3). This reproduction of the lubrication layer, with the help of the rheological measurements, provides a significant opportunity to determine the properties of the lubrication layer.

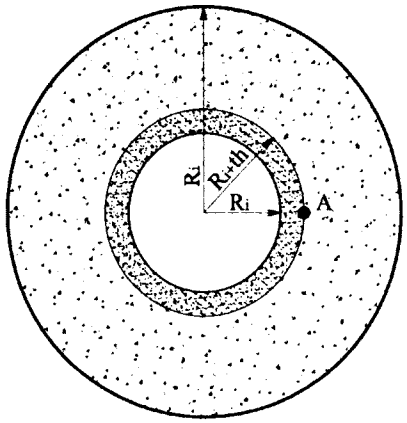


***Figure 5.3:*** *Schematic representation of the sheared concrete zone and the lubrication layer formed in the tribometer gap. $R_i$ and $R_o$ refer to the radii of the inner and outer cylinders, respectively, and th refers to the thickness of the lubrication layer.*

From Figure 5.3, assuming the Bingham behavior of concrete, and that the concrete is entirely sheared in the tribometer gap (due to its relatively low yield stress), the angular velocity within the lubrication layer ($\omega_{(r),l}$) can be calculated from the properties of the lubrication layer by integrating the shear rate across the lubrication layer with regard to $-r$:

$$\begin{aligned}
\omega_{(r)l} &= -\int \frac{\dot{\gamma}}{r} dr \\
&= -\int \left( \frac{\dfrac{T}{2\pi r^2 h} - \tau_{0l}}{r\mu_l} \right) dr \\
&= -\int \left( \frac{T}{2\pi r^3 \eta_l h} - \frac{\tau_{0l}}{r\mu_l} \right) dr \\
&= \frac{T}{4\pi r^2 h \mu_l} + \frac{\tau_{0l}}{\mu_l} \ln(r) + Constant
\end{aligned} \tag{5.5}$$

where

$\omega_{(r)l}$: angular velocity within the lubrication layer as a function of $r$ (rad/s)

$\dot{\gamma}$: shear rate within the lubrication layer at a distance $r$ from the center of the inner cylinder (1/s)

$r$: distance from the center of of inner cylinder (m)

$T$: torque measured in tribometer (N m)

$h$: height of inner cylinder submerged into concrete (m)

$\tau_{0l}$: yield stress of the lubrication layer (Pa), determined from the intercept of the torque-velocity relationship with the torque-axis

$\mu_l$: plastic viscosity of the lubrication layer (Pa s)

The integration constant is determined by applying the boundary condition. At a distance

$r = R_i$ (the radius of the inner cylinder), the velocity is equal to the angular velocity of the inner cylinder ($\Omega_i$) thus,

$$\Omega_{(r=R_i)l} = \Omega_i = \frac{T}{4\pi {R_i}^2 h\mu_l} + \frac{\tau_{0l}}{\mu_l}\ln(R_i) + Constant \tag{5.6}$$

$$Constant = \Omega_i - \frac{T}{4\pi {R_i}^2 h\mu_l} - \frac{\tau_{0l}}{\mu_l}\ln(R_i) \tag{5.7}$$

where

$\Omega_{(r=R_i)l}$: angular velocity within the lubrication layer at a distance $r=R_i$ (rad/s)
$\Omega_i$: angular velocity of the inner cylinder (rad/s)

Substituting the integration constant from equation 5.7 into equation 5.5 delivers the velocity within the lubrication layer as a function of $r$:

$$\begin{aligned}\omega_{(r)l} &= \frac{T}{4\pi r^2 h\mu_l} + \frac{\tau_{0l}}{\mu_l}\ln(r) + \Omega_i - \frac{T}{4\pi {R_i}^2 h\mu_l} - \frac{\tau_{0l}}{\mu_l}\ln(R_i) \\ &= -\frac{T(r^2 - R_i^2)}{4\pi r^2 {R_i}^2 h\mu_l} - \frac{\tau_{0l}}{\mu_l}\ln\left(\frac{R_i}{r}\right) + \Omega_i\end{aligned} \tag{5.8}$$

The velocity at any point $A$ located at the outer boundary of the lubrication layer (where $r = R_i + th$) can be calculated by substituting $r$ by $R_i + th$ in equation 5.8:

$$\omega_{(r=R_i+th)l} = \Omega_{Al} = -\frac{T\left[(R_i+th)^2 - {R_i}^2\right]}{4\pi(R_i+th)^2 {R_i}^2 h\mu_l} - \frac{\tau_{0l}}{\mu_l}\ln\left(\frac{R_i}{R_i+th}\right) + \Omega_i \tag{5.9}$$

where

$\omega_{(r=R_i+th)l}$, $\Omega_{Al}$: angular velocity at any point $A$ (located at the outer boundary of the lubrication layer) and calculated using the lubrication layer properties (rad/s)
$th$: thickness of the lubrication layer (m)

Similar to the lubrication layer, the angular velocity within the sheared concrete zone can be determined from concrete properties by integrating the shear rate with regard to $-r$:

$$\begin{aligned}\omega_{(r)c} &= -\int \frac{\dot{\gamma}}{r} dr \\ &= -\int \left(\frac{\frac{T}{2\pi r^2 h} - \tau_{0c}}{r\mu_c}\right) dr \\ &= -\int \left(\frac{T}{2\pi r^3 \mu_c h} - \frac{\tau_{0c}}{r\mu_c}\right) dr \\ &= \frac{T}{4\pi r^2 h\mu_c} + \frac{\tau_{0c}}{\mu_c}\ln(r) + Constant\end{aligned} \tag{5.10}$$

The integration constant is determined from the boundary conditions by considering that the outer cylinder is stationary, and thus the velocity at a distance $r = R_o$ is zero.

$$\Omega_o = 0 = \frac{T}{4\pi {R_o}^2 h\mu_c} + \frac{\tau_{0c}}{\mu_c}\ln(R_o) + Constant \tag{5.11}$$

$$Constant = -\frac{T}{4\pi {R_o}^2 h\mu_c} - \frac{\tau_{0c}}{\mu_c}\ln(R_o) \tag{5.12}$$

where

$\Omega_o$: angular velocity at the outer cylinder = 0

$\dot{\gamma}$: shear rate within the concrete at a distance $r$ from the center of the inner cylinder (1/s)

$R_o$: radius of outer cylinder (m)

$\tau_{0c}$: yield stress of concrete measured with the rheometer (Pa)

$\mu_c$: viscosity of concrete measured with the rheometer (Pa s)

By substituting the integration constant from equation 5.12 into equation 5.10, the velocity within the concrete section as a function of $r$ can be written as:

$$\begin{aligned}\omega_{(r)c} &= \frac{T}{4\pi r^2 h\mu_c} + \frac{\tau_{0c}}{\mu_c}\ln(r) - \frac{T}{4\pi {R_o}^2 h\mu_c} - \frac{\tau_{0c}}{\mu_c}\ln(R_o) \\ &= -\frac{T\left(r^2 - {R_o}^2\right)}{4\pi r^2 {R_o}^2 h\mu_c} - \frac{\tau_{0c}}{\mu_c}\ln\left(\frac{R_o}{r}\right)\end{aligned} \tag{5.13}$$

Using equation 5.13, the velocity at any point $A$ located at the outer boundary of the lubrication layer (where $r = R_i + th$) can be calculated:

$$\omega_{(r=R_i+th)c} = \Omega_{Ac} = -\frac{T\left[(R_i+th)^2 - {R_o}^2\right]}{4\pi(R_i+th)^2 (R_o)^2 h\mu_c} - \frac{\tau_{0c}}{\mu_c}\ln\left(\frac{R_o}{R_i+th}\right) \tag{5.14}$$

where

$\omega_{(r=R_i+th)c}$, $\Omega_{Ac}$: angular velocity at any point $A$ calculated using the concrete properties (rad/s)

As a result, the angular velocity $\Omega_{Al}$ at point $A$ (located at the outer boundary of the lubrication layer) can be calculated by equation 5.9 from the properties of the lubrication layer. Also, at the same point the angular velocity $\Omega_{Ac}$ can be calculated by equation 5.14 from the properties of the concrete. Physically, one point can only have one velocity, therefore:

$$\Omega_{Al} = \Omega_{Ac} \tag{5.15}$$

Substituting $\Omega_{Al}$ and $\Omega_{Ac}$ from equations 5.9 and 5.14 respectively, into equation 5.15 and rearranging gives:

$$-\frac{T\left[(R_i+th)^2-{R_o}^2\right]}{4\pi\left(R_i+th\right)^2{R_o}^2h\mu_c}-\frac{\tau_{0c}}{\mu_c}\ln\left(\frac{R_o}{R_i+th}\right)$$
$$+\frac{T\left[(R_i+th)^2-{R_i}^2\right]}{4\pi\left(R_i+th\right)^2{R_i}^2h\mu_l}+\frac{\tau_{0l}}{\mu_l}\ln\left(\frac{R_i}{R_i+th}\right)=\Omega_i \tag{5.16}$$

As indicated in equation 5.16, the angular velocity at the inner cylinder is expressed by the rheological properties of both concrete and the lubrication layer, the measured torque, the inner and outer radii of the tribometer, and the thickness of the lubrication layer. The rheological properties of concrete can be determined independently using a rheometer. Also, the yield stress of the lubrication layer can be determined from the intercept with the torque-axis of the torque-velocity relationship in the tribometer test. As a result, the only remaining unknown variables in equation 5.16 are the thickness and viscosity of the lubrication layer. Knowing this, performing two tribological experiments using different cylinders diameters will yield two equations similar to equation 5.16, thus allowing to solve for the thickness and viscosity of the lubrication layer.

It is noteworthy that the shear rate applied within the concrete should be set equal in both tribometers. Therefore, the diameters of the inner and outer cylinders of both tribometers should be carefully selected to guarantee identical shear rates.

## 5.7 Tribological parameters

The flow zones formed in the tribometer gap are similar to those formed across the pipe section during pumping. The lubrication layer in the tribometer is formed near the high-shear zone at the inner cylinder. The remaining concrete across the tribometer gap can be divided, depending on the yield stress of concrete, into sheared and unsheared zones. Within the unsheared zone (usually near the outer cylinder), the shear stress is insufficient to overcome the yield stress of concrete resulting in a unsheared concrete section (or plug flow). As the applied stress increases with decreasing the distance from the inner cylinder, it becomes sufficient to overcome the yield stress at a certain distance ($rp$), resulting in a sheared concrete zone beyond this point. The boundaries between the sheared and unsheared zones can vary depending on the magnitude of the applied stress on the concrete and its yield stress. The three following cases can be encountered during tribological measurements (see Figure 5.4):

- The concrete is entirely unsheared (the case of concrete with relatively high yield stress such as CVC).
- The concrete is entirely sheared (which is the case of highly-flowable concrete such as SCC).
- The concrete is partly sheared (this is the case of concrete with moderate yield stress like some types of SCC and HWC).

The different cases during tribological measurements can be detected by determining the plug radius ($rp$) from equation 5.17.

$$rp = \sqrt{\frac{T}{2\pi\tau_{0c}h}} \tag{5.17}$$

If the plug radius is larger than the outer radius ($R_o$), then the entire sample is sheared and the shear stress evolution across the tribometer gap is given by equation 5.18.

$$\tau_r = \frac{T}{2\pi h r^2} \tag{5.18}$$

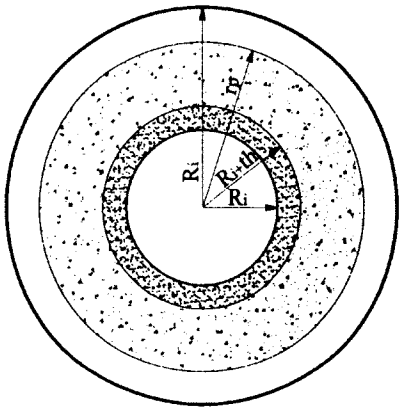


***Figure 5.4:*** *Schematic representation of the flow zones formed across the tribometer gap during testing. First zone ( with a thickness of* $R_i - R_{i+th}$ *) is the lubrication layer and the second one ( with a thickness of* $R_{i+th} - rp$*) is the sheared concrete. The third zone ( with a thickness of* $rp - R_o$ *) is the unsheared concrete.*

where

$\tau_r$: shear stress in the tribometer gap as a function of the distance from the center of the inner cylinder (Pa)

$r$: distance from the center of the inner cylinder (m)

In the case of an entirely sheared sample and assuming Bingham behavior for concrete, the shear rate within the sheared concrete zone can be written as:

$$\dot{\gamma}_r = \frac{\frac{T}{2\pi r^2 h} - \tau_{0c}}{\mu_{pc}} \tag{5.19}$$

By integrating equation 5.19 with regard to the radius $r$, and applying the boundary conditions where the velocity at the outer cylinder is zero, the angular velocity within the sheared concrete is obtained:

$$\omega_{(r)c} = \frac{T}{8\pi^2 h\mu_{pc}}\left(\frac{1}{r^2} - \frac{1}{R_o^2}\right) - \frac{\tau_{0c}}{2\pi\mu_{pc}}\ln\left(\frac{R_o}{r}\right) \tag{5.20}$$

In case the sample is partly sheared ($R_i < rp < R_o$), then $R_o$ should be replaced by $rp$ in equation 5.20. When the entire concrete sample is not sheared, which is most likely to happen in the case of CVC, the plug radius becomes smaller than the inner radius ($rp < R_i$) and consequently $\omega_{(r)c}$ is equal to zero.

From equation 5.20 the velocity at the outer boundary of the lubrication layer can be calculated by substituting $r$ by $R_i + th$. Assuming that the thickness of the lubrication layer relative to the radius of the inner cylinder is very small, the angular velocity of the concrete $\omega_{co}$ at the outer boundary of the lubrication layer can be approximated by:

$$\omega_{co} = \frac{T}{8\pi^2 h \mu_{pc}} \left( \frac{1}{R_i^2} - \frac{1}{R_o^2} \right) - \frac{\tau_{0c}}{2\pi \mu_{pc}} \ln \left( \frac{R_o}{R_i} \right) \tag{5.21}$$

Then, the velocity difference across the lubrication layer ($\omega_{ll}$) can be calculated by equation 5.22.

$$\omega_{ll} = \omega_{tot} - \omega_{co} \tag{5.22}$$

where

$\omega_{ll}$: resulting velocity difference over the lubrication layer (rad/s)
$\omega_{tot}$: total angular velocity imposed by the inner cylinder (rad/s)
$\omega_{co}$: angular velocity of concrete at the outer boundary of the lubrication layer (rad/s)

The resulting velocity difference across the lubrication layer ($\omega_{ll}$) can be expressed linearly:

$$V_{ll} = R_i \omega_{ll} \tag{5.23}$$

Similarly, the tangential velocities $V_{tot}$ and $V_{co}$ can be obtained:

$$V_{tot} = R_i \omega_{tot} \tag{5.24}$$

$$V_{co} = R_i \omega_{co} \tag{5.25}$$

As a result, three velocities ($V_{ll}, V_{co}, V_{tot}$) are obtained to describe the flow resistance of the different zones formed across the tribometer gap: $V_{co}$ for the concrete zone, $V_{ll}$ for the lubrication layer, and $V_{tot}$ for both of them combined. If the concrete is not sheared, as in the case of CVC, then $V_{co}$ becomes zero and the tribological measurements will only indicate the effect of the lubrication layer.

By plotting the three velocities versus the shear stress measured at the inner cylinder of the tribometer, three different relationships are obtained, as displayed in Figure 5.5. The blue line in Figure 5.5 presents the relationship between $V_{ll}$ and $\tau_{Ri}$ given by equation 5.26.

$$\tau_{Ri} = \tau_{0l} + Itrib_{ll} V_{ll} \tag{5.26}$$

where

$\tau_{Ri}$: shear stress measured at the inner cylinder (Pa)

$\tau_{0l}$: yield stress of the lubrication layer (Pa)

$Itrib_{ll}$: viscous constant (Pa s/m)

$V_{ll}$: resulting linear velocity difference across the lubrication layer (m/s)

The gradient of this relationship, denoted as $Itrib_{ll}$, was used first by Kaplan [3] as a viscous constant to indirectly determine the properties of the lubrication layer. From its unit (Pa s/m), the viscous constant can be considered as product of the viscosity-to-thickness ratio of the lubrication layer.

The green line in Figure 5.5 presents the relationship between $V_{co}$ and the shear stress ($\tau_{Ri}$). The slope, denoted as $Itrib_{co}$, can be considered a new tribological parameter, characterizing the contribution of the sheared concrete zone to the flow resistance. The third line (in red) presents the relationship between $V_{tot}$ and the shear stress. The slope of the green line, called the total flow resistance and referred to as $Itrib_{tot}$, is a function of $Itrib_{ll}$ and $Itrib_{co}$, since it comprises both effects of the lubrication layer and sheared concrete zone.

$Itrib_{ll}$ can be considered independent of the test geometry as the shear effect is taking place in a narrow gap (across the lubrication layer). On the other hand, $Itrib_{tot}$ and $Itrib_{co}$ can exhibit some dependency on the test geometry as the shear rate may vary across the gab they are measured in. Nevertheless, $Itrib_{tot}$ and $Itrib_{co}$ remain significant indicators to examine the effects of mix design parameters on the total flow resistance across the tribometer gap and pipe section.

By means of the three tribological parameters discussed above, the effects of each the lubrication layer and concrete properties on the concrete flow resistance in the tribometer can be evaluated independently. Furthermore, the parameters measured with the tribometer, can be employed to appraise concrete flow in pipes, since the flow conditions

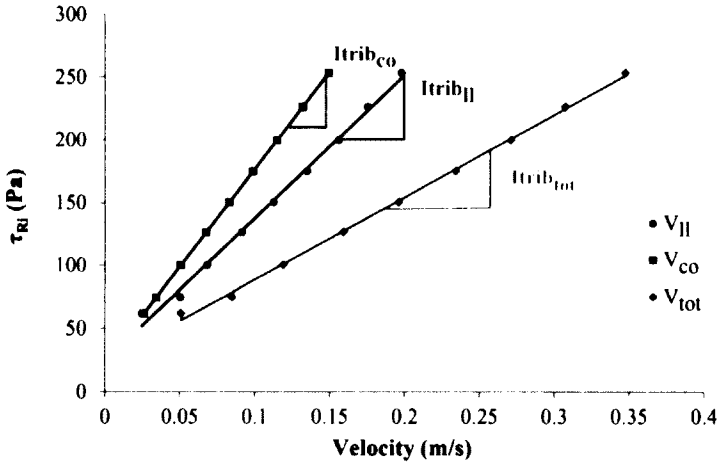


***Figure 5.5:*** *Illustrative example of the tribological parameters obtained from the tribometer test for mixture SCC14 (Table B.15) prepared with* w/cm *of 0.29, S/A of 0.53, and total binder content of 600* kg/m$^3$. *The tribological parameters are represented by the slope of each line.*

are similar in both cases. The tribological parameters also will further the understanding of the properties of the lubrication layer and their influence on pressure loss in pipes. Complete details concerning this matter are discussed in Chapter 7.

## 5.8 Velocity profiles across the pipe section

When highly-flowable concrete is pumped, three zones with different flow characteristics can be observed across the pipe section, as depicted in Figure 5.6. The first zone is the plug extending from the pipe center to a certain distance ($rp$) at which the applied shear stress is equal to the yield stress of the concrete. In this zone the stress is smaller than the yield stress, hence the concrete will move ahead in the pipe without being sheared. The second zone represents the sheared concrete spanning from the inner boundary of the first zone ($rp$) to the inner boundary of the lubrication layer ($R - th$). The concrete in this section is entirely sheared and the shear stress magnitude depends on the applied shear effect. The third zone is the lubrication layer located in the vicinity of the pipe wall with a thickness believed to lay in the range of 0.5-3.5 mm. The lubrication layer is also entirely sheared, but the shear stress generated within the lubrication layer is different than that in concrete as the lubrication layer has different rheological properties.

The boundaries of the different flow zones vary depending on the rheological properties of concrete and lubrication layer, the applied shear effect, and the radius of the pipe. In the case of highly-flowable concrete (with relatively low yield stress), the unsheared concrete zone is very small compared to the sheared one. In the case of CVC with relatively high yield stress, the sheared concrete zone disappears since the entire concrete section is unsheared resulting in only two flow zones, the unsheared concrete and the lubrication layer. The velocity profile of each flow zone in the case of highly-flowable concrete is detailed in the following sections, assuming the Bingham behavior of concrete.

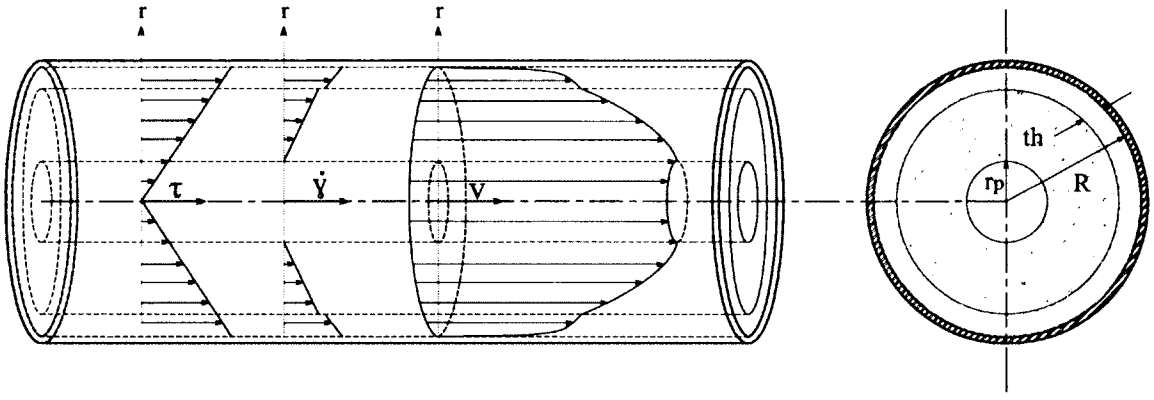


***Figure 5.6:*** *(reprint of Figure 5.2) Free body diagram for concrete pipe flow model, showing the three flow zones and their velocity profiles across the pipe section.*

### 5.8.1 Velocity profile across the lubrication layer

The shear stress at a radius $r$ from the pipe center line is a linear function of the shear stress at the wall, independent of the material properties [4, 7]:

$$\tau_{(r)} = \frac{\tau_w r}{R} \tag{5.27}$$

where

$\tau_{(r)}$: shear stress at a distance $r$ from the pipe center line (Pa)
$r$: distance from the pipe center line (m)

By applying equation 5.27 to the lubrication layer, the shear stress within the lubrication layer can be written:

$$\tau_{(r)l} = \frac{\tau_w r}{R} = \tau_{0l} + \mu_{pl}\dot{\gamma}_{(r)l} \tag{5.28}$$

where

$\tau_{(r)l}$: shear stress within the lubrication layer as a function of $r$ (Pa)
$\dot{\gamma}_{(r)l}$: shear rate within the lubrication layer at a distance $r$ from the pipe center line (1/s)
$\tau_{0l}$: yield stress of the lubrication layer (Pa)
$\mu_{pl}$: plastic viscosity of the lubrication layer (Pa s)

Rearranging equation 5.28 delivers the shear rate within the lubrication layer as a function of its properties and the radius $r$ ($R - th < r < R$):

$$\dot{\gamma}_{(r)l} = \frac{(\frac{\tau_w r}{R} - \tau_{0l})}{\mu_{pl}} \tag{5.29}$$

Using a different approach, the shear rate can also be determined from its 2D general equation:

$$\dot{\gamma}_{xy} = \frac{\partial v_x}{\partial y} + \frac{\partial v_y}{\partial x} \tag{5.30}$$

where

$v_x$: velocity component parallel to the pipe surface in the direction of the pipe main axes
$v_y$: velocity component normal to the pipe main axes

Assuming the laminar flow condition in equation 5.30, the velocity component in the direction normal to flow is then nullified and thus the shear rate across the lubrication layer becomes:

$$\dot{\gamma}_{(r)l} = \frac{\partial v_x}{\partial y} = \frac{\partial v_r}{\partial r} \tag{5.31}$$

where

$v_r$: velocity component within the lubrication layer in the direction of the pipe main axis

Substituting the shear rate from equation 5.29 into equation 5.31 and integrating with regard to $-r$ gives:

$$\begin{aligned} v_{(r)l} &= \int \dot{\gamma}_{(r)l} dr \\ &= -\int \frac{\frac{\tau_w r}{R} - \tau_{0l}}{\mu_{pl}} dr \\ &= -\frac{\frac{\tau_w r^2}{2R} - \tau_{0l} r}{\mu_{pl}} + Constant \end{aligned} \tag{5.32}$$

where

$v_{(r)l}$: velocity within the lubrication as a function of $r$ (m/s)

In equation 5.32, the integration constant is calculated from the boundary conditions as the velocity at the wall (where $r = R$) equals zero:

$$v_{(r=R)l} = 0 = -\frac{\frac{\tau_w R^2}{2R} - \tau_{0l} R}{\mu_{pl}} + Constant \tag{5.33}$$

$$Constant = R\left(\frac{\tau_w - 2\tau_{0l}}{2\mu_{pl}}\right) \tag{5.34}$$

By substituting the integration constant from equation 5.34 into equation 5.32, the velocity within the lubrication layer becomes:

$$v_{(r)l} = -\frac{\frac{\tau_w r^2}{2R} - \tau_{0l} r}{\mu_{pl}} + R\left(\frac{\tau_w - 2\tau_{0l}}{2\mu_{pl}}\right) \tag{5.35}$$

Simplifying equation 5.35 gives:

$$v_{(r)l} = (R - r)\left(\frac{\tau_w R + \tau_w r - 2R\tau_{0l}}{2\mu_{pl} R}\right) \tag{5.36}$$

The velocity at the inner boundary of the lubrication layer can be calculated from equation 5.36 by replacing $r$ by $R - th$:

$$v_{(r=R-th)l} = \frac{th}{\mu_{pl}}\left(\tau_w - \tau_{0l} - \frac{\tau_w th}{2R}\right) \tag{5.37}$$

where

$v_{(r=R-th)l}$: velocity at the inner boundary of the lubrication layer ($r = R - th$) (m/s)

$th$: thickness of the lubrication layer (m)

### 5.8.2 Velocity profile across the sheared concrete zone

Similar to the lubrication layer, the shear rate across the sheared concrete zone ($rp < r < R - th$) is expressed by the properties of concrete and the shear stress at the wall:

$$\dot{\gamma}_{(r)c} = \frac{\left(\frac{\tau_w r}{R} - \tau_{0c}\right)}{\mu_{pc}} \tag{5.38}$$

where

$\dot{\gamma}_{(r)c}$: shear rate within the sheared concrete zone at a distance $r$ from the pipe center line (1/s)

$\tau_{0c}$: yield stress of concrete (Pa)

$\mu_{pc}$: plastic viscosity of concrete (Pa s)

By integrating the shear rate in equation 5.38 with regard to $-r$, the velocity as a function of $r$ can be written:

$$\begin{aligned} v_{(r)c} &= \int \dot{\gamma}_{(r)c} dr \\ &= -\int \frac{\frac{\tau_w r}{R} - \tau_{0c}}{\mu_{pc}} dr \\ &= -\frac{\frac{\tau_w r^2}{2R} - \tau_{0c} r}{\mu_{pc}} + Constant \end{aligned} \tag{5.39}$$

where

$v_{(r)c}$: velocity within the sheared concrete as a function of $r$ (m/s)

$rp$: plug radius (m)

The integration constant can be calculated from the boundary conditions since the velocity at a the inner boundary of the lubrication layer (where $r = R - th$) is known from equation 5.37. Thus, replacing $r$ by $R - th$ in equation 5.39 and substituting equation 5.37 into equation 5.39, the integration constant is obtained:

$$v_{(r=R-th)c} = -\frac{\frac{\tau_w (R-th)^2}{2R} - \tau_{0c}(R-th)}{\mu_{pc}} + Constant$$
$$= \frac{th}{\mu_{pl}}\left(\tau_w - \tau_{0l} - \frac{\tau_w th}{2R}\right) \tag{5.40}$$

$$Constant = \frac{th}{\mu_{pl}}\left(\tau_w - \tau_{0l} - \frac{\tau_w th}{2R}\right) + \frac{\frac{\tau_w (R-th)^2}{2R} - \tau_{0c}(R-th)}{\mu_{pc}} \tag{5.41}$$

With equation 5.41, it is possible to complete equation 5.39 and solve for the velocity within the sheared concrete zone at any distance $r \in [rp, R]$:

$$v_{(r)c} = \frac{1}{2\mu_{pc}R}\left((R-th)(\tau_w R - \tau_w th - 2\tau_{0c}R) - \tau_w r^2 + 2\mu_{pc}R\tau_{0c}r\right)$$
$$- \frac{1}{2\mu_{pl}}\left(\frac{\tau_w (R-th)^2}{R} - 2\tau_{0l}(R-th) + R(\tau_w - 2\tau_{0l})\right) \tag{5.42}$$

### 5.8.3 Velocity profile across the unsheared concrete zone

At a distance $rp$ from the pipe center line, the shear stress induced by the pumping pressure is equal to the yield stress of concrete.

$$rp = \frac{\tau_{0c}R}{\tau_w} \tag{5.43}$$

Within this zone, the shear stress is insufficient to shear the concrete, resulting in a constant velocity. The constant velocity can be simply calculated from equation 5.42 by substituting $r$ by $rp$ from equation 5.43, yielding:

$$v_{(rp)c} = \frac{1}{\mu_{pc}}\left(\tau_w \frac{(R-th)^2}{2R} - \tau_{0c}(R-th) + \frac{\tau_{0c}^2 R}{2\tau_w}\right)$$
$$+ \frac{th}{\mu_{pl}}\left(\tau_w - \tau_{0l} - \frac{\tau_w th}{2R}\right) \tag{5.44}$$

where

$v_{(rp)c}$: velocity within the concrete plug (m/s)

## 5.9 Flow rates across the pipe section

Assuming laminar flow and the no-slip condition, the flow rate across each the lubrication layer, the sheared concrete zone, and the unsheared concrete zone can be obtained by integrating the velocity profile (of each zone) over its cross-sectional area, as detailed in the following sections.

### 5.9.1 The flow rate within the lubrication layer

Integrating the velocity profile of the lubrication layer from equation 5.36 over its cross-sectional area delivers the flow rate of the lubrication layer:

$$\begin{aligned} Q_l &= \int_0^{2\pi}\int_{R-th}^{R} v_{(r)l} r dr d\theta \\ &= \int_0^{2\pi}\int_{R-th}^{R} (R-r)\left(\frac{\tau_w R + \tau_w r - 2R\tau_{0l}}{2\mu_{pl}R}\right) r dr d\theta \end{aligned} \tag{5.45}$$

where

$Q_l$: flow rate of the lubrication layer ($m^3/s$)

By performing the integral in equation 5.45 and simplifying the answer, the flow rate becomes:

$$\begin{aligned} Q_l = 2\pi\Bigg(&-\frac{\tau_w\left(R^4-(R-th)^4\right)}{8R\mu_{pl}} + \frac{\tau_{0l}\left(R^3-(R-th)^3\right)}{3\mu_{pl}} \\ &+\frac{R(\tau_w-2\tau_{0l})\left(R^2-(R-th)^2\right)}{4\mu_{pl}}\Bigg) \end{aligned} \tag{5.46}$$

### 5.9.2 The flow rate within the sheared concrete zone

Integrating the velocity profile of the sheared concrete zone from equation 5.42 over its cross-sectional area gives its flow rate:

$$\begin{aligned} Q_c &= \int_0^{2\pi}\int_{rp}^{R-th} v_{(r)c} r dr d\theta \\ &= \int_0^{2\pi}\int_{rp}^{R-th}\Bigg[\frac{1}{2\mu_{pc}R}\left((R-th)(\tau_w R - \tau_w th - 2\tau_{0c}R) - \tau_w r^2 + 2\mu_{pc}R\tau_{0c}r\right) \\ &\quad -\frac{1}{2\mu_{pl}}\left(\frac{2\tau_w(R-th)^2}{2R} - 2\tau_{0l}(R-th) + R(\tau_w - 2\tau_{0l})\right)\Bigg] r dr d\theta \end{aligned} \tag{5.47}$$

where

$Q_c$: flow rate of the sheared concrete zone ($m^3/s$)

Performing the integral in equation 5.47 and rearranging the answer yields:

$$Q_c = 2\pi \left[ -\frac{\tau_w}{8R\mu_{pc}} \left( (R-th)^4 - \frac{{\tau_{0c}}^4 R^4}{{\tau_w}^4} \right) + \frac{\tau_{0c}}{3\mu_{pc}} \left( (R-th)^3 - \frac{{\tau_{0c}}^3 R^3}{{\tau_w}^3} \right) \right.$$
$$+ \left( \frac{R(\tau_w - 2\tau_{0l})}{4\mu_{pl}} + \frac{(R-th)(\tau_w R - \tau_w th - 2\tau_{0c} R)}{4\mu_{pc} R} \right.$$
$$\left. \left. - \frac{1}{2\mu_{pl}} \left( \frac{\tau_w (R-th)^2}{2R} - \tau_{0l}(R-th) \right) \right) \left( (R-th)^2 - \frac{{\tau_{0c}}^2 R^2}{{\tau_w}^2} \right) \right] \tag{5.48}$$

### 5.9.3 The flow rate within the unsheared concrete zone

Similarly, the flow rate of the plug is calculated by integrating its velocity profile given by equation 5.44 over the cross-sectional area of the plug:

$$Q_p = \int_0^{2\pi} \int_0^{rp} v_{(rp)c} r dr d\theta \tag{5.49}$$

$$Q_p = \int_0^{2\pi} \int_0^{rp} \left[ \frac{1}{\mu_{pc}} \left( \tau_w \frac{(R-th)^2}{2R} - \tau_{0c}(R-th) + \frac{\tau_{0c}^2 R}{2\tau_w} \right) \right.$$
$$\left. + \frac{th}{\mu_{pl}} \left( \tau_w - \tau_{0l} - \frac{\tau_w th}{2R} \right) \right] r dr d\theta \tag{5.50}$$

where

$Q_p$: flow rate of the plug ($m^3/s$)

Performing the integral in equation 5.50 and simplifying the answer yields:

$$Q_p = \frac{\pi {\tau_{0c}}^2 R^2}{{\tau_w}^2} \left[ \frac{{\tau_{0c}}^2 R}{2\mu_{pc}\tau_w} + \frac{(R-th)(\tau_w R - \tau_w th - 2\tau_{0c} R)}{2\mu_{pc} R} \right.$$
$$\left. - \frac{1}{\mu_{pl}} \left( \frac{\tau_w (R-th)^2}{2R} - \tau_{0l}(R-th) \right) + \frac{R(\tau_w - 2\tau_{0l})}{2\mu_{pl}} \right] \tag{5.51}$$

## 5.10 Total concrete pipe flow rate

The total flow rate across the pipe section is the sum of the three flow rates of the lubrication layer, sheared concrete section, and plug.

$$Q_{tot} = Q_l + Q_c + Q_p \tag{5.52}$$

where

$Q_{tot}$: total flow rate across the pipe section ($m^3/s$)

Substituting equations 5.46, 5.48, and 5.51 into equation 5.52 and rearranging delivers the total flow rate across the pipe section:

$$\begin{aligned} Q_{tot} = \frac{\pi}{12R{\tau_w}^3\mu_{pc}\mu_{pl}} \big( & -12\mu_{pl}{\tau_w}^4R^3th + 18\,\mu_{pl}\,{\tau_w}^4R^2th^2 - 12\,\mu_{pl}\,{\tau_w}^4Rth^3 \\ & - 4\,\tau_{0c}R^4\mu_{pl}\,{\tau_w}^3 + 12\,\mu_{pc}\,R^3{\tau_w}^4th - 18\mu_{pc}\,R^2{\tau_w}^4th^2 + 12\,\mu_{pc}\,R{\tau_w}^4th^3 \\ & + 12\,\tau_{0c}R^3\mu_{pl}\,{\tau_w}^3th - 12\,\tau_{0c}R^2\mu_{pl}\,{\tau_w}^3th^2 + 4\,\tau_{0c}R\mu_{pl}\,{\tau_w}^3th^3 \\ & - 12\mu_{pc}\,th\tau_{0l}R^3{\tau_w}^3 + 12\,\mu_{pc}\,th^2\tau_{0l}R^2{\tau_w}^3 - 4\,\mu_{pc}\,th^3\tau_{0l}R{\tau_w}^3 + {\tau_{0c}}^4R^4\mu_{pl} \\ & + 3\mu_{pl}\,{\tau_w}^4R^4 + 3\mu_{pl}\,{\tau_w}^4\,th^4 - 3\,\mu_{pc}\,{\tau_w}^4th^4\big) \end{aligned} \tag{5.53}$$

As indicated in equation 5.53, the total flow rate is expressed by the properties of concrete and the lubrication layer, shear stress at the wall, and the pipe radius. The shear stress at the wall can be replaced by a function of the pressure loss and the pipe radius (from equation 5.2). By doing so and rearranging, the total flow rate is depicted by the total pressure loss along the pipe, length of the pipe, pipe diameter, properties of concrete and lubrication layer:

$$\begin{aligned} Q_{tot} = \frac{\pi}{384L{\Delta p_{tot}}^3\mu_{pc}\mu_{pl}} \big( & -24\,\mu_{pl}\,{\Delta p_{tot}}^4D^3th + 72\,\mu_{pl}\,{\Delta p_{tot}}^4D^2th^2 - 96\,\mu_{pl}\,{\Delta p_{tot}}^4Dth^3 \\ & - 16\,\tau_{0c}D^3\mu_{pl}\,{\Delta p_{tot}}^3L + 24\,\mu_{pc}\,D^3{\Delta p_{tot}}^4th - 72\,\mu_{pc}\,D^2{\Delta p_{tot}}^4th^2 + 96\,\mu_{pc}\,D{\Delta p_{tot}}^4th^3 \\ & + 96\,\tau_{0c}D^2\mu_{pl}\,{\Delta p_{tot}}^3th\,L - 192\,\tau_{0c}D\mu_{pl}\,{\Delta p_{tot}}^3th^2L + 128\,\tau_{0c}\mu_{pl}\,{\Delta p_{tot}}^3th^3L \\ & - 96\,\mu_{pc}\,th\tau_{0l}D^2{\Delta p_{tot}}^3L + 192\,\mu_{pc}\,th^2\tau_{0l}D{\Delta p_{tot}}^3L - 128\,\mu_{pc}\,th^3\tau_{0l}{\Delta p_{tot}}^3L \\ & + 256\,{\tau_{0c}}^4\mu_{pl}\,L^4 + 3\,\mu_{pl}\,{\Delta p_{tot}}^4D^4 + 48\,\mu_{pl}\,{\Delta p_{tot}}^4th^4 - 48\,\mu_{pc}\,{\Delta p_{tot}}^4th^4\big) \end{aligned} \tag{5.54}$$

where

$L$: length of the pipe over which the total pressure loss is measured (m)
$\Delta p_{tot}$: total pressure loss over the length $L$ of the pipe (Pa)
$D$: pipe diameter (m)

By replacing the total pressure loss by the pressure loss per unit length times the length ($L$) of the pipe in equation 5.54, the flow rate can also be expressed by the pressure loss per unit length of the pipe, as indicated in equation 5.55.

$$\begin{aligned} Q_{tot} = \frac{\pi}{24R^4\Delta p^3\mu_{pc}\mu_{pl}} \big( & -12\mu_{pl}\Delta p^4R^7th + 18\mu_{pl}\Delta p^4R^6th^2 - 12\mu_{pl}\Delta p^4R^5th^3 \\ & - 8\tau_{0c}R^7\mu_{pl}\Delta p^3 + 12\mu_{pc}R^7\Delta p^4th - 18\mu_{pc}R^6\Delta p^4th^2 + 12\mu_{pc}R^5\Delta p^4th^3 \\ & + 24\tau_{0c}R^6\mu_{pl}\Delta p^3th - 24\tau_{0c}R^5\mu_{pl}\Delta p^3th^2 + 8\tau_{0c}R^4\mu_{pl}\Delta p^3th^3 \\ & - 24\mu_{pc}th\tau_{0l}R^6\Delta p^3 + 24\mu_{pc}th^2\tau_{0l}R^5\Delta p^3 - 8\mu_{pc}th^3\tau_{0l}R^4\Delta p^3 + 16{\tau_{0c}}^4R^4\mu_{pl} \\ & + 3\mu_{pl}\Delta p^4R^8 + 3\mu_{pl}R^4\Delta p^4th^4 - 3\mu_{pc}R^4\Delta p^4th^4\big) \end{aligned} \tag{5.55}$$

## 5.11 Analytical pressure prediction model

Equations 5.53, 5.54, and 5.55 furnish an analytical model to calculate the pressure loss at different flow rates based on the pipe size and the properties of concrete and lubrication layer.

At this stage, equation 5.55 was chosen to analytically describe the different effects and interactions between the parameters, in relation to the discharge rate and pressure loss. Since it is impossible to plot the range of changes of all variables in one graph, the model is represented through different contour diagrams, where only three parameters can vary at once. The resulting diagrams serve as a simple approach to predict the pressure loss on job sites for a wide range of concrete properties and pumping discharge rates. The ranges of the studied parameters in the following sections mainly cover the behavior of highly-flowable concrete such as SCC. Different ranges of parameters may be chosen and used in equation 5.55. The responses of variations in different parameters and their relationships are discussed in the following sections.

### 5.11.1 Influence of concrete properties

The effect of concrete viscosity on pressure loss of concrete pumped at different discharge rates and in different pipes sizes is illustrated through Figures 5.7 and 5.8. As indicated, concrete viscosity controls the pressure loss to a large extent. For a given discharge rate, the pressure loss significantly increases as viscosity increases; this effect becomes more pronounced in the range of high discharge rates and low viscosities. For example, at a discharge rate of 10 l/s, increasing viscosity from 20 to 40 Pa s increases the pressure loss by 30%, while for the same increase in viscosity from 60 to 80 Pa s the pressure loss only increases by around 10% (Figure 5.7). For a higher discharge rate of 20.5 l/s, the increase in viscosity from 20 to 40 Pa s results in an increase in the pressure loss of approximately 38%, while the same increase in viscosity from 60 Pa s to 80 Pa s increases the pressure loss by approximately 12%.

Apart from the direct influence of viscosity on pressure loss, viscosity is firmly interrelated with the properties of the lubrication layer. A separate section (5.11.3) is devoted to discuss these interactions in detail.

The effect of yield stress on the pressure loss at different discharge rates for 5-in. (127 mm) pipe is depicted in Figure 5.9. It can be inferred that, a weak correlation exists between the pressure loss and yield stress, although an increase in yield stress leads to a slight increase in the pressure loss for a given discharge rate. Evidently, the influence of the yield stress on the discharge rate is considerably less significant than viscosity. This is anticipated as the largest part of the concrete section across the pipe (in the studied case of highly-flowable concrete) is sheared due to its relatively low yield stress. Consequently, the flow pattern is governed by viscosity rather than yield stress. This finding is further confirmed through several empirical results presented in section 6.10.1.

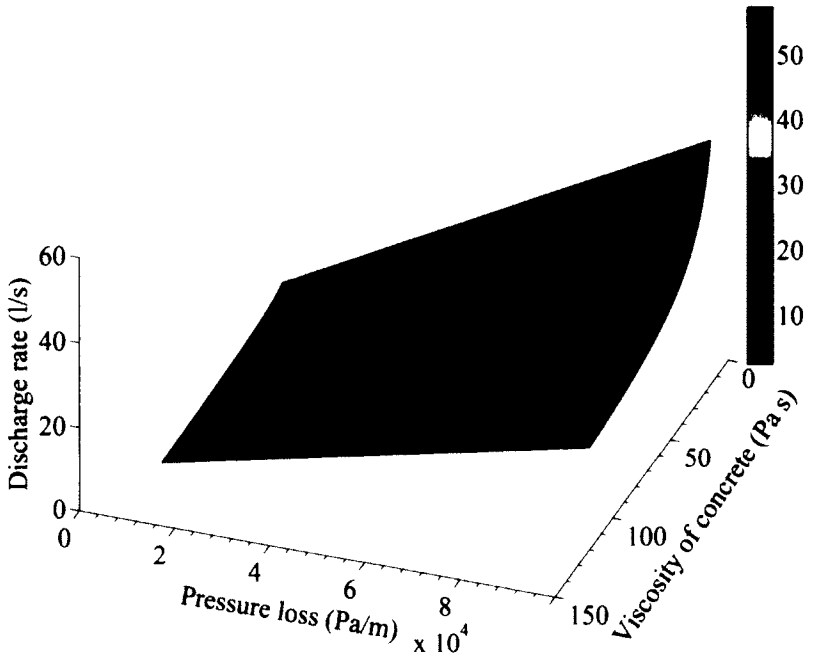


(a)

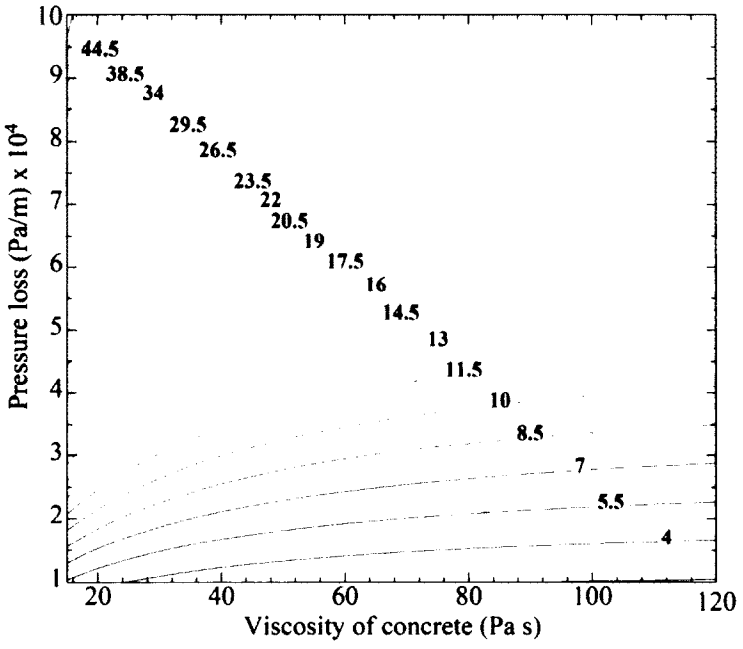


(b)

***Figure 5.7:*** *Relationship between concrete viscosity and pressure loss for different discharge rates, and given properties of the lubrication layer: (a) 3D plot; (b) contour diagram. Given: concrete yield stress = 30 Pa, viscosity of lubrication layer = 5 Pa s, thickness of lubrication layer = 1.5 mm, yield stress of lubrication layer = 1 Pa, and pipe diameter = 5 in. (127 mm).*

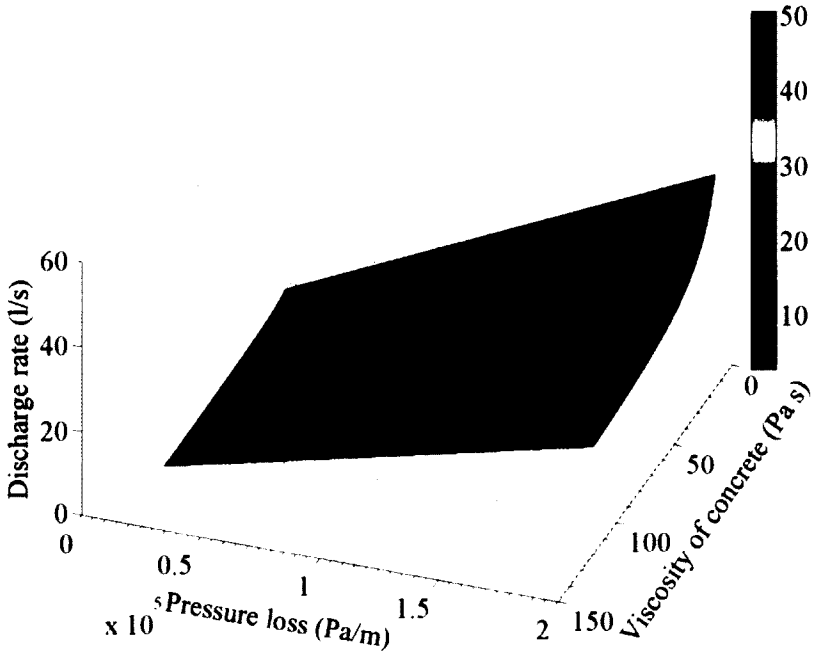


(a)

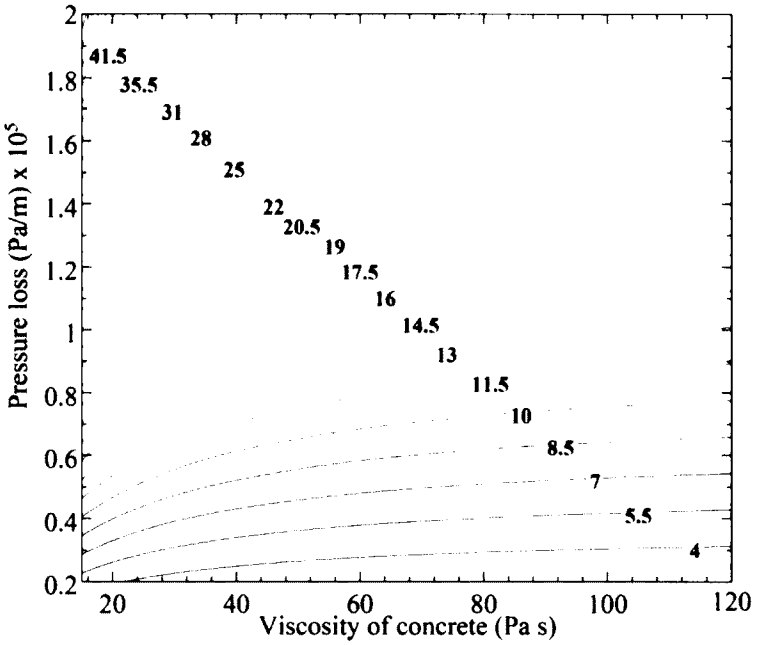


(b)

***Figure 5.8:*** *Relationship between concrete viscosity and pressure loss for different discharge rates, and given properties of the lubrication layer: (a) 3D plot; (b) contour diagram. Given: concrete yield stress = 30 Pa, viscosity of lubrication layer = 5 Pa s, thickness of lubrication layer = 1.5 mm, yield stress of lubrication layer = 1 Pa, and pipe diameter = 4 in. (102 mm).*

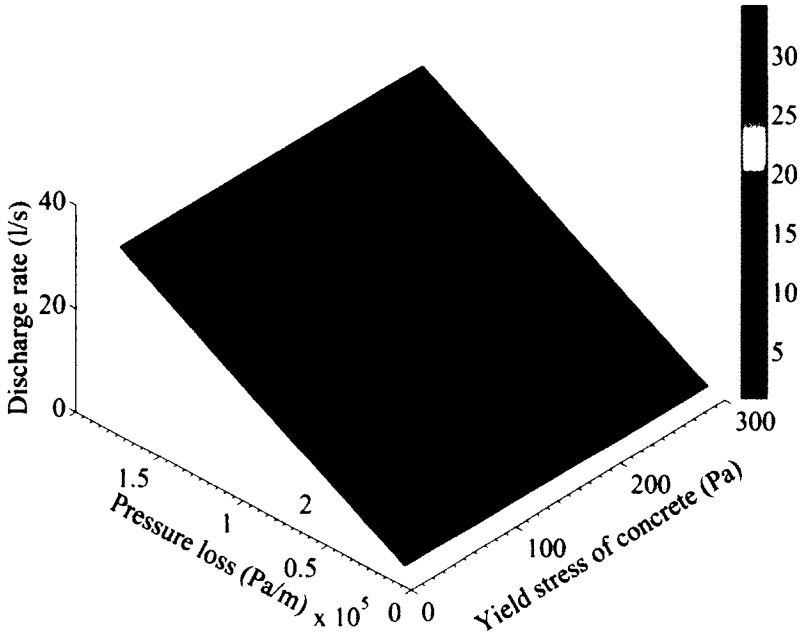


(a)

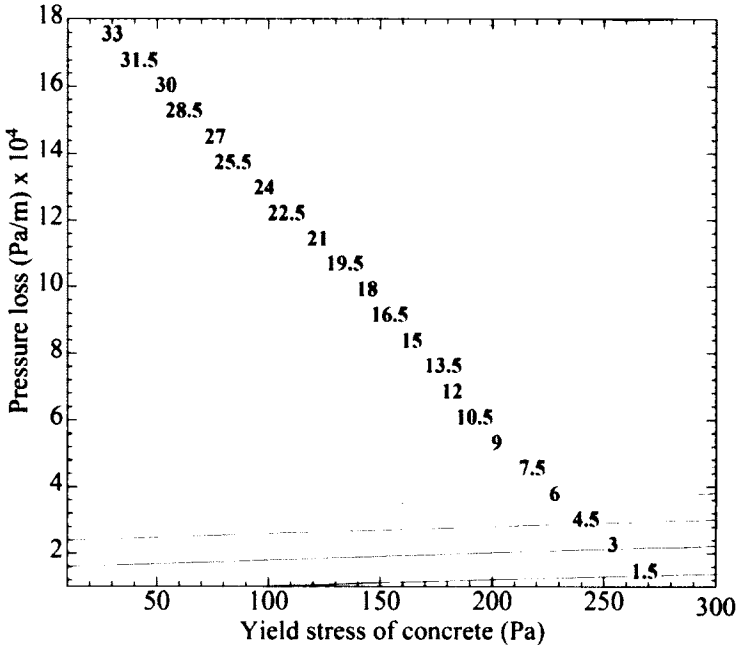


(b)

***Figure 5.9:*** *Relationship between yield stress of concrete and pressure loss for different discharge rates, and for given properties of the lubrication layer and concrete viscosity: (a) 3D plot; (b) contour diagram. Given: concrete viscosity = 50 Pa s, viscosity of lubrication layer = 5 Pa s, thickness of lubrication layer = 1.5 mm, yield stress of lubrication layer = 1 Pa, and pipe diameter = 5 in. (127 mm).*

### 5.11.2 Influence of the lubrication layer

The influence of the lubrication layer on the pressure loss is best described by considering its thickness and viscosity. As in the case of concrete, increasing viscosity increases pressure loss at a given discharge rate. This increase is more significant at low viscosities; a small change in viscosity on the order of 5 Pa s can change the pressure loss by arround 15% (Figure 5.10).

Thickness of the lubrication layer also has a profound influence on the pressure loss, as demonstrated in Figure 5.11. The pressure loss substantially declines as the thickness increases. This effect is more pronounced at high discharge rates and small thicknesses; a small increase in the thickness on the order of 0.5 mm can decrease the pressure loss by 15%.

For a given pressure loss, the viscosity and thickness of the lubrication layer seem not to be independent from each other. As shown in Figure 5.12, an increase in viscosity leads to an increase in thickness for a given concrete viscosity and pressure loss. In this case, the changes in thickness and viscosity are not only interrelated but also affected by the changes in concrete viscosity (see section 5.11.3). An increase in concrete viscosity leads to a decrease in viscosity of the lubrication layer and an increase in its thickness. On the other hand, the resulting decrease in viscosity of the lubrication layer leads, more than likely, to decreases its thickness. Since all these changes can occur simultaneously, the final change (increase or decrease) in the lubrication layer thickness is governed by the most dominating effect induced by both concrete and the lubrication layer viscosities. The coupled effect of viscosity and thickness of the lubrication layer on the pressure loss in relation with viscosity of concrete and its mix compositions can be further investigated by means of the tribological measurements, as described in Chapter 7.

The properties of the lubrication layer cannot be determined independently of the concrete mix compositions, among which the binder type and content are of prime importance. For example, two concrete mixtures displaying equal viscosities but prepared with different binder contents or types may result in different lubrication layer properties. In this connection, an early study has concluded that the thickness increases with the cement paste volume, $w/c$, the content of HRWRA, and decreases with increasing the fine sand content [8]. As the thickness and viscosity of the lubrication layer can evolve in different directions when a change in concrete viscosity is introduced, investigating their effects on pressure loss is not straightforward. To facilitate this process, employing the viscous constant (a viscosity-to-thickness ratio) and other tribological parameters can provide an indication of the changes in these properties and their effects on the pressure loss (section 5.7). The correlations between the viscous constant and other tribological parameters, and the pressure loss are established empirically and explained in further detail in section 6.10.2.

To conclude, the lubrication layer has the following effect on pressure loss: pressure loss increases with increasing viscosity but decreases with increasing thickness. For a given pressure loss, the changes in the properties of the lubrication layer can be related to the changes in concrete viscosity and may evolve in different directions. As a result, thickness and viscosity of the lubrication layer can yield opposite effects on the pressure loss and the final result then depends on which effect dominates. The influence of concrete mixture compositions on the properties of the lubrication layer cannot be captured

analytically. The experimental results of the tribological tests (presented in Chapter 7) provide a better understanding of this matter. In addition, the coupled effect of viscosity and thickness on the pressure loss in relation with viscosity of concrete are investigated.

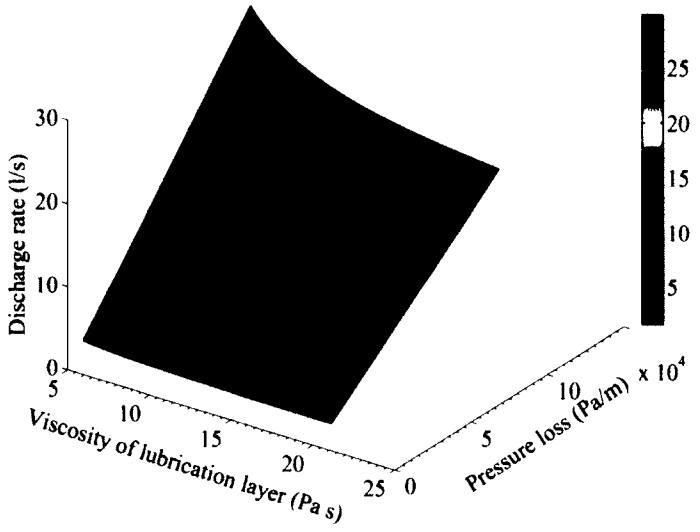


(a)

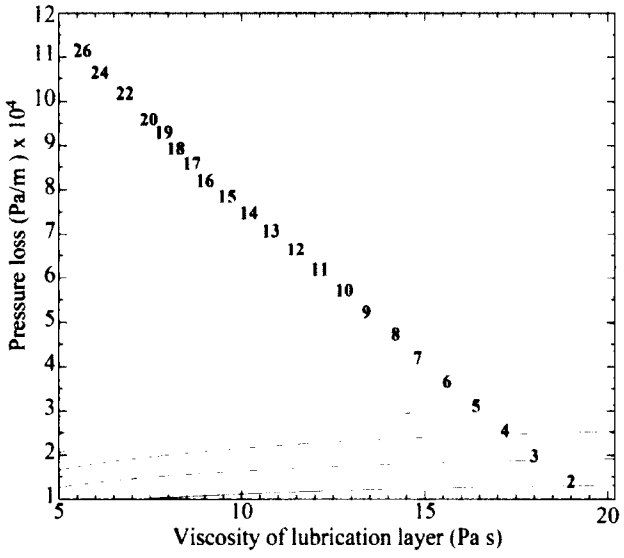


(b)

***Figure 5.10:*** *Relationship between the viscosity of the lubrication layer and pressure loss for different discharge rates, and given thickness of the lubrication layer and concrete properties: (a) 3D plot; (b) contour diagram. Given: concrete viscosity = 50 Pa s, yield stress of concrete = 30 Pa, thickness of lubrication layer = 1.5 mm, yield stress of lubrication layer = 1 Pa, and pipe diameter = 5 in. (127 mm).*

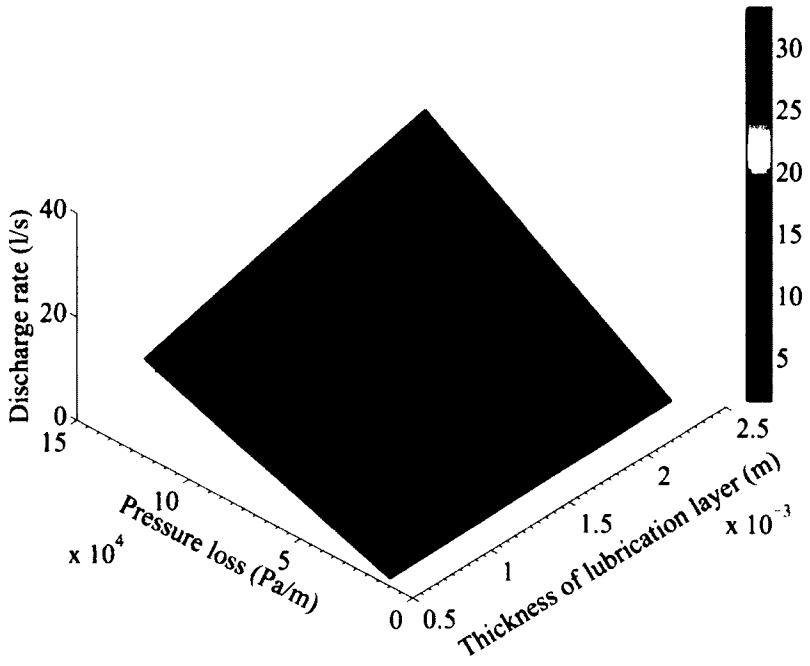


(a)

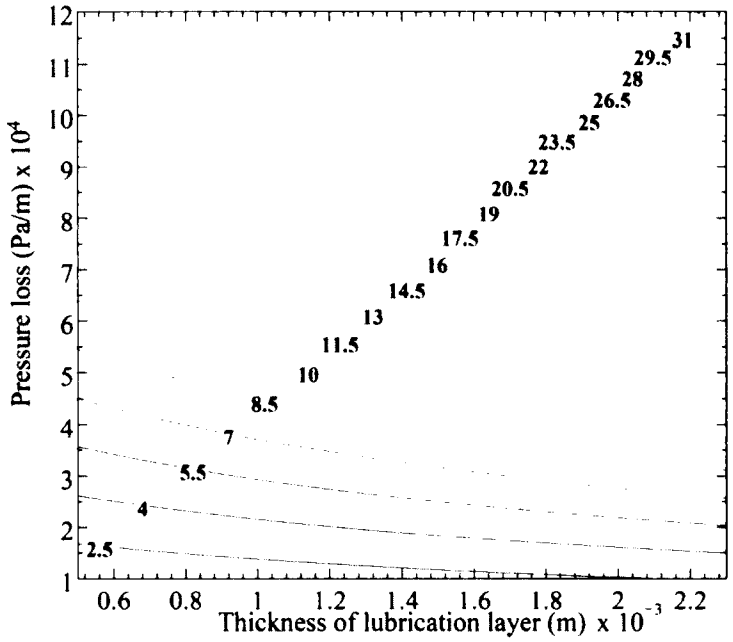


(b)

***Figure 5.11:*** *Relationship between the thickness of the lubrication layer and pressure loss for different discharge rates, and given properties of concrete and thickness of the lubrication layer: (a) 3D plot; (b) contour diagram. Given: concrete viscosity = 50 Pa s, yield stress of concrete = 30 Pa, viscosity of lubrication layer = 5 Pa s, yield stress of lubrication layer = 1 Pa, and pipe diameter = 5 in. (127 mm).*

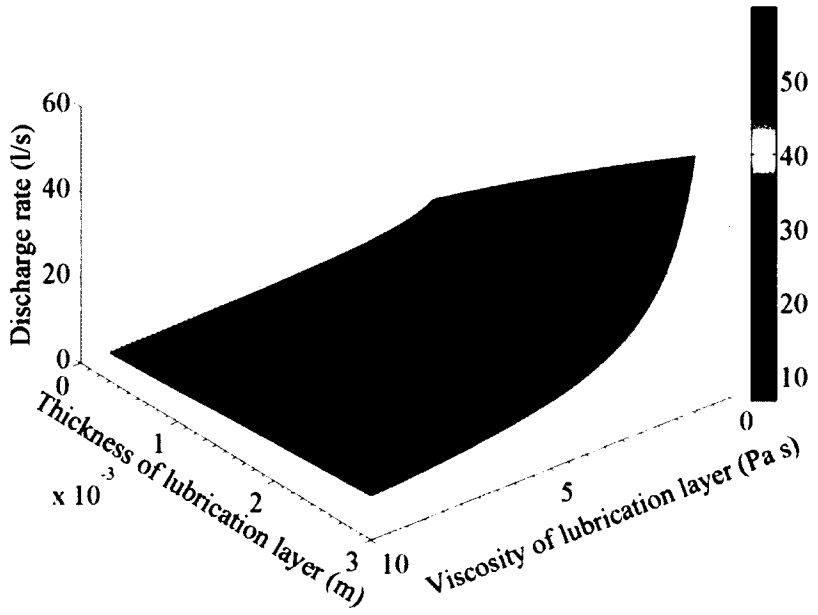


(a)

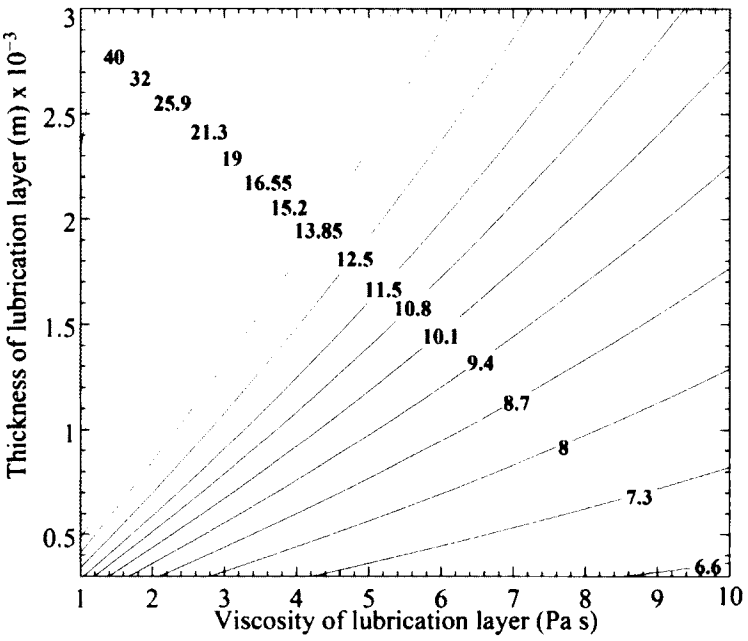


(b)

***Figure 5.12:*** *Relationship between the viscosity of the lubrication layer and its thickness for different discharge rates, and given pressure loss and concrete properties: (a) 3D plot; (b) contour diagram. Given: concrete viscosity = 50 Pa s, yield stress of concrete = 30 Pa, yield stress of lubrication layer = 1 Pa, pressure loss 50000 Pa/m, and pipe diameter = 5 in. (127 mm).*

### 5.11.3 Interactions between the properties of concrete and the properties of the lubrication layer

Determining the properties of the lubrication layer is difficult in practice, and determining its interactions with the concrete properties is even more so. A fixed pressure loss can be a helpful assumption to simplify the analysis at his stage. In this case, the properties of the lubrication layer are affected by the viscosity of the concrete, as outlined previously. Viscosity of the lubrication layer and viscosity of concrete evolve in opposite directions, as presented in Figure 5.13. For the given pressure loss, viscosity of the lubrication layer decreases with increasing viscosity of concrete. This phenomenon is evident in the range of low concrete viscosity (below 30 Pa s), while it becomes less significant for higher viscosities. This decrease can be explained by the lower flexibility of the free water droplets and fine particles to move within the concrete matrix at high viscosity. It follows that, only low-viscous paste and water droplets can migrate toward the high shear zone to form a low-viscous lubrication layer. Because of theoretical nature of this phenomenon, this is only a possible explanation and other causes may exist.

Assuming a constant pressure loss, the correlation between the thickness of the lubrication layer and the viscosity of concrete for different discharge rates is presented in Figure 5.14. For a given discharge rate, the thickness of the lubrication layer increases with the viscosity of concrete. A sharp increase is observed at low concrete viscosities (below 30 Pa s), while a lower one is observed at higher viscosities.

Reflecting on the above analysis, it suffices to say that the changes in the properties of the lubrication layer are related to those found in concrete at a given pressure loss. An increase in concrete viscosity decreases viscosity of the lubrication layer while increases its thickness. Each of these changes results in a different effect on the pressure loss, hence, the final effect is a function of all the changes in both the lubrication layer and concrete, with the latter showing the highest effect.

### 5.11.4 Influence of pipe diameter

Selecting the pipe radius is an important step in designing a pumping circuit since it is a key factor influencing the pressure loss along the streamline. In pumping concrete, the case becomes even more complicated as some properties of the lubrication layer exhibit a high dependency on the pipe size.

The analytical analysis proves the solid relationship between the pipe radius and the pressure loss at different discharge rates (see Figure 5.15). As expected, increasing the pipe diameter significantly reduces the pressure loss for a given discharge rate. This is attributed to a reduction in the flow velocity, resulting in lower energy dissipation.

Because of its influence on the flow velocity and the shear magnitude across the pipe, the pipe diameter is a substantial factor in determining the properties of the lubrication layer. Figure 5.16 exemplifies the relationship between the pipe radius and the thickness of the lubrication layer for a given pressure loss and concrete viscosity. In this case, increasing the pipe radius decreases the thickness of the lubrication layer, as indicated in Figure 5.16. This could be justified in light of the theory stating that the lubrication layer is formed as a consequence of the shear action taking place within the fresh concrete matrix. As a smaller radius results in a lower velocity (at a given discharge rate) and

shear rate within the concrete, fewer particles will migrate toward the high shear zone, resulting in a thinner lubrication layer. It should be noted that the above discussion is valid for a constant pressure loss and concrete viscosity. Changing the ranges of these affecting parameters may lead to different changes in the thickness of the lubrication layer.

From the above discussion, it can be concluded that the pipe radius is a controlling factor in the design of a pumping circuit as it primarily influences the properties of the lubrication layer and the pressure loss. Apart from questions of economy, selecting the pipe radius is therefore a matter of the properties of the pumped concrete and the required pumping height, as described in section 6.10.1.

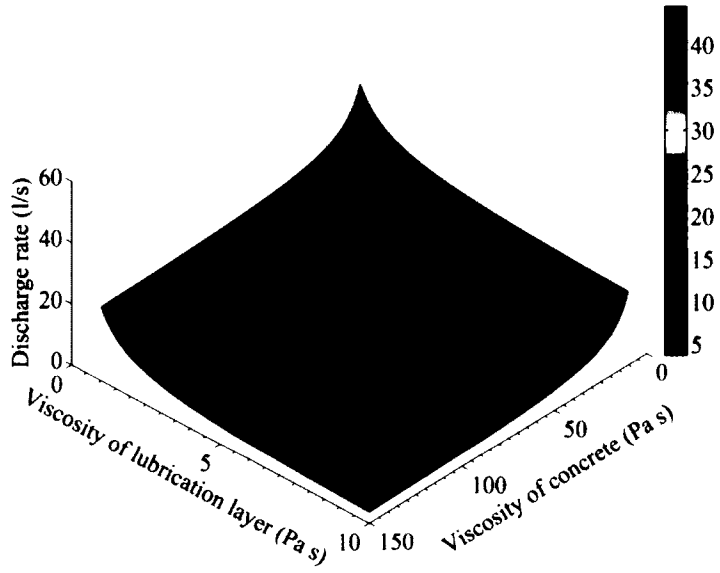


(a)

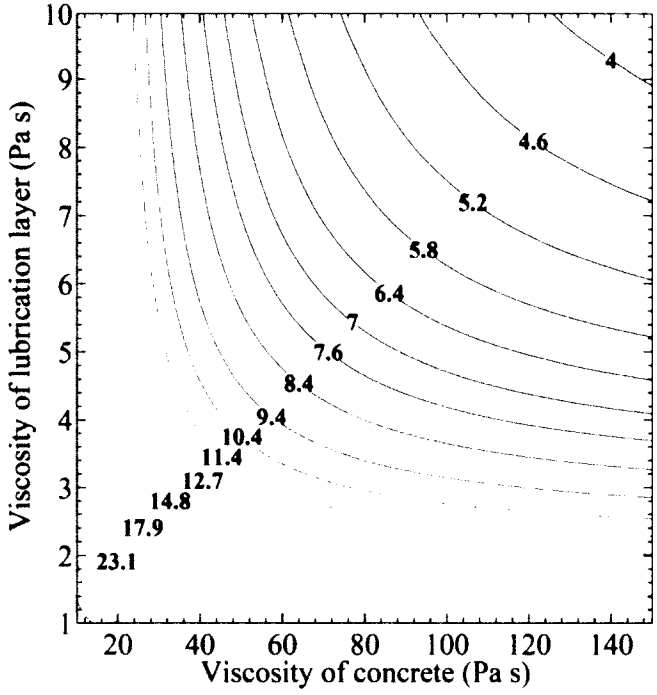


(b)

***Figure 5.13:*** *Relationship between the viscosity of concrete and viscosity of the lubrication layer for different discharge rates, and given pressure loss and thickness of the lubrication layer: (a) 3D plot; (b) contour diagram. Given: yield stress of concrete = 30 Pa, thickness of lubrication layer = 1.5 mm, yield stress of lubrication layer = 1 Pa, pressure loss = 40000 Pa/m, and pipe diameter = 5 in. (127 mm).*

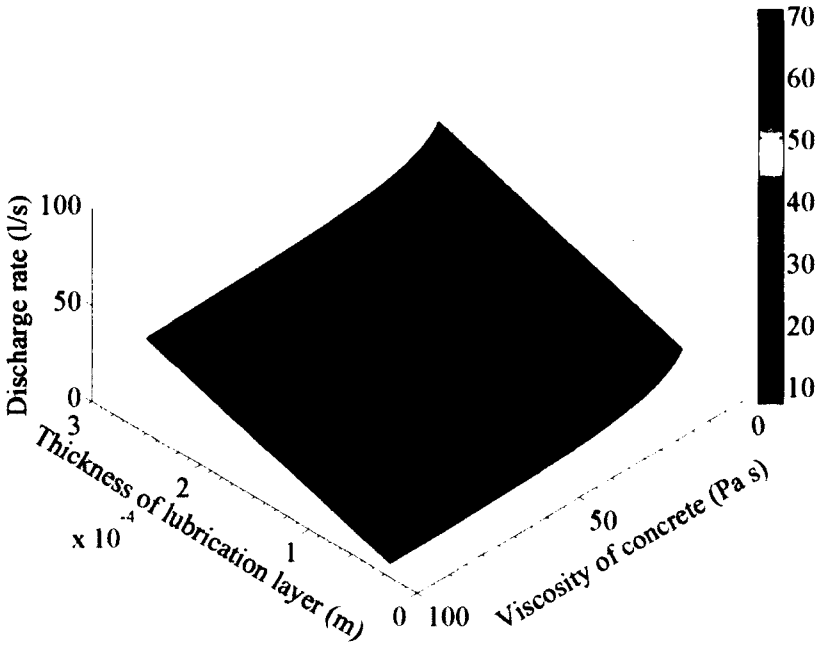


(a)

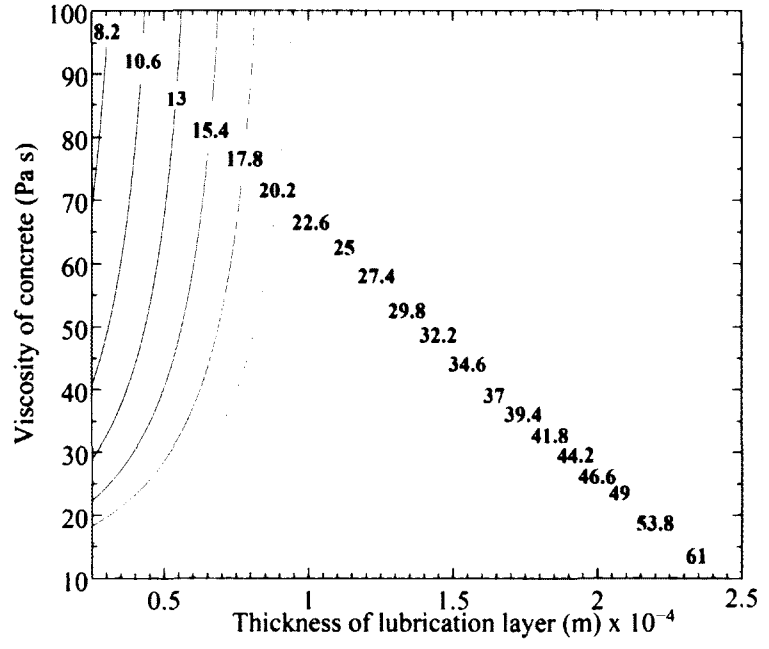


(b)

***Figure 5.14:*** *Relationship between the viscosity of concrete and the thickness of the lubrication layer for different discharge rates, and given pressure loss and viscosity of the lubrication layer: (a) 3D plot; (b) contour diagram. Given: yield stress of concrete = 30 Pa, viscosity of lubrication layer = 15 Pa s, yield stress of lubrication layer = 1 Pa, pressure loss = 40000 Pa/m, and pipe diameter = 5 in. (127 mm).*

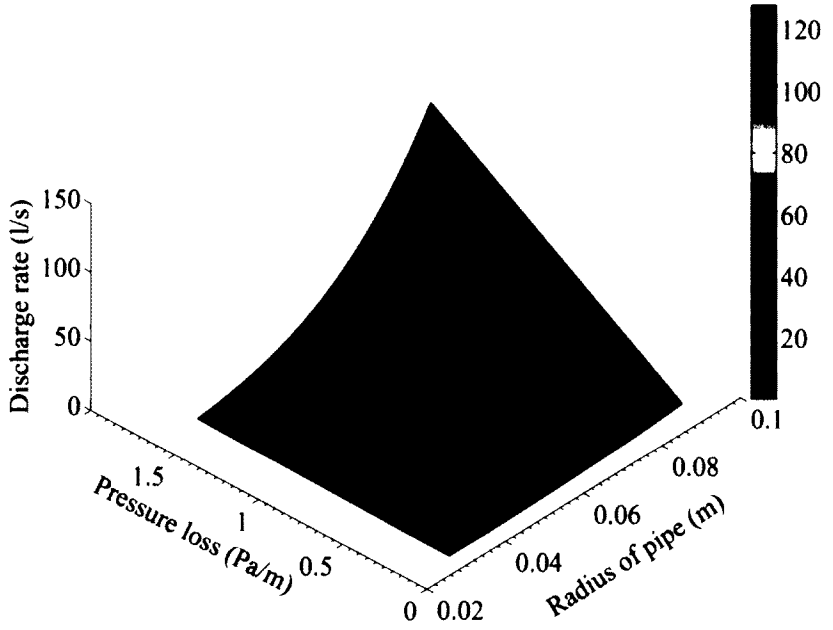


(a)

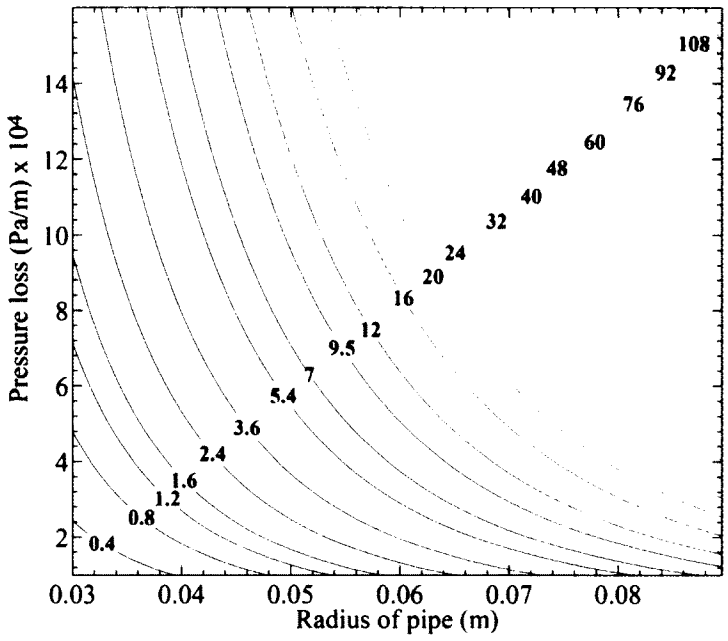


(b)

***Figure 5.15:*** *Relationship between the pipe radius and pressure loss for different discharge rates, and given properties of the lubrication layer and concrete viscosity: (a) 3D plot; (b) contour diagram. Given: concrete viscosity = 50 Pa s, yield stress of concrete = 30 Pa, viscosity of lubrication layer = 5 Pa s, yield stress of lubrication layer = 1 Pa, thickness of lubrication layer = 1.5 mm.*

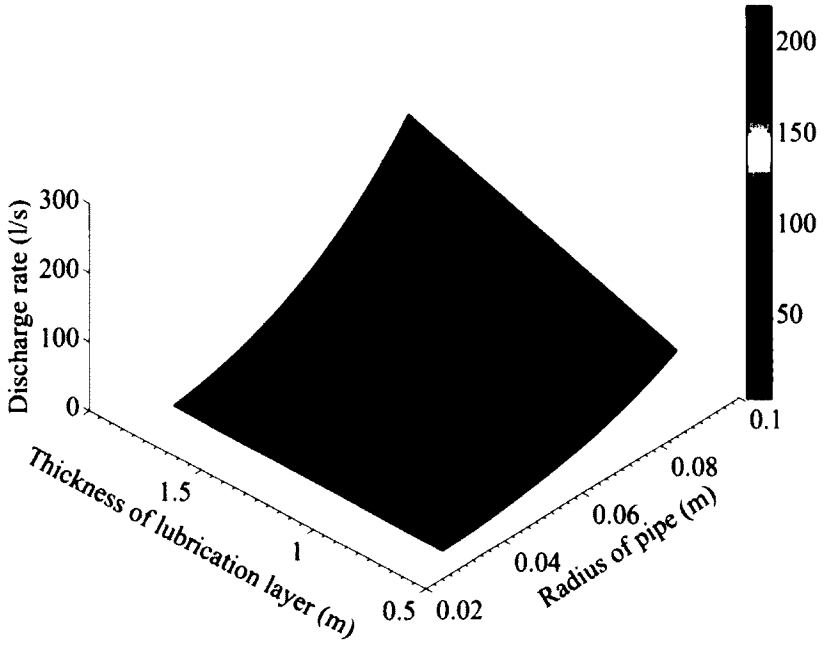


(a)

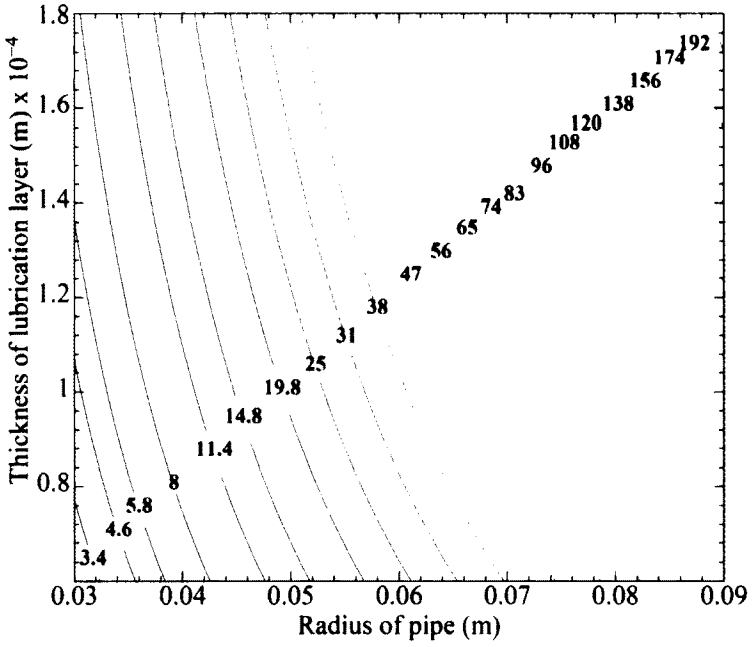


(b)

***Figure 5.16:*** *Relationship between the pipe radius and thickness of the lubrication layer for different discharge rates, and given pressure loss and concrete properties: (a) 3D plot; (b) contour diagram. Given: concrete viscosity = 50 Pa s, yield stress of concrete = 30 Pa, viscosity of lubrication layer = 5 Pa s, yield stress of lubrication layer = 1 Pa, pressure loss = 40000 Pa/m.*

### 5.11.5 Vertical pumping

For pumping to be successful, the power of the pump must overcome the various forms of energy losses along the streamline. The required head of the pump can be determined by an energy balance between two points, while considering pressure losses due to pipes and equipment. Applied to a case of vertical pumping, the energy provided by the pump must then balance for different effects: elevation, kinetic energy, friction losses ($\Delta F$), and minor losses due to equipment (fittings, valves, etc.) (see also section 4.6.3). The head that a pump can produce at various flow rates and constant speed is established through pump tests conducted by pump manufacturers. Many commercially available performance charts determine the pumping power needed for a wide scope of concrete pumps at different discharge rates and heads.

**Example**

Compute the pump horsepower needed to deliver concrete with a viscosity of 40 Pa s to a height of 1000 m at a flow rate of 12 l/s.

Assume: concrete yield stress = 30 Pa, concrete density = 2350 kg/m$^3$, pipe diameter = 5 in. (127 mm), thickness of lubrication layer = 1.5 mm, viscosity of lubrication layer = 5 Pa s, yield stress of lubrication layer = 1 Pa. Neglect all minor losses generated by the pump and the equipment along the streamline.

**Solution:**

***a.*** Applying the steady flow energy equation to two points on the streamline, the first at the free surface of the pump reservoir and the second at the pipe exist gives:

$$\left(h_1 + \frac{v_1^2}{2g} + \frac{p_1}{\rho_1 g}\right)_{in} = \left(h_2 + \frac{v_2^2}{2g} + \frac{p_2}{\rho_2 g}\right)_{out} + \Delta F - h_{pump} \tag{5.56}$$

where

$\rho$: concrete density (kg/m$^3$)
$v_1$: concrete flow velocity at the reservoir surface $\approx 0$ (m/s)
$v_2$: concrete flow velocity at the pipe exit (m/s)
$g$: gravitational constant = 9.81 (m/s$^2$)
$h_1$: reference height, considered 0 (m)
$h_2$: elevation above reference height (m)
$p_1$: atmospheric pressure at the reservoir surface (Pa)
$p_2$: atmospheric pressure at the pipe exit (Pa)
$\Delta F$: head loss along the pipeline (m)
$h_{pump}$: head of the pump (m)

Neglecting the concrete velocity at the reservoir surface, and assuming there is no change in concrete density along the stream, 5.56 equation is simplified to:

$$\left(0 + 0 + \frac{p_{atm}}{\rho g}\right)_{in} = \left(h_2 + \frac{v_2^2}{2g} + \frac{p_{atm}}{\rho g}\right)_{out} + \Delta F - h_{pump} \tag{5.57}$$

$$0 = \left(h_2 + \frac{v_2^2}{2g}\right)_{out} + \Delta F - h_{pump} \tag{5.58}$$

***b.*** Concrete velocity at the pipe exit can be calculated from the known flow rate and the pipe diameter:

$$v_2 = \frac{Q}{A} = \frac{12 \times 10^{-3}}{(\pi/4)(12.7 \times 10^{-2})^2} = 0.94\, m/s$$

***c.*** For the given parameters, the pressure loss per unit length of the pipe from Figure 5.7 is $3.8 \times 10^4$ Pa/m, and the total pressure loss over the pumping length is then $3.8 \times 10^4 \times 10^3 = 3.8 \times 10^7$ Pa. Expressing the pressure loss as a head loss gives:

$$\Delta F = \frac{3.8 \times 10^7}{\rho g} = \frac{3.8 \times 10^7}{2350 \times 9.81} = 1648.33\, m$$

***d.*** Substituting the individual terms and the total pressure loss in equation 5.58, yields:

$$h_{pump} = 1000\, m + \frac{(0.94)^2}{2 \times 9.81} + 1648.33\, m = 2648.37\, m \tag{5.59}$$

With the head pump known, the delivered pump horsepower can be computed:

$$P_{pump} = Q\, \rho\, g\, h_{pump} = 12 \times 10^{-3} \times 2350 \times 9.81 \times 2648.37 = 732.65\, kW = 982.48\, hp$$

As can be deduced from equation 5.59, for the given parameters, the pressure loss is the dominant parameter in determining the pump head, followed by the pumping height. This can change when lower concrete viscosity or larger pipe is used, as presented in Table 5.1.

By repeating the steps detailed above for the same pumping height, but different concrete viscosities, pipe diameters, and discharge rates, the resulting pressure losses and pump horsepower can be arranged in Table 5.1.

***Table 5.1:*** *Total pressure loss computed using the analytical model for different viscosities of concrete and pipe diameters.*

| Viscosity = 20 Pa s | | | | | | | | | | | |
|---|---|---|---|---|---|---|---|---|---|---|---|
| D = 4 in. (102 mm) | | | | | | D = 5 in. (127 mm) | | | | | |
| Q | $V_2$ | Δp | ΔF | $h_p$ | $P_{pump}$ | Q | $V_2$ | Δp | ΔF | $h_p$ | $P_{pump}$ |
| litre/sec | m/s | Pa/m | m | m | kW | litre/sec | m/s | Pa/m | m | m | kW |
| 6 | 0.73 | 30000 | 1301.3 | 2301.3 | 318.3 | 6 | 0.47 | 15000 | 650.7 | 1650.7 | 228.3 |
| 8 | 0.98 | 38000 | 1648.3 | 2648.4 | 488.4 | 8 | 0.63 | 17000 | 737.4 | 1737.4 | 320.4 |
| 10 | 1.22 | 48000 | 2082.1 | 3082.2 | 710.6 | 10 | 0.79 | 22000 | 954.3 | 1954.3 | 450.5 |
| 12 | 1.47 | 57000 | 2472.5 | 3472.6 | 960.7 | 12 | 0.95 | 27000 | 1171.2 | 2171.2 | 600.7 |
| 14 | 1.71 | 66000 | 2862.9 | 3863.1 | 1246.8 | 14 | 1.11 | 30000 | 1301.3 | 2301.4 | 742.8 |
| 16 | 1.96 | 72000 | 3123.2 | 4123.4 | 1520.9 | 16 | 1.26 | 35000 | 1518.2 | 2518.3 | 928.9 |
| 18 | 2.20 | 85000 | 3687.1 | 4687.3 | 1945.1 | 18 | 1.42 | 40000 | 1735.1 | 2735.2 | 1135.0 |
| 20 | 2.45 | 92000 | 3990.7 | 4991.0 | 2301.2 | 20 | 1.58 | 43000 | 1865.2 | 2865.4 | 1321.1 |
| Viscosity = 40 Pa s | | | | | | | | | | | |
| D = 4 in. (102 mm) | | | | | | D = 5 in. (127 mm) | | | | | |
| Q | $V_2$ | Δp | ΔF | $h_p$ | $P_{pump}$ | Q | $V_2$ | Δp | ΔF | $h_p$ | $P_{pump}$ |
| litre/sec | m/s | Pa/m | m | m | kW | litre/sec | m/s | Pa/m | m | m | kW |
| 6 | 0.73 | 40000 | 1735.1 | 2736.9 | 318.3 | 6 | 0.47 | 19000 | 824.2 | 1824.2 | 252.3 |
| 8 | 0.98 | 48000 | 2082.1 | 3085.4 | 488.4 | 8 | 0.63 | 25000 | 1084.4 | 2084.5 | 384.4 |
| 10 | 1.22 | 60000 | 2602.6 | 3607.7 | 710.6 | 10 | 0.79 | 29000 | 1257.9 | 2258.0 | 520.5 |
| 12 | 1.47 | 77000 | 3340.1 | 4347.4 | 960.7 | 12 | 0.95 | 38000 | 1648.3 | 2648.4 | 732.7 |
| 14 | 1.71 | 87000 | 3773.8 | 4783.8 | 1246.8 | 14 | 1.11 | 42000 | 1821.8 | 2821.9 | 910.8 |
| 16 | 1.96 | 95000 | 4120.8 | 5133.9 | 1520.9 | 16 | 1.26 | 48000 | 2082.1 | 3082.2 | 1136.9 |
| 18 | 2.20 | 110000 | 4771.5 | 5788.0 | 1945.1 | 18 | 1.42 | 55000 | 2385.8 | 3385.9 | 1405.0 |
| 20 | 2.45 | 120000 | 5205.3 | 6225.7 | 2301.2 | 20 | 1.58 | 60000 | 2602.6 | 3602.8 | 1661.1 |
| Viscosity = 60 Pa s | | | | | | | | | | | |
| D = 4 in. (102 mm) | | | | | | D = 5 in. (127 mm) | | | | | |
| Q | $V_2$ | Δp | ΔF | $h_p$ | $P_{pump}$ | Q | $V_2$ | Δp | ΔF | $h_p$ | $P_{pump}$ |
| litre/sec | m/s | Pa/m | m | m | kW | litre/sec | m/s | Pa/m | m | m | kW |
| 6 | 0.73 | 48000 | 2082.1 | 3083.9 | 318.3 | 6 | 0.47 | 22000 | 954.3 | 1954.3 | 270.3 |
| 8 | 0.98 | 55000 | 2385.8 | 3389.0 | 488.4 | 8 | 0.63 | 28000 | 1214.6 | 2214.6 | 408.4 |
| 10 | 1.22 | 67000 | 2906.3 | 3911.4 | 710.6 | 10 | 0.79 | 35000 | 1518.2 | 2518.2 | 580.5 |
| 12 | 1.47 | 85000 | 3687.1 | 4694.4 | 960.7 | 12 | 0.95 | 43000 | 1865.2 | 2865.3 | 792.7 |
| 14 | 1.71 | 97000 | 4207.6 | 5217.6 | 1246.8 | 14 | 1.11 | 49000 | 2125.5 | 3125.6 | 1008.8 |
| 16 | 1.96 | 108000 | 4684.8 | 5697.8 | 1520.9 | 16 | 1.26 | 55000 | 2385.8 | 3385.8 | 1248.9 |
| 18 | 2.20 | 126000 | 5465.5 | 6482.1 | 1945.1 | 18 | 1.42 | 63000 | 2732.8 | 3732.9 | 1549.0 |
| 20 | 2.45 | 139000 | 6029.5 | 7049.8 | 2301.2 | 20 | 1.58 | 70000 | 3036.4 | 4036.5 | 1861.1 |
| Viscosity = 80 Pa s | | | | | | | | | | | |
| D = 4 in. (102 mm) | | | | | | D = 5 in. (127 mm) | | | | | |
| Q | $V_2$ | Δp | ΔF | $h_p$ | $P_{pump}$ | Q | $V_2$ | Δp | ΔF | $h_p$ | $P_{pump}$ |
| litre/sec | m/s | Pa/m | m | m | kW | litre/sec | m/s | Pa/m | m | m | kW |
| 6 | 0.73 | 49000 | 2125.5 | 3127.3 | 318.3 | 6 | 0.47 | 24000 | 1041.1 | 2041.1 | 282.3 |
| 8 | 0.98 | 60000 | 2602.6 | 3605.9 | 488.4 | 8 | 0.63 | 30000 | 1301.3 | 2301.3 | 424.4 |
| 10 | 1.22 | 72000 | 3123.2 | 4128.3 | 710.6 | 10 | 0.79 | 37000 | 1605.0 | 2605.0 | 600.5 |
| 12 | 1.47 | 91000 | 3947.3 | 4954.7 | 960.7 | 12 | 0.95 | 46000 | 1995.4 | 2995.4 | 828.7 |
| 14 | 1.71 | 102000 | 4424.5 | 5434.5 | 1246.8 | 14 | 1.11 | 52000 | 2255.6 | 3255.7 | 1050.8 |
| 16 | 1.96 | 115000 | 4988.4 | 6001.4 | 1520.9 | 16 | 1.26 | 59000 | 2559.3 | 3559.3 | 1312.9 |
| 18 | 2.20 | 132000 | 5725.8 | 6742.3 | 1945.1 | 18 | 1.42 | 69000 | 2993.0 | 3993.1 | 1657.0 |
| 20 | 2.45 | 147000 | 6376.5 | 7396.9 | 2301.2 | 20 | 1.58 | 75000 | 3253.3 | 4253.4 | 1961.1 |
| Viscosity = 100 Pa s | | | | | | | | | | | |
| D = 4 in. (102 mm) | | | | | | D = 5 in. (127 mm) | | | | | |
| Q | $V_2$ | Δp | ΔF | $h_p$ | $P_{pump}$ | Q | $V_2$ | Δp | ΔF | $h_p$ | $P_{pump}$ |
| litre/sec | m/s | Pa/m | m | m | kW | litre/sec | m/s | Pa/m | m | m | kW |
| 6 | 0.73 | 51000 | 2212.2 | 3214.1 | 318.3 | 6 | 0.47 | 27000 | 1171.2 | 2171.2 | 300.3 |
| 8 | 0.98 | 63000 | 2732.8 | 3736.0 | 488.4 | 8 | 0.63 | 33000 | 1431.5 | 2431.5 | 448.4 |
| 10 | 1.22 | 76000 | 3296.7 | 4301.8 | 710.6 | 10 | 0.79 | 39000 | 1691.7 | 2691.7 | 620.5 |
| 12 | 1.47 | 97000 | 4207.6 | 5214.9 | 960.7 | 12 | 0.95 | 49000 | 2125.5 | 3125.5 | 864.7 |
| 14 | 1.71 | 107000 | 4641.4 | 5651.4 | 1246.8 | 14 | 1.11 | 56000 | 2429.1 | 3429.2 | 1106.8 |
| 16 | 1.96 | 120000 | 5205.3 | 6218.3 | 1520.9 | 16 | 1.26 | 63000 | 2732.8 | 3732.9 | 1376.9 |
| 18 | 2.20 | 138000 | 5986.1 | 7002.6 | 1945.1 | 18 | 1.42 | 73000 | 3166.5 | 4166.7 | 1729.0 |
| 20 | 2.45 | 150000 | 6506.6 | 7527.0 | 2301.2 | 20 | 1.58 | 79000 | 3426.8 | 4426.9 | 2041.1 |

## 5.12 Summary

In the first part of this chapter, an analytical derivation was described to determine the thickness and viscosity of the lubrication layer by means of tribological and rheological tests.

The different flow zones that form across the pipe section during pumping were analytically characterized. It was found that the boundaries between these zones and their velocity profiles are complex functions of the properties of concrete, the properties of the lubrication layer, and the pipe diameter. Using the velocity profiles, the contribution of each flow zone to the total flow rate across the pipe was determined assuming the Bingham behavior of concrete.

In the second part of this chapter, the effect of the rheological properties of concrete and those of the lubrication layer, and pipe size on pressure loss at different discharge rates were analytically investigated. It was demonstrated that concrete viscosity is a key parameter influencing pressure loss and the properties of the lubrication layer. Pressure loss increases with viscosity of concrete, but is not significantly influenced by yield stress. The effect of concrete viscosity on pressure loss is more pronounced in the range of low viscosity (below 30 Pa s) and high discharge rate.

The correlations between the properties of the lubrication layer and the pressure loss disclosed that the pressure loss increases with viscosity of the lubrication layer, while it decreases with increasing its thickness, for a given discharge rate and concrete viscosity. The analysis also revealed that, for a given pressure loss, the lubrication layer properties are not only interdependent with themselves but also correlated with concrete viscosity. The thickness and viscosity of the lubrication layer increase together. Also, an increase in concrete viscosity results in a decrease in the viscosity of the lubrication layer and an increase in its thickness. This decrease is evident for concrete viscosities below 30 Pa s, but it becomes less significant above this value. Because of their dependency on concrete viscosity, the changes in the lubrication layer properties can yield different effects on the pressure loss. As a result, the final effect is then a function comprising all the effects induced by the lubrication layer and concrete.

It was also found that, for a given discharge rate, increasing the pipe diameter can significantly decrease pressure loss and the thickness of the lubrication layer. Apart from questions of economy, selecting the pipe radius is therefore a matter of the properties of the pumped concrete and the required pumping height.

The analyses showed that, among the studied parameters viscosity is the most influential property on pressure loss followed by the thickness of the lubrication layer and its viscosity. On the other hand, yield stress of both concrete and lubrication layer only show a little influence on pressure loss.

The contour diagrams and 3D plots presented in this chapter provide a clear quantitative and qualitative description of the different parameters governing the pressure loss in pipes. By means of the presented diagrams, pumping pressure loss can be practically computed for a wide range of concrete rheological properties ($\tau_0, \mu_p$) and pipes geometries (L,R).

## 5.13 References

[1] Jacobsen S., Mork J.H., Lee S.F., Haugan L., "Pumping of concrete and mortar, state of the art, COIN Project report 5", Tech. Rep., 2008.

[2] Sakuta M., Kasanu I., Yamane S., Sakamoto A., "Pumpability of fresh concrete", Tokyo, 1989.

[3] Kaplan D., "Pumping of concretes", Ph.D. dissertation, Laboratoire Central des Ponts et Chausées, Paris, 2001.

[4] Feys D., "Interactions between rheological properties and pumping of self-compacting concrete", Ph.D. dissertation, Ghent University, 2009.

[5] Browne R.D., Bamforth P.B., "Tests to establish concrete pumpability", *ACI Journal*, vol. 74, pp. 193 203, 1977.

[6] Ede A.N., "The resistance of concrete pumped through pipelines", *Magazine of Concrete Research*, vol. 1957, no. 9, pp. 129 140,

[7] Macosko C.W., *Rheology principles, measurements and applications*, 10. Vch New-York, 1994.

[8] Ngo T.T., "Influence of concrete compositions on the pumpability parameters", Ph.D. dissertation, Cergy Pontoise, France, 2009.

# Chapter 6

# Pumping Tests

## 6.1 Introduction

This chapter is dedicated to discussing the full-scale pumping tests performed at the laboratory of the Université de Sherbrooke. The first half of this chapter details all aspects of the experimental program, including the circuit design, the mix design of the pumped concrete, and the testing methods that were used during the pumping program. The second half outlines the experimental results, which were submitted to an analytical assessment separated into three parts. In the first part, empirical relationships between pressure loss and the measured rheological and tribological properties of concrete are addressed. In the second part, the results are statistically modeled using multiple regression analysis to enable prediction of pressure loss based on concrete properties. Furthermore, quantitative descriptions of the effects of certain rheological and tribological properties on pressure loss are highlighted. Similar statistical analysis is performed for the V-funnel results, delivering a practical approach to predict pressure loss on job sites. In the third part of this chapter, the effect of pumping on concrete properties, the difference between SCC and CVC in pumping operations, and the development of a new testing apparatus to predict pressure loss on job sites are discussed.

## 6.2 Circuit design

A 30-m closed pumping circuit was installed at the laboratory of the Université de Sherbrooke. It was used to pump 26 concrete mixtures to evaluate the effects of different mix design parameters on pressure loss in two types of pipes. The circuit was constructed in two parts using 4-in. (102 mm) and 5-in. (127 mm) pipes. A schematic representation and a picture of the circuit are presented in Figures 6.1 and 6.2. Segments 2 to 8 of the pumping circuit were built with 4-in. (102 mm) pipes, while segments 10 to 20 were built with 5-in. (127 mm) pipes. The two parts were joined by a reducer (segment 9). Segments 8 and 10 were elbows with radii of 75 and 50 cm, respectively. Segment 9 was a vertical pipe installed at the end of the circuit, which dumped the concrete into the pump reservoir.

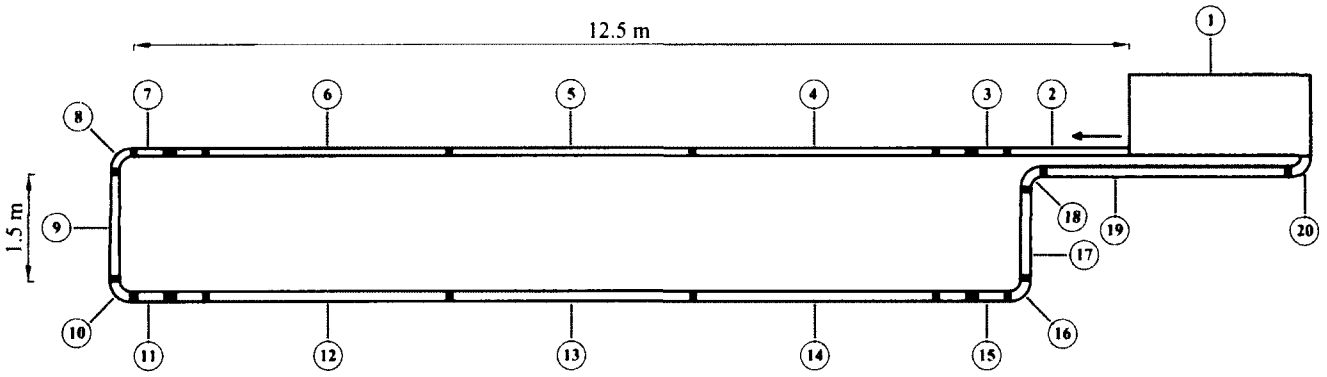


***Figure 6.1:*** *Schematic representation of the pumping circuit (scale 1/00). The pressure sensors are in red.*

Four pressure sensors were installed in the middle of segments 3, 7, 11, and 15, and connected to the data acquisition system so that the variation in pumping pressure could be monitored during testing.

## 6.3 Test setup

### 6.3.1 Concrete pump

Schwing BPL 900 pump: a hydraulic truck-mounted piston pump with a maximum pressure (on the concrete) of 60 bar (6000 kPa) and a maximum output of 90 $m^3/h$ was used. The pump has a 0.75 $m^3$ reservoir and is equipped with two hydraulic cylinders, each with a diameter of 20 cm and a stroke length of 2 m. The cylinders work alternatively: a sudden decrease and increase in both discharge rate and pressure can be recorded at the alternation point, while the discharge is approximately constant during the pushing phase of the cylinder. The pump comes equipped with a remote control, giving the user the option of changing the discharge instantaneously as per requested during testing.

#### Pipes

Standard steel pipe sections of 3 m and 1 m in length with inner diameters of 4 and 5 in. (102 and 127 mm) were assembled to build the pumping circuit. To connect the pipes with different diameters, a straight reducer (segment 9) was used. The similar pipes were connected to each other using adjustable clamps with rubber gaskets to ensure that the connections were watertight (see Figure 6.2).

#### Sampling

A wheelbarrow was used to take samples of concrete from the mixing truck at the arrival. Also, a wheeled container was employed to take samples of concrete after pumping and throughout the discharge calibration process.

## 6.4 Measuring systems

### 6.4.1 Pressure and temperature sensors

Four identical pressure sensors with a maximum capacity of 69 bar and a safety margin of 35 bar were installed in the middle of segments 3, 6, 10, and 13 (see Figure 6.3). The pressure sensors are equipped with a membrane that is connected to a set of strain gauges. The deformation of the membrane is translated into pressure reading. The sensors were connected to a data acquisition system (Vishay System 5000) capable of transforming the measured pressure into supply voltage (in mV) at a frequency of 10 Hz. The distance between the two adjacent pressure sensors was 10.18 m for the small pipes, and 10.01 m for the large pipes. The pressure loss per unit length was obtained by dividing the pressure difference between two adjacent sensors by the corresponding

***Figure 6.2:*** *Pumping circuit (top); pump reservoir (bottom left); and a clamp connecting two 5-in. (127 mm) pipes (bottom right).*

distance. Temperature sensors, coupled with each pressure sensor and using the same acquisition software, were installed to monitor the temperature changes during pumping.

***Figure 6.3:*** *Pressure sensor and strain gauges installed at the same location on the pipe wall.*

### 6.4.2 Strain gauges

In order to measure the deformation of the pipes under pressure, two strain gauges were glued to the outer surface of the pipes using the same layout as the pressure sensors (Figure 6.3). Since it is proven that the deformation of the pipe under pressure is well related to the applied pressure [1], the strain gauges can serve as a redundant measuring system of pressure loss in case the pressure sensors malfunction. The pressure loss then can be reproduced from the correlation between the deformation of the pipes under pressure and the pressure measured by the sensors (when they were working).

Unfortunately, all pressure sensors were broken at an early phase (at 1/3-1/2) in the experimental program, most likely as a result of the pressure surges they received during testing. Consequently, the pressure measurements later relied on the strain gauges using the approach described above. The average strain of each coupled gauges was correlated with the results of the corresponding sensor delivering the calibration formula for the strain gauges. The average strain was considered to reduce the fluctuations in the measurements, created by variations in pipe thickness, alignment, installation of the strain gauges, etc. It is noteworthy that some of the strain gauges displayed abnormal measurements. This can be attributed to the lateral movement of the circuit under the stroke of the pump. Such deviated results were excluded from the analysis.

### 6.4.3 Discharge control

The pump operating system was equipped with a discharge controller allowing changes in the discharge as required during testing. In virtue of the pump specifications, the theoretical volume of concrete discharged with each stroke of the pump was known. Hence, the discharge was calculated by dividing the total volume of concrete pumped with a certain number of strokes by the elapsed time. The number of strokes was clearly audible, and the elapsed time was measured with a stopwatch.

Another approach for measuring the time was provided by the pressure-time relationship registered by the acquisition system (Figure 6.4). As a result, the discharge could be determined using two different approaches and, in fact, both coincided nicely throughout the experimental program.

The discharge calculations at this stage was based on two assumptions: first, that the pump cylinders are completely filled with concrete, and second, that the pump provides a constant discharge during a stroke (Figure 6.5).

In fact, both of these assumptions were inaccurate and needed to be corrected. Practical experience has shown that the pump cylinders are not completely filled [2], and the discharge rates varies during the pump stroke from a maximum to a minimum peak resulting in a variable discharge rate, as displayed in Figure 6.4.

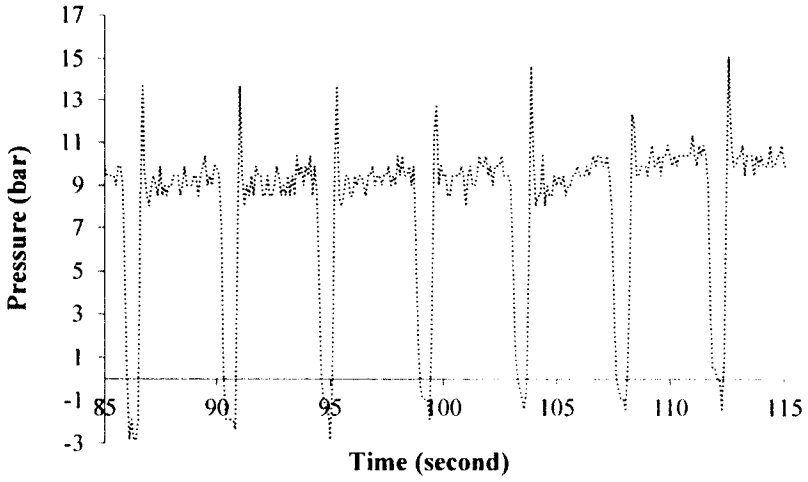


***Figure 6.4:*** *Concrete pressure during several pump strokes (1 bar = 100 kPa)*

### 6.4.4 Discharge calibration

In order to correct the inaccurate assumptions of the discharge rate calculation method, calibration tests were executed with the goal of bridging the gap between the calculated theoretical discharge rates and the actual discharge rates of the pump. One test was performed for each concrete delivering a relationship between the calculated and actual discharge rates. The obtained relationship was then employed to calculate the actual discharge rate for a certain concrete at any testing stage.

The calibration tests were executed using a sampling reservoir connected to a load measuring cell (with a frequency of 10 measurements per second) to measure the weight

of concrete exiting the pipe and entering the reservoir. Using the load cell to measure the weight variations, and the stopwatch (or the acquisition system) to measure the time, a precise idea of the mass flowing through the circuit, per stroke, was ascertained. Once the density and weight of the concrete have been measured, the initial data were converted to an accurate measurement of the volume variation with time. The calibration tests were repeated for several discharge rates for each concrete mixture. As a result, relationships between the actual and measured discharge rates were established and used to correct the initial discharge rates measured through different testing stages (Figure 6.6).

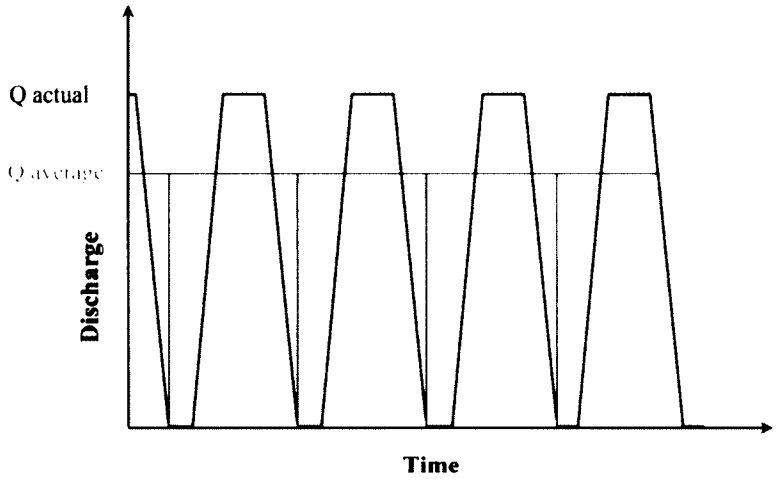


***Figure 6.5:*** *Assumed discharge rate (red curve) and actual discharge rate (black curve) during pumping tests. Adapted from [1].*

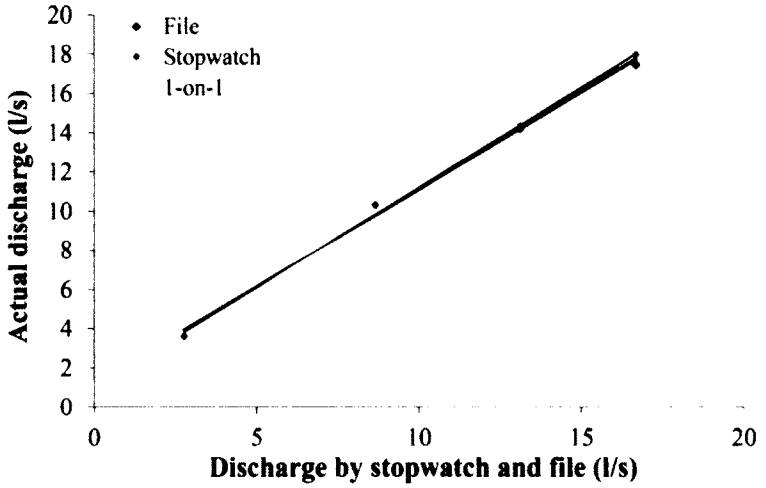


***Figure 6.6:*** *Illustrative example of the relationship between the actual discharge rates and the discharge rates measured using the load cell and stopwatch (black), and the data system (red). Grey line is 1-on-1 relationship assuming the complete filling of the cylinders.*

## 6.5 Cleaning

Cleaning with compressed air was the method of choice in this project as it is the most used in pumping applications. The cleaning procedure began by inserting a sponge ball driven by pressurized air in the pipes near the pump. As it moved further through the pipes, the sponge ball accelerated as the amount of concrete decreased. Therefore, for safety purposes the pressurized air was removed when the sponge reached two thirds of the total length of the circuit. Once the sponge left the circuit, all pipes, rubber gaskets, clamps, test equipment, and reservoirs, were dismantled and cleaned with water for the next use. A tight cloth, when needed, was pushed through the pipes by a rod to ensure the complete removal of any residual cement paste.

## 6.6 Mix design

Twenty six concrete mixtures including SCC, HWC, and CVC, were tested in the pumping circuit. Considering the future application of this research, SCC and HWC were the main focus, whereas the three CVC mixtures served only a comparative purpose. The tested mixtures cover a wide range of the most influential mix design parameters including *w/cm*, binder content, paste volume, slump flow consistency, and S/A. The complete mix designs and compositions are presented in Tables B.15 and B.16.

The SCC and HWC mix design parameters fall in the area of high-strength, highly flowable concrete within a slump flow range of 350-850 mm. As presented in Tables B.15 and B.16, *w/cm* varied between 0.22 and 0.34, and the S/A from 0.47 to 0.53. The binder content changed from 435 to 680 kg/m$^3$, and the paste volume from 358.5 to 407.5 l/m$^3$. A blend of two types of limestone aggregates with MSAs of 10 mm and 20 mm were used in different proportion depending on the S/A in question.

A local sand with a maximum particle size of 5 mm was used in all mixtures. The initial slump flow of SCC and HWC mixtures ranged from 410 to 815 mm, while the slump of the CVC mixtures from 180 to 235 mm. A combination of GU+25% Class C fly ash was used for SCC6, whereas the binder used for the remaining mixtures was a ready blend of GU+8% silica fume (except SCC5). Two commercially available polycarboxylate-based HRWRAs were used: Plastol 6200 and Plastol 5000. The foreseen quantity of the first HRWRA (Plastol 6200) was added at the concrete plant during mixing, while the second HRWRA (Plastol 5000) was added upon the arrival of the mixing truck, as needed. All mixtures were mixed at a local concrete plant in Sherbrooke (Demix Béton) and were received in a mixing truck 30-45 min after water-cement contact time.

## 6.7 Testing procedure

In total, 26 concrete mixtures were tested in the pumping circuit. In every case, the initial slump/slump flow test was performed upon the arrival of the concrete truck. Following this test, slump/slump flow was adjusted by adding the appropriate quantity of HRWRA in the mixing truck. Mixing continued for two minutes and slump/slump flow was measured again. Prior to initiating the testing program, the pipes were lubricated by

pumping a cement paste which was prepared separately using the Type GU cement. Lubricating the pipes was essential to avoid any paste reduction when introducing the virgin concrete. Upon completion of the lubrication, the mixing truck unloaded the concrete into the pump reservoir, and it was pumped through the circuit at a low discharge rate of 4 l/s to avoid any start-up blockage. Afterward, the concrete underwent a pumping cycle of 6-8 different discharge rates carried out in descending order. The range of the applied discharge rates varied from 1-18 l/s. Each rate was held constant for five strokes in order to provide stable pressure loss measurements. The number of strokes was reduced to 2-4 strokes, in the case of low discharge rates (below 4 l/s) to avoid excessive pumping time. The entire cycle was repeated five times, with an interval of 30 minutes between consecutive cycles. By so doing, the changes in concrete properties due to pumping over time could be investigated.

The concrete was kept at rest in the pipes between consecutive pumping cycles, and therefore a pre-pumping stage was needed to eliminate any thixotropic behavior before testing was restarted. At all testing stages, the pressure loss in the pipes was monitored by the pressure sensors (initially) and strain gauges.

Fresh properties tests involving, slump/slump-flow, V-funnel, L-box (when applicable), air content, and static segregation, were executed for non-pumped and pumped samples. Equally, the rheological and tribological properties of the concrete were determined for both types of samples.

The pumped samples were taken from the concrete falling directly out of the pipes into a special container (described in section 6.3.1) at the end of each pumping cycle. The samples of the non-pumped concrete were taken from another container filled with virgin concrete (after being accepted) from the mixing truck. The non-pumped concrete was kept at rest over the testing time, except when taking samples, a hand-mixing was applied to reduce the thixotropic effect within the concrete and facilitate the fresh properties testing.

## 6.8 Concrete testing

### 6.8.1 Rheology

The rheological properties of the tested mixtures were preliminarily measured with the ICAR rheometer and further corrected through a special procedure, as detailed in section 3.9. A description of the ICAR rheometer and its functionality are presented in section 3.8.2.

The testing procedure developed for the ICAR rheometer started by pre-shearing the concrete sample for 20 seconds at maximum rotational velocity (0.5 rps) to eliminate the effect of thixotropy on the measurements. The pre-shearing period was followed by a decrease in rotational velocity from 0.50 to 0.025 rps through 7 five-second increments. At each step, the velocity (N) and the corresponding torque (T) were registered and only then was the T-N relationship established. After excluding all data points that were deviated or not in equilibrium, the slope and interception of the T-N relationship (known as the G and H parameters) were obtained and transformed using the Reiner-Riwlin equation to obtain the plastic viscosity and yield stress. Plug flow was verified by

comparing the shear stress at the most outer point in the rheometer gap ($R_o$) with the yield stress of concrete. A shear stress value at $R_o$ lower than the yield stress of concrete was an indication of plug flow. A special iterative procedure was then used to correct the measurements and recalculate the rheological properties.

A comparative study between the ICAR and ConTec rheometers of the Université de Sherbrooke found that the ICAR rheometer underestimates viscosity, and in some cases, overestimates yield stress. Given the better accuracy of the ConTec rheometer, ICAR measurements were transformed into equivalent ConTec measurements by means of a correlation established between the rheological properties of a wide range of concrete mixtures measured in both rheometers (see section 3.9 for further details).

### 6.8.2 Tribology

A new Tribometer developed at the Université de Sherbrooke was used to assess the tribological properties of the tested mixtures. The tribometer geometry, working principle, data treatment, and testing procedure, are described in detail in the following sections.

#### Development of the UdS tribometer (2012)

The UdS tribometer is based on the Tattersall Mk-III rheometer as a modified version of the Ngo tribometer [3] (see Figure 6.7). The planetary motion of the impeller is removed and the H-impeller is replaced by a smooth steel cylinder that can rotate centrally at different velocities in a cylindrical reservoir. The inner cylinder is connected to a measuring cell that measures the corresponding torque. The diameters of the outer and inner cylinders are 237 mm and 125 mm, respectively, while their heights are 200 mm and 260 mm, respectively. The head of the inner cylinder is cone-shaped (with a height of 50 mm and an angle of 38.7°) to facilitate the penetration into the concrete. The clearance between the cone and the bottom of the reservoir is 5 mm, which is very low. The tribometer is connected to a computer through which the testing velocities and other testing parameters can be defined.

#### Testing procedure

The testing procedure started by pre-shearing the sample for 30 seconds at the maximum rotational velocity (of 0.9 rps) to eliminate the effect of thixotropy and form the lubrication layer near the rotating cylinder. The pre-shearing stage was followed by a 10-step regime decreasing rotational velocity from 0.90 to 0.015 rps. During each step, the rotational velocity was held constant for 5 seconds, while the corresponding torque was registered. The measured data including the imposed velocities (N) and the corresponding torques (T) were registered by the tribometer's computer for further data analysis.

#### Data treatment

The raw data were extracted from the tribometer and the torque was averaged at each of the ten different rotational velocity steps. The measured torque values were corrected by eliminating the side effect of the cone-shaped head of the inner cylinder, as detailed

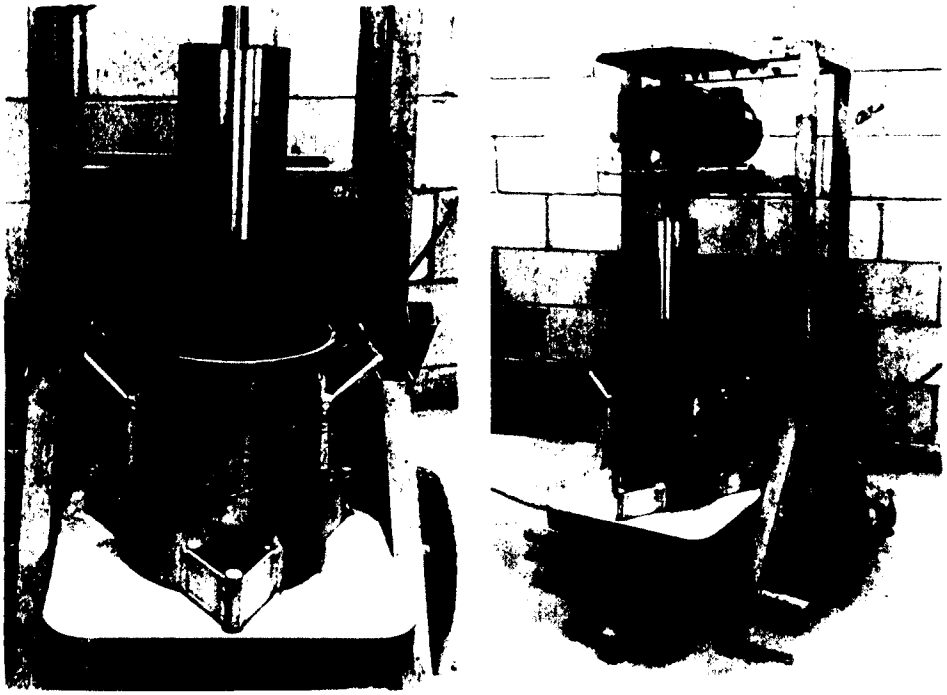

***Figure 6.7:*** *Tribometer developed at the Université de Sherbrooke (2012).*

in the following section. The correlation between the corrected torque and velocity was used to determine the tribological properties of concrete, as discussed at length in section 5.7.

### Effect of the cone

During testing, the cone-shaped head of the inner cylinder creates some disturbance in the flow at the level of the cone head. Several attempts were preliminarily made to eliminate this side effect. The first attempt comprised testing of nine concrete mixtures, with different rheological properties, at six different filling heights in the tribometer. A relationship was then established between the filling heights and the corresponding torques. By extrapolating and plotting this relationship, the side effect of the cone graphically corresponds to the intercept with the torque axis (at 0 filling height). Although this procedure is theoretically the best one (Macosko, 1994) [4], it did not deliver consistent results. The second attempt was made by measuring the corresponding torque only at the lowest filling height. Ideally, the filling height of the vertical part of the inner cylinder was 0 cm, indicating that only the cone-shaped head was submerged in the concrete. In special cases, when the filling height exceeded the cone height by 1 cm, the torque was corrected by taking the ratio of the contact surface of the cone to the sum of the total contact surface of the cone and the submerged part of the inner cylinder. The rotational velocity decreased in six steps from 0.9 to 0.1 rps for each tested concrete. The results at the two lowest rotational velocities showed doubtful accuracy due to the low torque registered; therefore, the four steps at the highest rotational velocities (from 0.3 to 0.9 rps) were only used to determine the influence of the cone.

The test results demonstrated that the measured torque is a function of the imposed

rotational velocity and the concrete viscosity, as presented in Figure 6.8. A clear distinction could be made for the tested mixture based on their viscosities (measured with the ConTec Viscometer 5).

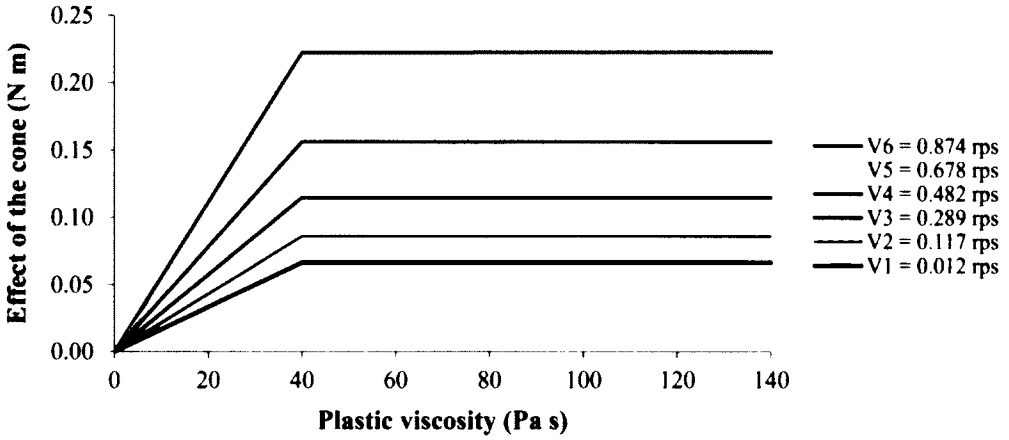


***Figure 6.8:*** *The cone effect of the inner cylinder as a function of the viscosity and rotational velocity. Perez-Schell A. et al. (2012).*

As a result, the correction procedure yielded two equations for the torque, equation 6.1 for concrete mixtures with plastic viscosity ($\mu_p$) within the range of 40-140 Pa s, and equation 6.2 for concrete mixtures with plastic viscosity lower than 40 Pa s. As indicated in equation 6.2, for concrete mixtures with plastic viscosity lower than 40 Pa s, the torque was shown to evolve linearly from zero at (theoretical) zero plastic viscosity to the value obtained at 40 Pa s plastic viscosity for each rotational velocity.

$$T_{cone} = \left(5.38 \times 10^{-4}\mu_p + 1.32 \times 10^{-1}\right) N + \left(4.28 \times 10^{-4}\mu_p + 4.41 \times 10^{-2}\right) \tag{6.1}$$

$$T_{cone} = 1.54 \times 10^{-1}\frac{\mu_p}{40}N + 6.12 \times 10^{-2}\frac{\mu_p}{40} \tag{6.2}$$

To conclude, the side effect generated by the cone can be eliminated through a correction procedure depending on concrete viscosity and the imposed rotational velocity. The corrected torque values can be used then for further analysis to determine the different tribological properties of concrete. Although the cone correction process is approximate and not straightforward, it is essential to perform the correction as the effect of the cone shows a sizable influence on the measured torque values.

### Tribological parameters

Several tribological parameters were derived from the tribology test, as discussed in section 5.7. The relationship between the velocity of the cylinder ($V_{tot}$) and the shear stress was established. The nature of this relationship, referred to as $Itrib_{tot}$, is such that it can be used to evaluate the total flow resistance of concrete. Also, the velocity of the lubrication layer ($V_{ll}$) was determined and correlated with the shear stress. The slope of this relationship, referred to as $Itrib_{ll}$, was used to evaluate the contribution

of the lubrication layer to the concrete flow in the tribometer. The final correlation to consider was the difference between $V_{tot}$ and $V_{ll}$ (denoted as $V_{co}$) and its relationship with shear stress. The slope of this relationship, referred to as $Itrib_{tot}$, was used to describe the flow resistance of the sheared concrete section in the tribometer gap. Further details concerning the tribological parameters and their mathematical derivations are available in section 5.7.

### 6.8.3 Assessment of the fresh properties

The fresh properties of the pumped mixtures were assessed using slump/slump-flow, air content, V-funnel, L-box, and static segregation tests (if applicable). Greater details concerning these test methods are presented in section 7.3.1. The pumped concrete samples were taken at the end of each pumping cycle, and the non-pumped concrete samples were taken from the mixture before being pumped.

Both types of samples were kept under 100% humidity condition at laboratory temperature of 23 ± 2 °C and tested for compressive strength at 7 and 28 days. The fresh properties of all tested mixtures are presented in Tables B.17-B.20, while the compressive strength results are presented in Table B.24.

## 6.9 Pressure loss data treatment

As mentioned previously, after the pressure sensors were broken, the pressure loss measurement later relied on the strain gauges. Although the average strain was considered to reduce the fluctuations in the measurements created by variations in pipe thickness, alignment, installation of the strain gauges, etc., some measurements were affected by a certain error in the strain gauges (as in SCC14 for example). Some of these errors can be attributed to the lateral movement of the circuit caused by the stroke of the pump.

Apart from the measuring system, certain concrete mixtures exhibited a considerable reduction in stability under pumping pressure (SCC5 for example), which in certain cases led to unreliable pressure loss measurements. Based on the above considerations, all deviated measurements and scattered data points were excluded from the analysis presented in the following sections. The raw data of the pressure loss presented can be found in Appendix C, and the excluded measurements of the pressure loss are presented in Tables B.25-B.28.

As mentioned before, during each pumping cycle the concrete was pumped at 6-8 different discharge rates. The range of the applied discharge rates varied from 1-18 l/s. Each rate was held constant for a certain number of strokes to provide stable pressure loss measurements. An example of the correlation between the pressure loss and discharge rate is presented in Figure 6.9. Since the discharge rate was controlled manually during testing, the applied discharge rates varied slightly from one pumping cycle to another, as shown in Figure 6.9. For the sake of simplicity, five discharge rates: 4, 8, 12, 16, and 20 l/s, were selected from the pressure loss-discharge rate relationship for each pumping test. In this way, with an acceptable approximation, the different fixed discharge rates could be easily compared through the results discussion and analysis. Note that the 20 l/s discharge was not attained during pumping tests but was obtained by extrapolating

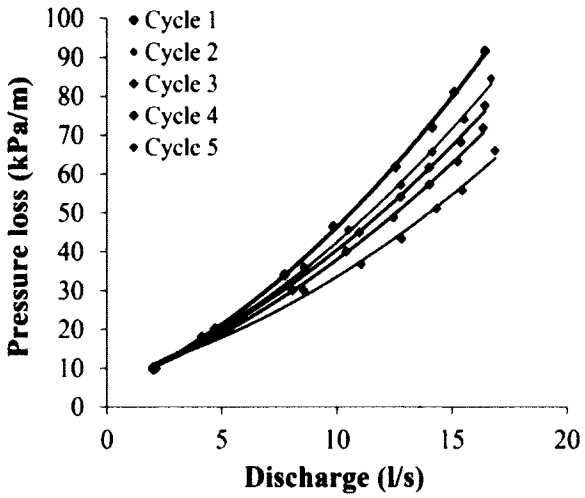


***Figure 6.9:*** *Relationship between pressure loss (in 4-in. pipes) and discharge rate at different pumping cycles of SCC4.*

the relationship between the tested discharge rates and pressure loss. The pressure loss corresponding to the fixed discharge rates are presented in Tables B.25-B.28, and the measured pressure loss and discharge rates are listed in Appendix C.

## 6.10 Test Results

The following data analyses consider different correlations obtained between the pressure loss and various properties of the tested mixtures. In order for the forthcoming statements to be true, it is necessary to make two assumptions at this stage. The first is that the properties of concrete do not change during the testing time of a given pumping cycle. The second is that concrete properties in the pipes under pressure are identical to those measured on concrete exiting the pipes at the end of each pumping cycle. When reading the following analyses, the pressure loss per unit length of pipe is referred to as 'pressure loss' unless otherwise stated.

### 6.10.1 Rheological properties and pressure loss

In this section the rheological properties represented by viscosity and yield stress are empirically correlated with the pressure loss of pumped concrete at different discharge rates, for the two types of pipes used in the experimental program.

#### Viscosity

The viscosities of the pumped SCC and HWC mixtures (measured at the end of each pumping cycle) are plotted versus their corresponding pressure losses at different discharge rates, as indicated in Figure 6.10. The pressure loss significantly increases with viscosity for both types of pipes at a given discharge rate, an effect amplified by increasing the discharge rate (Figure 6.10). For example, increasing viscosity by 30 Pa s can increase the pressure loss by 29% at a discharge rate of 8 l/s for 5-in. (127 mm) pipes.

For the same increase in viscosity at a higher discharge rate of 16 l/s, the pressure loss increases by 49%. This can be attributed to the increased viscous dissipation and interparticle friction [5, 6], leading to higher flow resistance and thus higher pressure loss. The obtained correlation between pressure loss and viscosity is in good agreement with a previous study conducted on SCC by Feys in 2009 [1]. However, the correlations presented in the literature [1] slightly under estimate the pressure loss for a given viscosity compared to those presented in Figure 6.10.

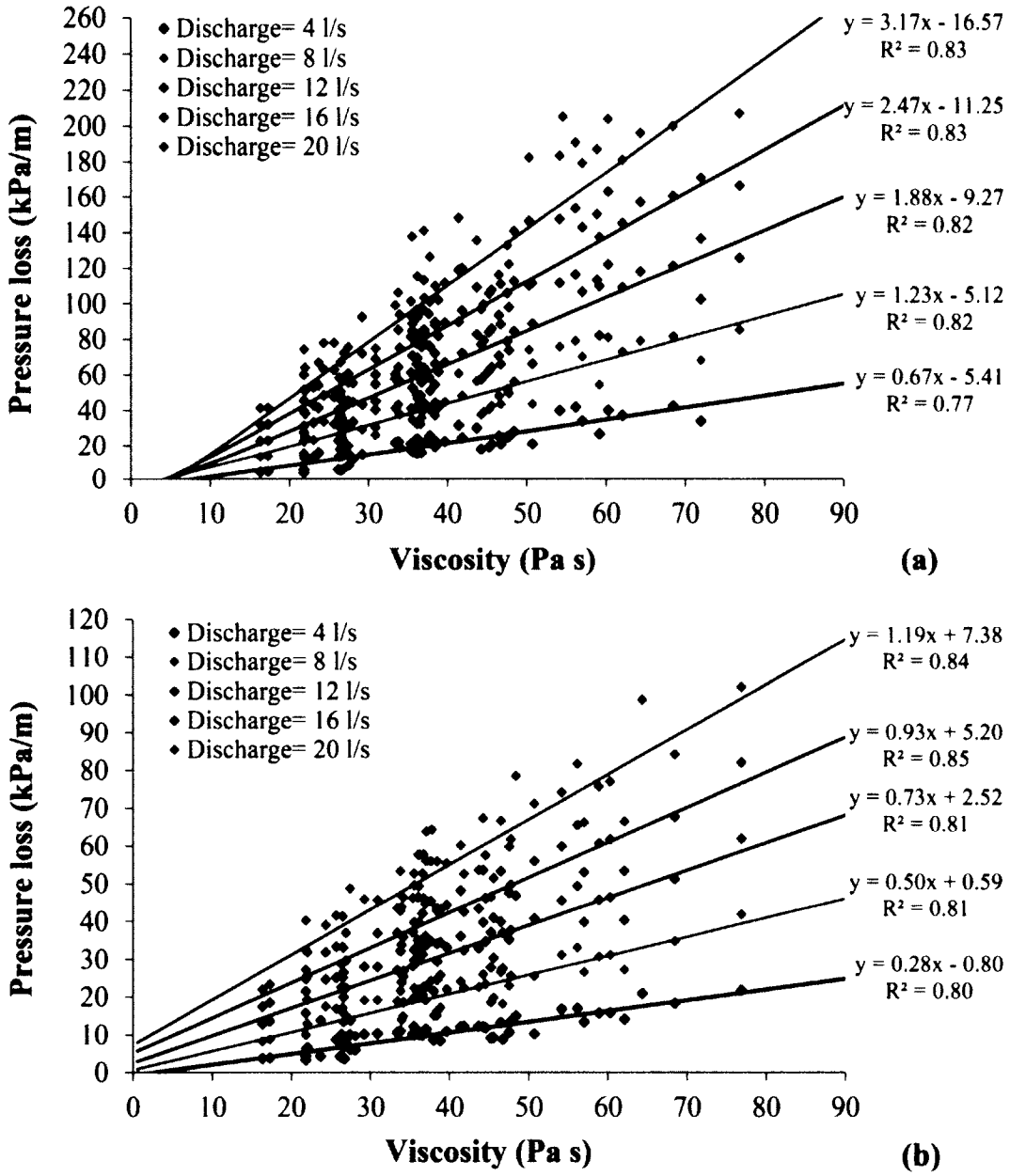


***Figure 6.10:*** *Relationship between viscosity and pressure loss for SCC and HWC mixtures at different discharge rates using (a) 4-in. (102 mm) pipes, and (b) 5-in. (127 mm) pipes.*

The empirical correlations (displayed in Figures 6.10a and 6.10b) coincide well with

the analytical correlations between viscosity and pressure loss (section 5.11.1). In both approaches, viscosity increases with pressure loss at a given discharge rate. On the other hand, a slight overestimation of the pressure loss by the analytical correlation can be reported in most cases. For example, the pressure loss reading in 5-in. (127 mm) pipes for a concrete viscosity of 40 Pa s and a discharge rate of 16 l/s is 43 kPa/m from the empirical correlation (Figure 6.10a), in contrast to 48 kPa/m from the analytical model for given lubrication layer properties (Table 5.1). This difference can be justified by the non-linear relationship between the pressure loss and viscosity in the analytical study, especially at high discharge rates.

Comparing Figures 6.10a and 6.10b signifies the influence of the pipe diameter on pressure loss. For a given viscosity and discharge rate, pressure loss can be reduced by more than 50% by increasing the pipe diameter by 1 in. (25.4 mm) from 5 in. to 4 in.. This can be rationalized by the theory that increasing the pipe diameter reduces the flow velocity, resulting in lower energy dissipation and consequently lower pressure loss. From a different angle, the stability of the pumped mixture is another parameter to consider when selecting the pipe size as the risk of segregation or phase separation increases by increasing the flow velocity or reducing the pipe diameter.

Unsurprisingly, in CVC, unlike SCC and HWC, pressure loss exhibits a weak dependency on viscosity. Because the flow pattern of CVC is such that the concrete remains unsheared, the effect of yield stress dwarfs that of viscosity.

### Yield stress

Figures 6.11a and 6.11b present pressure loss as a function of yield stress at different discharge rates for various mixtures investigated throughout the experimental program. Relative to viscosity, yield stress does not exhibit a significant influence on pressure loss in SCC and HWC. Nevertheless, increasing yield stress will likely increase pressure loss slightly at a given discharge rate. This observation is consistent with the results of the analytical correlation between pressure loss and yield stress (section 5.11.1) for highly-flowable concrete. Physically, the weak correlation between yield stress and pressure loss can be explained by the relatively low yield stress of SCC and HWC. It is this physical characteristic that causes the concrete section to be sheared across the pipe, allowing viscosity rather than yield stress to govern the displacement.

Relative to the literature on the subject [1], this investigation was not able to find a substantial correlation between the yield stress and pressure loss through either the analytical model or the experimental program.

In CVC, unlike in SCC and HWC, yield stress greatly influences pressure loss, as depicted in Figure 6.11b. This is justified by the relatively high yield stress of CVC which results in a large section of unsheared concrete across the pipe. Consequently, the energy needed to initiate movement of the concrete along the pipes is primarily governed by yield stress. The firm correlation obtained between yield stress and pressure loss are in agreement with the previous findings of Kaplan [2]. It should be noted here that only three CVC mixtures were tested in this phase, and that the number of data points are insufficient to make further statements for CVC at this stage of the pumping operation.

To conclude, the flow patterns of CVC and both SCC and HWC reflect the different relationships between the rheological properties of concrete and pressure loss. The most

influential parameter on pressure loss is viscosity in SCC and HWC, and yield stress in CVC.

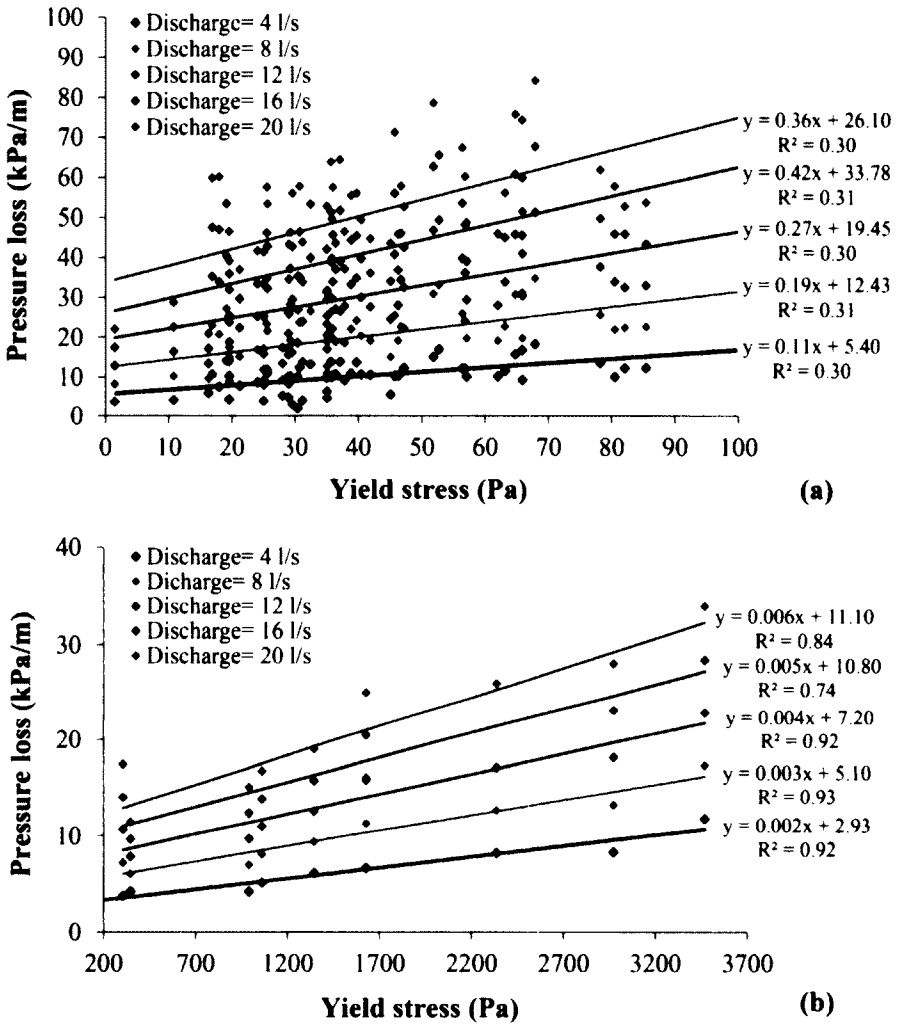


***Figure 6.11:*** *Relationship between yield stress and pressure loss at different discharge rates using 5-in. (127 mm) pipes for (a) SCC and HWC mixtures, and (b) CVC mixtures.*

## 6.10.2 Tribological properties of concrete and pressure loss

To best illustrate the influence of tribological properties on pressure loss, Figures 6.12 and 6.13 present pressure loss at different discharge rates as a function of $Itrib_{II}$, $Itrib_{co}$, and $Itrib_{tot}$ of the concrete (see section 5.7 for definition). The figures display cogent correlations between the tribological properties and pressure loss at different discharge rates. In the case of SCC and HWC, the pressure loss increases with $Itrib_{II}$, as indicated in Figure 6.12a. Since $Itrib_{II}$ is a product of the viscosity-to-thickness ratio of the lubrication layer, an increase in $Itrib_{II}$ can be attributed to an increase in viscosity (and/or) a reduction in thickness. In either case, the pressure loss will increase as proven by the analytical model detailed in section 5.11.2.

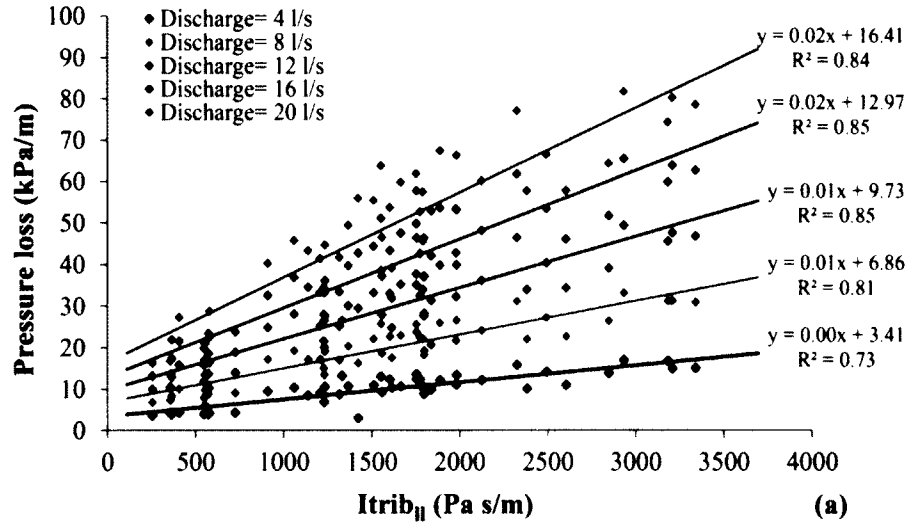


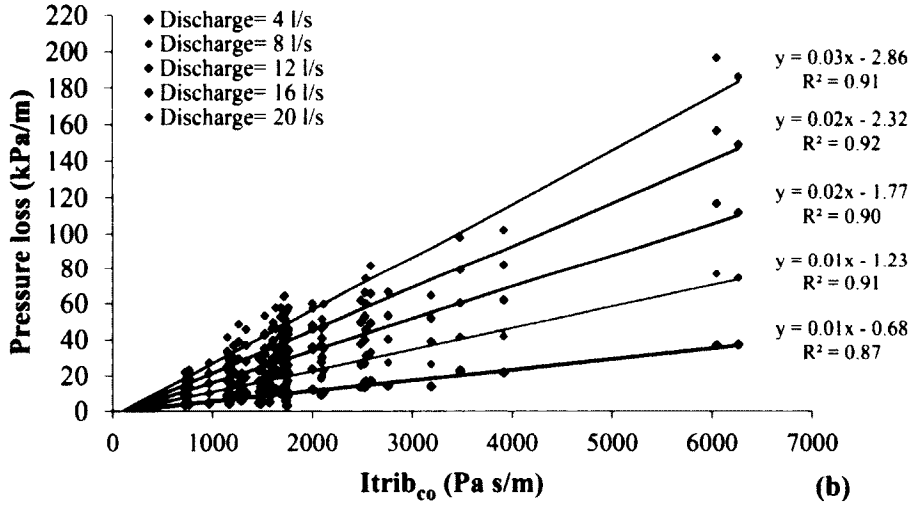


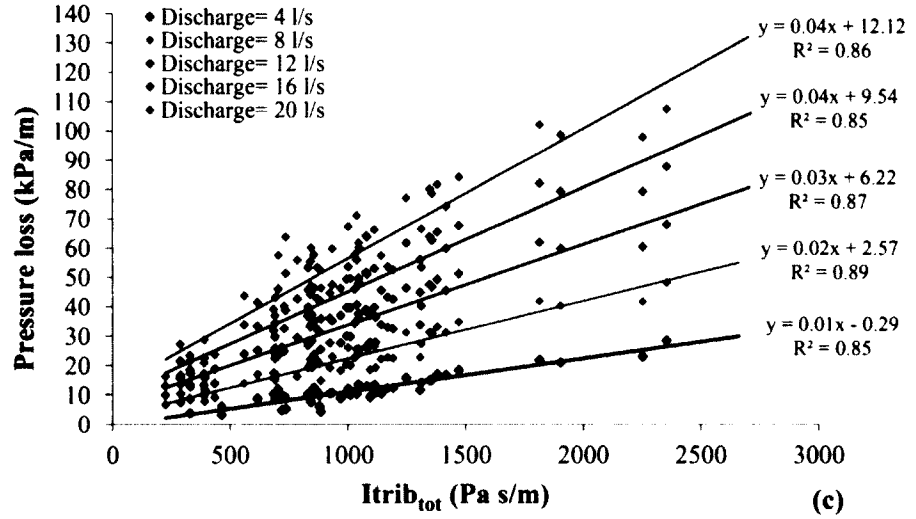


***Figure 6.12:*** *Relationship between pressure loss and (a) $Itrib_{ll}$, (b) $Itrib_{co}$, and (c) $Itrib_{tot}$, at different discharge rates using 5-in. (127 mm) pipes for SCC and HWC mixtures.*

Similarly to increasing $Itrib_{ll}$, increasing $Itrib_{co}$ increases pressure loss (Figure 6.12b), which can be justified in light of the strong relationship between viscosity and $Itrib_{co}$, as described earlier in equation 5.20. In essence then, an increase in $Itrib_{co}$ can be translated into an increase in concrete viscosity, leading to a higher pressure loss.

Lastly, Figure 6.12c demonstrates a strong correlation between $Itrib_{tot}$ and pressure loss. As $Itrib_{tot}$ comprises both the effects of the sheared concrete section and lubrication layer, an increase in $Itrib_{tot}$ can be related to an increase in the flow resistance of either concrete or the lubrication layer. For example, in concrete, as in the lubrication layer, increasing viscosity increases flow resistance and thus pressure loss (sections 5.11.1 and 5.11.2).

The scenario changes in CVC due to its low dependency on viscosity, which is translated into a weak correlation between $Itrib_{co}$ and pressure loss. On the other hand, solid correlations are obtained between both $Itrib_{ll}$ and $Itrib_{tot}$ and pressure loss (Figures 6.13a and 6.13b).

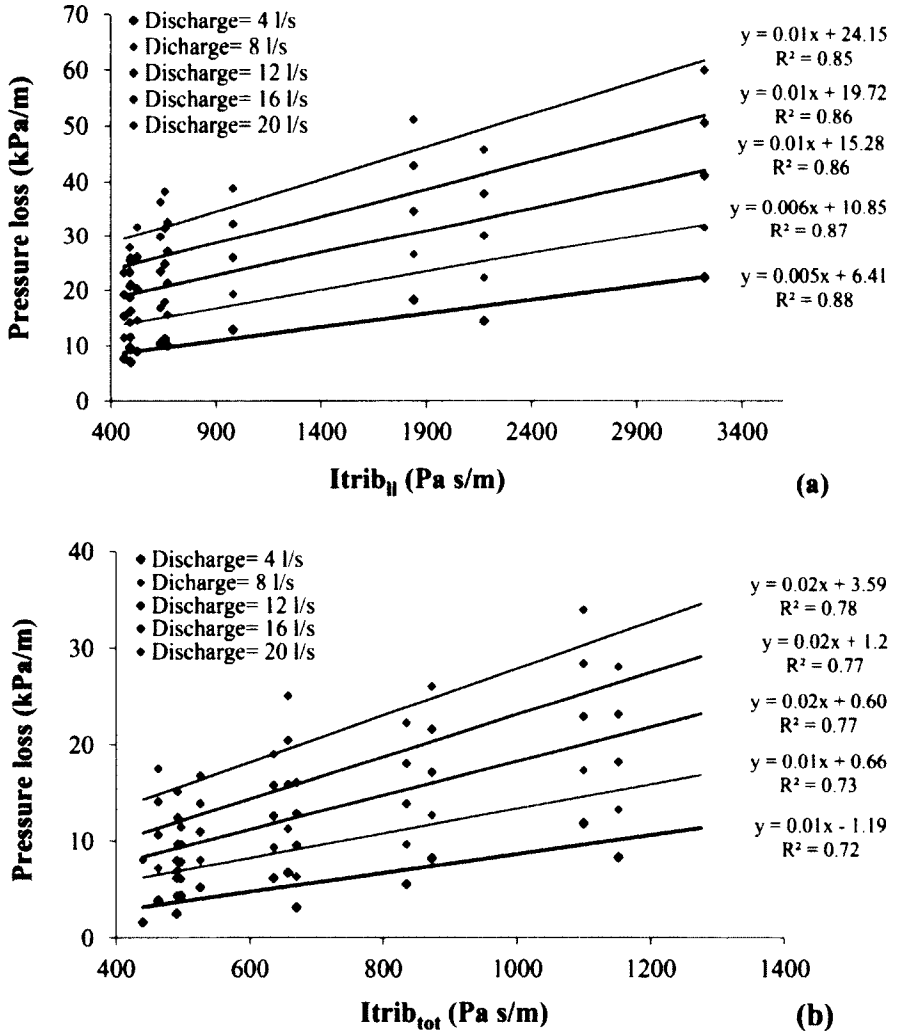


***Figure 6.13:*** *Relationship between pressure loss and (a) $Itrib_{ll}$, and (b) $Itrib_{tot}$, at different discharge rate using 5-in. (127 mm) pipes for CVC mixtures.*

An increase in $Itrib_{ll}$ or $Itrib_{tot}$ results in an increase in pressure loss. Knowing that

the concrete section is not sheared, this phenomenon can only be explained by either an increase in the flow resistance of the lubrication layer or a drastic increase in yield stress of the concrete.

To conclude, for SCC and HWC, all three tribological parameters demonstrate firm correlations with pressure loss. $Itrib_{co}$ (which is a function of concrete viscosity) showed slightly a higher coefficient of determination ($R^2$) than the $Itrib_{ll}$ and $Itrib_{tot}$. In the case of CVC, strong correlations are obtained between only $Itrib_{ll}$ and $Itrib_{tot}$, and pressure loss, whereas a weak relationship exists between $Itrib_{co}$ and pressure loss. Since $Itrib_{co}$ and $Itrib_{ll}$ present the unique contribution of the concrete and lubrication layer on concrete flow resistance, the effect of the lubrication layer and concrete on pressure loss can be assessed independently by means of Figures 6.12a and 6.12b. In addition, the influence of different mix design parameters on the tribological properties can be optimized to minimize the pressure loss. Further investigations concerning this matter are discussed in detail in Chapter 7.

### 6.10.3 Fresh properties of concrete and pressure loss

As established in the preceding sections, the rheological properties of concrete are key parameters that determine pumping pressure loss. Equally, the same properties govern to a significant extent the fresh properties of concrete. From this perspective, the goal of the following sections is to establish correlations between the fresh properties and pressure loss. As a consequence of these correlations, simple test methods, typically used to assess the fresh properties of concrete, will be employed as satisfactory measurements to estimate the pressure loss.

#### V-funnel

The flow time measured in the V-funnel tests (of SCC and HWC mixtures) reveals a strong relationship with pressure loss, as presented in Figure 6.14. The pressure loss increases as V-funnel time increases for a given discharge rate. This correlation can be justified in view of the good relationships between the V-funnel time and viscosity and tribological properties of concrete. As shown in Figure 6.15a, an increase in the V-funnel time indicates an increase in the viscosity, resulting in an increase in the pressure loss.

From a different aspect, the increase in the pressure loss with the V-funnel time can be justified by the positive correlations between the V-funnel and the tribological parameters $Itrib_{ll}$, $Itrib_{co}$, and $Itrib_{tot}$ (Figure 6.15). An increase in the V-funnel time can be translated into an increase in $Itrib_{ll}$, $Itrib_{co}$, or $Itrib_{tot}$, which in turn leads to an increase in the pressure loss, as pointed out in the previous section.

As a result, the solid correlation between pressure loss and V-funnel time validates the use of the V-funnel test as substitute to a complex rheological or tribological measurements for the estimation of the pressure loss on job sites.

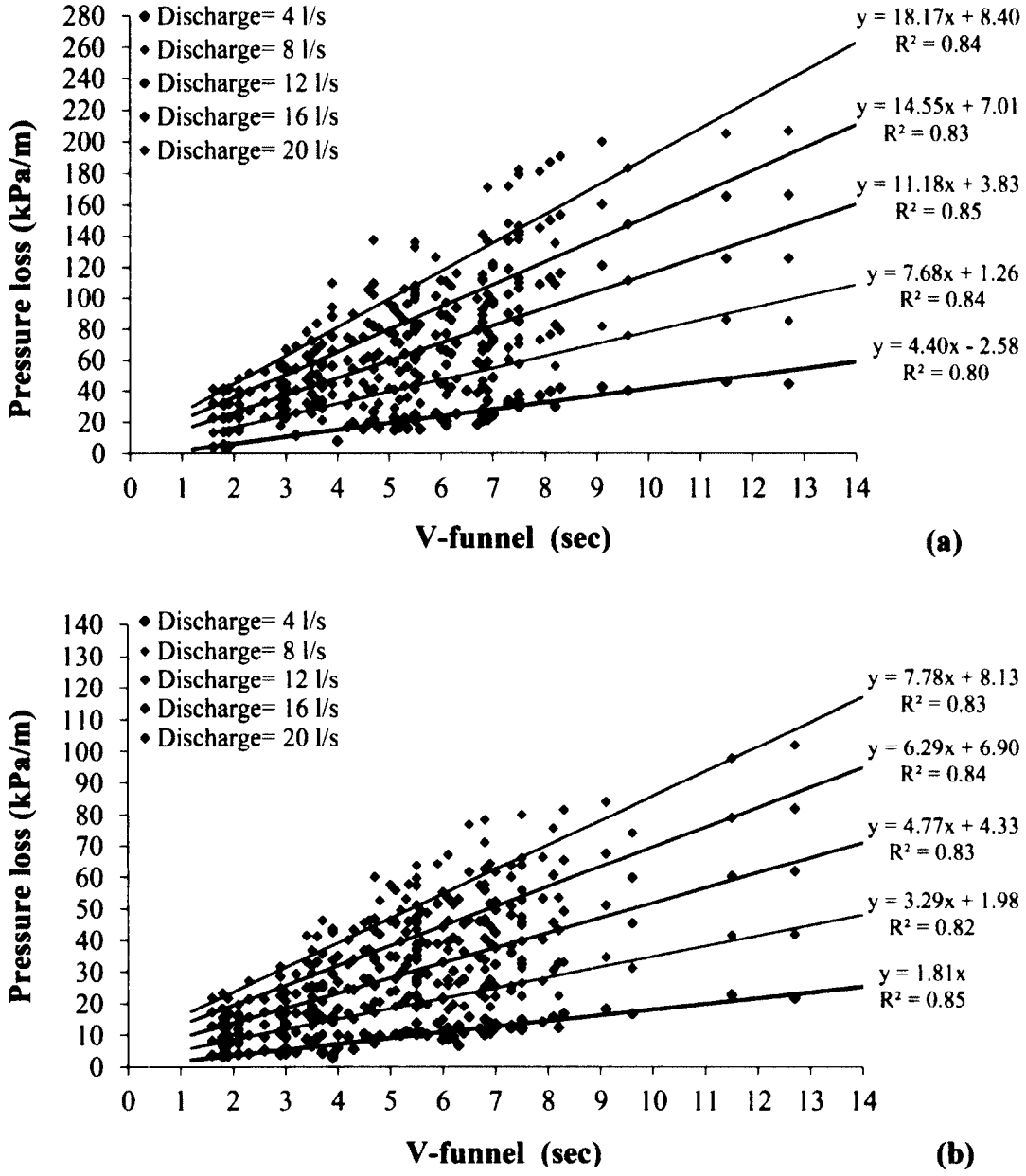


***Figure 6.14:*** *Relationship between the V-funnel time and pressure loss at different discharge rates for (a) 4-in. (102 mm) pipes and (b) 5-in. (127 mm) pipes for SCC and HWC mixtures.*

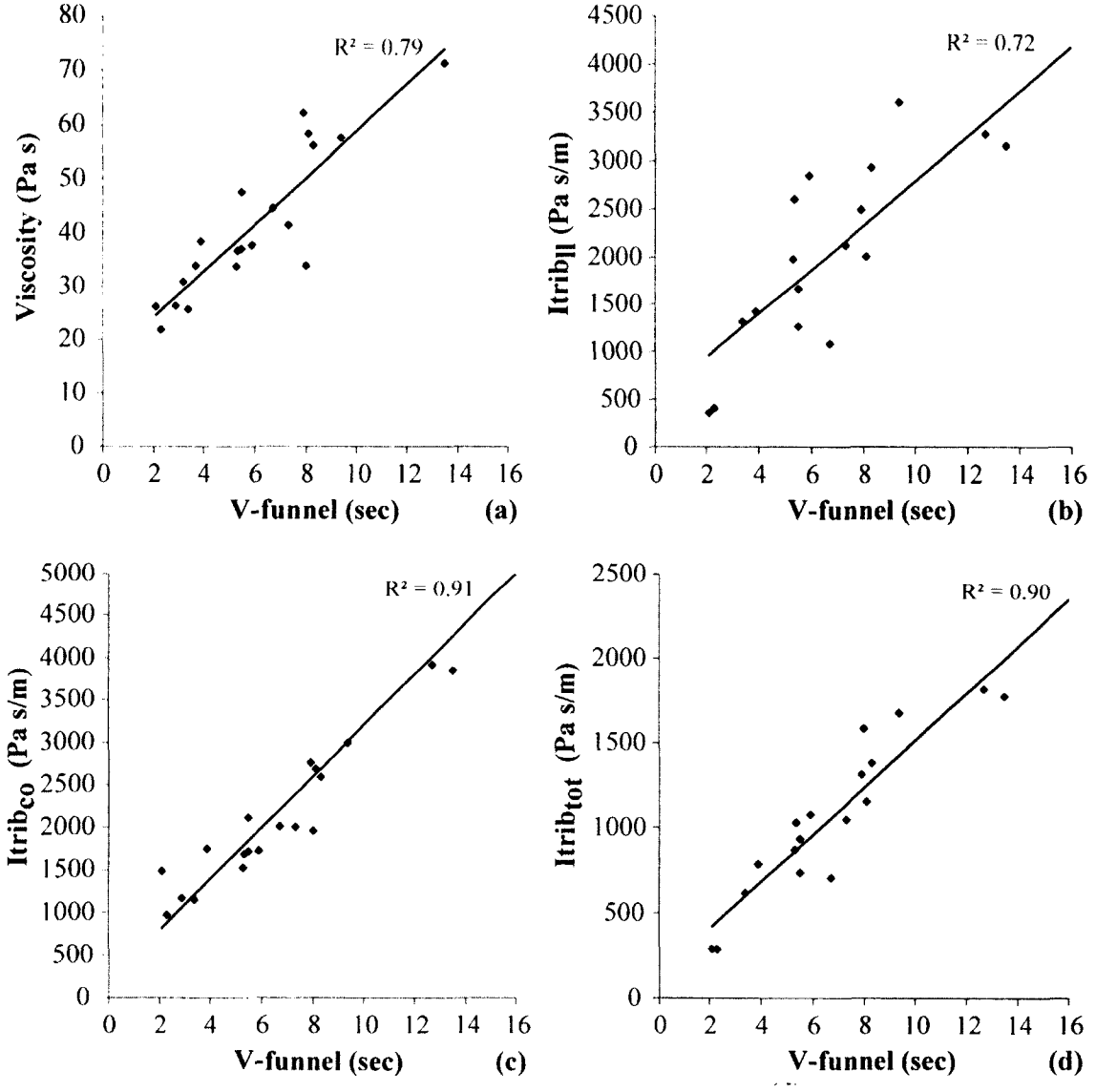


***Figure 6.15:*** *Relationship between V-funnel and (a) viscosity, (b) $Itrib_{II}$, (c) $Itrib_{co}$, and (d) $Itrib_{tot}$ measured at the end of the second pumping cycle for SCC and HWC mixtures.*

### Slump

In the case of CVC, a significant correlation was found between the pressure loss and slump (Figure 6.16) however, in the case of SCC and HWC, no substantial correlation was found. This is expected as the flow properties of CVC are highly dependent on yield stress that basically governs the slump test. As illustrated by Figure 6.16, an increase in the slump results in a reduction in the pressure loss at a given discharge rate. Applying this to SCC does not deliver accurate results because the flow properties of SCC are primarily related to viscosity rather than yield stress.

The literature on the subject contains a number of studies that employ the use of slump test as a simple method to predict the pressure loss for CVC [2, 7]. Despite the widespread use of this method to determine pumping pressure, unrealistic values can be obtained when applied to highly-flowable concrete (see section 4.3 for more details).

In view of the above discussion, it suffices to say that the slump test is an excellent and simple way to estimate pressure loss of CVC, but due to fundamentally different flow properties, it is not applicable to SCC. Rather, the V-funnel test can be used as an accurate method to determine the pressure loss in the case of SCC and HWC.

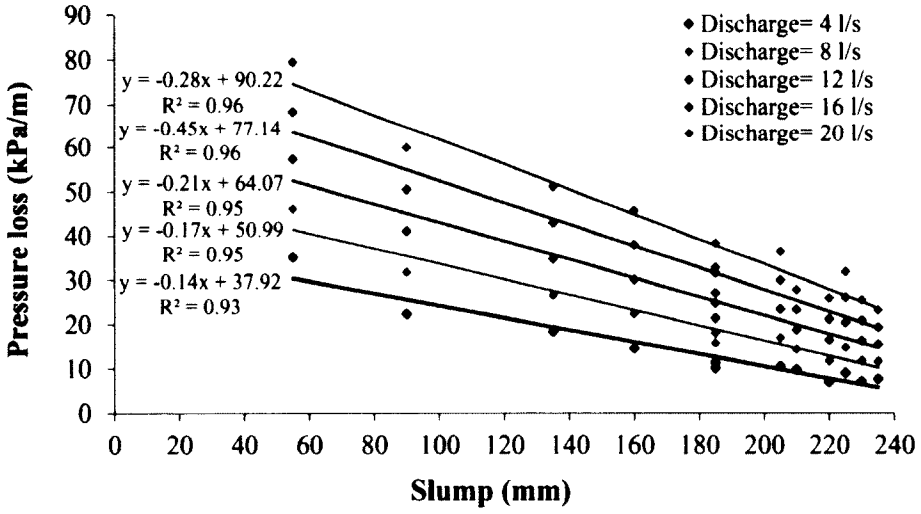


***Figure 6.16:*** *Relationship between the slump and pressure loss of CVC mixtures at different discharge rates in 5-in. (127 mm) pipes.*

## 6.11 Statistical models to predict pressure loss

### 6.11.1 Rheology and tribology

The empirical study previously outlined demonstrates that viscosity and $Itrib_{II}$ hold significant sway over the pressure loss of SCC and HWC. In order to furnish a quantitative description of these effects, a statistical approach using multiple regression analysis was undertaken. By means of the statistical analysis, the unique contribution of $Itrib_{II}$ and viscosity on the pressure loss can be disclosed. In addition, the analysis provides a tool to forecast how a particular change in these parameters would affect pressure loss. The

multiple regression analysis was performed using SPSS software with a confidence limit of 95%, indicating a probability value lower than 5%. The analysis was performed for two pipe diameters, considering the pressure loss as the dependent variable while viscosity and $Itrib_{ll}$ as the independent variables. An outcome of this study is a model expressing the pressure loss as a function of viscosity and $Itrib_{ll}$, discharge rate, and pipe diameter (equations 6.3 and 6.4). The results of the regression analysis are listed in Tables 6.1 and 6.2, and discussed in the following sections.

### Coefficient of determination ($R^2$)

The values presented in column 1 (in Tables 6.1 and 6.2) show that the statistical model is established with a high coefficient of determination ($R^2 = 0.69$ for 5-in. (127 mm) pipes and $R^2 = 0.85$ for 4-in. (102 mm) pipes), indicating a high correlation between the measured values and the predicted ones.

### Modeling

The weight of the independent variables (viscosity and $Itrib_{ll}$) are presented in column 3. By means of these values, the dependent variable (pressure loss) can be modeled as a function of the independent variables ($\mu$ and $Itrib_{ll}$ ), as presented in equations 6.3 and 6.4. The viscosity and $Itrib_{ll}$ are ranked as significant influential parameters as their corresponding probability values (in the significance column 4 ) are considerably lower than 5%.

For 5-in. (127 mm) pipes:

$$\Delta p = Q(0.058\,\mu + Itrib_{ll} \times 10^{-4} - 0.038) \tag{6.3}$$

For 4-in. (102 mm) pipes:

$$\Delta p = Q(0.133\,\mu + Itrib_{ll} \times 10^{-3} - 0.914) \tag{6.4}$$

where

$\Delta p$: pressure loss per unit length of pipe (kPa/m)
$Q$: discharge rate (l/s)
$\mu$: viscosity of concrete (Pa s)
$Itrib_{ll}$: viscous constant (Pa s/m)

### Part and partial values

The partial values presented in column 7 refer to the correlation between the dependent variable (pressure loss) and the independent variables (viscosity and $Itrib_{ll}$). For example, for the 5-in. (127 mm) pipes, the partial value of viscosity is 0.53, denoting that 53% of the variation in the pressure loss is accounted for by viscosity after $Itrib_{ll}$ has been held constant (see Figure 6.17a). Similarly, the partial value of $Itrib_{ll}$ is 0.20 implying that if viscosity is held constant, 20% of the variation in the pressure loss is induced by $Itrib_{ll}$. By comparing the partial values of viscosity and $Itrib_{ll}$, it can be deduced that viscosity

holds a greater influence over pressure loss. The semi-partial (or part) values presented in column 8 provide another statistical measure that describes the unique contribution of each variable to the dependent variable. For example, for the 5-in. (127 mm) pipes, the part value of viscosity is 0.35, indicating that 35% of the variation in the pressure loss is accounted for by the viscosity uniquely (after the interaction between viscosity and $Itrib_{II}$ is partialled out), as presented in Figure 6.17b. Similarly, the unique contribution of $Itrib_{II}$ is 0.08, indicating that 8% of the variation in the pressure loss is uniquely accounted for by $Itrib_{II}$. The unique contributions of both viscosity and $Itrib_{II}$ clearly signify their effects on the pressure loss. Among the two parameters, viscosity again holds the highest effect.

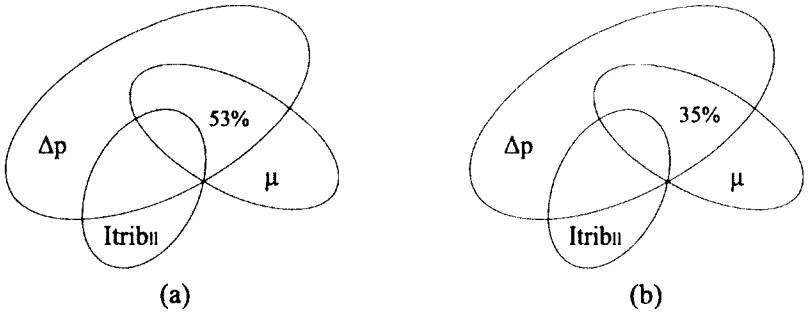


***Figure 6.17:*** *Sketch of (a) partial value and (b) part value of viscosity for the pressure loss in 5-in. (127 mm) pipes.*

By comparing the part values of viscosity and $Itrib_{II}$ for 5-in. pipes (in column 8, of Tables 6.1 to their counterpart values for 4-in. pipes in Table 6.2), it can be deduced that the influence of $Itrib_{II}$ increases with decreasing pipe diameter, while the effect of viscosity remains almost constant regardless of the pipe size. The increased importance of $Itrib_{II}$ with smaller pipes can be attributed to the sharp changes in the flow velocity, leading to significant changes in the properties of the lubrication layer (see section 5.11.4).

### Multicollinearity and quality of fit diagnose

Because viscosity and $Itrib_{II}$ are interrelated, it is important verifying whether their relationship affects the precision of the statistical model. This problem (called multi-collinearity), can be verified by the collinearity statistics presented by the tolerance and

***Table 6.1:*** *Results of the regression analysis used to calculate the pressure loss in 5-in. (127 mm) pipes using viscosity and* $Itrib_{II}$ .

| $R^2$ | Variable | Coefficients Beta | Sign. | 95.0% Confidence Interval for B | | Correlations | | Collinearity Statistics | |
|---|---|---|---|---|---|---|---|---|---|
| | | | | Lower Bound | Upper Bound | Partial | Part | Tolerance | VIF |
| (1) | (2) | (3) | (4) | (5) | (6) | (7) | (8) | (9) | (10) |
| | Constant | -0.038 | 0.79 | -0.32 | 0.24 | | | | |
| 0.69 | Viscosity | 0.058 | 2.7E-42 | 0.05 | 0.06 | 0.53 | 0.35 | 0.82 | 1.21 |
| | $Itrib_{II}$ | 3E-4 | 9.4E-14 | 2.1E-4 | 3.6E-4 | 0.20 | 0.08 | 0.82 | 1.21 |

***Table 6.2:*** *Results of the regression analysis used to calculate the pressure loss in 4-in. (102 mm) pipes using viscosity and* $Itrib_{II}$ .

| $R^2$ | Variable | Coefficients Beta | Sign. | 95.0% Confidence Interval for B | | Correlations | | Collinearity Statistics | |
|---|---|---|---|---|---|---|---|---|---|
| | | | | Lower Bound | Upper Bound | Partial | Part | Tolerance | VIF |
| (1) | (2) | (3) | (4) | (5) | (6) | (7) | (8) | (9) | (10) |
| | Constant | -0.914 | 3.5E-5 | -1.341 | -0.487 | | | | |
| 0.85 | Viscosity | 0.133 | 8.8E-75 | 0.123 | 0.143 | 0.72 | 0.41 | 0.87 | 1.15 |
| | $Itrib_{II}$ | 0.001 | 2.7E-39 | 0.001 | 0.001 | 0.49 | 0.15 | 0.87 | 1.15 |

the variance inflation factor (VIF) in columns 9 and 10, respectively. A tolerance value less than 0.01 and VIF greater than 10, are both signs of multicollinearity. Fortunately, all reported tolerance and VIF values are within the accepted limits, indicating that the correlation between viscosity and $Itrib_{II}$ does not affect the precision of the model.

Another worthy precaution is to assess the "quality of fit" of the derived models. A model may fit well but poorly estimate the independent variable, or in another case, it may fit poorly but estimate the independent variable correctly. Therefore, it is important to verify whether the model predicts the data accurately. To do this, the predicted pressure loss values, calculated by the prediction model (from the rheological and tribological properties of tested mixtures), are plotted versus the corresponding readings of the pressure sensors (Figure 6.18). The high coefficients of determination of the relationships (presented in Figure 6.18) between the predicted and measured pressure losses ($R^2$= 0.90 for 5-in. (127 mm) pipes, and $R^2$= 0.92 for 4-in. (102 mm) pipes) demonstrate the accuracy of the prediction model and the high "quality of fit".

To summarize, the pressure loss can be predicted through the derived statistical model on the basis of the rheological and tribological properties of concrete, for a given discharge rate and pipe diameter. Both viscosity and $Itrib_{II}$ play a consequential role on pressure loss. Viscosity holds the highest influence regardless of the pipe size (62% higher effect than $Itrib_{II}$ for 5-in. pipes and and 32% for 4-in. pipes), whereas the influence of $Itrib_{II}$ increases with decreasing the pipe size.

It is noteworthy that the models are delivered for SCC and HWC with viscosity and slump flow falling in the ranges of 22-200 Pa s, and 350-850 mm, respectively. Applying the models to concrete with a slump flow out of this range may result in different estimation of the pressure loss.

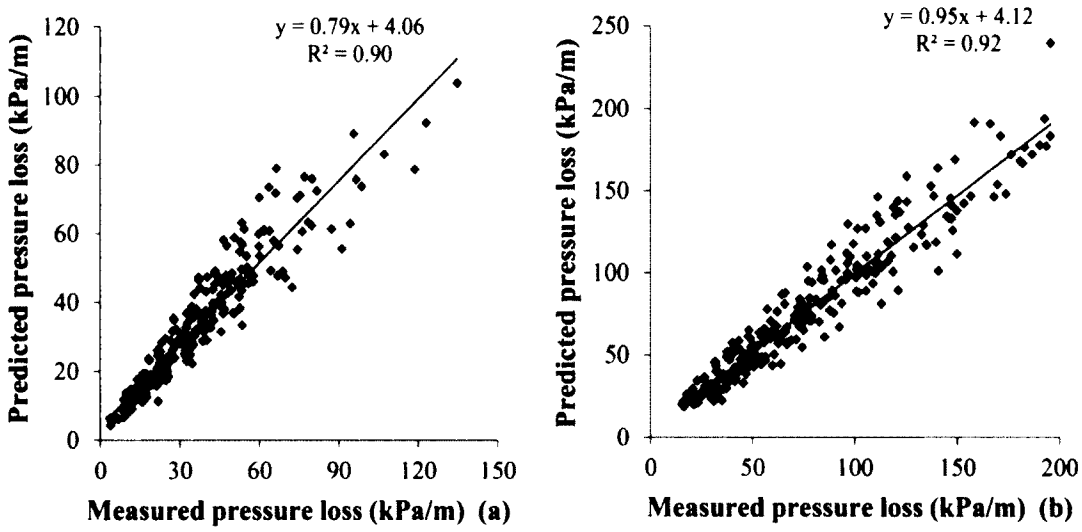


***Figure 6.18:*** *Measured pressure loss versus predicted pressure loss calculated for equations 6.3 and 6.4 for (a) 5-in. (127 mm) pipes and (b) 4-in. (102 mm) pipes.*

### 6.11.2 V-funnel

As demonstrated in section 6.10.3, V-funnel time is well correlated with pressure loss. With this correlation as an input, a multiple regression analysis was performed to establish a statistical model able to compute the pressure loss based on the V-funnel test. The regression analysis was executed with a confidence limit of 95% and the high coefficients of determination ($R^2 = 0.81$ for 5-in. pipes and $R^2 = 0.84$ for 4-in. pipes) presented in Tables 6.3 and 6.4 indicate a strong correlation between the measured values and the predicted ones. Pressure loss as a function of V-funnel time and discharge rate for 5-in. (127 mm) and 4-in. (102 mm) pipes is given by equations 6.5 and 6.6.

For 5-in. (127 mm) pipes:

$$\Delta p = Q(0.36\,V_F + 0.56) \tag{6.5}$$

For 4-in. (102 mm) pipes:

$$\Delta p = Q(0.93\,V_F + 0.34) \tag{6.6}$$

where

$\Delta p$: pressure loss per unit length of pipe (kPa/m)
$Q$: discharge rate(l/s)
$V_F$: V-funnel time (s)

The model given by equations 6.5 and 6.6 can be considered another practical approach to predict pressure loss on job sites. The high coefficient of determination ($R^2 = 0.81$ for 5-in. pipes and $R^2 = 0.84$ for 4-in. pipes) demonstrates a significant correlation between the predicted and measured values of pressure loss.

***Table 6.3:*** *Results of the regression analysis used to calculate the pressure loss in 5-in. (127 mm) pipes using V-funnel flow time.*

| $R^2$ | Variable | Coefficients Beta | Sign. | 95.0% Confidence Interval for B | | Correlations | | Collinearity Statistics | |
|---|---|---|---|---|---|---|---|---|---|
| | | | | Lower Bound | Upper Bound | Partial | Part | Tolerance | VIF |
| (1) | (2) | (3) | (4) | (5) | (6) | (7) | (8) | (9) | (10) |
| 0.81 | Constant | 0.56 | 2.6E-19 | 0.44 | 0.67 | | | | |
| | V-funnel | 0.36 | 7.8E-151 | 0.34 | 0. 37 | 0.90 | 0.90 | 1.0 | 1.0 |

***Table 6.4:*** *Results of the regression analysis used to calculate the pressure loss in 4-in. (102 mm) pipes using V-funnel flow time.*

| $R^2$ | Variable | Coefficients Beta | Sign. | 95.0% Confidence Interval for B | | Correlations | | Collinearity Statistics | |
|---|---|---|---|---|---|---|---|---|---|
| | | | | Lower Bound | Upper Bound | Partial | Part | Tolerance | VIF |
| (1) | (2) | (3) | (4) | (5) | (6) | (7) | (8) | (9) | (10) |
| 0.84 | Constant | 0.34 | 0.027 | 0.04 | 0.64 | | | | |
| | V-funnel | 0.93 | 1.3E-123 | 0.88 | 0.97 | 0.91 | 0.91 | 1.0 | 1.0 |

In order to assess the "quality of fit", the pressure losses calculated by equations 6.5 and 6.6 are plotted versus the corresponding pressure losses measured directly by the pressure sensors (Figure 6.19). The high coefficients of determination ($R^2$ = 0.92 for 5-in. pipes and $R^2$ = 0.90 for 4-in. pipes) shown in Figure 6.19 exemplifies the firm correlation between the predicted and measured values, indicating a high "quality of fit".

Reflecting on the above discussion, it can be concluded that pressure loss for SCC and HWC can be predicted using the V-funnel model in two types of pipes. This provides a practical approach to determine the pressure loss on job sites without the need for complex rheological and tribological properties.

### 6.11.3 CVC modelization

Since only three CVC mixtures were tested, the data points were insufficient to run a regression analysis that predicts the pressure loss with satisfactory accuracy. Helpful, in this connection, are several studies presented in the literature that use of the slump to determine the pressure loss [2, 7, 8]. Also, the empirical relationships executed on Figure 6.16 can be favorably used to determine the pressure loss of CVC. In the presented relationships, the yield stress of the tested mixtures falls within the range of 300-3500 Pa. Accordingly, changing the range of the yield stress may lead to inaccurate pressure loss estimation.

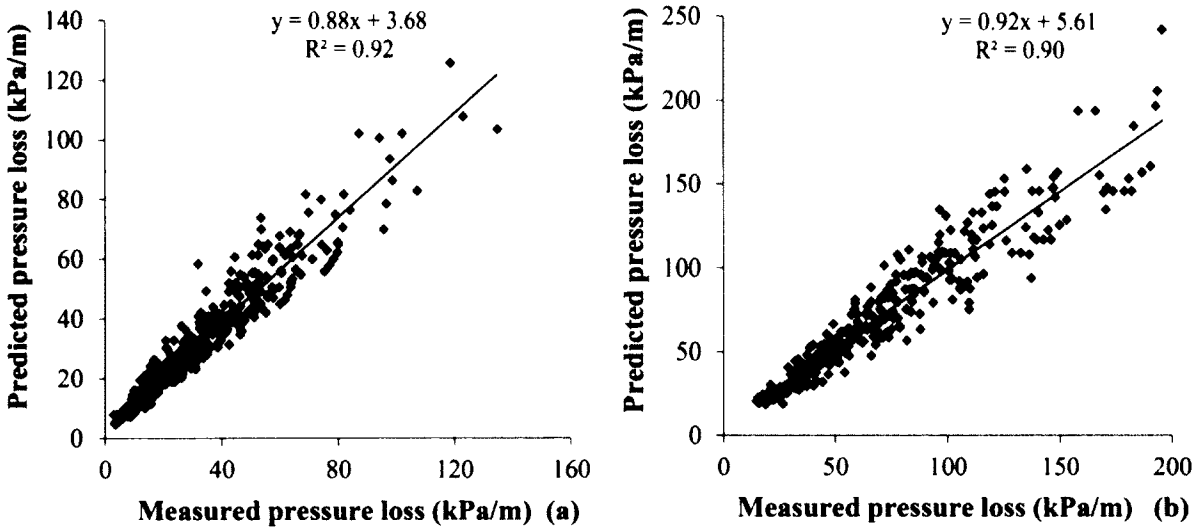


***Figure 6.19:*** *Measured pressure loss versus predicted pressure loss calculated using equations 6.5 and 6.6 for (a) 5-in. (127 mm) pipes and (b) 4-in. (102 mm) pipes.*

## 6.12 Changes in concrete properties due to pumping

Pumping is considered a pressurized flow causing various changes in concrete properties. These changes are related to several parameters including the magnitude of the applied pressure, concrete mix composition, and pumping duration. The most significant changes in concrete properties observed throughout the pumping tests are addressed in the following sections.

### 6.12.1 Temperature

The concrete temperature in pumping pipes was monitored continuously throughout testing. The temperature increase per unit of time (°C/min) was determined at each discharge rate, and the temperature of the pumped concrete samples was measured at the end of each pumping cycle. As shown in Figure 6.20a, temperature increases over the pumping cycles because part of the mechanical energy applied to maintain the flow is converted into heat. This can be attributed to the viscous dissipation and the interparticle friction during flow [5, 6]. Figure 6.20b indicates that the rate of temperature increase is linearly related to the pressure loss and that the rate is more pronounced at high pressure losses. At low pressure losses, the rate can be very low, and even negative in some cases due to low temperatures in the pumping laboratory. Even though it is believed that the rate of temperature increase is strongly related to mixture composition, there were no indication of relationships with any other parameter besides pressure loss. However, a general trend can be observed between aggregate content and concrete temperature during pumping, as shown in Tables B.16 and B.18; mixtures with higher aggregate contents exhibited higher temperatures during pumping. This is expected as higher aggregate content leads to more solid-solid interactions and consequently greater heat

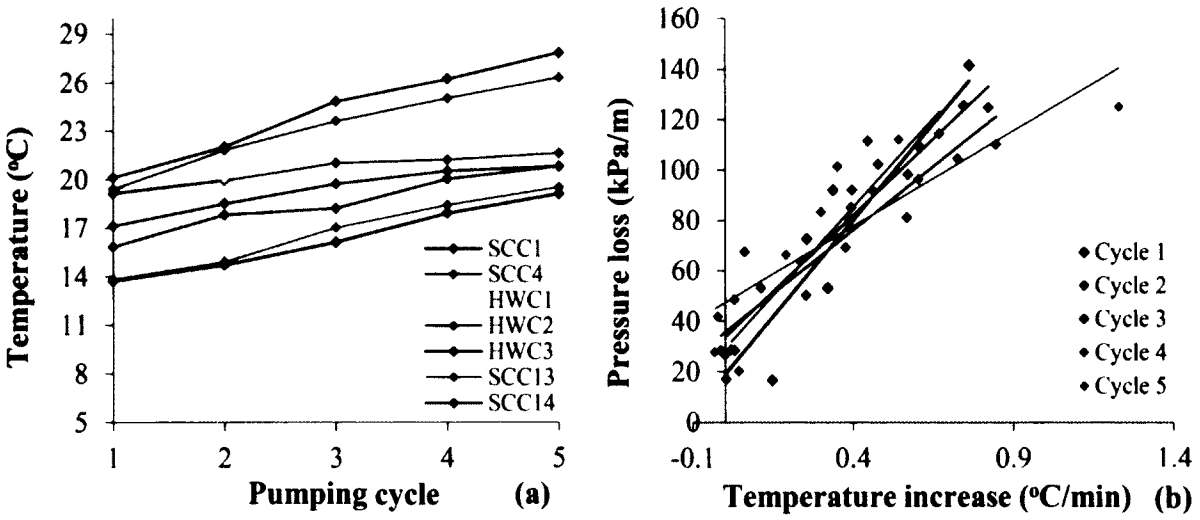


***Figure 6.20:*** *(a) Temperature changes over the pumping cycles for several concrete mixtures. (b) Example of temperature increase rate at different pumping cycles as a function of the pressure loss for HWC3. The temperature was measured with a thermal sensor located near sensor 1.*

dissipation. Nevertheless, this is not a universal rule since temperature can evolve in different directions depending on other parameters, particularly *w/cm*, HRWRA dose and type, and cement type [9]. The area of research to reveal the mutual interactions between temperature and pumping is still open for investigation.

## 6.12.2 Air content

Air content is a key factor affecting the rheological properties of concrete and can be the cause of several properties changes during pumping. The air content was determined for all pumped mixtures at the end of each pumping cycle (Table B.19). Illustrative examples of variation in air content (measured as described in 7.3.1) during the pumping cycles are presented in Figure 6.21. Indistinct fluctuations in air content due to pumping can be observed, but the general trend is an increase in air content due to pumping.

Previous researchers attributed the increase in air content to the incomplete filling of the pump cylinders during pumping [1]. It follows that the unfilled space consists of air that, when pumped, mixes up with concrete pushed through the pumping pipes. Another reason could be that when concrete falls back inside the pump reservoir, new air bubbles get trapped and mixed with the concrete [1]. On the other hand, the reduction in air content, in certain cases, can be attributed to the dynamic air-bubbles dissolution caused by the increasing pressure during pumping [10]. When the pressure increases, the smaller bubbles are dissolved into nearby water droplets. When the pressure becomes lower (close to the exit of the hose), the small pressurized air bubbles, which have not been fully dissolved, appear mainly as larger bubbles [10], which can easily escape from the mixture resulting in a reduction in the air content. Officially, the real cause behind the changes in air content during pumping is uncertain. Additional analysis on such parameters as air bubble size and distribution is required. Unfortunately, none of these analyses were performed in this investigation as they are unrelated to the project objectives.

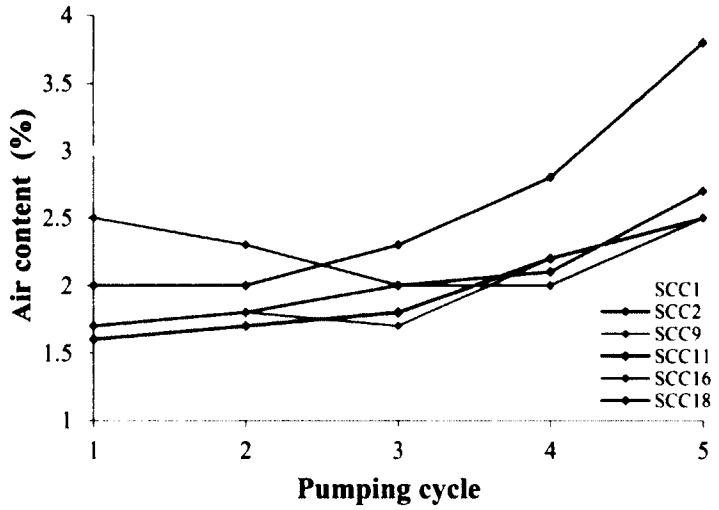


***Figure 6.21:*** *Example of the changes in air content during pumping for various concrete mixtures.*

### 6.12.3 Rheology

Determining the changes in the rheological properties of concrete throughout pumping is central to understanding the evolution of pressure loss during pumping. In consequence, viscosity and yield stress of the pumped mixtures were determined at the end of each pumping cycle. The changes were evaluated during only the first 4 pumping cycles for two reasons: the first because not all mixtures underwent 5 pumping cycles, and the second because certain mixtures tested at cycle 5 exhibited a sharp loss of workability uncharacteristic of the other cycles, as presented in Tables B.17-B.20. For example, SCC2 showed a slump flow loss of 505 mm (from 815 to 310 mm) between the first and last pumping cycle, while SCC4 displayed only a loss of 35 mm (from 680 to 635 mm). A possible explanation for this could be the decline of the HRWRA dispersing action over time for certain mixtures.

As a general statistical indicator of the overall trend, average viscosity and yield stress of all mixtures were calculated for each pumping cycle. Changes in rheological properties of all pumped mixtures at the different testing stages can be found in Tables B.21 and B.22.

#### Viscosity

The general tendency for concrete viscosity is to decrease with each pumping cycle (Figure 6.22a). By the end of pumping cycle 4, the average viscosity of all pumped mixtures had decreased by 24% relative to the average viscosity at the end of cycle 1 (Figure 6.22b). There exist several possible explanations for this behavior. The first attributes this reduction to the high shear effect that takes place in the pumping pipes and that magnifies the effect of structural break-down. The second explanation relates the decrease in viscosity to the changes in air content and bubble distribution within concrete throughout pumping [1].

Researchers weigh the influence of air bubbles by the capillary number defined by the ratio of the shearing forces on the air bubbles to the surface tension forces [11].

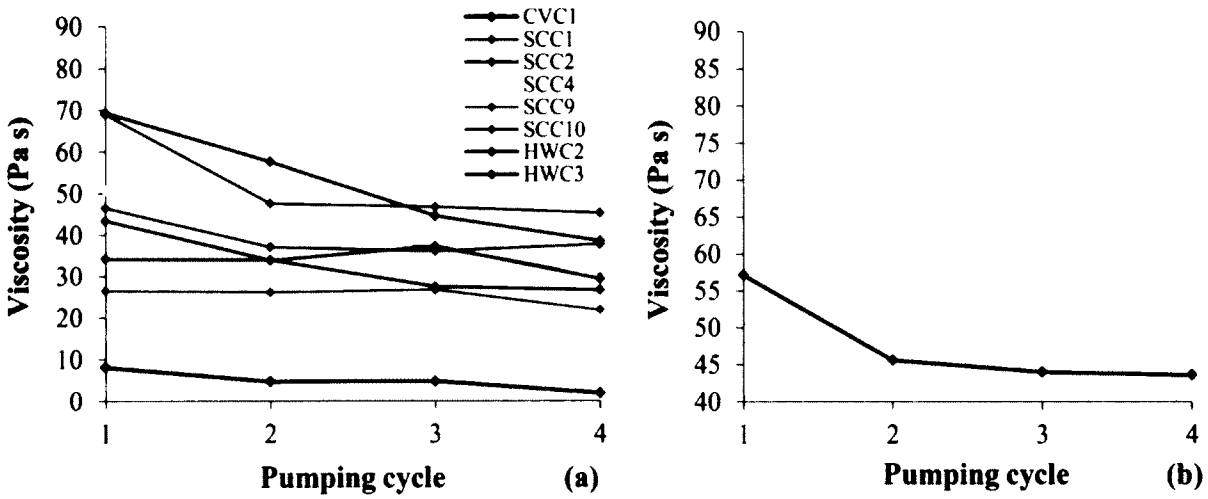


***Figure 6.22:*** *(a) Evolution of viscosity over 4 pumping cycles for several concrete mixtures; (b) average viscosity of all tested mixtures at the end of each cycle.*

At high capillary numbers, the bubbles deform in the flow zone and the flow resistance declines, and at low capillary numbers, the bubbles remain spherical resulting in higher flow resistance. The larger the amount of bubbles, the greater is the influence. Under the high shear effect induced in the pumping pipes, air bubbles are more likely to deform, forming smaller air bubbles [1]. Considering this phenomenon, the decrease in viscosity during pumping can be justified by the (potential) increase in small air bubbles generated within the pumped concrete. This provides a theoretical explanation, but ultimately, more specific analysis is required to validate the theory for the relationship.

A final explanation interpreting the viscosity reduction can be related to the temperature increase due to pumping. Previous studies concluded that a drop in temperature usually decreases yield stress and substantially increases viscosity of mortars with PC-based HRWRA [12]. Also, from a workability point of view, a temperature increase enhances the fluidity of cement pastes [13] due to an increase in the Brownian motion of the particles, weakening the interactions between the agglomerates [14].

Ideally, the initial reduction in viscosity caused by the structural break-down effect should be followed by a dramatic increase after a certain duration of pumping, as the loss of workability should eventually take over the structural-break down effect. Oddly enough, some mixtures showed a continuous reduction in viscosity throughout the entire pumping experiments. This contrary behavior can be attributed to the high dose of HRWRA used for certain mixtures.

In the case of CVC, the changes in viscosity are considerably less evident than those of SCC (Table B.22). This is expected as the effect of viscosity is less significant in the CVC's unsheared medium.

### Yield stress

As shown in Figure 6.23a, yield stress tends to increase due to pumping for the majority of the three types of concrete. This increase is significant in certain mixtures, while it is less pronounced in others. As shown in Figure 6.23b, the average yield stress of the tested mixtures increases by around 78% over the 4 pumping cycles. Although a general trend

of increasing yield stress is observed, special consideration should be given to analyze the results as the increase in yield stress varies from extreme to insignificant in the pumped mixtures.

Since yield stress is a function of energy, a possible explanation of the increase in yield stress can be related to the shear history that concrete accumulates during pumping. In each pumping cycle the shear effect that concrete undergoes, adds to the shear history that the concrete has accumulated to that point. Eventually, this accumulation leads to an increase in the yield stress of concrete. Generally, the higher and longer the shear effect, the greater is the energy needed to overcome yield stress.

Another possible cause could be the temperature increase associated with pumping, which can result in an increased yield stress. The chemical composition of the cement, and the type and dose of HRWRA interfere strongly into the changes in yield stress under different temperatures. These effect have been proved on concrete mortars, especially when PC based-HRWRA is used [12].

Another possible explanation for the increase in yield stress can be attributed to the significant increase of small air bubbles within the pumped concrete. Since the yield stress test is performed under low shear effect, the air bubbles are prone to remain spherical resulting in a lower capillary number and thus higher flow resistance [1] (as pointed out in the previous section). It should be noted here that the effect of air content on yield stress can be countered by the structural-breakdown, and thus the change in yield stress depends on which effect dominates [1]. In the case where structural-breakdown dominates, the yield stress should decrease, whereas in the case where air content prevails, the yield stress should increase. This can be a possible explanation of the decrease in yield stress for certain mixtures, as presented in Table B.22.

To summarize, the dominant rheological properties relate to pumping duration, depending on the type of concrete used. SCC and HWC mixtures experience a significant reduction in viscosity and in most cases an increase in yield stress with pumping duration. The increase in yield stress is evident in certain mixtures, whereas it is considerably

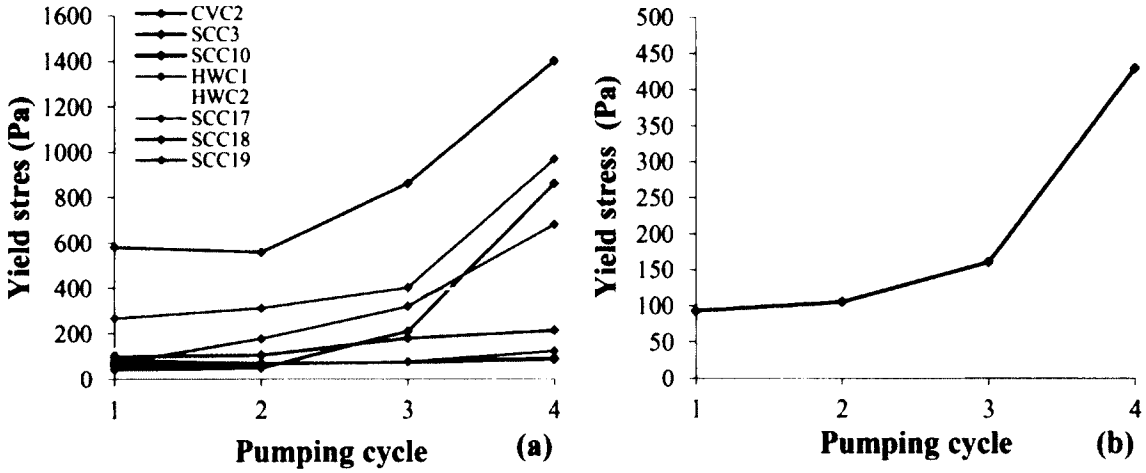


***Figure 6.23:*** *(a) Evolution of yield stress over 4 pumping cycles for several concrete mixtures; (b) average yield stress of all tested mixtures at the end of each cycle.*

less significant in other mixtures. CVC exhibits a substantial increase in yield stress and a minor increase in viscosity with pumping duration. Different theoretical justifications for these changes in connection with changes in temperature and the air void system were explained. The door of research to further understand these effects is open to investigation.

### 6.12.4 Tribology

Changes in the tribological properties of concrete are intertwined with the changes in concrete viscosity and those in viscosity and thickness of the lubrication layer. As these changes can evolve in different directions throughout pumping, the tribological properties become dictated by the most dominating change.

The changes in the tribological parameters for several mixtures throughout the 4 pumping cycles are presented in Figures 6.24a, 6.24c, and 6.24e. Illustrative examples of the changes in the average values of $Itrib_{ll}$, $Itrib_{co}$, and $Itrib_{tot}$ calculated at each pumping cycle are presented in Figures 6.24b, 6.24d, and 6.24f, respectively. As shown in Figure 6.24b, $Itrib_{ll}$ increases by approximately 21% by the end of cycle 3, and drops drastically after this point. The initial increase can be justified by the correlation between the properties of concrete and those of the lubrication layer. As detailed in section 5.11.3, continous pumping reduces concrete viscosity, which in turn increases the viscosity of the lubrication layer, and consequently, increasees $Itrib_{ll}$. Despite this evidence, the real reason behind the decrease (or in some cases increase) in $Itrib_{ll}$ at cycle 4 remains inconclusive. It could be that the ability of concrete to form a lubrication layer in the tribometer subsides over time due to successive pumping cycles. As a result, precisely measuring $Itrib_{ll}$ in the tribometer at cycle 4 would become more difficult and even less representative of the real case in pumping pipes where the lubrication layer has already been formed during previous pumping cycles.

Unlike $Itrib_{ll}$, $Itrib_{co}$ shows a steady reduction during the first 3 pumping cycles, but it tends to increase during cycle 4 (Figure 6.24c). The $Itrib_{co}$ average decreases by around 66% during the first 3 pumping cycles. This is expected as $Itrib_{co}$ is directly related to the viscosity of concrete, which also decreases with pumping. On the other hand, the increase in $Itrib_{co}$ during the last pumping cycle can be attributed to the loss of workability resulted from prelonged pumping.

Likewise, $Itrib_{tot}$ decreases throughout the first 3 pumping cycles and increases during the final cycle (Figure 6.24e). The $Itrib_{tot}$ average decreases by around 7% by the end of cycle 3 but sharply increases at the last cycle (Figure 6.24f). Given that $Itrib_{tot}$ is a function of $Itrib_{ll}$ and $Itrib_{co}$, the reduction in $Itrib_{tot}$ with pumping can be justified by the reduction in concrete viscosity, while its increase can be rationalized by the increase in $Itrib_{co}$.

Reflecting on the previous discussion, it can be concluded that the changes in tribological properties of concrete can evolve in different directions depending on the changes in rheological properties of concrete and those in the lubrication layer. Generally, $Itrib_{ll}$ is prone to increase whereas $Itrib_{co}$ and $Itrib_{tot}$ tend to decrease with pumping. It must be kept in mind that these changes yield significant effects on pressure loss. They are therefore critical to consider in the mix design phase to prevent any undue pressure loss.

Further investigations concerning the effects of mix design parameters on tribological properties and pressure loss are discussed at length in Chapter 7.

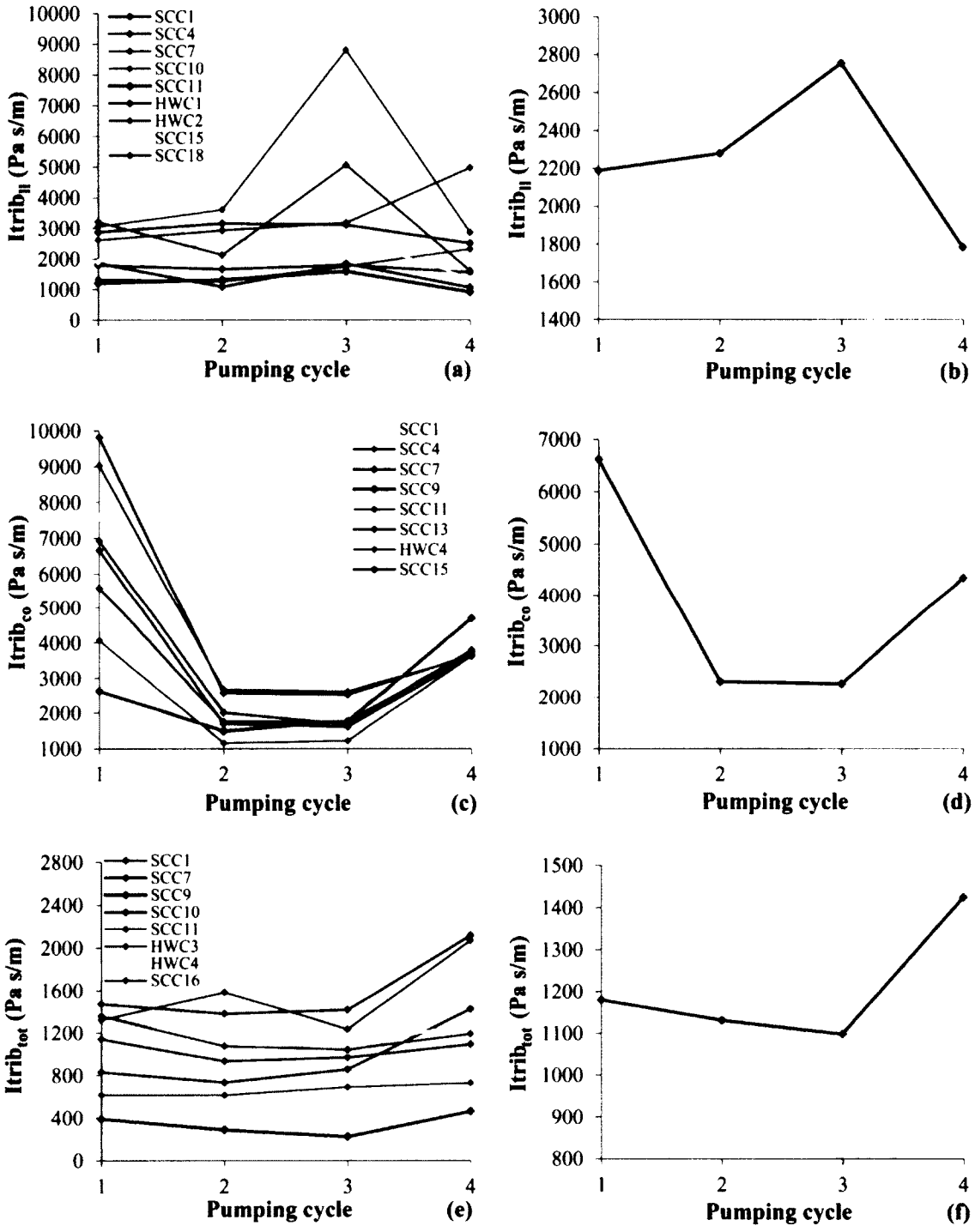


***Figure 6.24:*** *Examples of changes in (a) $Itrib_{ll}$, (c) $Itrib_{co}$, and (e) $Itrib_{tot}$ over 4 pumping cycles; average values of (b) $Itrib_{ll}$, (d) $Itrib_{co}$, and (f) $Itrib_{tot}$.*

## 6.13 Comparison of pumpability of different types of concrete

Given that SCC and CVC display different flow patterns when pumped, changes in their rheological properties due to pumping interfere differently in their flow characteristics. The primary changes for both types of concrete due to pumping can be mainly described by viscosity reduction and yield stress augmentation. Since one of these parameters is vital to the flow of one type of concrete and minor to the other, different pressure loss behaviors can be detected throughout pumping.

Figure 6.25 exemplifies the time evolution of pressure loss over the 5 pumping cycles at different discharge rates for SCC, HWC, and CVC. For SCC, in most cases pressure loss decreases continuously at the beginning, while it tends to increase in the end during cycles 4-5 (Figures 6.25a, 6.25d, and 6.25g. The increase in pressure loss (after a certain number of pumping cycles) varied in the tested mixtures from high (SCC2) to insignificant (SCC18), as indicated in Figure 6.25. Moreover, the time (or pumping cycle) at which this increase in pressure loss occurs changed from a mixture to another. For certain mixtures, this increase started at an early stage during pumping (for example at cycle 3 for SCC2), while it started at later stages in other mixtures (at cycle 4 for SCC16). Since viscosity decreases due to pumping during all pumping cycles, the reduction in pressure loss during the early cycles can be justified by the reduction in viscosity. On the other hand, a possible cause of the increase in pressure loss at the last pumping cycles can be attributed to the changes in tribological properties during the last pumping cycle, as discussed in the previous section.

The reduction in the viscosity of SCC due to pumping is not infinite. At a certain stage, viscosity starts to increase when the loss of workability begins to take over. The point at which this occurs depends on several aspects related to the mix design, type of HRWRA, type and content of the binder in use. Further explanations concerning the effect of concrete constituent materials on the rheological properties and pressure loss during pumping are discussed in Chapter 7.

For the tested CVC mixtures, the scenario changes since the yield stress is the most influential parameter on pressure loss. The sharp increase in yield stress due to pumping leads to an increase in pressure loss, as presented in Figure 6.25b, e, and h.

In the case of HWC, the time evolution of pressure less during pumping seems to be less intense than those in SCC or CVC, as shown in Figure 6.25c, 6.25f, and 6.25i. In most cases, especially at low discharge rates, the pressure loss displays a slight change during the pumping cycles. The less significant changes in the pressure loss of HWC can be rationalized by the nature of its flow, in which both viscosity and yield stress can play a significant role. The reduction in pressure loss caused by the decrease in viscosity could be countered by the increase in pressure loss resulted from the reduction in the yield stress, leading to a more or less constant pressure loss. In this context, the changes in the pressure loss can be explained by the dominant effect of one of these parameter over the another.

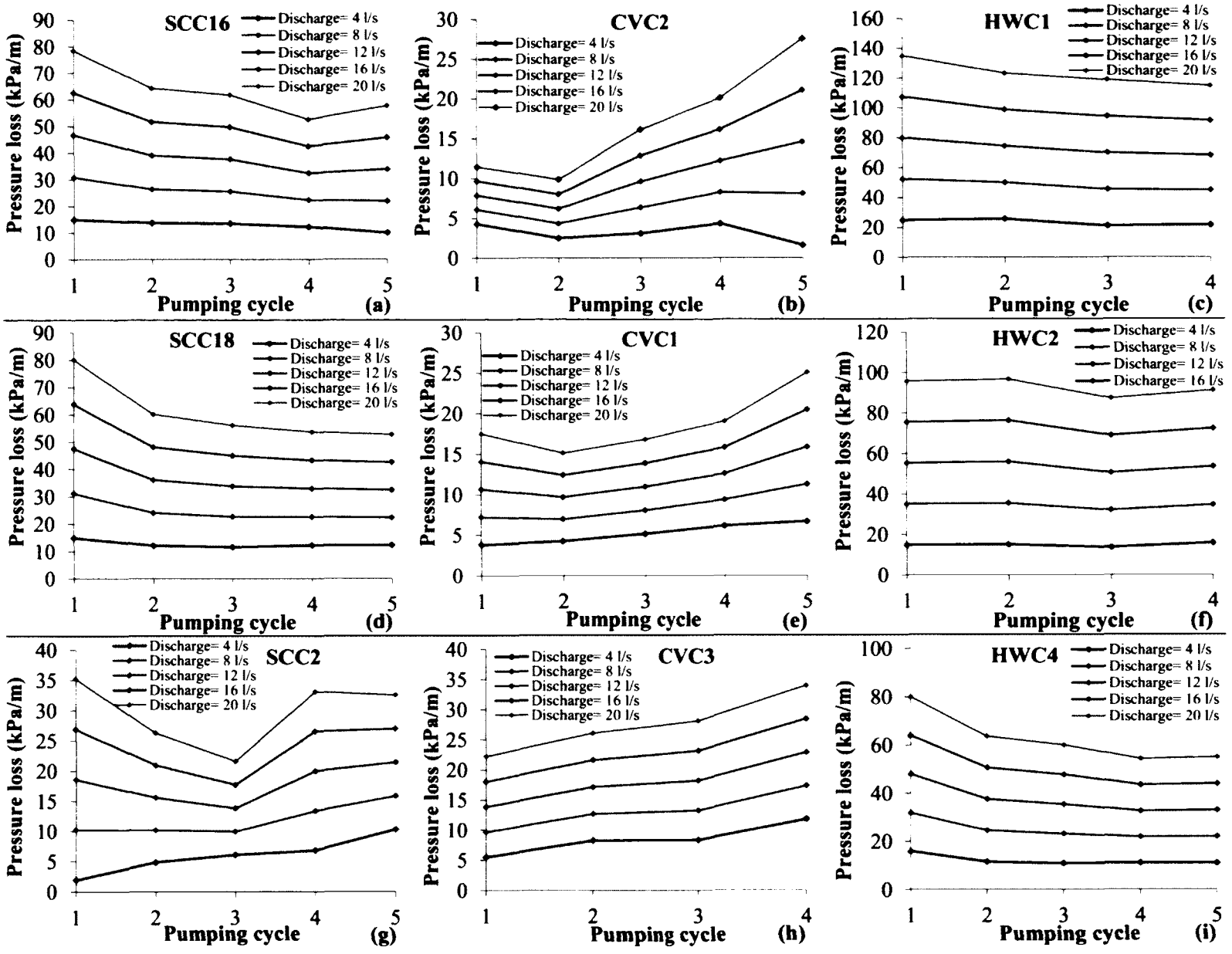


***Figure 6.25:*** *Comparative example of the evolution of pressure loss for SCC, HWC, and CVC in 4-in. (102 mm) pipes at different discharge rates.*

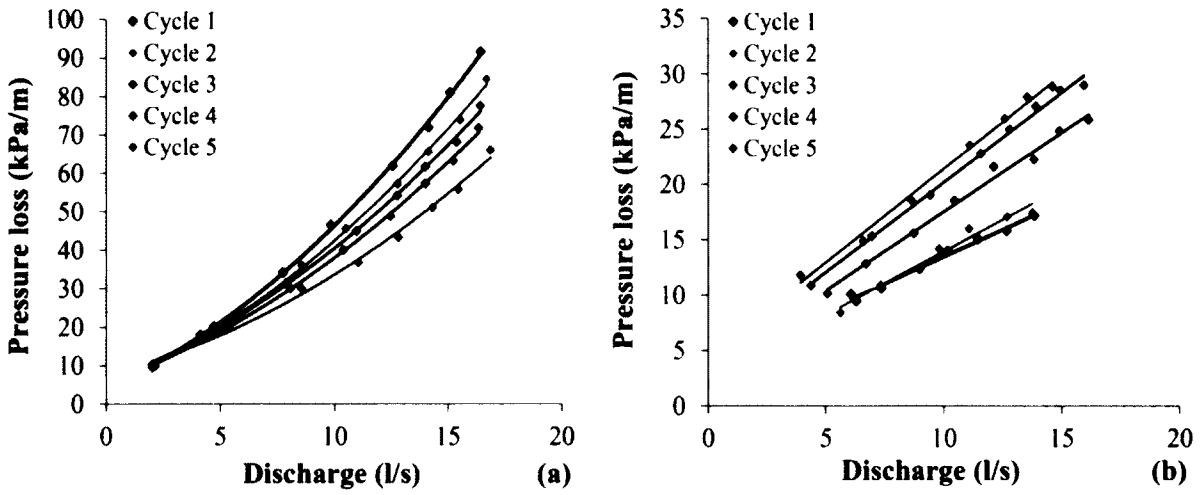


***Figure 6.26:*** *Illustrative example of the discharge-pressure loss relationship for (a) SCC4 and (b) CVC2 in 4-in. (102 mm) pipes at different discharge rates.*

The divergence between SCC and CVC extends also to the relationship between the pressure loss and discharge rate. In the case of CVC, a linear relationship was found while for SCC a slightly non-linear one that balances out for high discharge rates was found (Figure 6.26).

In conclusion, the behavior of SCC and CVC due to pumping varies notably because of their vastly different flow patterns. Generally, in SCC viscosity decreases resulting in a reduction of the pressure loss, whereas in the case of CVC yield stress increases leading to an increase in pressure loss. For HWC, both effects of increasing yield stress and decreasing viscosity intervene in the changes of pressure loss, resulting in less significant changes.

As a result of the above discussion, it can be deduced that SCC favors long-distance pumping (such as in high-rise constructions) since the reduction in viscosity during pumping is accompanied by a reduction in pressure loss. However, stability can become a crucial concern for SCC and HWC if viscosity reduces significantly, and yield stress does not increase sufficiently to maintain proper consistency of the pumped mixture [1]. Placing emphasis on the increase in yield stress, special care should be taken when pumping CVC for long distances as the risk of blocking is probable due to the increase in pressure loss with pumping.

## 6.14 The pipe flow test

### 6.14.1 Scope

The empirical results of the pumping tests demonstrate that the rheological and tribological properties of concrete are key parameters influencing the flow behavior of SCC, and thus the pressure loss associated with pumping such type of concrete. Determining these properties on job sites in relation to the pressure loss is usually difficult. The proposed pipe flow test (PFT) furnishes a simple approach to assess these properties and correlate

them with the pressure loss without the need for complex rehaological and tribological measurements.

### 6.14.2 Description

The pipe apparatus consists of a standard steel pumping pipe with an inner diameter of 4 in. (102 mm), a length of 950 mm and two valve gates installed at the ends (Figure 6.27). The pipe is placed on 4 rotating wheels fixed to a board, allowing the pipe to rotate around its longitudinal axis. The pipe is mobile and can be lifted and moved by a single operator.

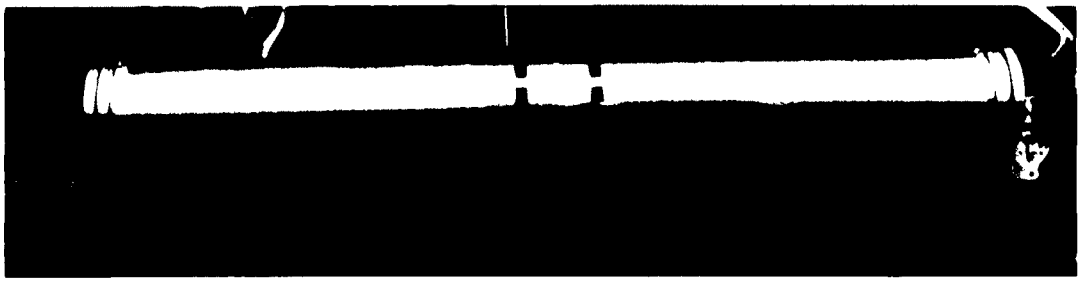

***Figure 6.27:*** *The pipe flow apparatus placed on rotating wheels.*

### 6.14.3 Principle

The lubrication layer in pumping pipes is built and stabilized under the shear effect generated by the pumping pressure. In order to induce such a shear effect in the testing pipe, the concrete is subjected to a spinning motion generated by rotating the pipe around its longitudinal axis. The generated shear effect enables the lubrication layer to form and stabilize near the inner wall of the pipe. The newly formed lubrication layer will change the flow behavior (or resistance) of the concrete in the pipe. This effect can be evaluated by the time that a certain amount of concrete takes to evacuate from the pipe having a fully developed lubrication layer. The measured time (referred to as the flow time $t_f$) can be related to the viscosity of the tested concrete and further to the pressure loss in pumping pipes.

### 6.14.4 Testing procedure

The testing procedure comprises two phases, the first is dedicated to forming the lubrication layer, and the second is meant to evaluate the flow properties of concrete with the newly formed lubrication layer. The two phases are detailed as follows:

- Phase I: Forming the lubrication layer
  The objective of this phase is to form the lubrication layer through rotating the pipe in a set of 50 clockwise time-controlled rotation cycles; this is accomplished by the following steps:
  1- Close the bottom valve.
  2- Fill the pipe with concrete up to a height of 75 cm.

3- Close the upper gate and place the pipe on the rotating wheels.
4- Rotate the pipe around its main axis through 50 time-controlled cycles (1 rotation/second).
5- Remove the pipe from the wheels and set it vertically.
6- Open the valve and wait for 60 seconds until the residual concrete evacuates from the pipe.

- Phase II: Evaluating flow
  The goal of this phase is to evaluate the flow properties of the concrete with the presence of the lubrication layer created in phase I:
  1- Close the lower valve gate, and without cleaning the pipe, refill it with concrete up to the same previous height (75 cm).
  2- Open the valve and measure the flow time ($t_f$) corresponding to the interval between the opening of the valve and the moment light appears through the pipe.
  3- Relate $t_f$ to the rheoligical and tribological properties of concrete and to the pressure loss during pumping.

### 6.14.5 Development of the testing procedure

The lubrication layer has a dynamic characteristic defined by the time and shear magnitude needed to form it. These two aspects in the testing pipe are described by the number of the applied rotating cycles during testing (in Phase I). The number of cycles (50 cycles) was optimized from testing a range of cycles varying from 10 to 400 cycles. Test results showed that the lubrication layer is fully developed only after a certain number of cycles, above which increasing the number of cycles does not significantly change the flow time. For example, applying a low number of cycles (below 25) results in an unstable or partially developed lubrication layer, delivering inaccurate flow time measurements. On the other hand, applying a high number of cycles (above 50) does not considerably change the flow time measurements. After several trials using different numbers of cycles, it was found that applying 50 cycles is adequate to form and stabilize the lubrication layer without significantly prolonging the testing time of the experiment.

### 6.14.6 Mix design

In total, 14 SCC mixtures covering a wide scope of SCC's constituent materials and viscosities (from 22 to 129 Pa s) were tested. Three control concrete mixtures were employed to establish the single-operator relative error of the measured properties. The binder content of the tested mixtures varied from 575 to 686 kg/m$^3$, while w/cm from 0.22 to 0.28. Two binder compositions were used: first, Type GU cement (conforming to ASTM C150 [15]) with 6% silica fume replacement (conforming to ASTM C1240 [16]), and second, Type GU cement with 6% silica fume and 25% Class C Fly ash (complying with ASTM C618 [17]). S/A of 0.53, 0.5, and 0.59 were used in the tested mixtures. A blend of two types of aggregate having MSAs of 10 and 20 mm was used for SCC27-SCC38, in addition to a blend of two types of sand (crushed-aggregate sand and dune sand). For SCC39-SCC43, coarse aggregate with MSA of 14 mm and sand with maximum size distribution of 5 mm were employed. Two types of polycarboxylate-based HRWRAs

were used. Plastol 5000 was used in SCC27-SCC38 and Epsilon HP 570 was incorporated in SCC39-SCC43. Detailed mix designs and compositions of the tested mixtures are presented in Tables 6.5 and 6.6.

### 6.14.7 Mixing and testing procedure

Mixing and testing procedure were carried out as described in section 7.3.4. The pipe flow test was performed at several testing ages: 55, 80, and 125 min after water-cement contact time, as presented in Table 6.7.

### 6.14.8 Test results

Viscosity of the tested mixtures demonstrates a strong correlation with the flow time measured in the testing pipe, as presented in Figure 6.28. The obtained correlation signifies the influence of viscosity and the lubrication layer on the flow resistance of SCC in pipes, and supports previous research findings presented in Chapter 5. As a main asset of the obtained correlation (Figure 6.28), viscosity of the tested concrete can be estimated by the flow time ($t_f$) measured in the testing pipe, providing a practical method to evaluate viscosity in the field without the need for complex rheological measurements. Another application of the obtained correlation is that the flow time ($t_f$) can be indirectly linked to the pumping pressure loss, using existing correlations between viscosity and pressure loss. The above discussed approach is exemplified in the following exercise.

**Example**

What is the estimated viscosity and pressure loss per unit length in 4- and 5-in. pipe associated with pumping a concrete at a discharge rate of 12 l/s, knowing that the concrete showed a flow time of 2.5 seconds in the pipe flow test?

**Solution:**

***a.*** From Figure 6.28, for a flow time $t_f = 2.5$ seconds, viscosity reading is 68 Pa s.

***b.*** From Figures 6.29a and 6.29b, for a given viscosity of 68 Pa s and at a discharge rate of 12 l/s, pressure loss readings in 4- and 5-in. pipe are 119 and 52 kPa/m, respectively.

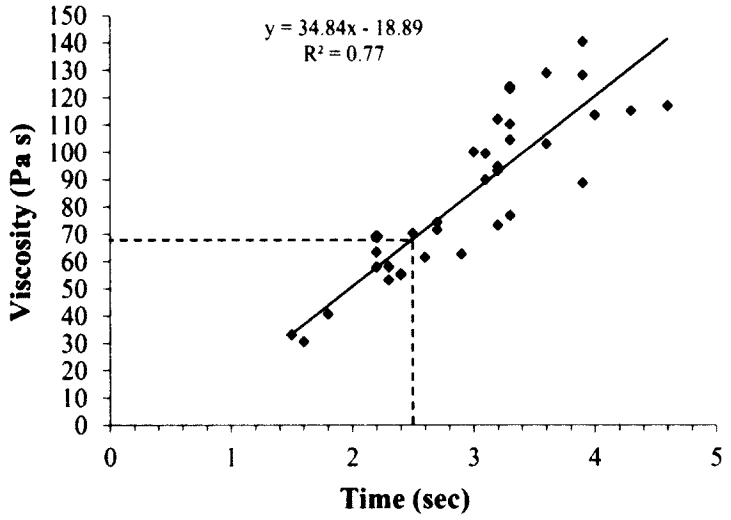


***Figure 6.28:*** *Relationships between $t_f$ (time flow) and viscosityof the tested mixtures.*

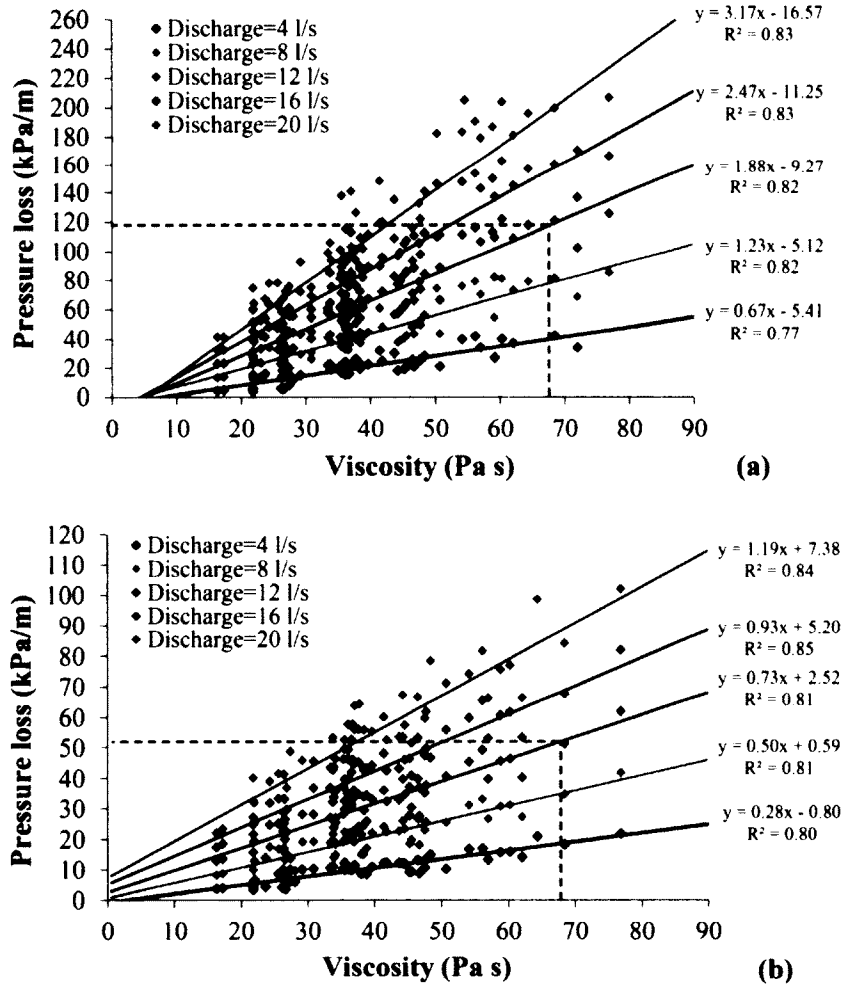


***Figure 6.29:*** *Reprint of Figure 6.10: Relationship between viscosity and pressure loss for SCC and HWC mixtures at different discharge rates using (a) 4-in. (102 mm) pipes, and (b) 5-in. (127 mm) pipes.*

***Table 6.5:*** *Mix designs of the mixtures tested in the PFT.*

| Mixture | Binder | | | Paste | S/A | Sand | | | Aggregate | | | Cement GU | Fly ash C | Silica fume | *w/cm* | HRWRA |
|---|---|---|---|---|---|---|---|---|---|---|---|---|---|---|---|---|
| | GU | FAC | SF | kg/m$^3$ | *l*/m$^3$ | S/A | Crushed | Dune | Normal | 10 mm | 20 mm | 14 mm | kg/m$^3$ | kg/m$^3$ | kg/m$^3$ | - | *l*/m$^3$ |
| SCC27GM | 69% | 25% | 6% | 575 | 375 | 0.59 | 45.0% | 14.0% | - | 32.5% | 8.5% | 8.5% | 396.8 | 143.8 | 34.5 | 0.28 | 3.59 |
| SCC28GM | 69% | 25% | 6% | 575 | 375 | 0.56 | 42.7% | 13.3% | - | 34.9% | 9.1% | 9.1% | 396.8 | 143.8 | 34.5 | 0.28 | 3.36 |
| SCC29GM | 69% | 25% | 6% | 575 | 375 | 0.53 | 40.4% | 12.6% | - | 37.3% | 9.7% | 9.7% | 396.8 | 143.8 | 34.5 | 0.28 | 3.45 |
| SCC31GM | 69% | 25% | 6% | 575 | 375 | 0.59 | 45.0% | 14.0% | - | 32.5% | 8.5% | 8.5% | 396.8 | 143.8 | 34.5 | 0.28 | 3.59 |
| SCC32GM | 69% | 25% | 6% | 605 | 375 | 0.59 | 45.0% | 14.0% | - | 32.5% | 8.5% | 8.5% | 417.5 | 151.3 | 36.3 | 0.25 | 4.86 |
| SCC34GM | 94% | 0% | 6% | 618 | 375 | 0.59 | 45.0% | 14.0% | - | 32.5% | 8.5% | 8.5% | 580.9 | - | 37.1 | 0.28 | 4.59 |
| SCC35GM | 94% | 0% | 6% | 650 | 375 | 0.59 | 45.0% | 14.0% | - | 32.5% | 8.5% | 8.5% | 611.0 | - | 39.0 | 0.25 | 6.55 |
| SCC37GM | 94% | 0% | 6% | 618 | 375 | 0.59 | 45.0% | 14.0% | - | 32.5% | 8.5% | 8.5% | 580.9 | - | 37.1 | 0.28 | 3.91 |
| SCC38GM | 94% | 0% | 6% | 600 | 364 | 0.59 | 45.0% | 14.0% | - | 32.5% | 8.5% | 8.5% | 564.0 | - | 36.0 | 0.28 | 4.77 |
| SCC39 | 94% | 0% | 6% | 618 | 375 | 0.52 | - | - | 52% | - | - | 48% | 580.9 | - | 37.1 | 0.28 | 5.11 |
| SCC40 | 94% | 0% | 6% | 618 | 375 | 0.53 | - | - | 53% | - | - | 47% | 580.9 | - | 37.1 | 0.28 | 5.23 |
| SCC41 | 94% | 0% | 6% | 618 | 375 | 0.53 | - | - | 53% | - | - | 47% | 580.9 | - | 37.1 | 0.28 | 5.63 |
| SCC42 | 94% | 0% | 6% | 618 | 375 | 0.53 | - | - | 53% | - | - | 47% | 580.9 | - | 37.1 | 0.28 | 5.45 |
| SCC43 | 94% | 0% | 6% | 618 | 375 | 0.53 | - | - | 53% | - | - | 47% | 580.9 | - | 37.1 | 0.28 | 3.97 |

*Table 6.6: Mixture compositions of the mixtures tested in the PFT.*

| Mixture | Fresh properties | | | | | | | | | | | |
|---|---|---|---|---|---|---|---|---|---|---|---|---|
| | Slump-flow (mm) | | | | T-50 (sec) | | | | V-funnel | | | |
| (hrs) | 0:15 | 0:45 | 1:15 | 1:45 | 0:15 | 0:45 | 1:15 | 1:45 | 0:15 | 0:45 | 1:15 | 1:45 |
| SCC27GM | 745 | 725 | 710 | 710 | 3.1 | 3.9 | 3.9 | 4.4 | 8.3 | 8.6 | 8.9 | 9.6 |
| SCC28GM | 715 | 710 | 710 | 700 | 3.6 | 3.5 | 3.2 | - | 10.2 | 9.9 | 10.5 | 10.4 |
| SCC29GM | 720 | 685 | 700 | 695 | 2.9 | 4 | 3.6 | 3.5 | 10.2 | 12 | 12.3 | 12.2 |
| SCC31GM | 725 | 700 | 700 | 685 | 2.8 | 2.8 | 3.2 | 3.2 | 8.9 | 8.6 | 9 | 9 |
| SCC32GM | 750 | 740 | 765 | 735 | 3 | 4.5 | 3.9 | 5 | 12.7 | 14.7 | 13.3 | 15 |
| SCC34GM | 710 | 645 | 650 | 605 | 2.7 | 3.8 | 3.7 | 5 | 7.8 | 10.3 | 11.1 | 14.5 |
| SCC35GM | 715 | 680 | 675 | 670 | 4.9 | 6.5 | 5.6 | 5.9 | 13.9 | 18.2 | 17.1 | 18.4 |
| SCC37GM | 705 | 710 | 685 | 695 | 3.1 | 2.7 | 2.5 | 1.9 | 8.4 | 9.2 | 7.4 | 5.7 |
| SCC38GM | 725 | 700 | 700 | 695 | 2.9 | 3.7 | 3.0 | 3.9 | 9.2 | 10.9 | 10.5 | 12.7 |
| SCC39 | 760 | 660 | 640 | 630 | 2.9 | 3.1 | 5.2 | 8.3 | 12.1 | 17.8 | 15.3 | 24.8 |
| SCC40 | 750 | 660 | 645 | 620 | 3.2 | 3.6 | 4.0 | 5.3 | 11.7 | 16.1 | 16.0 | 19.3 |
| SCC41 | 760 | 700 | 660 | 640 | 3.1 | 3.2 | 5.4 | 6.1 | 10.7 | 16.0 | 17.5 | 20.9 |
| SCC42 | 755 | 710 | 680 | 650 | 3.0 | 3.4 | 5.6 | 7.1 | 9.2 | 14.6 | 14.9 | 19.2 |
| SCC43 | 530 | 650 | 770 | 820 | 5.3 | 4.1 | 3.5 | 3.1 | 16.3 | 13.0 | 11.0 | 7.1 |

*Table 6.7: Rheological properties and flow times of the mixtures tested in the PFT.*

| Mixture | Differential viscosity (Pa s) | | | | Yield stress (Pa) | | | | Flow time (sec) | | |
|---|---|---|---|---|---|---|---|---|---|---|---|
| (hrs) | 0:30 | 1:00 | 1:30 | 2:00 | 0:30 | 1:00 | 1:30 | 2:00 | 0:55 | 1:20 | 2:05 |
| SCC27GM | 61.9 | 69.2 | 70.4 | 71.5 | 8.7 | 27.9 | 32.8 | 2.2 | 2.2 | 2.5 | 2.7 |
| SCC28GM | 64.5 | 62.7 | 63.4 | 61.4 | 16.8 | 19.9 | 20.5 | 2.9 | 2.9 | 2.2 | 2.6 |
| SCC29GM | 65.9 | 76.8 | 73.2 | 74.3 | 18.9 | 13.8 | 29.8 | 3.3 | 3.3 | 3.2 | 2.7 |
| SCC31GM | 59.3 | 57.9 | 53.1 | 55.1 | 27 | 6.8 | 36.1 | 2.2 | 2.2 | 2.3 | 2.4 |
| SCC32GM | 117.8 | 112.8 | 123.2 | 128.1 | 8.6 | 14.7 | 10.4 | 2.6 | - | 3.3 | - |
| SCC34GM | 56.2 | 56.7 | 62.3 | 55.1 | 29.1 | 16.4 | 6.9 | 2.2 | - | - | 2.4 |
| SCC35GM | 128 | 128.9 | 124.1 | 110.3 | 19.8 | 21.5 | 14 | 3.6 | 3.6 | 3.3 | 3.3 |
| SCC37GM | 45.4 | 40.7 | 33.1 | 30.6 | 4.9 | 6.9 | 26.3 | 1.8 | 1.8 | 1.5 | 1.6 |
| SCC38GM | 57.4 | 59.2 | 58.0 | 55.5 | 1.1 | 4.4 | 7.2 | 13 | - | 2.3 | 2.4 |
| SCC39 | 100.9 | 112.0 | 140.3 | 115.1 | 9.1 | 33.3 | 76.4 | 88.2 | 3.2 | 3.9 | 4.3 |
| SCC40 | 77.8 | 100.1 | 103.1 | 113.5 | 19.6 | 34.7 | 60.2 | 70.3 | 3 | 3.6 | 4 |
| SCC41 | 68.6 | 93.1 | 128.1 | 116.9 | 9.6 | 15.5 | 14.2 | 37.9 | 3.2 | 3.9 | 4.6 |
| SCC42 | 76.2 | 90.0 | 104.5 | 88.7 | 5.5 | 10.0 | 12.0 | 28.1 | 3.1 | 3.3 | 3.9 |
| SCC43 | 121.9 | - | 99.4 | 94.8 | 125.3 | 97.7 | 15.6 | 12.1 | 4.7 | 3.1 | 3.2 |

### 6.14.9 Repeatability

Three control concrete mixtures (SCC40-SCC42) having the same mix design were carried out to establish the single-operator error of the measured properties. Mixtures compositions and test results of the tested mixtures are presented in Tables 6.5-6.7. The mean values, absolute errors, and the relative errors of several measured properties are presented in Table 6.8.

***Table 6.8:*** *Relative error of different properties of the control mixtures measured at 30 min.*

| Measurement | Mean | Absolute error | Relative error (%) |
|---|---|---|---|
| Slump flow (mm) | 755 | 33.3 | 4.41 |
| V-funnel (sec) | 10.53 | 0.89 | 8.45 |
| Pipe flow time (sec) | 3.1 | 0.1 | 3.22 |
| Viscosity (Pa s) | 74.2 | 3.7 | 4.99 |

### 6.14.10 Remarks

The PFT simulates, to a significant extent, the flow behavior of concrete in pumping pipes. The test results revealed a strong correlation between the flow time ($t_f$) measured in the testing pipe and viscosity of the tested concrete. The obtained correlation is in line with previous research findings stating that the flow behavior of SCC is primarily affected by its rheological and tribological properties. Based on the $t_f$-viscosity relationship, the PFT grants a practical tool to predict viscosity of SCC on job sites without undertaking typical rheological experiments. Moreover, the obtained correlation can be successfully extended to predict the pumping pressure loss by means of existing relationships between viscosity and pumping pressure loss.

## 6.15 Summary

The full scale pumping experiments performed in a pumping circuit at the laboratory of the Université de Sherbrooke were described in this chapter. Details of the circuit layout, calibration tests, testing procedures, and concrete properties testing were outlined as well.

The test results of the 26 pumped concrete mixtures were presented in three main parts. In the first part, several empirical relationships were established between the pressure loss and the properties of both concrete and the lubrication layer. In the second part, statistical analyses were performed in order to derive prediction models to compute the pressure loss on the basis of the properties of concrete and the lubrication layer. In the third part, changes in concrete properties due to prolonged pumping were detailed. In addition, comparisons between the behavior of SCC and CVC during pumping were made. Lastly, the development of a new simple test method to determine the pressure loss on job sites was described.

In the first part, the established empirical relationships revealed that viscosity, rather than yield stress, is a key parameter determining the pressure loss for SCC and HWC mixtures. An increase in concrete viscosity leads to a considerable increase in pressure loss, with more sizable losses at higher discharge rates. Overall, these empirical findings were in great agreement with those obtained from the analytical study (presented in section 5.11).

In the case of CVC, the opposite is true, yield stress, instead of viscosity, primarily controls the pressure loss. Therefore, an increase in yield stress results in an increase in pressure loss when pumping CVC. It was also found that the new introduced tribological parameters displayed cogent correlations with the pressure loss when using SCC and CVC. These correlations will help further the understanding of the consequences of changes in $Itrib_{ll}$ and viscosity on pressure loss (Chapter 7)

In virtue of the circuit layout, the influence of the pipe size on pressure loss was also investigated; it was found that for a given viscosity, pressure loss decreases with increasing the pipe size. On the other hand, decreasing the pipe size can negatively affect the mixture's stability. Pipe size selection is therefore a difficult compromise between reaching the total head and maintaining mixture stability.

In the second part, as a result of the statistical analyses, several models that precisely predict the pressure loss on the basis of the measured rheological and tribological properties of concrete were derived. The statistical analyses revealed the substantial effects of viscosity and $Itrib_{ll}$ on pressure loss. Among both parameters affecting pressure loss, viscosity showed the highest effect followed by the increasing effect of $Itrib_{ll}$ with decreasing the pipe diameter. Simple test methods including the V-funnel and slump tests were also modelized to easily compute the pressure loss for SCC and CVC, on job sites without the need for rheological and tribological measurements.

In the third part, the empirical results indicated that pumping leads to significant changes in concrete properties. Generally, viscosity decreases due to pumping while yield stress, temperature, and air content all increase. The tribological changes due to pumping can be summarized as an increase in $Itrib_{ll}$ and a reduction in $Itrib_{co}$ and $Itrib_{tot}$. This is justified by the reduction in concrete viscosity and the changes in the properties of the lubrication layer, both of which due to pumping.

The comparison between SCC and CVC highlighted their different flow patterns in pipes. SCC, in most cases, exhibits a slight-non linear relationship between pressure loss and discharge rate, while CVC shows a clear linear correlation. Overall, SCC can be advantageous for long-distance pumping because its ability to reduce pressure loss with pumping. At the same time, when pumping SCC stability issues can be induced by viscosity reduction and insufficient increase in yield stress. Unlike SCC, the range of the tested CVC mixtures exhibited an increase in pressure loss due to pumping, which may hamper its applicability for long-distance pumping.

Lastly, the developed pipe flow test (PFT) is considered a practical method to assess the flow behavior of SCC in pipes. Based on the flow time-viscosity relationship, the PFT test grants a practical tool to predict viscosity of SCC on job sites without undertaking typical rheological and tribological experiments. Moreover, the obtained correlation can be successfully extended to predict the pumping pressure loss by means of existing relationships between viscosity of SCC and pumping pressure loss.

## 6.16 References


[1] Feys D., "Interactions between rheological properties and pumping of self-compacting concrete", Ph.D. dissertation, Ghent University, 2009.

[2] Kaplan D., "Pumping of concretes", Ph.D. dissertation, Laboratoire Central des Ponts et Chausées, Paris, 2001.

[3] Ngo T.T., "Influence of concrete compositions on the pumpability parameters", Ph.D. dissertation, Cergy Pontoise, France, 2009.

[4] Macosko C.W., *Rheology principles, measurements and applications*, 10. Veh New-York, 1994.

[5] Winter H. H., "Viscous dissipation term in energy equation", *American Institute of Chemical Engineers*, 1987.

[6] Li Z., Ohkubo T-A., Tanigawa Y., "Flow performance of highly-fluidity concrete", *Materials in Civil Engineering*, vol. 16, pp. 588–596, 2004.

[7] Eckardstein K., Ernst V., "Concrete and concrete pumps; a concrete placing manual", Schwing, Tech. Rep., 1983, p. 133.

[8] Stephenson T.O., "Concrete pumping, pumpable concrete", *Australian civil Engineering*, pp. 24–27, 1968.

[9] Jacek Golaszewski, Janusz Szwabowski, "Influence of superplasticizers on rheological behaviour of fresh cement mortars", *Cement and Concrete Research*, vol. 34, no. 2, pp. 235–248, 2004.

[10] Dyer R.M, "An investigation of concrete pumping and effects of pressure on the air void systeme of concrete", Master thesis, university of Washington, 1991, p. 222.

[11] Rust A.C., Manga M., "Effect of bubble deformation on the viscosity of dilute suspensions", *Non-Newtonian Fluid Mechanics*, vol. 104, pp. 53–63, 2002.

[12] Golaszewski J., Szwabowski J., "Influence of superplasticizers on rheological behaviour of fresh cement mortars", *Cement and Concrete Research*, vol. 34, pp. 235–248, 2004.

[13] Jolicoeu C., Sharman C., Otis N., Lebel A., Simard M.-A., Pagé M., "The influence of temperature on the rheological properties of superplasticized cement pastes", in *Superplasticizers and Other Chemical Admixtures in Concrete, Ed. V.M. Malhotra*, Rome, 1997, pp. 379–415.

[14] Fernàndez-Altable V., Casanova I., "Influence of mixing sequence and superplasticiser dosage on the rheological response of cement pastes at different temperatures", *Cement and Concrete Research*, vol. 36, pp. 1222–1230, 2006.

[15] ASTM C150 / C150M - 11, "Standard specification for portland cement", *American Society for Testing and Materials*,

[16] ASTM C1240 - 11, "Standard specification for silica fume used in cementitious mixtures", *American Society for Testing and Materials*,

[17] ASTM C618 - 08a, "Standard specification for coal fly ash and raw or calcined natural pozzolan for use in concrete", *American Society for Testing and Materials*,

# Chapter 7

# Mix Design Optimization to Reduce Pumping Pressure

## 7.1 Introduction

One of the definitive lessons of the previous chapter was that pumping pressure loss can be effectively reduced by decreasing the viscosity and tribological flow resistance of concrete. Hence, mix design parameters that induce a reduction in concrete viscosity will lead to reduction in pressure loss. Reducing pumping pressure by adjusting the mix design parameters is the main concern of this chapter. The investigation begins with tests on the Concrete Equivalent Mortar scale (CEM), which provides a systematic scan of the following mix design parameters:

- cementitious materials (Class C and Class F fly ash, slag, and silica fume) at different substituting rates;
- water-to-cement ratio ($w/cm$); and
- paste volume.

With the research findings from the CEM scale as input, the investigation extends to the concrete scale to further confirm the results and examine several mix design parameters that could not be captured through the CEM scale. The effects of the following mix design parameters on rheological and tribological properties of concrete are in focus:

- water-to-cement ratio;
- binder content and combination;
- paste volume;
- maximum size of aggregate (MSA);
- sand-to-total aggregate ratio (S/A);
- air content; and
- slump flow consistency.

Throughout the analysis, the results of the previous chapter are recalled in order to disclose the different correlations between pressure loss and the targeted investigated mix design parameters.

## 7.2 CEM testing

CEM is widely used in concrete research to project causal relationships onto the concrete scale since several correlations exist between the properties measured in CEM and their counterparts in corresponding concrete mixtures [1]. The CEM scale is therefore considered an efficient way to systematically scan the different effects of concrete mix design parameters with reduced laboratory work and cost.

The CEM mix design concept is based on replacing all aggregate larger than 5 mm in the concrete mixture by an equivalent amount of sand having the same surface area

of the aggregate. The total surface area of the aggregate and the sand is calculated from the grain size distribution, assuming a spherical shape of grains.

Despite the merit of CEM in investigating the effects of mix design parameters, the real interactions between the aggregate and the other constituent materials in the mixture remain hard to capture accurately. Therefore, validating the results of CEM on the concrete scale is considered an important extension, particularly when investigating aspects related to the granular system.

### 7.2.1 Raw materials

All mixtures were prepared with GU Type cement (ordinary Portland cement) conforming to ASTM C150 [2], Class C and F fly ash, a normal-Blaine slag, and silica fume that all comply with ASTM C618, ASTM C989, and ASTM C1240, respectively [3–5]. Two types of sands, with a maximum aggregate size of 5 mm and complying with the recommendations of ASTM C33 [6], were chosen. A commercially available polycarboxylate-based HRWRA (Epsilon HP 570) with high workability retention was used and the dose was optimized through several trial batches. Chemical compositions and physical properties of the GU cement and the cementitious materials are listed in Tables A.3-A.11. The grain size distribution of the sand and aggregate used are presented in Figures A.1-A.3, and the physical properties are listed in Table A.1.

### 7.2.2 Mix design and preparation

The tested mixtures were all based on a corresponding SCC reference mixture having a total binder content of 550 kg/m$^3$, a paste volume of 375 l/m$^3$, S/A of 0.54, and $w/cm$ of 0.28. The paste volume and $w/cm$ changed when investigating their effects on viscosity and compressive strength. The HRWRA dose was adjusted to reach a target mini-slump of 225 $\pm$ 10 mm at 15 minutes after water-cement contact time. By fixing the mini-slump, it was possible to explore the mix design variations capable of attaining the same target value. In addition, the existing knowledge on the correlation between CEM and SCC shows that this value corresponds to a SCC slump flow of around 720 mm [1].

Mixing was performed in an 8-liter Hobard mixer as follows. Sand was added to the mixer and homogenized to determine its humidity. Half the mixing water was added and mixed for 30 seconds. All cementitious materials were added with the remaining water, and the reference time was set the moment cement and water came in contact. After 2 minutes of mixing, the HRWRA was added, and the mortar was mixed for 2 more minutes. The mixture was kept at rest for 1 minute, then mixed for another minute. Afterward, the mini-slump flow was tested at 15 minutes after cement-water contact time. If needed, the slump was adjusted by adding another dose of HRWRA to the mixture and mixing it for 2 more minutes, then repeating the test. Mortars that failed to reach the desired slump flow at 17 minutes were discarded.

*Table 7.1: Mix designs and fresh properties of the tested mortars.*

| Mixture | Sand | Cement | Slag | Silica | Fly ash C | Fly ash F | Added water | SP | Mini slump | | V-funnel | |
|---|---|---|---|---|---|---|---|---|---|---|---|---|
| | | | | | | | | | 15min | 80min | 25min | 85min |
| | kg/m$^3$ | kg/m$^3$ | kg/m$^3$ | kg/m$^3$ | kg/m$^3$ | kg/m$^3$ | kg/m$^3$ | kg/m$^3$ | mm | mm | sec. | sec. |
| Reference mixture | 1402.1 | 790.2 | - | - | - | - | 216.0 | 7.01 | 235 | 220 | 15 | 16 |
| 20% slag | 1396.8 | 631.4 | 157.9 | - | - | - | 217.2 | 5.06 | 230 | 170 | 33.6 | 49.2 |
| 25% slag | 1395.4 | 591.8 | 197.3 | - | - | - | 217.9 | 4.03 | 230 | 150 | 25.2 | 63 |
| 30% slag | 1394.1 | 552.2 | 236.7 | - | - | - | 217.7 | 4.29 | 234 | 200 | 26.1 | 20.5 |
| 40% slag | 1391.5 | 473.1 | 315.4 | - | - | - | 217.8 | 3.90 | 233 | 160 | 31.4 | 45.3 |
| 15% Fly ash C | 1332.0 | 652 | - | - | 115.0 | - | 215.0 | 4.6 | 227.5 | 182.5 | 16.7 | 15.6 |
| 20% Fly ash C | 1318.0 | 612 | - | - | 153.0 | - | 214.0 | 3.8 | 230.0 | 175.0 | 11.9 | 16 |
| 25% Fly ash C | 1304.0 | 572 | - | - | 191.0 | - | 214.0 | 3.1 | 227.5 | 160.0 | 18.7 | 14 |
| 30% Fly ash C | 1291.0 | 532 | - | - | 228.0 | - | 213.0 | 2.7 | 225.0 | 192.5 | 17.2 | 15.3 |
| 15% Fly ash F | 1348.0 | 654 | - | - | - | 115.0 | 215.0 | 5.6 | 230.0 | 200.0 | 12.6 | 14.4 |
| 20% Fly ash F | 1339.0 | 615 | - | - | - | 154.0 | 215.0 | 4.8 | 225.0 | 170.0 | 12.3 | 19.3 |
| 25% Fly ash F | 1331.0 | 575 | - | - | - | 192.0 | 215.0 | 4.6 | 227.5 | 175.0 | 18.6 | 22.2 |
| 6% silica+20 % Fly ash C | 1340.3 | 577.3 | - | 46.8 | 156.0 | 156.0 | 213.6 | 6.36 | 230 | 200 | 14 | 15.5 |
| 6% silica+25 % Fly ash C | 1328.5 | 536.9 | - | 46.7 | 194.5 | 194.5 | 212.7 | 6.88 | 235 | 235 | 11 | 11 |
| 6% silica+30 % Fly ash C | 1316.6 | 496.8 | - | 46.6 | 232.9 | 232.9 | 212.8 | 6.10 | 235 | 235 | 13.5 | 14.5 |
| 6% silica+10 % Fly ash F | 1371.1 | 659.5 | - | 47.1 | 78.5 | 78.5 | 215.0 | 6.49 | 225 | 21 | 14.6 | 18 |
| 6% silica+15 % Fly ash F | 1362.5 | 619.1 | - | 47.0 | 117.6 | 117.6 | 215.5 | 5.19 | 225 | 215 | 11.1 | 19 |
| 6% silica+20 % Fly ash F | 1353.8 | 578.9 | - | 46.9 | 156.5 | 156.5 | 214.9 | 5.45 | 225 | 195 | 16.1 | 19.2 |
| 25% Fly ash C+4 % silica | 1332.9 | 553.0 | - | 31.2 | 194.7 | 194.7 | 213.1 | 6.62 | 235 | 235 | 12.7 | 14 |
| 25% Fly ash C+8 % silica | 1324.1 | 520.9 | - | 62.2 | 194.4 | 194.4 | 212.5 | 6.88 | 235 | 235 | 10.5 | 12.5 |
| 15% Fly ash F+4 % silica | 1366.9 | 635.4 | - | 31.4 | 117.7 | 117.7 | 213.8 | 7.79 | 225 | 195 | 20 | 21.5 |
| 15% Fly ash F+8 % silica | 1358.0 | 602.9 | - | 62.6 | 117.4 | 117.4 | 212.7 | 8.70 | 225 | 205 | 16.5 | 19 |
| 2% silica | 1397.6 | 773.6 | - | 15.8 | - | - | 215.7 | 7.14 | 230 | 180 | 23.3 | 29 |
| 4% silica | 1393.0 | 757.1 | - | 31.5 | - | - | 215.3 | 7.40 | 230 | 205 | 16.2 | 23.1 |
| 5% silica | 1390.8 | 748.9 | - | 39.4 | - | - | 216.4 | 5.84 | 230 | 160 | 25 | 27 |
| 6% silica | 1388.5 | 740.7 | - | 47.3 | - | - | 214.9 | 7.66 | 235 | 230 | 13 | 16.2 |
| 8% silica | 1384.0 | 724.2 | - | 63.0 | - | - | 213.6 | 9.09 | 235 | 215 | 16.1 | 22.2 |
| 8% silica.rep.* | 1384.0 | 724.2 | - | 63.0 | - | - | 214.6 | 7.79 | 230 | 205 | 12.23 | 14.7 |
| 10% silica | 1379.5 | 707.8 | - | 78.6 | - | - | 214.4 | 7.66 | 235 | 1955 | 20.1 | 24.4 |
| 15% silica | 1368.3 | 667.0 | - | 117.7 | - | - | 212.2 | 10.00 | 225 | 215 | 13.2 | 15.5 |
| 6% silica - 0.22 *w/cm* | 1490.1 | 756.3 | - | 48.3 | - | - | 155.2 | 29.10 | 225 | 195 | 66 | 15 |
| 6% silica - 0.25 *w/cm* | 1438.8 | 748.4 | - | 47.8 | - | - | 188.8 | 13.60 | 225 | 195 | 40 | 16 |
| 6 % silica - 0.28 *w/cm* | 1388.5 | 740.7 | - | 47.3 | - | - | 213.4 | 9.61 | 235 | 220 | 13.2 | 15.5 |
| Paste volume = 300 l/m$^3$ | 1461.0 | 667.0 | - | 43.0 | - | - | 199.0 | 14.8 | 225.0 | 210.0 | 33.2 | 35.0 |
| Paste volume = 367 l/m$^3$ | 1264.0 | 782.0 | - | 50.0 | - | - | 233.0 | 9.7 | 225.0 | 218.0 | 15.9 | 16.4 |
| Paste volume = 400 l/m$^3$ | 1171.0 | 836.0 | - | 53.0 | - | - | 249.0 | 10.3 | 235.0 | 233.0 | 10.6 | 11.2 |

* All subsequent mixtures were prepared with sand 2, while precedent mixtures were prepared with sand 1.

***Table 7.2:*** *Compressive strength of the tested mortars.*

| Mixture | 28-days | 56-days |
|---|---|---|
| | MPa | MPa |
| Reference mixture | 87 | 92 |
| 20% slag | - | - |
| 25% slag | 82 | 90 |
| 30% slag | - | - |
| 40% slag | 80 | 90 |
| 15% Fly ash C | 86 | - |
| 20% Fly ash C | 82 | - |
| 25% Fly ash C | 79 | - |
| 30% Fly ash C | 78 | - |
| 15% Fly ash F | 89 | - |
| 20% Fly ash F | 88 | - |
| 25% Fly ash F | 81 | - |
| 6% silica+20 % Fly ash C | 86 | 94 |
| 6% silica+25 % Fly ash C | 82 | 89 |
| 6% silica+30 % Fly ash C | 76 | 93 |
| 6% silica+10 % Fly ash F | 93 | 97 |
| 6% silica+15 % Fly ash F | 94 | 101 |
| 6% silica+20 % Fly ash F | 89 | 93 |
| 25% Fly ach C+4 % silica | 84 | 85 |
| 25% Fly ach C+8 % silica | 86 | 100 |
| 15% Fly ash F+4 % silica | 86 | 92 |
| 15% Fly ash F+8 % silica | 83 | 89 |
| 2% silica | 98 | 107 |
| 4% silica | 96 | 100 |
| 5% silica | 98 | 101 |
| 6% silica | 104 | 107 |
| 8% silica.rep.* | 86 | 93 |
| 10% silica | 107 | 114 |
| 15% silica | 103 | 107 |
| 6% silica - 0.22 *w/cm* | 91 | - |
| 6% silica - 0.25 *w/cm* | 88 | - |
| 6 % silica - 0.28 *w/cm* | - | - |
| Paste volume = 300 l/m$^3$ | 95 | - |
| Paste volume = 367 l/m$^3$ | 92 | - |
| Paste volume = 400 l/m$^3$ | 92 | - |

* All subsequent mixtures were prepared with sand 2, while the precedent mixtures were prepared with sand 1.

### 7.2.3 Test methods and procedures

The flowability of the tested mixtures was evaluated through the mini-slump flow and the mini V-funnel flow time, according to ASTM C1437-07 and EFNARC (2002), respectively [7, 8]. The rheological properties were measured with the ConTec Viscometer 6 (described in section 3.8.1).

The following tests were performed when the required mini-slump flow of 225 $\pm$ 10 mm was attained: mini-slump flow at 15 and 80 minutes, mini V-funnel at 25 and 85 minutes, and rheometer at 20 minutes. All samples at the different testing ages were taken from the mixer preceded by a remixing period of 30 seconds to eliminate any

thixotropic effect on the measurements. Compressive strength was tested at 1, 7, 28, and 56 days, on 50 mm cubes cured under standard moisture curing conditions (100% humidity and 23 ± 2 °C).

### 7.2.4 Assessment of the rheological properties

Rheological tests with the ConTec Viscometer 6 began with a pre-shearing period of 30 seconds at the maximum rotational velocity (0.7 rps) to eliminate the effect of thixotropy. The pre-shearing period was followed by a decrease in the rotational velocity from 0.7 rps to 0.025 rps through 10 five-second increments. The average torque (T) and rotational velocity (N) were calculated at each step from the data points measured in equilibrium for further analysis.

Preliminarily analysis of the rheological measurements showed that the mortars exhibit non-linear shear-thinning behavior and even, in some cases, combined shear-thickening and shear-thinning behaviors. Although the physical cause of these behaviors is still under investigation, it could be attributed to the high concentration of solid materials in the mixtures, or to insufficient mixing energy. Considering that there is no model available for these special cases, the following procedure was used to transform the rheological raw data into fundamental parameters. Firstly, the Bingham model was applied to all data points measured at a rotational velocity equal to or lower than 0.3 rps and the plastic viscosity ($\mu_p$) was obtained, as indicated in Figure 7.1. Secondly, for all data measured at rotational velocities higher than 0.43 rps, the corresponding shear stress was divided by the shear rate, delivering the apparent viscosity ($\mu_{app}$) (the slope of the line connecting the measurement point with the origin). The reported apparent viscosity is the average value of the four data points in the zone. The ranges of measurements for the apparent and plastic viscosity are presented in Figure 7.1.

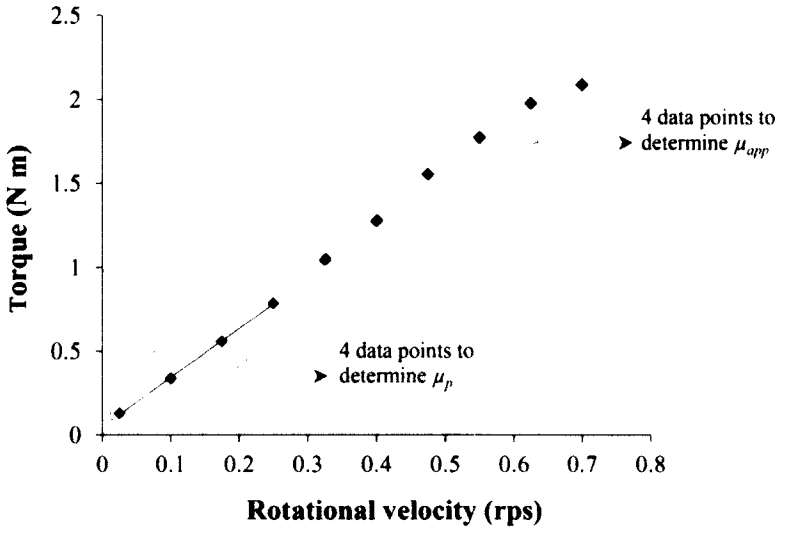


***Figure 7.1:*** *Example of the plastic viscosity ($\mu_p$) and apparent viscosity ($\mu_{app}$) determined by the flow curve.*

### 7.2.5 Effect of mix design parameters on the properties of CEM

This phase aims to optimize mix design parameters that are efficient in reducing viscosity and meeting the high strength requirements. The investigated parameters include the type and substituting rate of the cementitious materials, *w/cm*, and paste volume. Mixtures proportioning and fresh properties of the tested mixtures are listed in Table 7.1, and the compressive strengths in Table 7.2.

### 7.2.6 Influence of cementitious materials

The investigation into the influence of cementitious materials can be divided into two stages. In the first stage, the GU cement was replaced at different levels by one of 4 different cementitious materials including silica fume, Class C and Class F fly ash, and slag. In the second stage, blends of two cementitious materials were used in ternary binders with the GU cement. Based on the results emanating from both stages, different replacement levels of cementitious materials were optimized by the highest reduction in plastic viscosity, and were considered for further investigation on the concrete scale.

#### Silica fume

Seven mixtures with silica fume replacement rates of 2%, 4%, 5%, 6%, 8%, 10%, and 15%, were prepared to optimize the silica fume substituting level (see Table 7.1). The changes in plastic and apparent viscosities, as a function of the replacement rate of silica fume, are shown in Figure 7.2. The values are expressed relative to the viscosity of the reference mixture (prepared with 100% GU cement). As indicated in Figure 7.2, the plastic viscosity decreases significantly (by approximately 52%) as the silica fume replacement increases to 6%-8%, while beyond this point only a slight reduction in viscosity is obtained. The observed reduction can be justified by the improved packing density of the binder combination provided by the silica fume replacement at low rates.

In reference to the literature, the results are in partial agreement; early research states that replacing the GU cement with silica fume up to a certain level reduces viscosity while beyond this point an increase is obtained [9, 10]. This follows the general orientation of the test results, however, two differences can still be highlighted. The first is that viscosity does not show the same dramatic increase at high silica fume replacement rates. The second is that the optimal rate (giving minimum viscosity) that was found during testing is somewhat higher than those reported in literature (5-7%). The reasons for these differences are still unknown, but a possible explanation could be attributed to the high concentration of silica fume particles in the tested samples. It follows that a considerable part of these particles remains coagulated during mixing or testing and consequently limits the negative effect of silica fume. This incomplete dispersion of the silica fume particles can be attributed to insufficient mixing energy or the dispersing action of the HRWRA used.

The compressive strength results (presented in Table 7.2) indicate that, generally, compressive strength increases with the silica fume replacement rate. The highest strength

value of 114 MPa (at 56 days) was obtained at a replacement level of 10%, while a compressive strength of 107 MPa was obtained for a substitution rate of 6%.

In conclusion, replacing the GU cement by 6%-8% silica fume reduces viscosity by more than 50%, while at approximately the same rate (6%), the compressive strength can reach 107 MPa at 56 days. Taking into consideration the viscosity reduction and compressive strength development, a replacement rate of 6% silica fume was considered the optimized substitution rate to be used in the future phases.

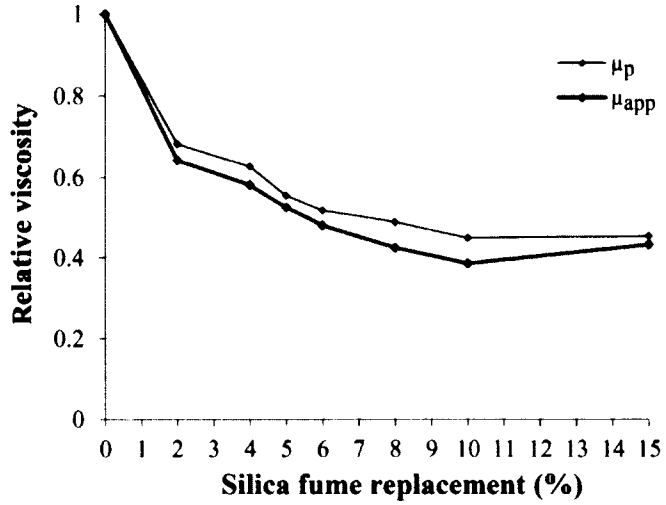


***Figure 7.2:*** *Plastic and apparent viscosities as a function of silica fume replacement rate. The values are relative to the viscosity of the reference mixtures measured at 20 min.*

## Fly ash

Previous studies on the rheological behavior of mortar and concrete concluded that for a given *w/cm*, viscosity can be considerably decreased by adding fly ash [11–14]. For concrete pumping requirements, the optimal rate falls in the range of 15%-20% [15], varying depending on *w/cm* and HRWRA dose [16]. Therefore, to optimize the replacement level of fly ash, several mixtures were prepared with two types of fly ash (Class C and F) and replacement rates varying from 15 to 30% (mix designs and fresh properties are presented in Table 7.1).

The resulting plastic and apparent viscosities of the tested mixtures as a function of fly ash replacement are depicted in Figure 7.3. For both types of fly ash, the curves exhibit similar tendencies at different replacement rates. In general, the apparent viscosity is 10%-20% higher than the plastic viscosity indicating a slight shear thickening behavior. As presented in Figure 7.3a, increasing the fly ash replacement in the case of Class C fly ash reduces both plastic and apparent viscosities, with the minimum values obtained at 25%. For Class F, the minimum plastic and apparent viscosities are obtained at a replacement rate of 15% (see Figure 7.3b).

Comparing the results of both types of fly ash affirms that Class C fly ash is more efficient in reducing viscosity than Class F. This can be explained by the different chemical composition of both types of fly ash, resulting in different HRWRA adsorption rates. The

low HRWRA adsorption of Class C fly ash justifies its superior viscosity reduction. This is because more particles of HRWRA are available in the mortar matrix resulting in higher dispersing action for the cement grains.

The compressive strength results listed in Table 7.2 indicate that replacing the GU cement by either class of fly ash reduces the compressive strength below that of the reference mixture without any fly ash. The reduction in compressive strength is a well-known disadvantage when using fly ash. Considering the viscosity reduction and the compressive strength development, replacement rates of 25% and 15% were taken as the optimized levels for Class C and F fly ash, respectively.

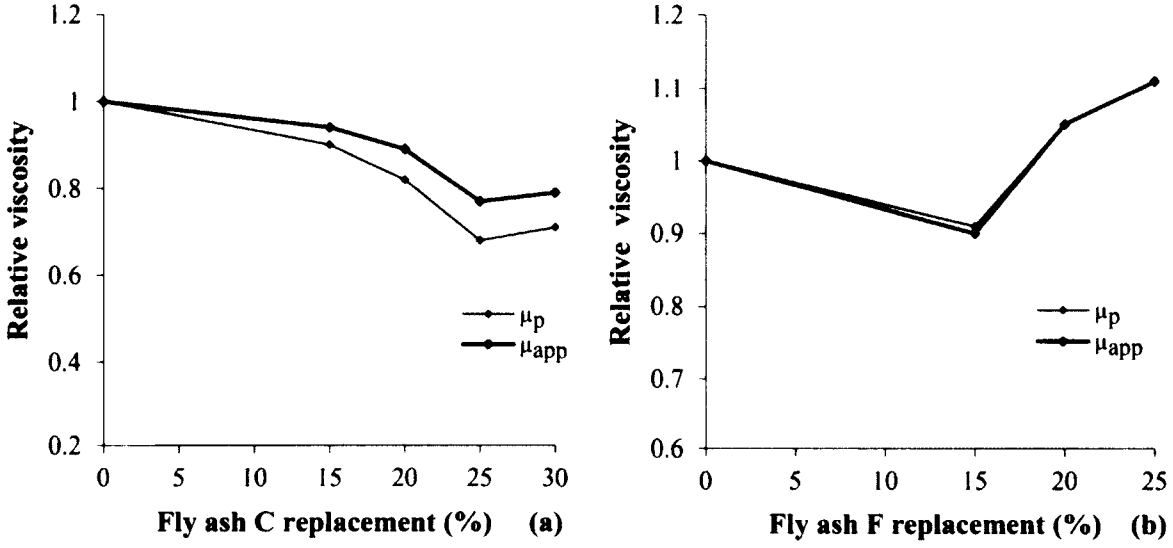


***Figure 7.3:*** *Plastic and apparent viscosities as a function of the replacement level of (a) Class C fly ash and (b) Class F fly ash. The values are expressed relative to the viscosity of the reference mixture measured at 20 min.*

## Slag

Four mixtures containing different slag replacement rates of 20%, 25%, 30%, and 40% were tested. The plastic and apparent viscosities as a function of slag replacement relative to the reference mixture without any slag are plotted in Figure 7.4. The lowest plastic and apparent viscosities are obtained for the substitution rate of 25%, providing a viscosity reduction of around 20%. Higher slag replacements of 30%-40% lead to steady increases in both plastic and apparent viscosities, as depicted in Figure 7.4. For all replacement rates, the plastic viscosity considerably exhibits lower values than the apparent viscosity, indicating a shear thickening behavior. This type of behavior increases viscosity and is unfavorable in applications with high shear rates such as pumping, because it results in an increase in the required pumping pressure.

On the subject of compressive strength, the results presented in Table 7.2 indicate that the replacement rates of 25% and 40% do not have any effect on the compressive strengths at 28 and 56 days. Taking into consideration the previously discussed inconveniences, slag was no longer used in the proceeding phases of the optimization.

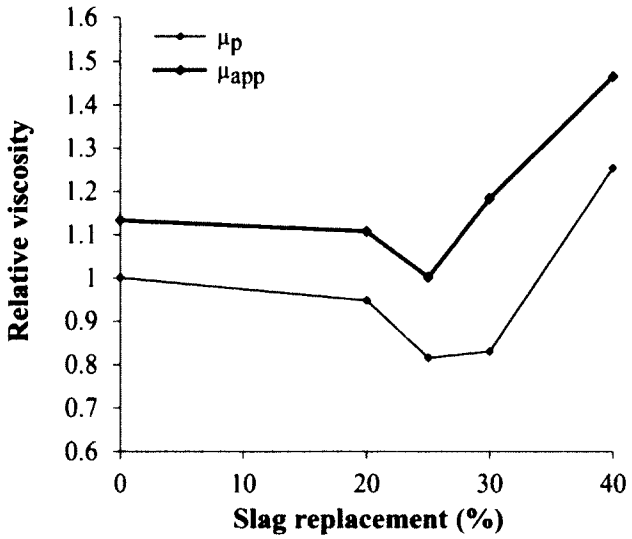


***Figure 7.4:*** *Plastic and apparent viscosities as a function of slag replacement. The values are expressed relative to the viscosity of the reference mixture measured at 20 minutes.*

## Silica fume and fly ash blend

It is well established that combining of silica fume and fly ash can significantly reduce viscosity [17]. The investigation into the combination of silica fume and fly ash comprises two stages. In the first stage, the silica fume replacement levels were varied, while the fly ash substitution levels were fixed. As a result, 6 mixtures in the first stage were prepared with various silica fume replacement rates varying by ± 2% around the optimized rate of 6% and fixed optimized fly ash rates of 25% for Class C and 15% for Class F.

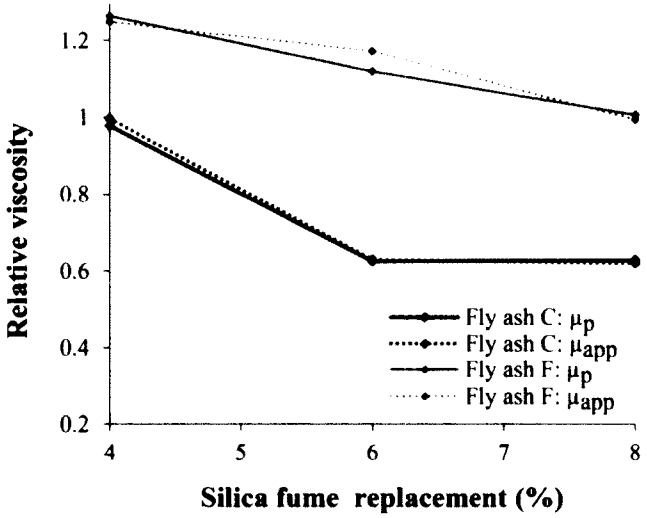


***Figure 7.5:*** *Plastic and apparent viscosities as a function of silica fume replacement for mixtures with fixed substitution rates of 25% and 15% for Class C and Class F fly ash, respectively. The values are relative to the plastic viscosity of the mixture prepared with only 6% silica fume.*

The resulting changes in plastic and apparent viscosities of the tested mixtures are presented in Figure 7.5. The values are expressed relative to the viscosity of the reference mixture prepared with 6% silica fume. As demonstrated in Figure 7.5, combining any replacement rate of silica fume with 15% Class F fly ash does not lead to any significant reduction in viscosity. On the other hand, using 6% or 8% silica fume replacement combined with 25% Class C fly ash leads to a sizable decrease in viscosity compared to the reference mixture. Hence, it can be concluded that combining silica fume with 15% Class F fly ash does not contribute to viscosity reduction, whereas combining 6% silica fume with 25% Class C fly can decrease viscosity by about 30%. The compressive strength results (presented in Table 7.2) demonstrate that all mixtures prepared with fly ash exhibit lower compressive strength than the reference mixture, further confirming that fly ash can adversely affect the compressive strength. The highest compressive strength of 101 MPa (at 56 days) was obtained for the combination of 6% silica fume and 15% of Class F fly ash. In the case of Class C fly ash, the highest compressive strength of 100 MPa was obtained by the combination of 8% silica fume and 25% fly ash.

In the second stage of the investigation into the influence of cementitious materials, the silica fume substitution level was fixed at 6%, while the fly ash replacements were varied by ± 5% around the optimized rates of both types of fly ash. As a result, 6 mixtures were carried out with silica fume replacement of 6%, Class C replacement of 20%, 25%, and 30%, and Class F replacement of 10%, 15%, and 20%. The resulting plastic and apparent viscosities of tested mixtures are presented in Figure 7.6. As demonstrated in Figure 7.6a, for Class C fly ash, viscosity reduces relatively by 30% for a replacement rate of 25%, while for Class F, no significant reduction was observed (see Figure 7.6b). The compressive strength results presented in Table 7.2 confirm that the addition of fly ash to mixtures contain silica fume reduces their resistance. This reduction is more pronounced in the case of Class C fly ash.

Based on the results emanating from the two stages discussed above, it can be concluded that the combination of 25% Class C fly ash and 6% silica fume is the optimal substitution rate. This blend shows a viscosity reduction of about 30% relative to the mixture with only 6% silica fume. On the other hand, combining Class F fly ash with silica fume does not lead to further reduction in viscosity. The compressive strength results indicate that the addition of fly ash adversely affects the results; however, a compressive strength of 89 MPa (at 56 days) was attained by the optimized blend.

### 7.2.7 Influence of mix design parameters

#### Paste volume

The paste volume is a key factor in determining the rheological properties of concrete as it characterizes the liquid phase of the fresh matrix. The required paste volume firmly depends on the granular characteristics of the aggregates; for a given aggregate size and content there is a minimum amount of paste volume below which the concrete exhibits poor deformability [18]. As previously outlined, it is difficult to capture with sufficient accuracy the effect of paste volume in relation to aggregate characteristic through CEM trials. Nevertheless, the research findings of this phase will help better understand the

influence of paste volume on the rheological properties of CEM. Further validation on concrete scale to confirm these findings is still required.

The influence of paste volume on CEM viscosity was investigated through 4 mixtures with corresponding concrete paste volumes of 300, 333, 367, and 400 l/m$^3$. All mixtures were prepared with a binder combination of 94% GU cement and 6% silica fume. The mix designs and fresh properties of the tested mixtures are presented in Table 7.1. The resulting plastic and apparent viscosities relative to the reference mixture (with a paste volume of 333 l/m$^3$) are depicted in Figure 7.7.

The results show that viscosity declines as paste volume increases from 300 to 333 l/m$^3$, and from this point it does not change significantly. The decrease in viscosity can be justified by the increasing number of the hydrodynamic interactions and the decreasing number of the solid-solid ones created by increasing the paste volume.

Among the investigated paste volumes, the volume of 333 l/m$^3$ seems to be a critical value beyond which the studied parameters do not significantly decrease viscosity. This finding is further confirmed through the investigation on the concrete scale.

### *w/cm*

The influence of *w/cm* on CEM viscosity was evaluated through two groups of mixtures prepared with different binders. The first binder is a combination of the GU cement with 6% silica fume, and the second consists of the GU cement with substitution rates of 6% silica fume and 25% Class C fly ash. In the first group, three *w/cm* of 0.28, 0.25, and 0.22 were used, whereas only 0.28 and 0.25 were used for the second group.

Figure 7.8 shows the influence of *w/cm* on the plastic and apparent viscosities of the tested mixtures. For the first group, a reduction of *w/cm* from 0.28 to 0.22 leads to a substantial 300% increase in viscosity. Likewise, for the second group, a reduction in

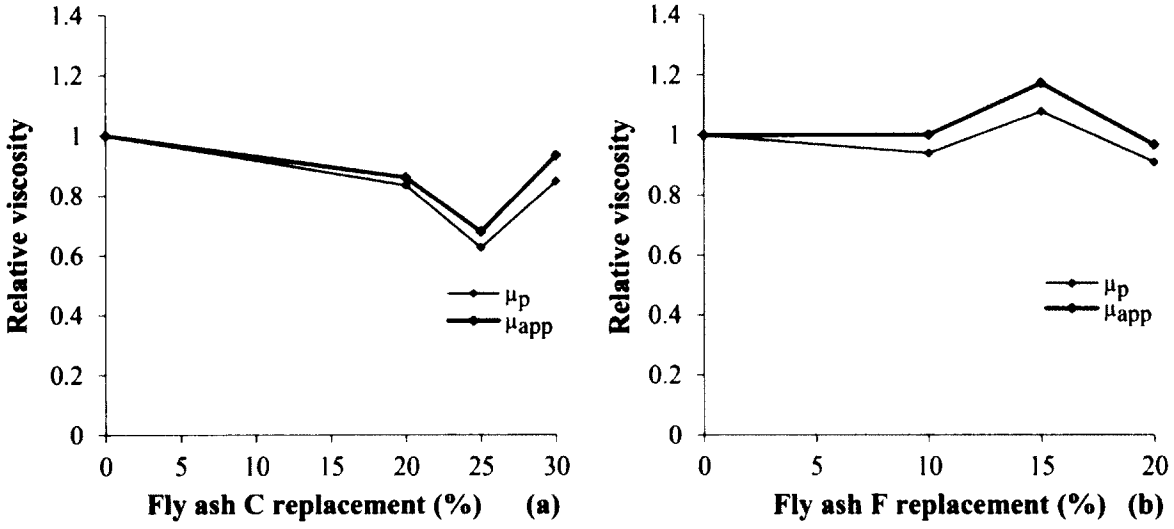


***Figure 7.6:*** *Plastic and apparent viscosities as a function of the replacement rate of (a) Class C fly ash and (b) Class F fly ash for mixtures containing 6% silica fume. The values are expressed relative to the plastic viscosity of the mixture with only 6% silica fume.*

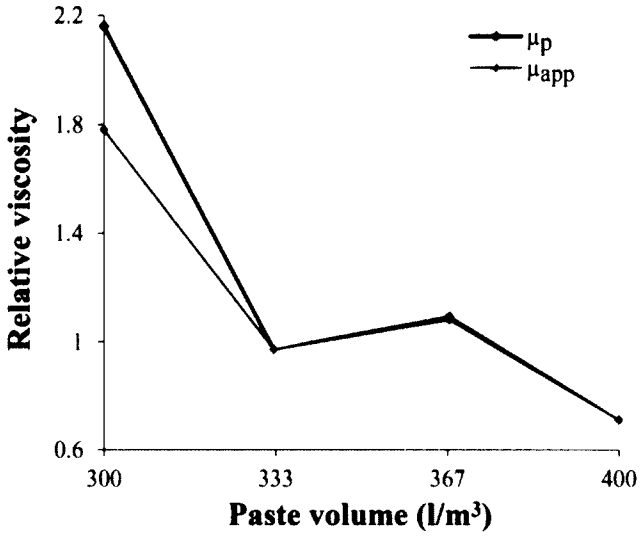


***Figure 7.7:*** *Plastic and apparent viscosities as a function of paste volume. The values are expressed relative to the viscosity of the reference mixture.*

*w/cm* from 0.28 to 0.25 increases viscosity by approximately 100%. The large variation in viscosity induced by small changes in *w/cm* renders the finding that *w/cm* is the most influential parameter on CEM viscosity. Its effect is considerably higher for mixtures prepared with 6% silica fume and 25% Class C fly ash than for those prepared with only 6% silica fume, indicating that the effect of *w/cm* on viscosity depends on the binder type.

As expected, the compressive strength results demonstrate that compressive strength increases with reducing *w/cm* (Table 7.2). The obtained results are in line with previous research findings on the subject [19].

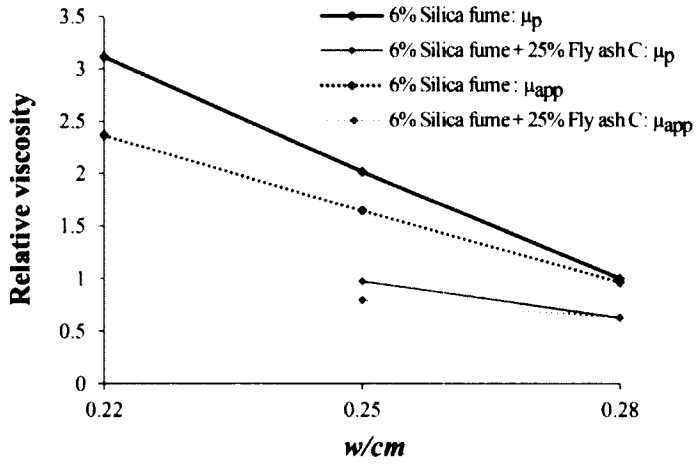


***Figure 7.8:*** *Plastic and apparent viscosities as a function of w/cm. The values are expressed relative to the plastic viscosity of the mixture with 6% of silica fume and w/cm of 0.28.*

### 7.2.8 Summary

From the first phase of the experimental program it was found that replacing the GU cement by silica fume or/and Class C fly ash can significantly reduce viscosity of CEM. A replacement level of 6% silica fume can reduce viscosity by 50%, while a substitution level of 25% Class C fly ash or 15% Class F fly ash can reduce viscosity by 30%, and 10%, respectively. Class C fly ash is therefore considered more efficient than Class F in reducing viscosity. It was also demonstrated that the use of slag is not recommended as it results in undue shear thickening behavior and leads to reduction in the compressive strength.

When investigating the combination of silica fume and fly ash it was observed that a blend of silica fume and fly ash can further reduce viscosity relative to their individual applications. A combination of 25% Class C fly ash with 6% silica fume replacement rates can decrease viscosity by 30% relative to the mixture without any fly ash. On the other hand, combining Class F fly ash with silica fume does not have a profound effect on viscosity. With regards to the compressive strength, replacing the GU cement by silica fume increases the compressive strength while both types of fly ash adversely affect the compressive strength.

The investigation into the effect of mix design parameters showed that, among the investigated parameters, *w/cm* has the highest effect on viscosity reduction; viscosity increases as much as threefold by decreasing *w/cm* from 0.28 to 0.22. CEM trials varying paste volume prove 333 l/m$^3$ to be a threshold value beyond which viscosity does not change significantly.

As a result, the optimized blends of 6% silica fume with 25% Class C fly ash, or 15% Class F fly ash display an impressive ability to reduce viscosity and meet the strength requirements. In light of these research findings, the investigation will be extended to the concrete scale where various mix design parameters that could not be captured through CEM trials are also investigated.

## 7.3 Concrete Scale

Workability requirements of concrete depend primarily on the type of transportation, construction, placement, and consolidating methods applied. When pumping high-strength SCC (H-S SCC) difficulties arise because of the low *w/cm* and poor flowabilty characteristics of such type of concrete, resulting in a high pumping pressure. Increasing *w/cm* is one way to improve the flowabilty of concrete, but with it comes the overall decrease in quality and the risk of segregation during pumping. In this sense, the challenge is to adjust the mixture proportioning to enhance flowability while meeting the stability and strength requirements. Improving flowability and thus decreasing pressure loss can be successfully accomplished by reducing viscosity and tribological flow resistance of concrete.

Applying the results from the CEM trials, the investigation presented in the following sections aims to optimize several mix design parameters to reduce viscosity and tribological resistance and pumping pressure loss of concrete. The results presented in the following sections are the products of two main phases carried out on concrete mixtures. The first phase involves mixtures tested at the laboratory of the UniversitÃ Ì de Sherbrooke, while the second phase includes the full-scale pumping tests carried out on a pumping circuit and discussed in Chapter 6.

### 7.3.1 Assessment of the fresh properties

The fresh properties of concrete were evaluated using the following test methods.

#### Slump/slump flow and T-50 flow test

The slump test is typically used to evaluate the ability of concrete to deform under its own weight using the slump (or Abram) cone. For SCC, this test (ASTM C 143) consists of determining the mean diameter of concrete spread at the end of a slump test and the time needed for the concrete to spread 500 mm (T-50). In the case of CVC, the test is executed by casting concrete in three layers and rodding each layer 25 times. For HWC, the concrete is inserted in one layer and consolidated by rodding 10 times. For SCC the same procedure is followed but no consolidation is needed.

#### L-box test

The L-box test (ACI 237) is used to assess the passing ability of concrete in confined flow conditions such as heavy reinforcement. The L-box consists of a reservoir, a slide gate, three reinforcement bars as obstacles, and a test basin. One minute after filling the reservoir, the slide gate is opened and the time it takes the concrete to reach the leading edge of the test basin is measured. Upon stoppage of the concrete flow, the vertical section ($h_1$= 600-$H_1$) and that at the leading edge ($h_2$= 150-$H_2$) are measured. The $h_2/h_1$ ratio is calculated, indicating the self-leveling ability of the concrete. A high $h_2/h_1$ value implies a greater passing ability. For HWC, a slight modification is introduced to the test where only 2 bars (instead of 3) are used and the concrete is vibrated for 5

seconds at the flow stoppage before taking the measurements. In both cases, any blocking of the flow by coarse aggregate behind the reinforcement bars can be detected visually.

#### V-funnel

The V-funnel flow time test is used to evaluate the deformability of concrete and can be related to its filling and passing ability and viscosity. The test apparatus consists of a V-shaped funnel reservoir with a straight narrow opening and a gate. The test is executed within 10 seconds after filling the reservoir to avoid any thixotropic influence on the results. The interval time between the opening of the gate and the moment the observer can see through the gate is measured and considered the V-funnel flow time. The shorter the time, the greater is the concrete ability to deform.

#### Sieve stability

This test is used to weigh the static resistance of SCC to segregation by measuring the portion of a concrete sample that passes through a sieve under its own weight. The ratio presented by the weight of the mortar separated from the sample to its total weight indicates the stability of the mixture. The lower the ratio, the higher is the concrete stability. The test is performed by pouring 5.0 $\pm$ 0.2 kg of concrete on a sieve with 5 mm opening. The sample is kept at rest on the sieve for 2 minutes, and the mortar that passes through the sieve is weighed and then expressed relative to the total mass of the sample. In this project, the French standard of maximum 15% passing was used to determine whether the SCC is stable or not. The test was not executed on CVC or HWC.

#### Air content

Air content is typically measured using the pressure method (ASTM C 231). In this method the fresh concrete is squeezed by compressed air to about twice normal atmospheric pressure. Since air is the only compressible component in the concrete, the change in the volume of the sample indicates the air content in the measured sample. The test consists of filling the 7-liter base of the air-content test device, latching the top of the test apparatus over the base, and then filling the air gap between the surface of the concrete and the underside of the top of air meter with water. The pressure meter is then zeroed with the built-in hand pump, the pressure is stabilized and then released, and finally the air content is measured. As a secondary function of this apparatus, the fresh concrete density can be determined by weighing the fresh concrete content and dividing by the known volume of the base.

### 7.3.2 Rheological properties

The rheological properties of concrete reported in this phase were determined using the ConTec Viscometer 5. This device is a coaxial concrete rheometer with a design similar to the mortar rheometer ConTec Viscometer 6 described in section 3.8.1. The radii of the inner and outer cylinders are 10 cm and 14.5 cm, respectively. The height of the measurement section submerged in concrete should be measured after each test and

corrected to a reference height of 12 cm. The torque values at different velocities are measured by the load cell and registered for further data treatment.

### Testing procedure and data treatment

The testing procedure began with pre-shearing the concrete sample for 20 seconds at the highest rotational velocity (0.5 rps) to eliminate any thixotropy influence on the measurements. The sample was then subjected to a 10-step decrease in rotational velocity, from the maximum rotational velocity to 0.025 rps. During each 5-second step, the average velocity and the corresponding torque were measured and registered for further analysis. The relationship between the measured torque and velocity was established, and the fundamental rheological parameters were calculated using the Reiner-Riwlin equations (3.20 and 3.21).

Preliminarily analysis of the results revealed that the vast majority of the flow curves exhibited a slight shear thickening behavior. Applying the linear Bingham model (equation 7.1) to the results can deliver negative yield stress values, which is physically impossible. On the other hand, neglecting the shear thickening behavior can result in a significant under estimation of the pumping pressures. In order to overcome this difficulty, the following approach was applied to the results: the modified Bingham model (presented in equation 7.2) was applied when the ratio of $c/\mu > 0.001$, otherwise the results were confirmed linear and the Bingham model was applied.

$$\tau = \tau_0 + \dot{\gamma}\mu_p \tag{7.1}$$

$$\tau = \tau_0 + \mu\dot{\gamma} + c\dot{\gamma}^2 \tag{7.2}$$

where

$\tau$: shear stress (Pa)
$\tau_0$: yield stress (Pa)
$\mu_p$: plastic viscosity (Pa s)
$\mu$: viscosity factor (Pa s)
$c$: second order parameter (Pa s$^2$)
$\dot{\gamma}$: shear rate (1/s)

Since two different models were applied to the results, a way to compare the results was needed. The differential viscosity, defined by the slope of the rheological curve at a certain shear rate, was well suited for this task. For the Bingham model, the differential viscosity was equal to the plastic viscosity, while in the case of the modified Bingham model, the differential viscosity was taken at shear rate of 5.5 l/s (approximately two-thirds of the maximum shear rate) to avoid overestimation of viscosity, particularly in the case of shear thickening behavior. Applying this procedure, the obtained differential viscosities of both models compared well. When calculating the yield stress, no significant difference was noticed between the two models.

It should be mentioned here that rheological properties of the pumped mixtures reported in the forthcoming sections were obtained through a different data treatment procedure than that detailed in section 6.8.1.

### 7.3.3 Tribological properties

The tribological properties were determined in the tribometer developed at the UniversitÃ de Sherbrooke. Detailed description of the tribometer and its operating principle are located in section 3.10.6.

#### Testing procedure and data treatment

The testing procedure applied with the tribometer was similar to those for the rheometer test. It began with a pre-shearing period of 20 seconds at the maximum rotational velocity (0.9 rps), in order to form the lubrication layer and eliminate the effects of thixotropy. Afterwards, the rotational velocity was decreased in 10 steps, from 0.9 rps to 0.01 rps, and held constant at each step for 5 seconds so that the rotational velocity and torque could be registered.

The registered torque was corrected for the "side effect" caused by the cone head of the tribometer as detailed in section 6.8.2. The tribological properties including $Itrib_{ll}$, $Itrib_{co}$, and $Itrib_{tot}$ were determined from the torque-velocity relationship, as indicated in section 5.7.

The total flow resistance ($Itrib_{tot}$) measured with the tribometer is an indication of the flow resistance of concrete being pumped through pipes. It comprises both the effects of the lubrication layer and those induced by the concrete itself. Because it is strongly related to viscosity, all parameters affecting viscosity are prone to have a significant effect on $Itrib_{tot}$. Normally, the higher the $Itrib_{tot}$, the higher is the flow resistance of concrete. From this perspective, one of the main objectives at this stage is to reduce $Itrib_{tot}$ in order to facilitate concrete flow and reduce the pressure loss along the pipes. More details concerning the derivation of the tribological parameters used to assess the flowability of concrete are described in detail in section 5.7.

### 7.3.4 Mixing and testing procedure

All mixtures were prepared using a drum mixer at its maximum capacity (100 liters). Mixing was executed as follows. First, coarse aggregate and sand were inserted and mixed with half the mixing water for 2 minutes to ensure a good homogeneity of the mixture. Second, cementitious materials were introduced and mixed for 30 seconds. Third, HRWRA diluted in the second half of the mixing water was added during mixing. After 3 minutes, mixing was stopped for 2 minutes, during which the mixture was homogenized manually by scraping the walls of the mixer. Finally, the concrete was mixed for 2.5 minutes and kept at rest for 2 more minutes, then the concrete was evaluated visually and using the slump flow test to verify whether the target slump flow was attained. If necessary, an additional HRWRA dose was added, mixing was resumed for 1 minute and slump flow was then retested. Mixtures that failed to reach the desired slump flow after 15 minutes (of the water-cement contact time) were discarded.

For the accepted mixtures, the following testing procedure was followed to evaluate workability, rheology, and tribology. Note that the time is taken relative to the water-cement contact time.

- Slump/slump flow, density, air content, V-funnel, L-box and sieve stability tests at

15 minutes;
- Rheology and tribology tests at 30 minutes;
- Slump/slump flow, and V-funnel tests at 45 minutes;
- Rheology and tribology tests at 60 minutes;
- Slump/slump flow, and V-funnel tests at 75 minutes;
- Rheology and tribology tests at 90 minutes;
- Slump/slump flow, density, air content, V-funnel, L-box and sieve stability tests at 105 minutes; and
- Rheology and tribology tests at 120 minutes.

The rhelogical, tribogical, and fresh properties measured at different testing ages are presented in Tables B.4-B.6 and Tables B.10-B.13. The discussed rheological and tribloical properties of concrete (in the first phase of the concrete scale) were measured 30 minutes after water-cement contact time. The pumped concrete mixtures (in the second phase) were received from a ready mix company and mixed through different procedures. More details concerning the testing procedures of the pumping tests can be found in section 6.7.

### 7.3.5 Materials

Through the experimental program, two sets of constituent materials were used throughout two testing stages. In the first stage, two types of local sand (sand 1 and sand 2) with a maximum aggregate size of 5 mm, complying with ASTM C33 recommendations [20] were used. Different types of aggregate with MSAs of 10 mm and 14 mm were used in different proportions. The granular distribution of the aggregate and sand used in the first stage are presented in Figures A.1 and A.3.

A different set of materials, typically used in the Arabic Gulf to produce SCC, were used in the second stage. This includes two different types of sand: the first, dune sand, the second, crushed aggregate sand. Also, two types of aggregate with MSAs of 10 mm and 20 mm, were used in different proportions, as detailed in Table B.8. The granular distributions of the sand and aggregate used in the second stage are presented in Figures A.4-A.7.

The GU Type cement conforming to ASTM C150 was used in all mixtures [2]. Also, Class C fly ash and silica fume complying with ASTM C618 and ASTM C1240, respectively, were incorporated as cementitious materials [3, 5]. Physical and chemical properties of the cementitious materials are presented in Tables A.3-A.11. Epsilon HP570, a commercially available polycarboxylate-based HRWRA with high workability retention, was employed in the mixtures.

### 7.3.6 Mix design

The investigated mixtures cover a broad range of concrete properties so that the effects of mix design variations on the flow properties of concrete may be assessed. Various mix design parameters were investigated at different levels including: *w/cm*, binder content and type, paste volume, S/A, MSA, air content, and slump flow consistency. All mixtures were prepared with *w/cm* of 0.28 except when investigating the effect of *w/cm* variation.

The binder content was fixed at 575 kg/m$^3$ except when examining the effect of variation in binder content. Also, the S/A was fixed at 0.53 ratio in the first stage and at 0.59 in the second one except when addressing the effect of S/A variation. The HRWRA dose was adjusted to reach the target slump flow at 15 minutes. Tables B.3, B.8, and B.9 list the mix design and proportioning of all tested mixtures used in stages 1 and 2 of this experimental phase.

## 7.4 Test results

The influences of several mix design parameters on the rheological and tribological properties and the pumping pressure loss are presented in the subsequent sections.

### 7.4.1 Effect of *w/cm*

The research findings from the CEM investigation showed that *w/cm* is the most influential mix design parameter on viscosity. In order to validate this finding on the concrete scale, 3 mixtures (SCC33, SCC32, and SCC31) were prepared with *w/cm* of 0.22, 0.25, and 0.28, respectively, while other mix design parameters were held constant (Table B.8).

As shown in Figure 7.9a, the resulting viscosity dramatically decreases (by around fivefold) from 320 Pa s to 132 Pa s, and finally to 62 Pa s, as the *w/cm* increases from 0.22 to 0.25, and finally to 0.28. This steady reduction can be attributed to the low *w/cm* levels where a small change in *w/cm* can have a profound impact on viscosity. These results are in accordance with the results obtained from the CEM trials, although the effect on viscosity is more significant in concrete than it is in CEM for the same change in *w/cm*.

The evolution of the total flow resistance as a function of *w/cm* is presented in Figure 7.9b. Similarly to viscosity, the total flow resistance considerably increases as *w/cm* decreases. For example, the total flow resistance increases by 66% as *w/cm* decreases from 0.28 to 0.22, indicating a significant influence of *w/cm* on flow resistance.

As expected, the compressive strength results (presented in Table B.14) show that reducing *w/cm* increases compressive strength. A reduction of 3% in *w/cm* can result in an increase of 10% in the compressive strength. These results are in line with those obtained from the CEM scale and previous researches stating that *w/cm* is the most influencial mix design parameter on compressive strength [19].

The influence of *w/cm* on pressure loss was investigated through 3 mixtures: SCC8, SCC10, and SCC9, prepared with *w/cm* of 0.245, 0.295, and 0.340, respectively. Mix designs and compositions, the rheological and tribological properties of the tested mixtures are presented in Tables B.15, B.16, and B.21-B.23, respectively. The pressure loss at different discharges as a function of *w/cm* for the tested mixtures is plotted in Figure 7.10. As demonstrated, pressure loss exhibits a substantial decrease with increasing *w/cm*. For example, the pressure loss at a discharge rate of 8 l/s decreases by 77% as *w/cm* reduces by 9.5% (from 0.340 to 0.245). The dramatic reduction in pressure loss can be attributed to the reduction in viscosity and $Itrib_{tot}$ of the pumped mixtures, as presented in Tables B.21-B.23.

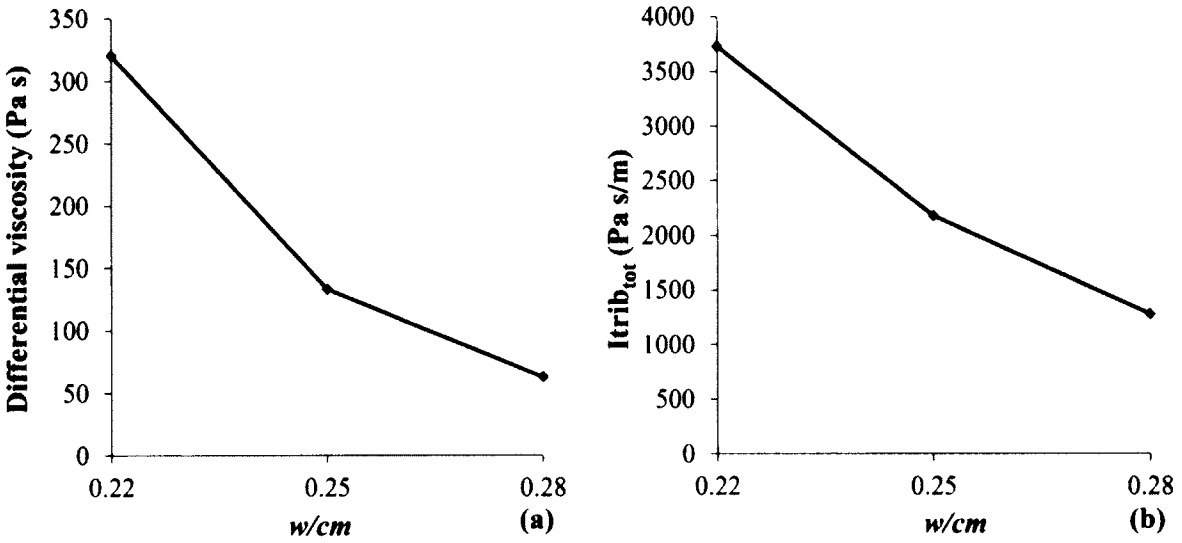


***Figure 7.9:*** *(a) Differential viscosity and (b) $Itrib_{tot}$ as a function of w/cm of the tested mixtures.*

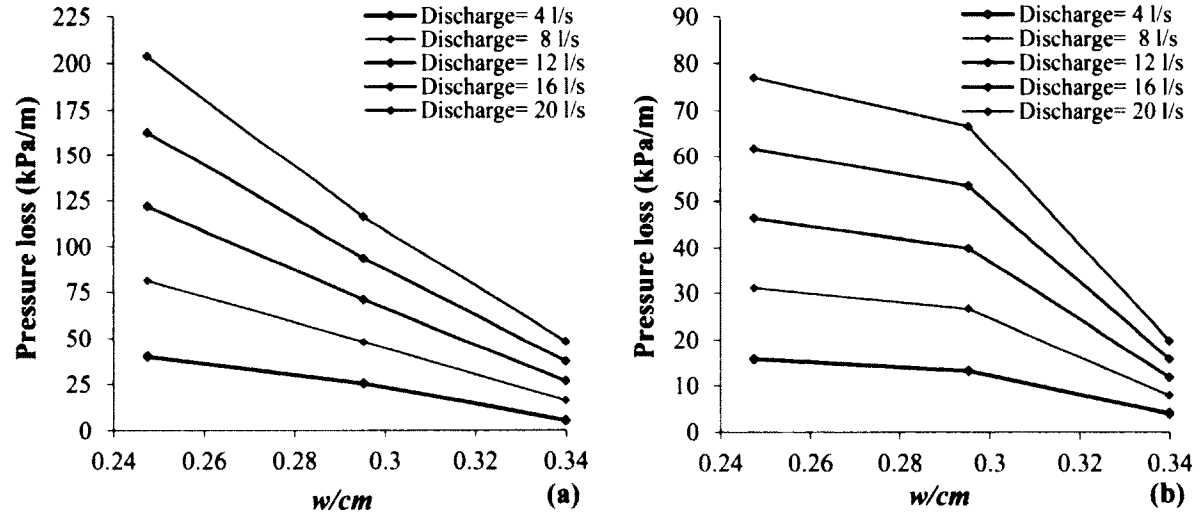


***Figure 7.10:*** *Pressure loss as a function of w/cm at different discharges for the tested mixtures using (a) 4-in pipes and (b) 5-in pipes. Pressure loss was measured during the first pumping cycle.*

It should be noted here that the plotted pressure losses are obtained during the first pumping cycle. Similar results were obtained during later pumping cycles as indicated in Tables B.25-B.28.

## 7.4.2 Influences of binder content and type

The influence of binder type was previously examined through CEM, and it was concluded that replacing the GU cement by 6% silica fume and 25% Class C fly ash delivers the lowest viscosity. It was also found from the CEM scale that incorporating fly ash can adversely affect the compressive strength. In order to verify these results on the concrete scale and further investigate the consequences of omitting the fly ash on the viscosity

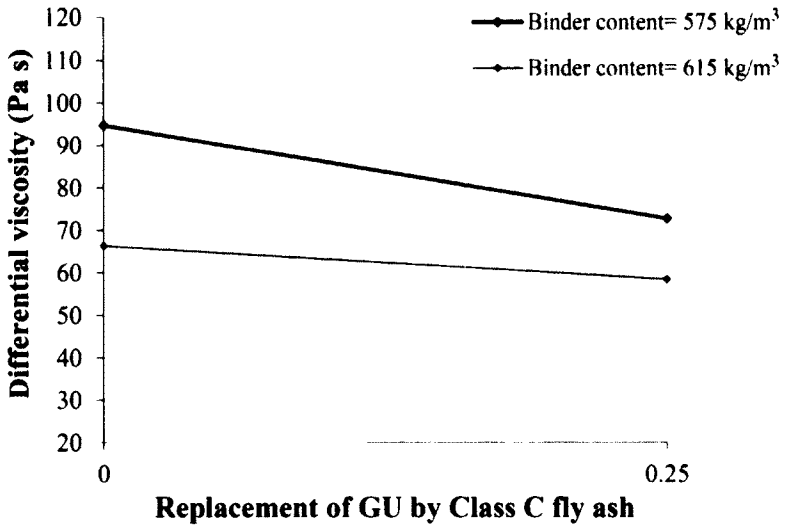


***Figure 7.11:*** *Differential viscosity of the tested mixtures as a function of Class C fly ash replacement rate for two binder contents.*

and flow resistance, 4 mixtures were prepared with two binders combinations. For each blend, two binder contents of 575 kg/m$^3$ and 615 kg/m$^3$ were used in order to examine the effect of binder content on the viscosity and the flow resistance. SCC3 and SCC6 mixtures incorporated a replacement of the GU cement by 25% of Class C fly ash and 6% silica fume and binder contents of 575 kg/m$^3$ and 615 kg/m$^3$, respectively. SCC7 and SCC8 incorporated a replacement of the GU cement by 6% of silica fume while the binder contents were 575 kg/m$^3$ and 615 kg/m$^3$, respectively. All mixtures were prepared with *w/cm* of 0.28, and S/A of 0.53. The mix designs and compositions are presented in Table B.3.

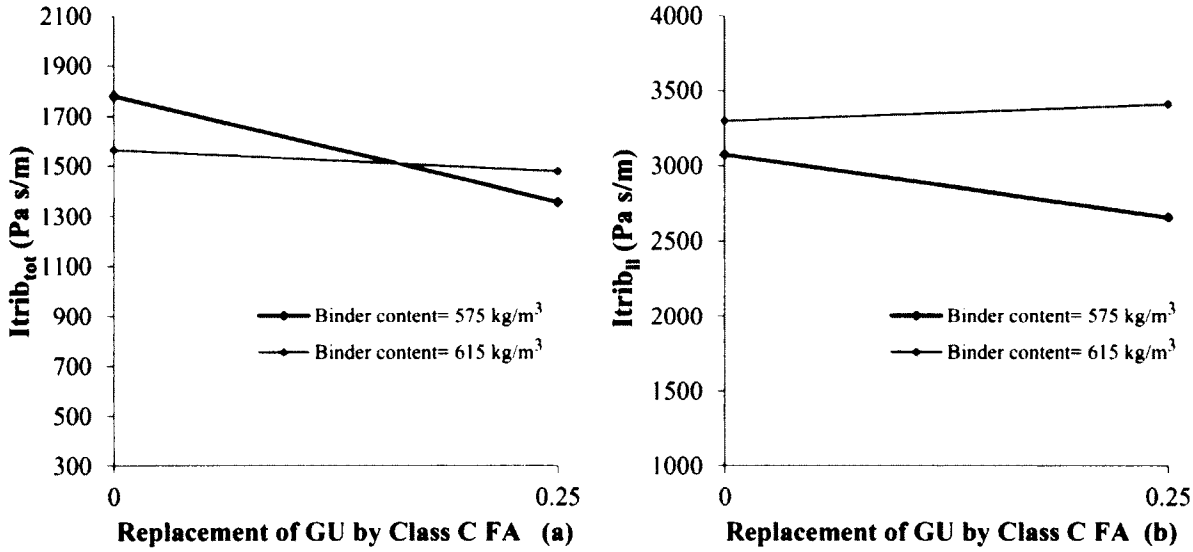


***Figure 7.12:*** *(a) Itrib$_{tot}$ and (b) Itrib$_{II}$ as a function of Class C fly ash replacement rate for two binder contents.*

### Binder content

Viscosity as a function of Class C fly ash replacement rates for both binder contents are displayed in Figure 7.11. Increasing the binder content from 575 kg/m$^3$ to 615 kg/m$^3$ reduces viscosity, with a more pronounced effect when no fly ash is used.

Similarly, $Itrib_{tot}$ decreases as the binder content increases when no fly ash is used, but when fly ash is employed $Itrib_{tot}$ remains almost constant as the binder content increases (Figure 7.12a). Giving the consideration that $Itrib_{tot}$ is a function of the properties of both concrete and the lubrication layer, this constant value of $Itrib_{tot}$ (when fly ash is used) can be attributed to the increase in $Itrib_{ll}$ at high binder content, as demonstrated in Figure 7.12b. More specifically, an increase in the binder content is more likely to produce a thicker lubrication layer [21] and thus increase $Itrib_{ll}$ by increasing the viscosity of the lubrication layer (which is normally accompanied with a reduction in concrete viscosity). Further details concerning the interactions between the properties of the lubrication layer and the properties of concrete can be found in section 5.11.3.

The compressive strength results (presented in Table B.7) indicate that increasing the binder content increases the compressive strength for a given binder combination. For example, SCC7 and SCC8, prepared with binder contents of 575 kg/m$^3$ and 615 kg/m$^3$, exhibited compressive strengths of 92 MPa and 97 MPa, respectively.
To conclude, increasing the binder content usually decreases viscosity but it is not always an effective way to reduce the flow resistance. As witnessed in this data analysis, it can result in higher $Itrib_{tot}$ especially when Class C fly ash is used. The compressive strength can be improved by increasing the binder content for a given binder combination.

### Binder type

As presented in Figure 7.11, the results of the concrete mixtures coincide well with the research findings emanating from the CEM scale; replacing the GU cement by 25% Class C fly ash reduces viscosity. This reduction is more remarkable in the mixtures prepared with lower binder content, indicating the lower efficiency of using fly ash to reduce viscosity when high binder content is used (Figure 7.11). Like viscosity, $Itrib_{tot}$ can be effectively reduced by replacing the GU cement by Class C fly ash. Again this effect becomes less significant when using higher binder content (of 615 kg/m$^3$) as indicated in Figure 7.12a.

The compressive strength results of the tested mixtures (presented in Table B.3) concure with those obtained through the CEM scale. As demonstrated, the replacement of the GU cement by Class C fly ash reduces the compressive strength compared to a mixture prepared only with silica fume.

In conclusion, replacing the GU cement by 6% silica fume and 25% Class C fly ash is an effecient method to reduce viscosity and flow resistance of concrete. This influence is more significant when low binder contents (of 575 kg/m$^3$) are used. In this respect, the choice of using Class C fly ash for further reduction in the viscosity or flow resistance should be carefully made based on the binder content in use.

### 7.4.3 Influence of paste volume

The flowability of concrete is primarily affected by the paste volume as it greatly influences the number of interparticle interactions in the fresh matrix. Increasing the paste volume can enhance the flowability of concrete, but it also can reduce its stability. Therefore, an optimal paste volume is a compromise between flowability and stability, a state achieved by proper suspension of aggregate within the mixture. The CEM investigation concluded that increasing the paste volume up to a certain limit (around 333 l/m$^3$) reduces viscosity, after which only a slight reduction in viscosity is obtained. The investigation into paste volume was extended to concrete scale using various paste volumes and binder combinations. Three mixtures, SCC5, SCC4, and SCC6, with paste volumes of 350 l/m$^3$, 375 l/m$^3$, and 400 l/m$^3$, respectively, were prepared with a blend of the GU cement and Class C fly ash replacement rate of 25% and silica fume substitution rate of 6%. Additionally, 2 mixtures, SCC7 and SCC8, with paste volumes of 350 l/m$^3$, and 375 l/m$^3$, respectively, were prepared without any fly ash replacement. All mixtures were proportioned with *w/cm* of 0.28 and S/A of 0.53. The HRWRA dose was adjusted to reach an initial slump flow of 745 ± 20 mm for SCC5, SCC4 and SCC6, and 700 ± 10 for SCC7 and SCC8. Mix compositions, fresh properties, rheological and tribological properties of the tested mixtures are presented in Tables B.3-B.6.

As presented in Figure 7.13, the differential viscosity decreases as the paste volume increases from 350 l/m$^3$, to 375 l/m$^3$, but beyond this threshold it does not significantly change. This can be explained by the limited influence of the paste volume. In other words, up to certain limits, increasing paste volume augments the distance between aggregates in a way that facilitates flow and lowers viscosity. Beyond these limits, an increase in distance induced by an increase in the paste volume does not significantly affect viscosity. The test results displayed in Figure 7.13 are in accordance with those of the CEM scale, indicating that an increase in paste volume up to a certain value (depending on the other mix design parameters) reduces viscosity, while increasing the paste volume beyond this point does not lead to further reduction in viscosity. Nevertheless, the major

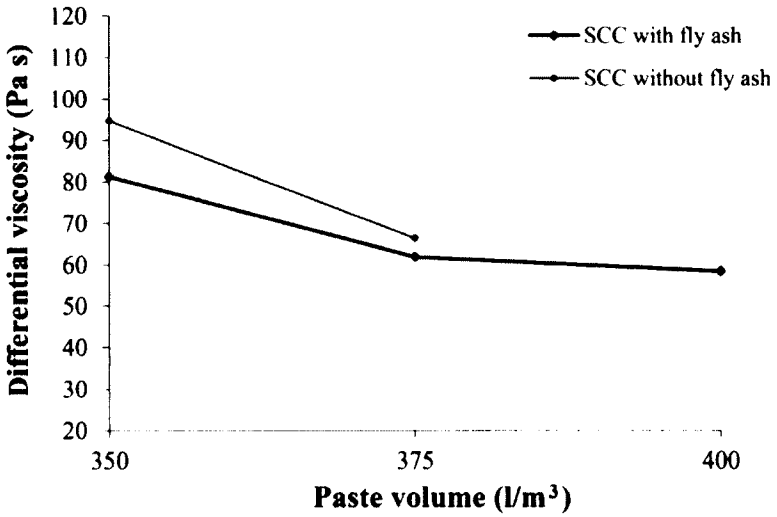


***Figure 7.13:*** *Differential viscosity as a function of paste volume of the tested mixtures using two binder combinations.*

difference between the results of CEM and concrete scales is that the limits of paste volume beyond which viscosity does not significantly change, are different. This can be attributed to the presence of the coarse aggregate in the concrete mixture, introducing substantial effects which cannot be captured through CEM mixtures. More specifically, the coarse aggregate affects concrete packing density, a key parameter of its rheological properties. Therefore, it is recommended to investigate the effect of variations in paste volume through concrete mixtures rather than mortars.

The correlations between the paste volume, $Itrib_{tot}$, and $Itrib_{II}$ of the tested mixtures are depicted in Figure 7.14. Similarly to viscosity, increasing the paste volume from 350 l/m$^3$ to 375 l/m$^3$ reduces $Itrib_{tot}$, while increasing the paste volume from 375 l/m$^3$ to 400 l/m$^3$ leads only to a slight increase in $Itrib_{tot}$. Because $Itrib_{tot}$ is a function of $Itrib_{II}$, this increase can be attributed to the 22% increase in $Itrib_{II}$ when the paste volume increases from 375 l/m$^3$ to 400 l/m$^3$ (see Figure 7.14b). It is believed that the increase in paste volume leads to an increase in thickness of the lubrication layer [21]; in this context, the increase in $Itrib_{II}$ along with the increase in paste volume can be justified by the increase in the viscosity of the lubrication layer. In fact, the increase in viscosity of the lubrication layer seems more significant than the increase in its thickness, for concrete prepared without fly ash. This can be justified by the relationship between viscosity of concrete and viscosity of the lubrication layer. A sharp decrease in concrete viscosity (as in the case when no fly ash is used) can result in a sharp increase in viscosity of the lubrication layer. Further details concerning the interactions between the properties of concrete and lubrication layer are pointed out in section 5.11.3. The compressive strength results presented in Table B.7 demonstrate that the resistance is not significantly affected by changes in paste volume. This can be explained by the similar resistance of the aggregate and the hardened cement paste, which indicates that changes in the paste volume do not significantly affect the compressive strength.

In view of the previous discussion, it suffices to say that for each binder combination there is an optimal paste volume that results in minimum viscosity and total flow

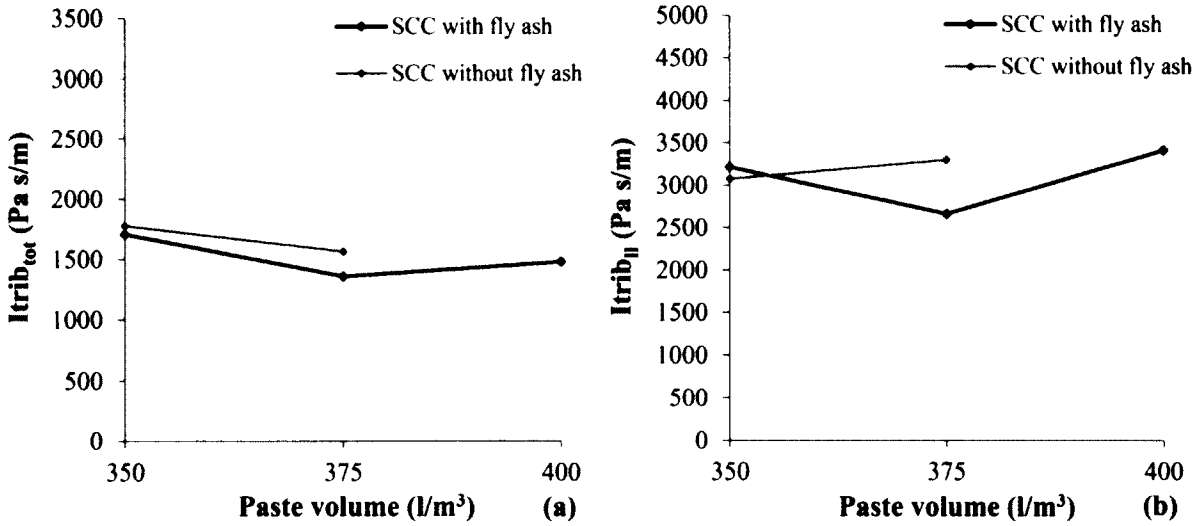


***Figure 7.14:*** *(a) $Itrib_{tot}$ and (b) $Itrib_{II}$ as a function of paste volume of the tested mixtures for two binder combinations.*

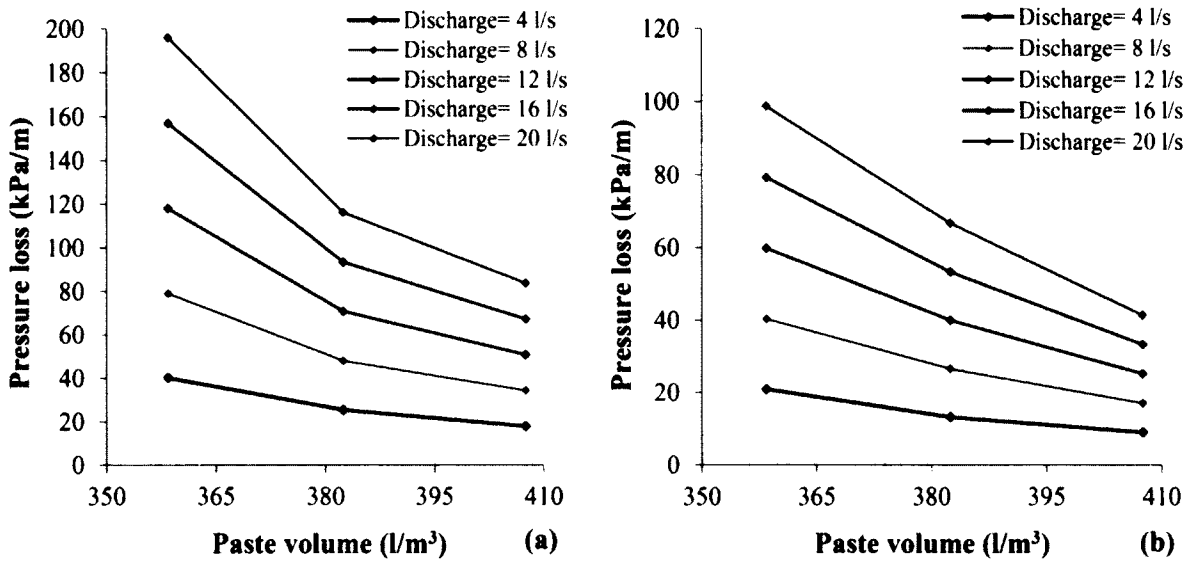


***Figure 7.15:*** *Pressure loss at different discharges as a function of paste volume in (a) 4-in pipes and (b) 5-in pipes.*

resistance. Beyond this value, increases in paste volume do not further reduce viscosity or $Itrib_{tot}$ significantly. Within the range of the investigated paste volumes, this optimal value was found to be around 375 l/m$^3$ for concrete prepared with or without fly ash.

Considering the prime importance of paste volume on viscosity, its connection with pressure loss was anticipated. This connection was investigated through 3 mixtures: SCC12, SCC10, and SCC11, prepared with paste volumes of 358.5 l/m$^3$, 382.5 l/m$^3$, and 407.5 l/m$^3$, respectively. The rheological and tribological properties presented in Tables B.21-B.23 indicate that viscosity and $Itrib_{tot}$ decrease as the paste volume increases from 358.5 l/m$^3$ to 382.5 /m$^3$, but beyond this point no significant decrease in viscosity and $Itrib_{tot}$ are observed. The changes in viscosity and $Itrib_{tot}$ due to changes in paste volume are directly reflected on the pressure loss of the pumped mixtures (Figure 7.15). In general, increasing the paste volume decreases the pressure loss, but again this effect has its limits. As demonstrated in Figure 7.15a, at a discharge of 8 l/s, an increase in the paste volume from 358.5 l/m$^3$ to 382.5 l/m$^3$ reduces the pressure loss by 39%, but a further increase in paste volume from 382.5 l/m$^3$ to 407.5 l/m$^3$ results in a 29% reduction.

As predicted, pressure loss decreases as the paste volume increases, but on the other hand, the stability of the pumped mixture is adversely proportioned to the paste volume. For example, SCC12 and SCC11, prepared with paste volumes of 358.5 l/m$^3$, and 407.5 l/m$^3$, show initial segregation indexes, as expressed by the sieve stability test, of 7% and 13%, respectively (Table B.20). From this perspective, special consideration should be given to the paste volume so that an optimal balance between the stability of the concrete mixture and pressure loss is guaranteed.

In conclusion, changes in pressure loss in relation to paste volume can be attributed to changes in viscosity and $Itrib_{tot}$. Increasing paste volume decreases pressure loss but can adversely influence the stability of pumped mixture. Finally, there is an optimal range of paste volume beyond which pressure loss does not significantly change.

### 7.4.4 Influence of MSA

In order to investigate the effect of MSA on rheological and tribological properties of concrete, 2 concrete mixtures (SCC10 and SCC11) were prepared with MSAs of 14 mm and 10 mm, respectively. The binder used was a blend of the GU cement with 25% Class C fly ash and 8% silica fume. Both mixtures had a binder content of 600 kg/m$^3$ and *w/cm* of 0.28. Complete details for mixture composition can be found in Table B.3.

Theoretically, increasing MSA increases the gaps between the fine and coarse aggregate, resulting in a reduction in the packing density and thus higher viscosity. The experimental results concord with this theory; as shown in Figure 7.16a, viscosity increases by 17% as MSA increases from 10 mm to 14 mm. Similarly, $Itrib_{tot}$ increases by 20% with the same increase in MSA (Figure 7.16b).

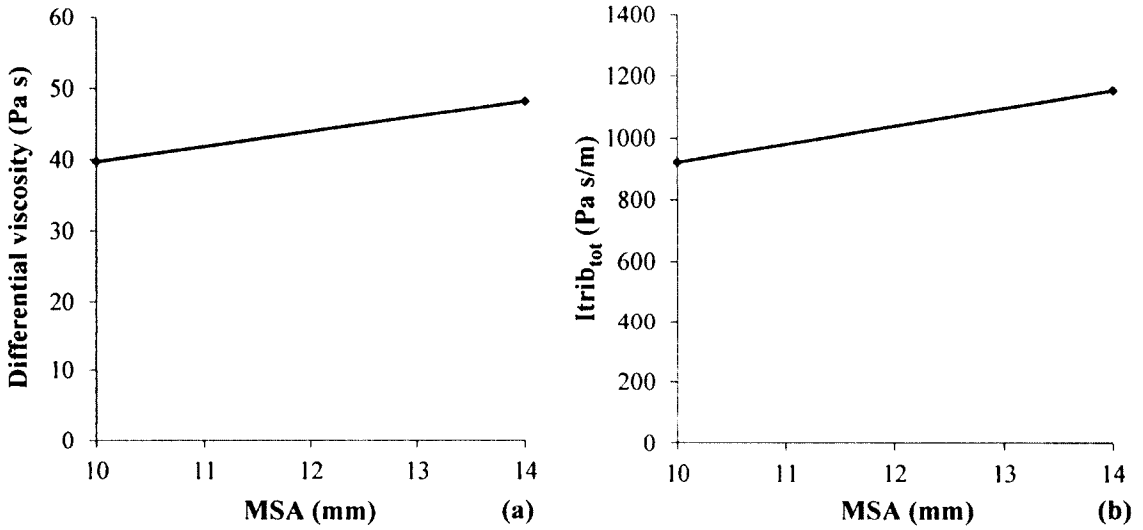


***Figure 7.16:*** *(a) Differential viscosity and (b) $Itrib_{tot}$ of tested mixtures as a function of MSA.*

Besides the increase in viscosity and $Itrib_{tot}$, the results of the fresh properties demonstrate that the risk of segregation increases with increasing MSA. For example, the segregation index increases by 23% as the MSA increases from 10 mm to 14 mm (Table B.5). Moreover, the mixture prepared with MSA of 10 mm shows slightly a higher compressive strength than that prepared with MSA of 14 mm. This can be justified by a greater aggregate-paste interface surface area, resulting in a better adherence between the aggregate and the cement paste, and thus higher compressive strength.

No pumping tests were executed to investigate the effect of MSA on the pressure loss. However, since reducing MSA reduces viscosity and $Itrib_{tot}$, it is anticipated that reducing MSA will lead to a sizable reduction in the pressure loss.

To summarize, within the frame of the tested mixtures, reducing the maximum aggregate size from 14 mm to 10 mm is an efficient practice to reduce viscosity and $Itrib_{tot}$ of concrete. The effect of MSA is not independent of other aspects concerning the aggregate and sand granular distribution. Hence, the effect of MSA on the rheological

and tribological properties can yield different effects than what has been found in this investigation, if different aggregate or sand are used.

### 7.4.5 Influence of S/A

Proportioning and the granular characteristic of the sand and aggregate are vital properties determining the packing density, and consequently, the viscosity of concrete. Generally, increasing the sand content improves the deformability of concrete, although this effect can vary depending on the granular distribution of the sand and aggregate. For example, two mixtures with the same aggregate and sand proportion but different granular distributions can yield entirely different rheological behaviors. Apart from the effect of MSA presented in the previous section, the only sand and aggregate property investigated at this stage was proportioning expressed as S/A. The effect of S/A was explored through two stages using different constituent materials and ranges. In the first stage, 3 mixtures, SCC17, SCC16, and SCC15, prepared with S/A of 0.47, 0.50, and 0.53, respectively, were investigated. The resulting changes in viscosity and $Itrib_{tot}$ as a function of S/A are depicted in Figure 7.17. As demonstrated, increasing S/A from 0.47 to 0.50 results in an increase in viscosity, while a further increase from 0.50 to 0.53 leads to a reduction. These changes in viscosity induced by increasing S/A can be attributed to variations in packing density, which is a straightforward function of the aggregate and sand size distributions and shapes. $Itrib_{tot}$ exhibits a behavior similar to that of viscosity and the minimum value is obtained at S/A of 0.53, as indicated in Figure 7.17b.

The effect of S/A on pressure loss at different discharges is illustrated by Figure 7.18. As can be noticed, the variations of pressure loss in relation to S/A coincide with the corresponding changes in viscosity and $Itrib_{tot}$. For example, at a discharge rate of 8 l/s, increasing S/A from 0.47 to 0.53 increases viscosity by 27%, $Itrib_{tot}$ by 17%, and pressure loss by around 26% (in 4-in pipes).

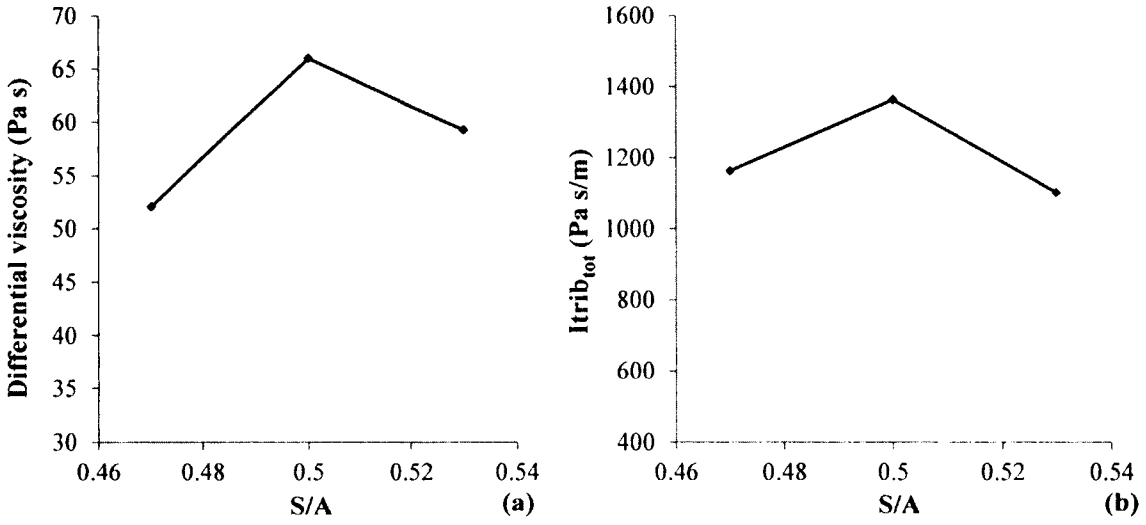


***Figure 7.17:*** *(a) Differential viscosity and (b) $Itrib_{tot}$ and of SCC17, SCC16, and SCC15.*

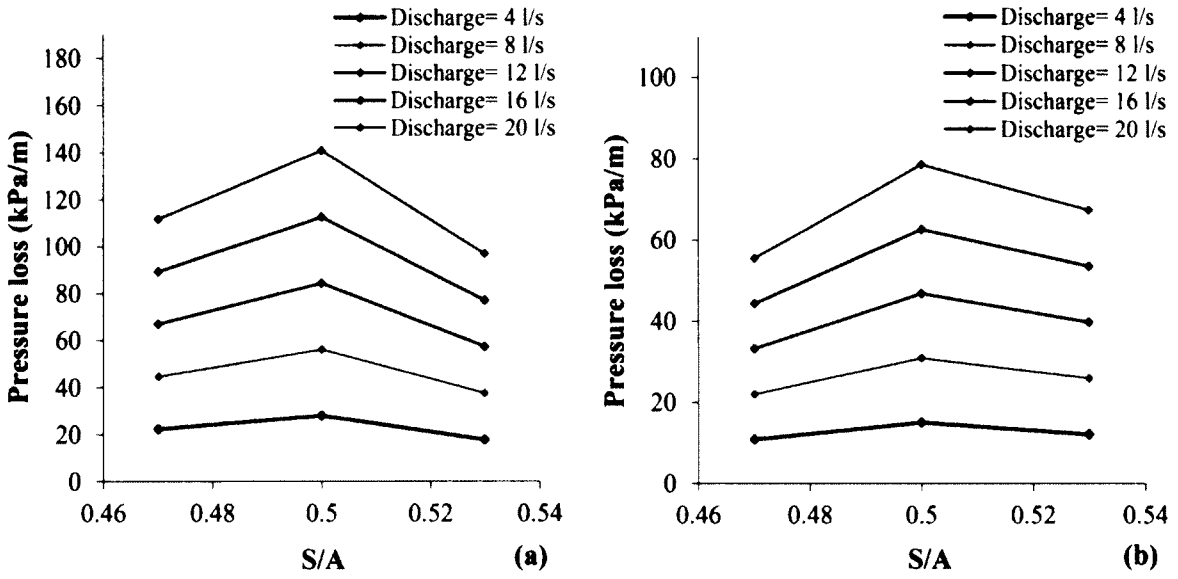


***Figure 7.18:*** *Pressure loss at different discharges as a function of S/A for SCC17, SCC16, and SCC15 in(a) 4-in pipes and (b) 5-in pipes.*

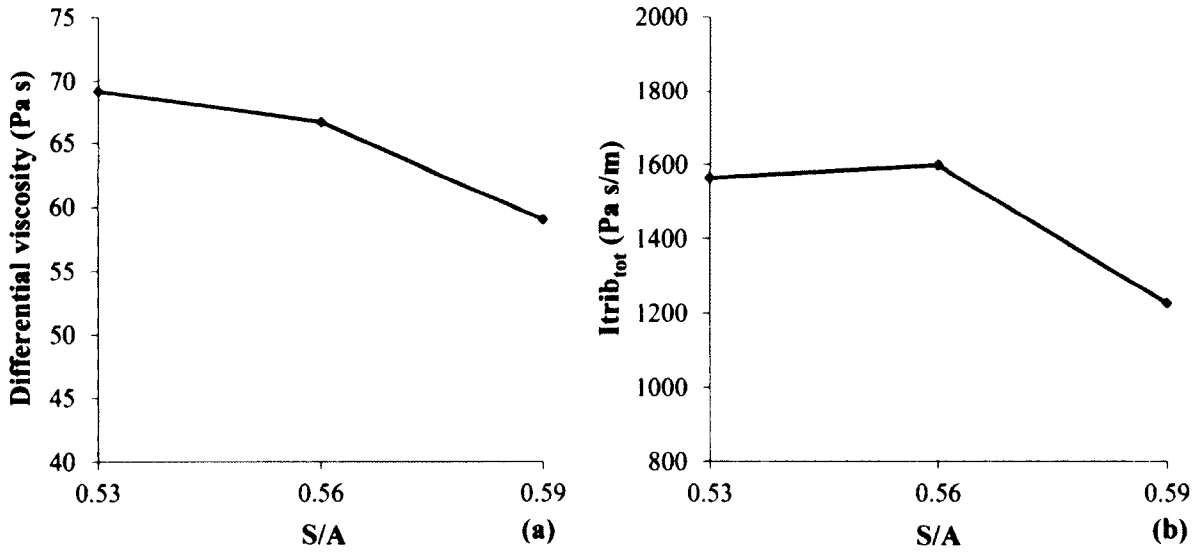


***Figure 7.19:*** *(a) Differential viscosity and (b) $Itrib_{tot}$ as a function of S/A for SCCGM29, SCCGM28, and SCCGM30.*

In the second stage, the investigation was extended to cover another proportioning range through 3 mixtures: SCCGM29, SCCGM28, and SCCGM30, prepared with S/A of 0.53, 0.56, and 0.59, respectively. These mixtures were prepared with constituent materials different than those used in the first stage. All mixtures were prepared with a total binder content of 575 kg/m$^3$ using the GU cement incorporated 25% Class C fly ash and 8% silica fume replacements. The *w/cm* was fixed at 0.28 and the initial slump flow, at 725 ± 20 mm. Complete mix compositions, fresh properties, and rheological and tribological properties are presented in Tables B.9-B.13.

Unlike the results of the first stage, the results of the second one, presented in Figure

7.19, clearly demonstrate that viscosity decreases as S/A increases. This reduction can be attributed to the improvement of the packing density induced by the increase in sand content, resulting in a facilitated flow. By comparing the viscosity variations of Figures 7.17 and 7.19, it can be inferred that increasing S/A does not always reduce viscosity. Instead, there is an optimal range of S/A in which viscosity is minimal.
No further investigation was undertaken at this stage, but it is believed that the optimal range is firmly related to the packing density of the granular system in question.

The results of $Itrib_{tot}$ are somewhat similar to those of viscosity, as shown in Figure 7.19b. Increasing S/A from 0.53 to 0.56 does not significantly affect $Itrib_{tot}$, whereas increasing S/A from 0.56 to 0.59 decreases $Itrib_{tot}$ by around 23%. This reduction can be justified by the facilitated flow induced by the increased sand content in the mixtures. The compressive strength results presented in Table B.14 demonstrate that no significant increase in compressive strength is obtained by increasing the S/A. Greater changes in S/A may result in more profound effects on compressive strength, but such trials did not form part of the presented study.

To summarize, changing S/A can be an effective way to decrease viscosity and $Itrib_{tot}$ of concrete and thus pressure loss during pumping. Optimal values of S/A vary widely depending on the characteristics and size distributions of the sand and aggregate employed. In this respect, performing a granular distribution analysis is indispensable in order to optimize sand and aggregate proportioning and minimize viscosity.

### 7.4.6 Influence of air content

The effect of air content on viscosity and $Itrib_{tot}$ was investigated through a single concrete mixture (SCC37) by increasing its air content during testing time. Several doses of an air-entraining agent were added every 30 minutes during the two-hour test. The tested mixture was prepared with S/A of 0.59, $w/cm$ of 0.28, and a blend of the GU cement and 8% silica fume with a total content of 618 kg/m$^3$. The initial air content before introducing any air-entraining agent was 2.3% and was measured at 20 minutes after water-cement contact time. The air content and rheological and tribological properties were measured similtanneously at different testing ages. Considering that the HRWRA demonstrated good workability retention for mixture similar to the tested one, the effect of workability loss on the rheological and tribological properties during testing time was neglected.

The resulting viscosity and $Itrib_{tot}$ as a function of air content are depicted in Figure 7.20. As demonstrated, increasing the air content dramatically decreases viscosity: an increase of 4.3% (from 3.2% to 7.5%) decreases viscosity by 40%. The effect of air content is similar on $Itrib_{tot}$; an increase in air content from 3.2% to 7.5% results in a reduction of 26% in $Itrib_{tot}$, indicating that the air content yields somewhat lower effect on $Itrib_{tot}$ than that on viscosity. The reduction in viscosity and $Itrib_{tot}$ brought about by the increase in air content can be explained by the increased inter-particle distance and consequent increased volume ratio of the paste fraction created by higher air contents. In addition to this, the air bubbles act as small ball bearings by reducing the inter-particle friction and overall shear resistance of the concrete. Moreover, the air bubbles collapse and deform easily under shear forces, resulting in a considerable reduction in viscosity [22]. In essence, the effect of air content in concrete can be understood on the basis of

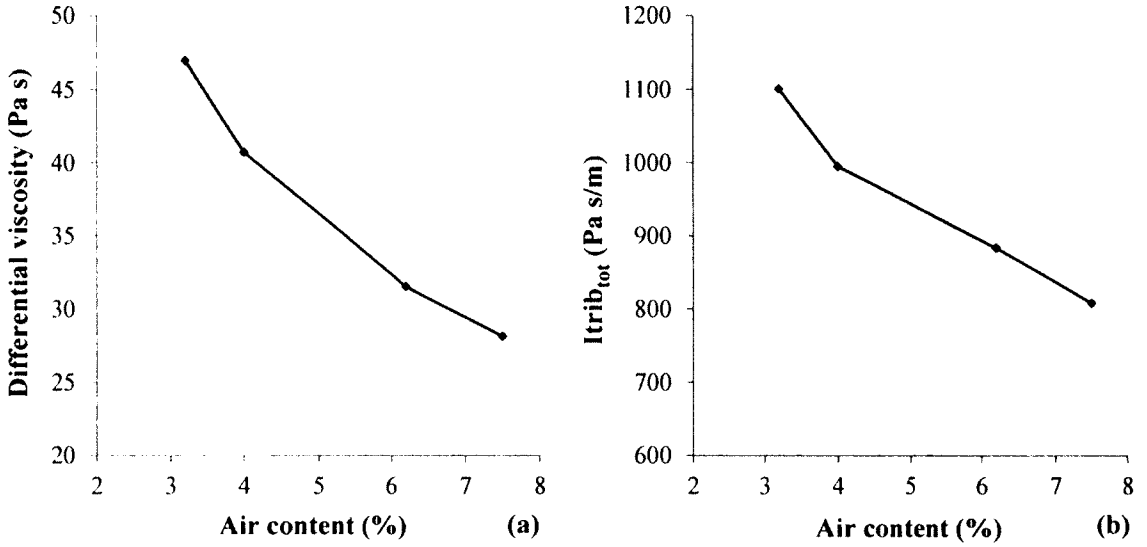


***Figure 7.20:*** *(a) Differential viscosity and (b) $Itrib_{tt}$ as a function of air content for SCC37.*

air bubble characteristics such as size, shape, and spacial distribution. These physical characteristics are also affected by the properties of the constituent materials in the concrete mixture and the mixing procedures. For example, the aggregate shape, gradation, surface properties, and quantity affect the size distribution of air bubbles by influencing the shearing and impact actions in the system during mixing. Also, an increase of fine materials passing sieve No. 100 (0.15 mm) decreases the air content, probably because of the decreased air bubble size caused by the shear action of particles whose sizes are close to air bubbles [23].

On the microstructure scale, it is believed that the spacing factor and maximum size of the air bubbles are decisive factors in stabilizing or destabilizing the fine particles and water droplets that form the lubrication layer. In other words, the properties of the lubrication layer including thickness and viscosity are directly affected by the characteristics of the air bubbles in the mixture. This area of research is still open to investigation to determine the exact effect of air bubbles on the properties of the lubrication layer.

According to the previous correlations found between viscosity, $Itrib_{tot}$ and pressure loss, it is more than likely that an increase in air content will lead to a reduction in pressure loss. On the other hand, excessive air content may weaken the cohesive coating between the aggregate and paste, which in turn can increase the risk of segregation leading to other stability problems.

Through the pumping tests, only one mixture (SCC13) was employed to investigate the changes in air content when air-entraining agent is used. Oddly enough, air content did not exhibit a significant change during the pumping cycles, as presented in Table B.19. However, a reduction in viscosity and increase in yield stress, as described in section 6.12.3, can be reported.

### 7.4.7 Slump flow consistency

Two groups of SCC mixtures were prepared in order to investigate the effect of slump flow consistency on the rheological and tribological properties of concrete and pressure loss. In the first group, 4 mixtures, SCC1, SCC2, SCC3-b, and SCC4-b, were prepared with the same compositions but different HRWRA contents to reach the target slump flows of 620 mm, 670 mm, 720mm, and 765 mm, respectively. A total binder content of 575 kg/m$^3$ of the GU cement with 6% silica fume, and paste volume of 375 l/m$^3$ were used in these mixtures. MSA of 14 mm was used for all mixtures, while S/A was fixed at 0.53, and *w/cm* at 0.28. Tables B.9-B.11 present the detailed mixture proportions and consequent fresh properties of the tested mixtures.

The resulting viscosity and $Itrib_{tot}$ values in relation to slump flow are presented in Figure 7.21. Both viscosity and the total flow resistance ($Itrib_{tot}$) are weakly influenced by the increase in slump flow. This can be attributed to the flow pattern of SCC in which yield stress (which mainly governs the slump flow) does not play a major role, as demonstrated analytically and empirically in sections 5.11.1 and 6.10.1.

Yield stress as a function of slump flow is displayed in Figure 7.22a. As demonstrated, yield stress remarkably decreases as slump flow increases. From a different angle, the fresh properties show that the decrease in yield stress can adversely affect the stability of the concrete; mixtures with higher slump flow display lower segregation resistance (see Table B.5).

The compressive strength results presented in Table B.7 indicate that increasing slump flow can slightly increase compressive strength. This increased value could be due to a better dispersion of the cement particles, resulting in higher compressive strength. However, the increase is too insignificant to warrant further analysis.

Since the increase in slump flow is not well correlated with viscosity of SCC, it is anticipated that it also does not significantly influence pressure loss.

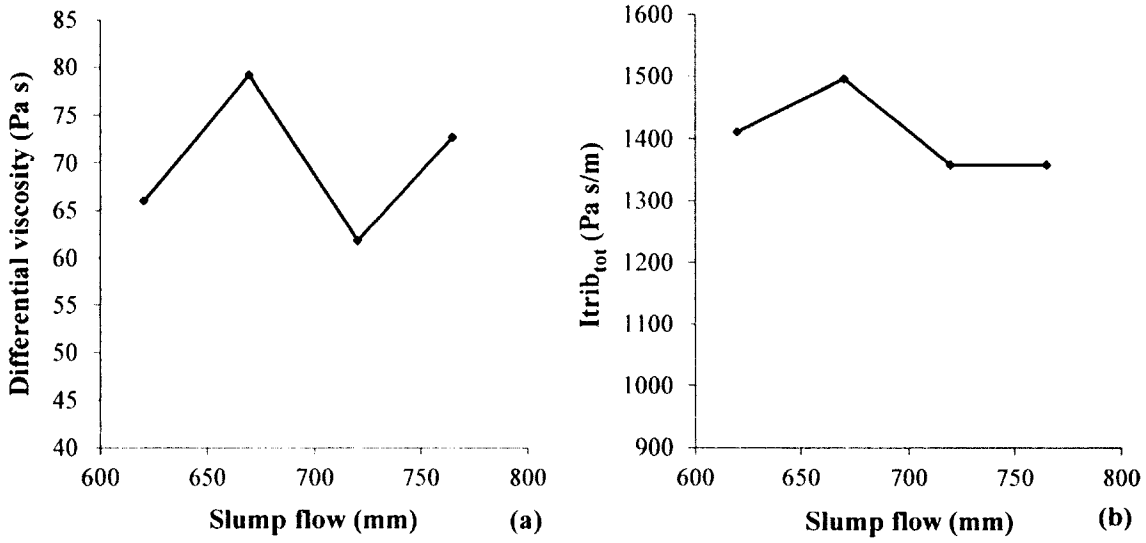


***Figure 7.21:*** *(a) Differential viscosity and (b) $Itrib_{tot}$ of as a function of slump flow for SCC1, SCC2, SCC3-b, and SCC4-b.*

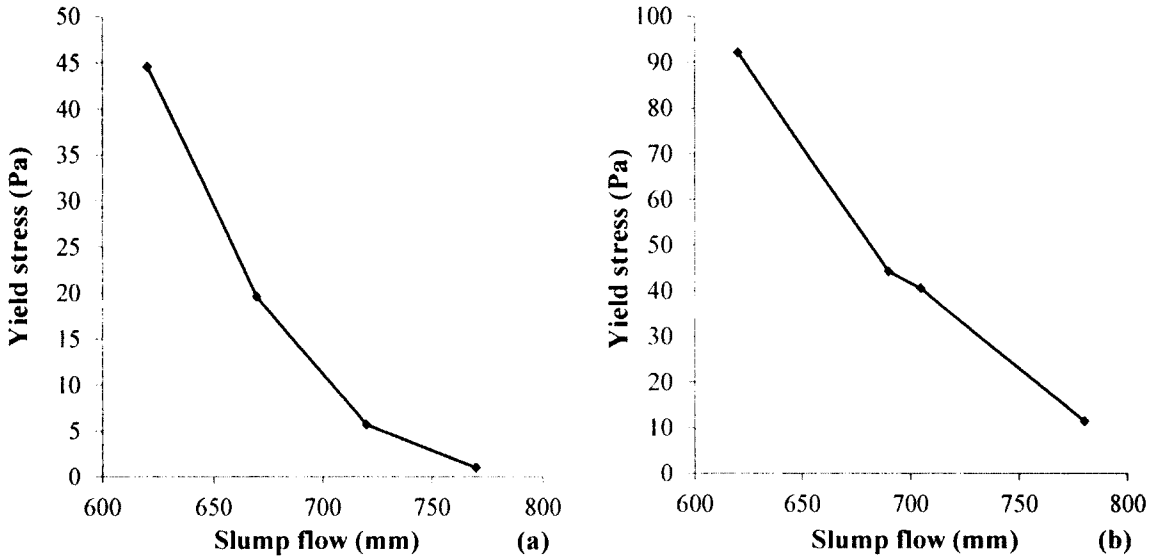


***Figure 7.22:*** *Relationship between the yield stress and slump flow for (a) SCC1, SCC2, SCC3-b, and SCC4-b; and (b) for SCC7, SCC10, SCC1, and SCC2.*

This theory was later supported through a second group of trials. Four mixtures, SCC7, SCC10, SCC1, and SCC2, were prepared with the same composition, but with slump flow values of 620 mm, 690 mm, 705 mm, and 780 mm, respectively. Complete rheological and tribological properties of the tested mixtures are listed in Tables B.21-B.23. Similarly to the results of the first group, the increase in slump flow is translated into a reduction in the yield stress (Figure 7.22b). Likewise, no clear relationship between slump flow and viscosity or $Itrib_{tot}$ can be observed, as indicated in Tables B.21-B.23. Results from this group also yielded a negative correlation between slump flow and stability. It was found that the increase in the slump flow from 615 mm to 765 mm increases the segregation index by 64%, as presented in Table B.20.

Finally, the pressure loss at different discharges was measured for the second group of mixtures with variable slump flow (Figure 7.23). As predicted, the slump flow does not exhibit a clear effect on the pressure loss at the different discharge rates. This finding is in line with the results obtained from the analytical model presented in section 5.11.1 and the empirical studies detailed in section 6.10.1.

Reflecting on the previous discussion, it suffices to say that the increase in slump flow of a concrete decreases its yield stress and has no significant effect on viscosity or $Itrib_{tot}$. Despite that increasing slump flow results in a more workable concrete, it can adversely affect stability without benefiting the pressure loss. From a practical stand, workability and stability requirements, rather than the pressure loss, should be the main consideration in selecting the slump flow. In other words, the slump flow of concrete to be pumped should be carefully selected to attain an adequate comprise between workability and stability before considering the rheological and tribological criteria.

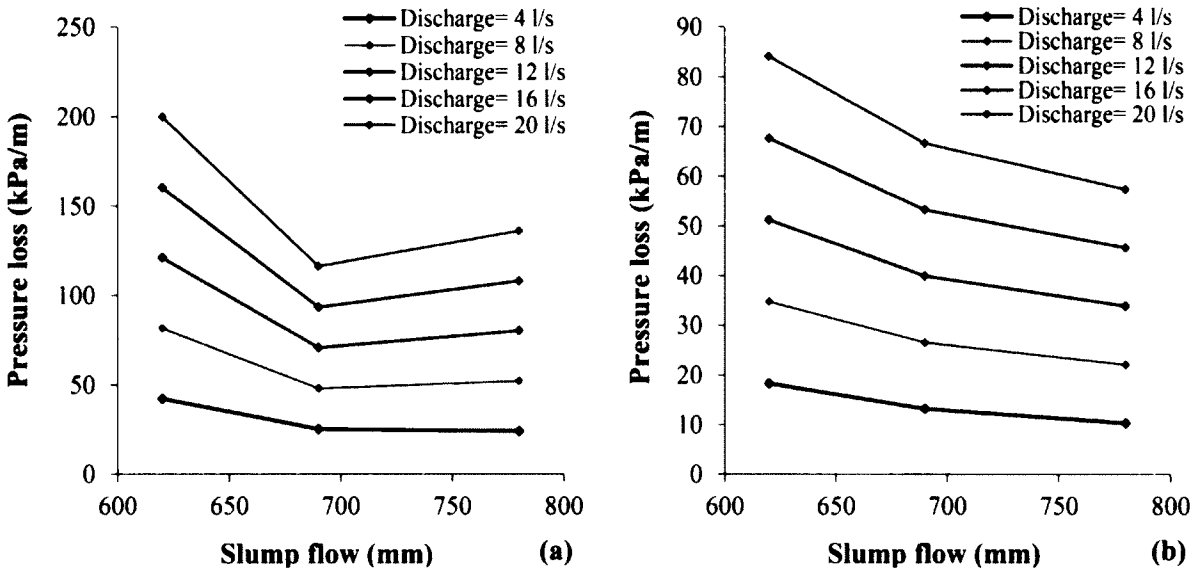


***Figure 7.23:*** *Pressure loss as a function of slump flow at different discharges for SCC7, SCC10, SCC1, and SCC2 in (a) 4-in pipes and (b) 5-in pipes.*

## 7.4.8 Summary

With the research findings of CEM scale as input, the investigation was expanded to the concrete scale with the same goal of reducing pumping pressure loss. The test results demonstrated that viscosity, $Itrib_{tot}$ and consequently pressure loss can be effectively reduced by adjusting the mix design parameters. Among the investigated parameters, *w/cm* has the most significant effect. It was found that a 6% increase in *w/cm* can cause a 5-fold reduction in viscosity, and that a 9% decrease can cause a 77% reduction in pressure loss.

The use of cementitious materials was proved an efficient approach to reduce viscosity. Replacing the GU cement by 6% silica fume and 25% Class C fly ash can considerably reduce the viscosity and $Itrib_{tot}$ of concrete. This effect is more pronounced when low binder contents (around 575 kg/m$^3$) are used. The results also revealed that the choice of binder content is a question of the binder type in use. In general, increasing binder content can decrease viscosity and $Itrib_{tot}$ but can also increase $Itrib_{II}$ depending on the type of binder used, such as when using fly ash.

It was also found that, generally, increasing the paste volume decreases viscosity, $Itrib_{tot}$, and pressure loss. For every concrete mix, there is an optimal range of paste volume that results in minimum viscosity and pressure loss. Beyond this range, the pressure loss does not change significantly but can considerably reduce the stability of the mixture. Thus, paste volume optimization is considered a delicate balance between the pressure loss and stability.

The investigation on the influence of MSA disclosed that reducing MSA decreases viscosity and $Itrib_{tot}$. The effect of MSA on the pressure loss was not assessed through pumping trials, but because of the positive correlations between viscosity, $Itrib_{tot}$ and pressure loss, it is believed that reducing MSA reduces pressure loss.

The results indicated that optimizing S/A can be an effective practice to reduce viscosity, $Itrib_{tot}$, and pressure loss. Generally speaking, for S/A higher than 0.50, an

increase in S/A results in a decrease in the viscosity, $Itrib_{tot}$, and pressure loss. However, the optimal range of S/A, which results in the minimum viscosity and $Itrib_{tot}$, varies depending on the characteristics and size distributions of the sand and aggregate in use.

The air content analysis demonstrated that increasing the air content severely decreases viscosity and $Itrib_{tot}$, whereas excessive air content can remarkably reduce the stability of the mixture. Due to the multitude possibility of air systems for a given air content, characterization of the air bubbles can provide better understanding of the underlying reasons behind viscosity reduction.

Finally, a firm correlation was found between the slump flow and yield stress, whereas no meaningful relationships could be established between the slump flow and viscosity, $Itrib_{tot}$, or pressure loss. An increase in the slump flow (brought about by increasing HRWRA) does not hold a substantial effect on pressure loss reduction, but it can significantly decrease the stability of the pumped mixture. Therefore, workability and stability requirements, rather than the pressure loss, should be the main consideration in selecting the slump flow of the pumped mixture.

## 7.5 References

[1] Erdem K., Khayat K.H., Yahia A., "Correlating rheology of self-consolidating concrete to corresponding concrete-equivalent mortar", *ACI Materials Journal*, pp. 154 160, 2009.

[2] ASTM C150 / C150M - 11, "Standard specification for portland cement", *American Society for Testing and Materials*,

[3] ASTM C618 - 08a, "Standard specification for coal fly ash and raw or calcined natural pozzolan for use in concrete", *American Society for Testing and Materials*,

[4] ASTM C989 - 10, "Standard specification for slag cement for use in concrete and mortars", *American Society for Testing and Materials*,

[5] ASTM C1240 - 11, "Standard specification for silica fume used in cementitious mixtures", *American Society for Testing and Materials*,

[6] ASTM C 33, "Standard specifications for concrete aggregates", *American Society for Testing and Materials*,

[7] ASTM C1437 - 07, "Standard test method for flow of hydraulic cement mortar", *American Society for Testing and Materials*,

[8] EFNARC, "EFNARC (2002) Specifications and guidlines for self-compacting concrete", Tech. Rep., p. 2002.

[9] Wallevik J.E., "Rheology of particle suspensions of fresh concrete, mortar and cement paste with various types of lignosulfonates", Ph.D. The Norwegian University of Science and Technology, 2003.

[10] Kubens K., Peng H., Oesterheld S., and Wallevik O.W., "Some effects of silica fume on variations in rheology of mortar due to production date of cement", 2008.

[11] Tattersall G.H., Banfill P.F.G., *The rheology of fresh concrete*. Great Britain: Pitman Books Limited, 1983.

[12] Douglas R.P, "Properties of self-consolidating concrete containing type F fly ash", PhD thesis, Northwestern University, 2004.

[13] Khatib R., Perez-Schell A., Feys D., Khayat K.H., "Reducing viscosity of High-Strength, Self-Consolidating Concrete to decrease pumping pressure", in *Twelfth International Conference on Recent Advances in Concrete Technology*, Prague, 2012.

[14] Khatib R., Feys D., Khayat K.H., "Effect of mix design parameter on reducing High-Strength CEM to reduce pumping pressure", in *Fifth North American Conference on the Design and Use of Self-Consolidating Concrete*, Chicago, 2013.

[15] Yucel K. T., "Effect of fly ashes on the rheological properties of fresh cement mortars", *International Journal of Thermophysics*, vol. 27, no. 3, pp. 906 921, 20061.

[16] Ferraris C.F., Karthik H.O., Russell H., "The influence of mineral admixtures on the rheology of cement paste and concrete", *Cement and Concrete Research*, vol. 31, no. 2, pp. 245–255, 2001.

[17] Rouis F., "Effect of cementitious materials on rheological properties of concrete-equivalent mortar of SCC consistency", Ph.D. dissertation, University of Sherbrooke, 2013.

[18] Bui V.K., Akkaya Y., Shah S.P., "Rheological model self-consolidating concrete", *ACI Materials Journal*, vol. 99, no. 6, pp. 549–559, 2002.

[19] Shamsai A., Rahmani K., Peroti S., Rahemi L., "The effect of water-cement ratio in compressive and abrasion strength of the nano silica concretes", *World Applied Sciences*, vol. 4, no. 17, pp. 540 545, 2012.

[20] ASTM C 33, "Standard specification for concrete aggregates", *American Society for Testing and Materials*,

[21] Ngo T.T., "Influence of concrete compositions on the pumpability parameters", Ph.D. dissertation, Cergy Pontoise, France, 2009.

[22] Chia K. S., Zhang M. H., "Effect of chemical admixtures on rheological parameters of fresh lightweight aggregate concrete", in *28th Conference on Our World in Concrete and Structures*, Singapore, 2003.

[23] Du L., J. Folliard K., "Mechanisms of air entrainment in concrete", *Cement and Concrete Research*, vol. 35, pp. 1463–1471, 2005.

# Chapter 8

# Conclusions

# 8.1 Conclusions of this research project

After a long journey of exploring the flow pattern of SCC and HWC in pipes and developing a solid understanding of the key parameters governing this flow, time has come to conclude this PhD dissertation and highlight its most significant findings. The following sections outline the conclusions of the analytical, statistical, and empirical studies provided by the last three chapters.

## 8.1.1 Properties of the lubrication layer

The analysis presented in section 5.6 demonstrated that concrete flow behavior in pumping pipes can be successfully simulated by means of tribological tests. On this basis, a new analytical formula was derived to calculate the thickness and viscosity of the lubrication layer. The properties of the lubrication layer were shown to be functions of the rheological properties of concrete and the applied stress in the tribometer's gap. Additionally, new tribological parameters were educed to describe the concrete flow resistance in the tribometer gap. The derived tribological parameters demonstrated high proficiency (through the experimental phases) in quantifying the concrete flow resistance in pumping pipes.

## 8.1.2 Concrete flow in pipes

The analyses undertaken in Chapter 5 showed that different flow behaviors can be characterized across the pipe section, depending on the pumping pressure, the properties of both concrete and the lubrication layer, and the distance from the pipe center. In the case of highly-flowable concrete, three zones with distinctive flow characteristics can be defined across the pipe section. In the first zone, the plug, the concrete moves along the pipe without being sheared, and in the second zone, the sheared concrete, the concrete section is entirely sheared as it moves along the pipe. The third zone, the lubrication layer, displays unique physical and flow characteristics compared to the other two zones. The analyses proved that the different flow zones across the pipe section can be analytically identified with the properties of both concrete and the lubrication layer. It was well established that the boundaries between these zones and their velocity profiles are complex functions of the properties of both concrete and the lubrication layer, and the pipe diameter. Using these affecting parameters, the contribution of each flow zone to the total flow rate across the pipe were precisely determined.

## 8.1.3 Analytical pressure prediction model

A master analytical formula to compute the pressure loss was derived in function of the rate, the rheological properties of both concrete and the lubrication layer, thickness of the lubrication layer, and pipe radius. The resulting formula is analytically grounded and can be applied to any type of highly-flowable concrete, obeying Bingham behavior. The effects of several parameters on the pressure loss, including the properties of both concrete and the lubrication layer, and the pipe size, were investigated independently

through the analytical model. The interactions between these parameters in relation to the pressure loss were also examined.

The analysis revealed that, in highly-flowable concrete, viscosity plays a fundamental role in determining the pressure loss, whereas yield stress displays only a minor effect.

The correlations between the properties of the lubrication layer and the pressure loss disclosed that pressure loss increases with the viscosity of the lubrication layer while it decreases with increasing its thickness.

The analysis also showed that, for a given pressure loss, the lubrication layer properties are not only interdependent, but they also depend on concrete viscosity. The thickness of the lubrication layer increases with its viscosity. On the other hand, if a constant discharge rate is assumed, an increase in concrete viscosity results in a decrease in the viscosity and an increase in the thickness of the lubrication layer. This decrease is sharp for concrete viscosities below 30 Pa s, while it becomes less significant beyond this range. As a result, variations in concrete viscosity can induce different changes in the viscosity and thickness of the lubrication layer, leading to opposite effects on the pressure loss.

Apart from the materials properties, the pipe diameter was proven to be influential parameter on pressure loss to a significant extent. For a given discharge, increasing the pipe diameter decreases pressure loss, but it can also lead to a reduction in the thickness of the lubrication layer and thus an increase in the pressure loss.

The analyses also revealed that, among the studied parameters viscosity is the most influential property on pressure loss followed by the thickness of the lubrication layer and its viscosity. On the other hand, yield stress of both concrete and lubrication layer only have a little influence on pressure loss.

The different effects of the parameters incorporated in the analytical model were presented through a set of contour diagrams (Figures 5.7-5.16). These diagrams bring to life a new promising approach that can determine the pressure loss for a wide range of concrete rheological properties and pipe sizes.

### 8.1.4 Pumping pressure loss and rheological and tribological properties

The results of the analytical study were further confirmed through the full-scale pumping tests conducted at the laboratory of the Université de Sherbrooke (Chapter 6). In the case of SCC and HWC, a solid positive correlation at different discharge rates exists between the pressure loss and viscosity. For CVC, the scenario changes, and instead, yield stress is strongly related to the pressure loss while viscosity has only a minor effect. The tribological parameters measured in the tribometer ($Itrib_{ll}$, $Itrib_{co}$, $Itrib_{tot}$) demonstrated cogent relationships with pressure loss. The derived tribological parameters were proved definitive indicators of the variations in the properties of the lubrication layer and their influences on the pressure loss.

### 8.1.5 Job-site estimation of pressure loss

Through the several empirical correlations established during the full-scale pumping tests, simple test methods were introduced to determine the pressure loss in field. The test

method varies according to the concrete type: the V-funnel test is adapted for SCC and HWC and the slump test for CVC. The outstanding advantage of these approaches is that the pressure loss can be easily estimated on job sites without the need for complex rheological and tribological measurements.

### 8.1.6 Statistical models to calculate pressure loss

Applying the same full-scale pumping test results as input, critical statistical analyses were undertaken in order to quantify the influence of concrete properties on pressure loss. Both viscosity and $Itrib_{ll}$ proved highly influential parameters on pressure loss; among both affecting parameters, viscosity has the highest effect followed by the increasing effect of $Itrib_{ll}$ with decreasing the pipe diameter. The statistical analyses also demonstrated that pressure loss can be accurately predicted on the basis of viscosity and $Itrib_{ll}$ of concrete. Statistical models for two pipe sizes were derived to determine the pressure loss as a function of the viscosity and $Itrib_{ll}$ of concrete. Incorporating $Itrib_{ll}$ improved the accuracy of the models by representing the influence of the lubrication layer on the flow resistance. Another statistical model to calculate the pressure loss was educed as a function of the V-funnel time. The simplicity of the V-funnel test makes this statistical model one of the most advantageous to predict the pressure loss on job sites without the need for rheological and tribological machinery.

### 8.1.7 The pipe flow test (PFT)

A new test method was developed to simulate the flow behavior of concrete in pipes (section 6.14). Test results showed that the flow time measured in the PFT is well correlated with the viscosity of concrete. The obtained correlation can be successfully extended to predict the pumping pressure loss, using existing relationships between viscosity and pumping pressure loss. This makes the PFT a practical tool to predict both viscosity and pressure loss on job sites without undertaking typical rheological and tribological experiments. One of the distinct privilege of the PFT over the standardized test methods used to predict pressure loss (such as the V-funnel test) is that the lubrication layer is fully developed through the testing procedures, resulting in more precise readings of the estimated pressure loss.

### 8.1.8 Influence of pumping on concrete properties

The changes in concrete properties due to prolonged pumping were assessed during the full-scale pumping experiments conducted at the laboratory of the Université de Sherbrooke (section 6.12). The test results signified the changes in concrete temperature and air content with pumping time. Concrete temperature was shown to increase with pumping duration due to the accumulation of the dissipated heat generated by the solid-solid particles interactions in the viscous flow. Temperature was also found to increase with the discharge rate because of the increased number of particles interactions at higher discharge rates. Air content also exhibited an increase with pumping pressure, but no definitive justification could be found. The changes in concrete temperature and air content were hypothesized to be the primary causes of the observed changes in viscosity

and yield stress. Viscosity displayed a significant reduction during pumping while yield stress exhibited an increase in most cases. The changes in the tribological properties can be summerized by an increase in $Itrib_{ll}$ and a reduction in $Itrib_{co}$ and $Itrib_{tot}$. These two parameters were found to be directly related to the thickness and viscosity of the lubrication layer during pumping.

### 8.1.9 Reducing pumping pressure

The experience gained from the full-scale pumping tests was applied one last to direct the optimization phase of the project (Chapter 7). Beginning on the CEM scale and continuing later on the concrete scale, viscosity and tribological resistance were targeted for reduction by optimizing several mix design parameters. The results revealed that pumping pressure can be most effectively reduced by increasing $w/cm$, but due to the accompanied reduction in stability and strength, it was not considered the most favorable method. The use of cementitious materials was found to remarkably reduce viscosity and consequently the pressure loss. A replacement level of 6% silica fume can reduce viscosity by 50%, while a substitution level of 25% Class C fly ash or 15% Class F fly ash can reduce viscosity by 30%, and 10%, respectively, relevant to the reference mixture prepared with only GU cement. Class C fly ash therefore proved more efficient than Class F for viscosity reduction. A replacement of the GU cement by a blend of 6% silica fume and 25% Class C fly ash can further decrease CEM viscosity by 30% without significantly decreasing its compressive strength. On the contrast, slag was found inappropriate for pumping applications as it results in undue shear thickening behavior and leads to reduction in the compressive strength.

With the research findings of CEM scale as input, the investigation was expanded to the concrete scale with the same goal of reducing pumping pressure loss. The results indicated that the effect of the investigated cementitious materials is more pronounced when high binder contents are used. Although increasing binder content can decrease viscosity and $Itrib_{tot}$, it can also increase $Itrib_{ll}$. Therefore, the choice of the binder content is a straightforward question of the binder type in use.

The investigation into the influence of the paste volume disclosed that, depending on the binder in use, increasing the paste volume can dramatically reduce viscosity, and as a consequence the required pumping pressure. However, beyond certain limits, increases in paste volume have no sizable effect on pressure loss, but can increase the risk of segregation and cause other instability issues. Therefore, for every mix design there exists a range of paste volumes in which flowability and stability are in harmony; outside of this range the concrete becomes less appropriate for pumping applications.

The study on the granular effect proved that optimizing the granular system of the mixture can be an effective practice to reduce viscosity, $Itrib_{tot}$, and thus pressure loss. It was observed that the influence of MSA varies in function of the granular distributions in place. Although, the general trend indicated a decrease in viscosity, $Itrib_{tot}$, and consequently pressure loss with decreasing MSA. Adjusting S/A was also found to be a practical way to decrease pumping pressure. As with MSA, increasing S/A does not always cause a reduction in pressure loss; instead optimal values of S/A can vary widely depending on the granular characteristics in use.

Finally, a firm correlation was found between the slump flow and yield stress, whereas no meaningful relationships could be established between the slump flow and viscosity, $Itrib_{tot}$, or pressure loss (except for CVC). Although an increase in the slump flow (brought about by increasing HRWRA) does not hold a substantial effect on reducing the pressure loss, it can significantly decrease the stability of the pumped mixture. Therefore, workability and stability requirements, rather than the pressure loss, should be the main consideration in selecting the slump flow of the pumped mixture.

### 8.1.10 Comparison of pumpability of different types of concrete

Because of their markedly different pipe flow characteristics, SCC and CVC yield similar yet at times contrary relationships. It was observed that CVC exhibits a linear correlation between pressure loss and discharge rate, while SCC exhibits a slightly non-linear relationship. The diverging behavior patterns of the two materials is best exemplified when considering pumping effect. For SCC, in most cases, pressure loss decreases continuously at early stages of pumping, while it tends to increase after a certain period of time during pumping. The decrease in the pumping pressure at early stages of pumping can be related to the reduction in viscosity associated with prolonged pumping. On the other hand, the increase in the pressure loss at late stages in the pumping operation can be attributed to the changes in tribological properties brought with prolonged pumping.

In the range of CVC, the scenario changes since the yield stress is the most influential parameter on pressure loss. The increase in yield stress due to pumping can lead to an increase in pressure loss.

The time evolution of pressure less in HWC during pumping can be considered less significant than those in SCC or CVC. These less important changes in the pressure loss of HWC during pumping can be attributed the characteristic of its flow, in which both viscosity and yield stress play a significant role.

Because of its unique ability to decrease pressure loss with pumping distance, SCC becomes a preferable choice for high-rise and other long-distance pumping applications. The only risk for long-distance SCC pumping remains the increased instability of the mix, an effect brought by the decreasing viscosity of pumped mixture with time. CVC on the other hand can increase pressure loss with pumping time, and therefore special care should be applied to prevent the potential occurrence of blockages.

### 8.1.11 Closing remarks

As can be gathered after reading the pages of this dissertation, the science of pumping SCC is far removed from the rudimentary notions that guided its early design efforts. The complicated flow environment in pumping pipes lent itself nicely to research efforts directed towards developing models to predict and reduce pressure loss. The outcome of this research will hopefully put into practice indispensable lessons on pumping SCC and help the concrete industry to push modern pumping technologies one step further.

## 8.2 Future research

### 8.2.1 Lubrication layer

A model was derived in this research project to determine the thickness and rheological properties of the lubrication layer with the help of tribological and rheological experiments. Unfortunately, validation of this model using two tribometers could not be completed due to some technical difficulties. Validating the proposed model and empirically determining the properties of the lubrication layer would be useful research work in the future.

### 8.2.2 Correlation between the properties of concrete and lubrication layer

Since the lubrication layer is a product of the shear effect in concrete, a certain link exists between the concrete constituent materials and the viscosity and thickness of the lubrication layer. As this correlation cannot be captured through analytical modeling, experimental studies are needed to define the relationship between the properties of the lubrication layer and the properties of the concrete constituent materials.

### 8.2.3 Pipe material

Most pipes available on the market are made of steel. Future structural applications intend to replace existing pipes with more "handy" types of pipes in terms of weight and cost. Determining the pressure loss in pumping pipes made of materials different than steel, for example PVC or rubber, will open the door for new pumping applications geared toward reaching places that are difficultly accessed with traditional steel pipes.

### 8.2.4 Pipe flow test

The pipe flow test developed in this investigation showed that the flow time in the testing pipe is well correlated with the viscosity and tribological properties of the tested concrete. Since these properties correlated with the flow time are well correlated with pressure loss, the flow time can be considered as an indication of pressure loss during pumping. From this perspective, the pipe flow test can be a practical tool to determine the pressure loss of concrete without the need for complex rheological and tribological experiments. Further validation of this theory on a full-scale pumping circuit is needed.

### 8.2.5 Air content and characterization

At many occasions during this investigation, changes in air content and system were considered to have a high impact on the rheological properties of concrete. At this point, researchers are able to identify several mechanisms through which the air can possibly affect the rheological properties, but solidly affirming through empirical investigations has proved difficult. This leaves open avenues for further research to fully understand the underlying mechanisms of these changes during pumping.

### 8.2.6 Long-distance pumping

During the pumping tests, each test was carried out over a certain period of time, which could not be exceeded due to some technical restraints. In practice, pumping can be continued for a long period of time, especially in very long circuits (above 3000 m, as in the cases of grout pumping down in mines, for example). Consequently, the flow behavior of concrete can significantly change due to the prolonged pumping, with a higher magnitude than that observed during short-time pumping. This change in the flow behavior can lead to important changes in the pressure loss along the stream line over time. Further investigation is still needed to look into the changes in the flow behavior associated with long-distance pumping and their effect on pressure loss along the pipe lines.

### 8.2.7 Pumpability of different types of concrete

Different types of concrete including SCC, HWC, and CVC were tested in the pumping circuit. The results of this research and those of a previous research carried out by Feys (2009) yield similar yet at times different correlations. Some of these differences can be attributed to the sensitivity of concrete, especially SCC and HWC, to the changes in the constituent materials and admixtures, which vary from country to another and even from a region to another. Research should therefore be continued to establish a wider database on the performance of SCC (and other types of highly-flowable concrete) in pumping pipes for a wider range of concrete constituent materials and admixtures.

### 8.2.8 Effect of pumping on long-term properties of concrete

The high shear effect induced during pumping can significantly affect the rheological and fresh properties of concrete. Most of these changes are associated with changes in the air content and temperature in the pumped concrete. In this context, the effect of pumping on the fresh properties can extend to the durability and long-term properties in concrete. A more comprehensive study is therefore needed to disclose the correlations between pumping and the long-term properties of concrete, and to evaluate the effect of pumping on the durability properties in pumped concrete.

## 8.3 Conclusions générale

Après une longue exploration du modèle d'écoulement de la BAP dans les tuyaux et développer une compréhension solide des paramètres clés régissant ce flux, le temps est venu de conclure cette thèse et mettre en évidence ses résultats les plus significatifs. Les sections suivantes décrivent les conclusions des études analytiques, statistiques et empiriques fournies par les trois derniers chapitres.

### 8.3.1 Propriétés de la couche de lubrification

L'analyse présentée dans la section 5.6 démontre que le comportement de l'écoulement du béton dans les tuyaux de pompage peut être simulé avec succès au moyen de tests tribologiques. Sur cette base, une nouvelle formule analytique a été dérivée pour calculer l'épaisseur et la viscosité de la couche de lubrification. Les propriétés de la couche de lubrification ont été présentées comme des fonctions des propriétés rhéologiques du béton et du couple appliqué à l'écart du tribomètre. En outre, les nouveaux paramètres tribologiques sont déduits pour décrire la résistance à l'écoulement du béton à l'écart du tribomètre. Les paramètres tribologiques dérivés ont montré une grande maîtrise (à travers les phases expérimentales) pour quantifier la résistance à l'écoulement du béton dans l'écoulement du béton dans les tuyaux de pompage.

### 8.3.2 Écoulement du béton dans les tuyaux

Les analyses réalisées au Chapter 5 ont montré que les différents comportements de flux peuvent être caractérisés, en fonction de la pression de pompage, les propriétés à la fois du béton et la couche de lubrification, et la distance du centre du tube. Dans le cas du béton très fluide, trois zones ayant des caractéristiques distinctives de flux peuvent être définies à travers la section du tuyau. Dans la première zone, le bouchon, le béton se déplace le long du tuyau sans être cisaillé, et dans la deuxième zone, le béton cisaillé, qui est entièrement cisaillé lorsqu'il se déplace le long du tuyau. La troisième zone, la couche de lubrification, présente des caractéristiques physiques et de flux uniques par rapport aux deux autres zones. Les analyses ont montré que les différentes zones d'écoulement à travers la section du tuyau peuvent être analytiquement identifiées par les propriétés à la fois du béton et de la couche de lubrification. Il a été bien établi que les frontières entre ces zones et leurs profils de vitesse sont des fonctions complexes des propriétés à la fois du béton et la couche de lubrification et le diamètre du tuyau. En utilisant ces paramètres affectants, la contribution de chaque zone d'écoulement pour le débit total a été déterminée avec précision à travers le tuyau.

### 8.3.3 Modèle analytique de prédiction de pression

Une formule analytique principale pour calculer la perte de charge a été déduite en fonction du débit, des propriétés à la fois du béton et la couche de lubrification, et le rayon de la conduite. La formule résultante est analytiquement bien établie et peut être appliquée à tout type de béton très fluide, en supposant que le comportement Bingham. Les effets de plusieurs paramètres sur la perte de pression, y compris les propriétés à la fois du

béton et la couche de lubrification, et la taille du tuyau, ont été étudiés de façon indépendante par le modèle analytique. Les interactions entre ces paramètres par rapport à la perte de pression ont également été examinées. L'analyse a révélé que, dans le béton très fluide, la viscosité joue un rôle fondamental dans la détermination de la perte de pression, tandis que la limite d'élasticité est affiche un effet négligeable. Les corrélations entre les propriétés de la couche de lubrification et de la perte de pression révèle que la perte de pression augmente avec la viscosité de la couche de lubrification tandis qu'elle diminue avec l'augmentation de son épaisseur. L'analyse a également montré que les propriétés de la couche de lubrification sont non seulement interdépendantes, mais elles dépendent aussi de la viscosité du béton. L'épaisseur de la couche de lubrification augmente avec la viscosité. D'autre part, une augmentation de la viscosité du béton résulte de la diminution de la viscosité et de l'augmentation de l'épaisseur de la couche de lubrification. Cette baisse est forte pour des viscosités de béton inférieures à 30 Pa s, alors qu'elle devient moins importante au-delà de cette fourchette. En conséquence, les variations de la viscosité du béton peuvent induire différentes variations de la viscosité et de l'épaisseur de la couche de lubrification, ce qui conduit à des effets opposés sur la perte de pression. Outre les propriétés des matériaux, le diamètre du tuyau a été prouvé pour être un paramètre influent sur la perte de pression dans une large mesure. L'augmentation du diamètre du tuyau diminue la perte de pression, mais elle peut aussi conduire à une réduction de l'épaisseur de la couche de lubrification et donc, une augmentation de la perte de pression. Les différents effets des paramètres intégrés dans le modèle d'analyse ont été présentés par un ensemble de diagrammes de contour (Figures 5.7-5.16). Ces diagrammes donnent vie à une nouvelle approche prometteuse qui peut déterminer avec précision la perte de pression pour une large gamme de propriétés du béton et de la taille des tuyaux.

### 8.3.4 Perte de pression de pompage et les propriétés rhéologiques et tribologiques

Les résultats de l'étude analytique ont été confirmés par les essais de pompage à grande échelle Les tests effectués au laboratoire de l'Université de Sherbrooke (Chapter 6). Dans le cas de BAP et HWC, une corrélation positive solide à différents débits existe entre la perte de pression et la viscosité. Pour BC, les changements de scénario, et à la place, la limite d'élasticité est fortement liée à la perte de pression tandis que la viscosité n'a qu'un effet mineur. Les paramètres tribologiques mesurés dans le tribomètre ($Itrib_{ll}$, $Itrib_{co}$, $Itrib_{tot}$) ont démontré des relations convaincantes avec la perte de pression. Les paramètres tribologiques dérivés ont été prouvés indicateurs définitifs des variations dans les propriétés de la couche de lubrification et de leurs influences sur la perte de pression.

### 8.3.5 Estimation de la perte de pression sur le chantier

A travers les quelques corrélations empiriques établies au cours des essais de pompage à grande échelle, méthodes d'essai simples ont été introduites afin de déterminer la perte de pression dans le domaine. Le test méthode varie selon le type de béton: V-entonnoir est adapté pour la BAP et HWC et l'essai de tassement pour BC. L'avantage exceptionnel de

ces approches est que la perte de pression peut être facilement estimée sur les chantiers sans avoir besoin de complexe mesures rhéologiques et tribologiques.

### 8.3.6 Les modèles statistiques pour calculer la perte de pression

En appliquant les mêmes résultats d'essais de pompage à grande échelle en entrée, les analyses statistiques essentielles ont été menées afin de quantifier l'influence des propriétés du béton sur la perte de pression. Les deux viscosités et $Itrib_{\mu}$ sont prouvés comme paramètres très influents sur la perte de pression; parmi les deux paramètres affectants, la viscosité a l'effet le plus élevé, suivie par l'effet de l'augmentation dans $Itrib_{\mu}$ avec la diminution du diamètre du tuyau. Les analyses statistiques ont également montré que la perte de pression peut être prédite avec précision en fonction de la viscosité et $Itrib_{\mu}$ de béton. Les modèles statistiques pour deux tailles de tuyaux ont été calculés pour déterminer la la perte de pression en fonction de la viscosité et $Itrib_{\mu}$ de béton. Intégrer $Itrib_{\mu}$ améliore la précision des modèles en représentant l'influence de la couche de lubrification sur la résistance à l'écoulement. Un autre modèle statistique pour le calcul de la perte de charge a été déduit comme fonction du temps V- entonnoir. La simplicité du test V- entonnoir rend ce modèle statistique l'un des plus avantageux pour prédire la perte de pression sur les chantiers sans avoir besoin de machines rhéologiques et tribologiques.

### 8.3.7 Test d'écoulement dans la conduite ( PFT )

Une nouvelle méthode de test qui simule l'écoulement dans les tuyaux en béton a été développée au laboratoire de l'Université de Sherbrooke (section 6.14). Les résultats des tests ont montré que le temps d'écoulement par le PFT est bien corrélé avec la viscosité et les propriétés tribologiques du béton testé. Ces propriétés peuvent ensuite réfléchir sur la perte de pression de pompage, ce qui donne un outil précis de prédire la perte de pression au moyen de procédures de tests simples. Un des privilèges distincts de la PFT sur les méthodes d'essai normalisées utilisées pour prédire la perte de pression (comme le test de l'entonnoir V) est que la couche de lubrification est entièrement développée par les procédures d'essai, ce qui entraîne des lectures plus précises de la perte de charge estimée. Toutefois, d'autres tests sur un essai de pompage à grande échelle sont encore nécessaires pour valider la méthode d'essai PFT.

### 8.3.8 Influence du pompage sur les propriétés du béton

Les changements dans les propriétés du béton en raison du pompage prolongé ont été évalués au cours des expériences de pompage à grande échelle effectuées au laboratoire de l'Université de Sherbrooke (section 6.12). Les résultats des tests signifiaient les changements de température du béton et de teneur en air en fonction du temps de pompage. La température du béton a été montrée pour augmenter la durée de pompage en raison de l'accumulation de la chaleur dissipée générée par l'interaction des particules solide-solide dans l'écoulement visqueux. La température a été également constaté qu'elle augmentait avec le taux de décharge en raison de l'augmentation du nombre des interactions de

particules à débit supérieur. La teneur en air présentait également une augmentation de la pression de pompage, mais pas de justification définitive n'a pu être trouvé. Les variations de la température du béton et de la teneur en air ont émis l'hypothèse d'être les principales causes des changements observés dans la viscosité et le seuil de cisaillement. La viscosité affichait une réduction significative pendant le pompage pendant que la limite d'élasticité présentait une augmentation systématique. Les changements dans les propriétés tribologiques peuvent être résumés par une augmentation dans $Itrib_{ll}$ et une réduction de la $Itrib_{co}$ et $Itrib_{tot}$. Ces deux paramètres ont été trouvés à être directement lié à l'épaisseur et la viscosité de la couche de lubrification pendant le pompage.

### 8.3.9 Réduction de la pression de pompage

L'expérience acquise lors des essais de pompage à grande échelle a été appliquée une dernière fois pour diriger la phase d'optimisation du projet (Chapter 7). En commençant à l'échelle CEM et en poursuivant plus tard sur l'échelle de béton, la viscosité et la résistance tribologiques ont été ciblés pour la réduction en optimisant plusieurs paramètres de formulation. Les résultats ont révélé que la pression de pompage peut être plus efficacement réduite en augmentant $w/cm$, mais en raison de la diminution accompagnée de la stabilité et de la force, il n'a pas été considéré comme la méthode la plus favorable. L'utilisation de matériaux à base de ciment a été trouvée pour réduire remarquablement la viscosité et par conséquent, la perte de pression. Un niveau de remplacement de 6% de fumée de silice peut réduire la viscosité de 50%, alors qu'un taux de substitution de 25% de cendres volantes de classe C, soit 15% de cendres volantes de classe F peut réduire la viscosité de 30% et 10%, respectivement, en rapport avec le mélange préparé avec référence avec seulement le ciment GU. La classe C de cendres volantes s'est donc avérée plus efficace que la classe F pour la réduction de viscosité. Un remplacement du ciment GU par un mélange de 6% de fumée de silice et 25% Classe C de cendres volantes peut encore diminuer la viscosité CEM de 30% sans diminuer significativement sa résistance à la compression. Sur le contraste, le laitier était inadapté pour les applications de pompage tel qu'il résulte du comportement de l'épaississement de cisaillement excessif et conduit à une réduction de la résistance à la compression. Avec les résultats de recherche d'échelle CEM en entrée, l'enquête a été élargie à l'échelle du béton avec le même objectif de réduire la perte de pression de pompage. Les résultats indiquent que l'effet des matériaux cimentaires étudiés est plus prononcé lorsque des teneurs élevées de liants sont utilisées. Bien que l'augmentation de liants peut diminuer la viscosité et $Itrib_{tot}$, elle peut aussi augmenter $Itrib_{ll}$. Par conséquent, le choix de la teneur en liant est une simple question du type de liant utilisé. L'enquête sur l'influence du volume de pâte a révélé que, selon le liant utilisé, ce qui augmente le volume de la pâte permet de réduire considérablement la pression de pompage requise. Cependant, au-delà de certaines limites, l'augmentation de volume de pâte n'a pas d'effet considérable sur la perte de pression, mais peut augmenter le risque de ségrégation et causer d'autres problèmes d'instabilité. Par conséquent, pour chaque conception de mélange, il existe une gamme de volumes de pâte dans laquelle la fluidité et la stabilité sont en harmonie, en dehors de cette plage, le béton devient moins approprié pour les applications de pompage. L'étude sur l'effet granuleux prouve que l'optimisation du système granulaire du mélange peut être une pratique efficace pour réduire la viscosité, $Itrib_{tot}$, et donc la perte de pression.

Cela a été observé que l'influence du MSA varie en fonction des distributions granulaires en place. Bien que la tendance générale indiquait une diminution de la viscosité, $Itrib_{tot}$, et perte de pression avec la baisse MSA. Le réglage S/A a également été trouvé pour être un moyen pratique pour diminuer la pression de pompage. Comme avec MSA, en augmentant S/A ne provoque pas toujours une réduction de la perte de pression; les valeurs optimales au lieu de S/A peuvent varier considérablement en fonction des caractéristiques granulaires utilisées. Enfin, une corrélation ferme a été trouvée entre l'affaissement et la limite d'élasticité, alors qu'aucune des relations significatives ne pourraient être établis entre le flux de tassement et de la viscosité, $Itrib_{tot}$, ou la perte de pression. Bien que l'augmentation du flux de tassement (provoquée par l'augmentation HRWRA) ne détienne pas un effet important sur la réduction de la perte de pression, il peut diminuer de façon significative la stabilité du mélange pompé. Par conséquent, les exigences en matière de maniabilité et de stabilité, plutôt que la perte de pression, doivent être la principale considération dans le choix du flux de tassement du mélange pompé.

### 8.3.10 Comparaison des BAP et BC

En raison de leurs très différentes caractéristiques d'écoulement des tuyaux, BAP et BC ont un rendement similaire encore, parfois des relations contraires. Il a été observé que, dans la plupart des cas, BC présente une corrélation linéaire entre la perte de charge et la décharge, tandis que BAP présente une relation légèrement non linéaire. Les divergences de comportements des deux matériaux est le meilleur exemple lorsque l'on considère l'effet de pompage. Parce que la viscosité diminue le seuil de cisaillement et augmente le rendement prolongé avec le pompage, la pompabilité de BAP est améliorée avec le temps tandis que celle de BC est finalement calmée. C'est cette capacité assez unique de BAP de diminuer la perte de pression à distance, qui en fait un choix préférable pour les applications de pompage de longue distance de grande hauteur et autres pompages. Le seul risque pour les longues distances de pompage de BAP reste l'augmentation de l'instabilité du mélange, un effet apporté par la viscosité diminue le mélange pompé avec le temps. D'autre part BC augmente la perte de pression avec le temps de pompage et de soins, et par conséquent une attention particulière devra être appliquée à prévenir l'apparition éventuelle de blocages.

### 8.3.11 Mot final

On peut comprendre après avoir lu les pages de cette thèse, que la science de pompage BAP est loin des notions rudimentaires qui ont guidé ses efforts précoces de la conception. L'environnement de flux compliqué dans les tuyaux de pompage se prêtait bien aux efforts de recherche orientée vers le développement de modèles pour prédire et réduire la perte de pression. Le résultat de cette recherche, nous l'espérons mettra en pratique des leçons indispensables sur le pompage BAP et aidera l'industrie du béton pour pousser les technologies modernes de pompage un peu plus loin.

# Appendices

# Appendix A

# Materials properties

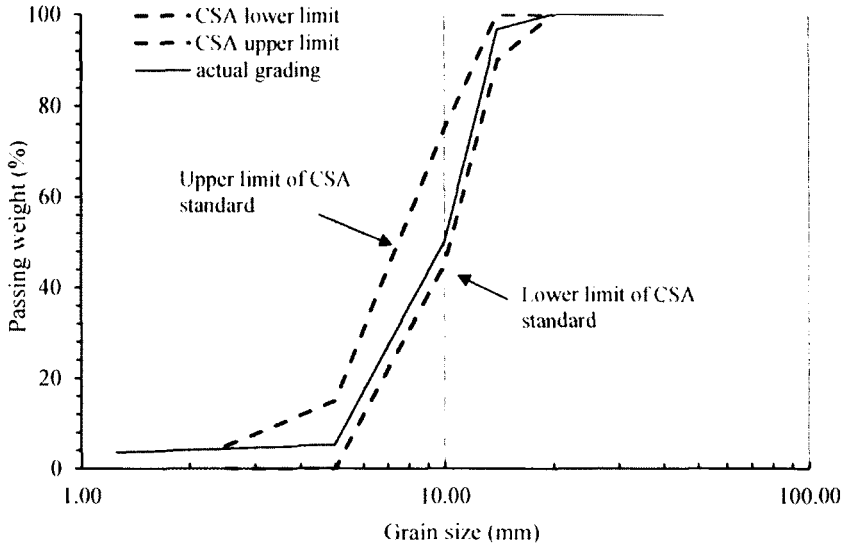


***Figure A.1:*** *Granular distribution of the 14-mm local aggregate used in phase 1 of the concrete scale.*

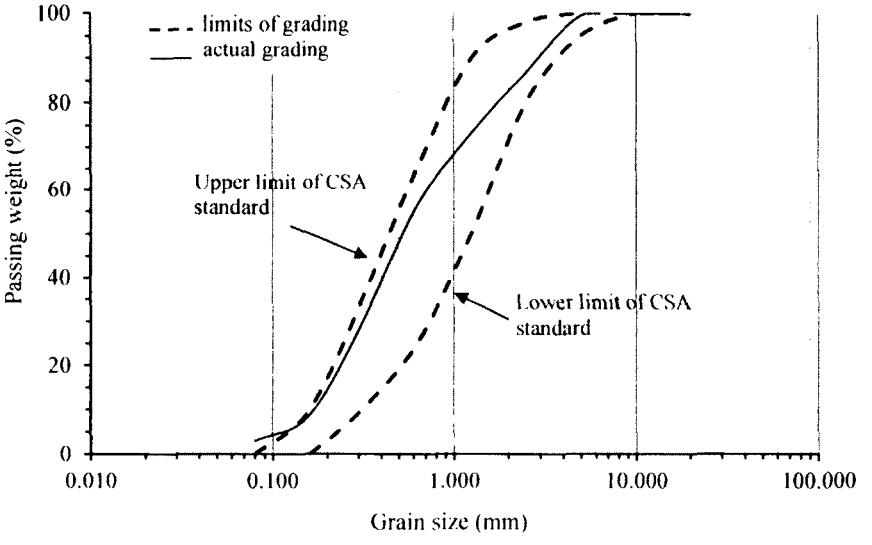


***Figure A.2:*** *Granular distribution of the local sand 1 used in phase 1 of the mortar scale.*

***Table A.1:*** *Density of the local sand and aggregate used in phase 1 of the concrete and mortar scales.*

| Material | Density (gr/cm$^3$) | Fineness modulus |
|---|---|---|
| Sand (1) | 2.65 | 2.48 |
| Sand (2) | 2.60 | 2.54 |
| Aggregate 14 mm | 2.74 | - |
| Aggregate 10 mm | 2.77 | - |

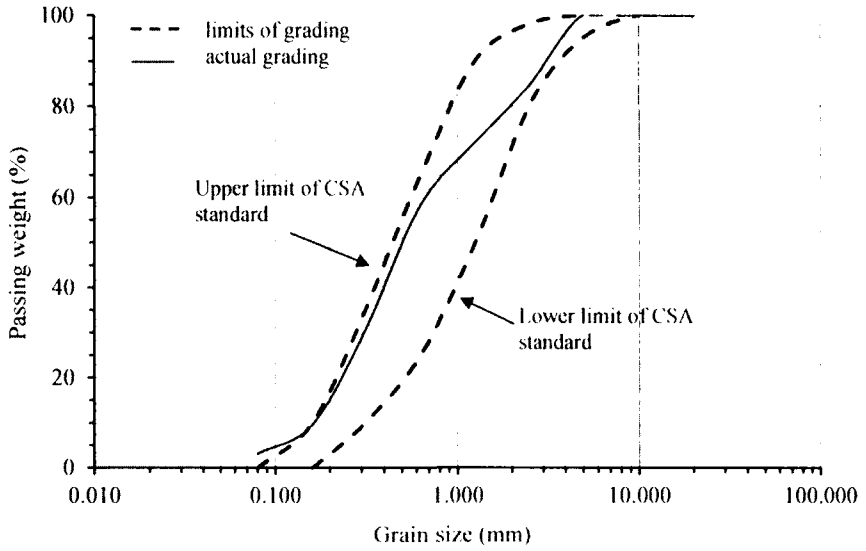


***Figure A.3:*** *Granular distribution of the local sand 2 used in phase 1 of the concrete and mortar scales.*

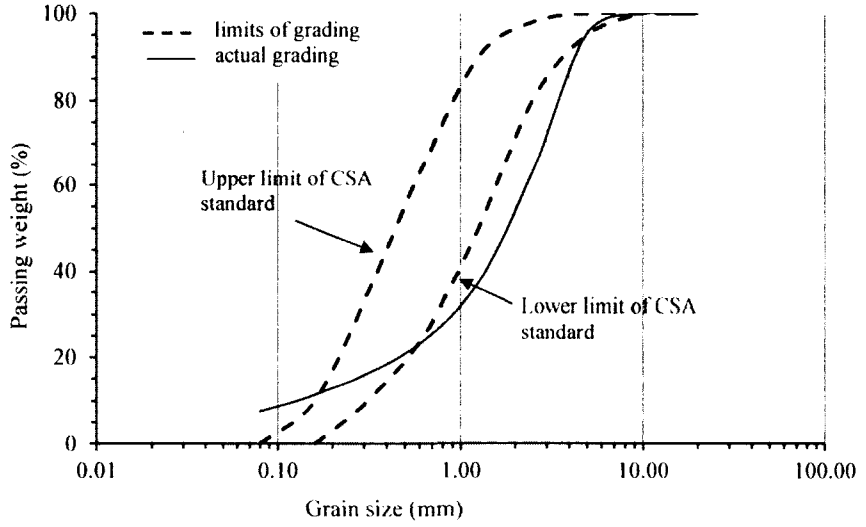


***Figure A.4:*** *Granular distribution of the crushed-aggregate sand (from the Arabic Gulf) used in phase 2 of the concrete scale.*

***Table A.2:*** *Density of the sand and aggregate (from the Arabic Gulf) used in phase 2 of the concrete scale.*

| Material | Density (gr/cm$^3$) | Fineness modulus |
|---|---|---|
| Sand 1 (dune sand) | 2.7 | 5.41 |
| Sand 2 (crushed-aggregate sand) | 2.63 | 2.47 |
| Aggregate 10 mm | 2.81 | - |
| Aggregate 20 mm | 2.8 | - |

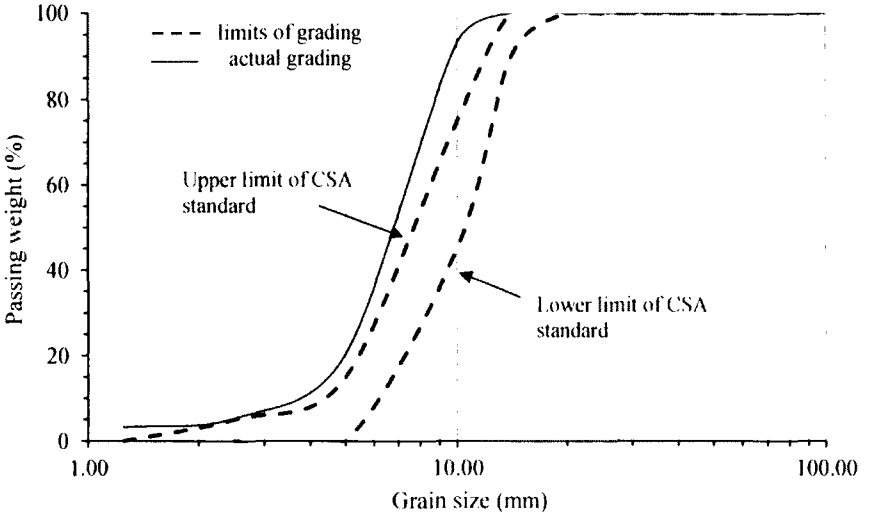


***Figure A.5:*** *Granular distribution of the 10-mm aggregate (from the Arabic Gulf) used in phase 2 of the concrete scale.*

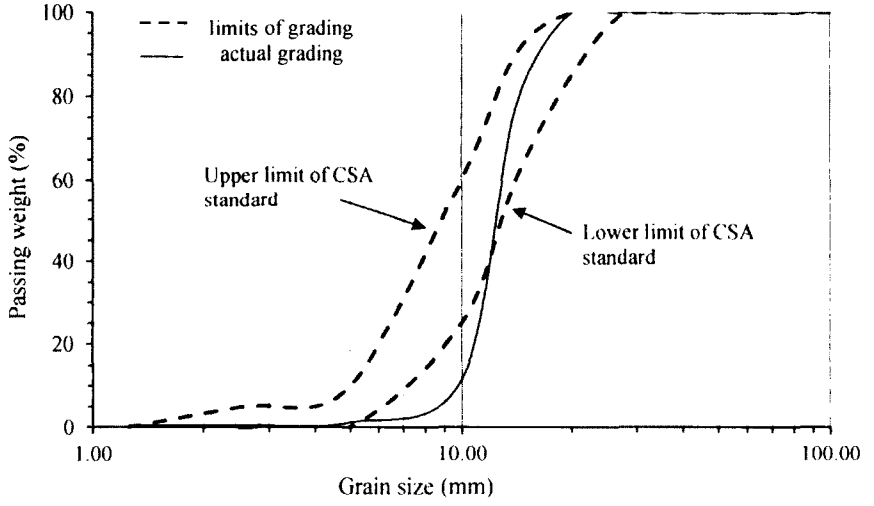


***Figure A.6:*** *Granular distribution of the 20-mm aggregate (from the Arabic Gulf) used in phase 2 of the concrete scale.*

***Table A.3:*** *Chemical analysis of GU Cement.*

| Chemical analysis of GU Cement | |
|---|---|
| Silicon dioxide ($Sio_2$) | 20.40% |
| Aluminium oxide ($Al2O_3$) | 4.60% |
| Sulphur Trioxyde ($SO_3$) | 2.80% |
| Iron Oxide ($Fe_2O_3$) | 3.40% |
| Calcium Oxide (CaO) | 62.70% |
| Magnesium Oxide (MgO) | 1.90% |
| Moisture content | 0.03% |
| Loss of ignition | 0.40% |
| Total Alkalies as Equiv $Na_2O$ | 0.80% |

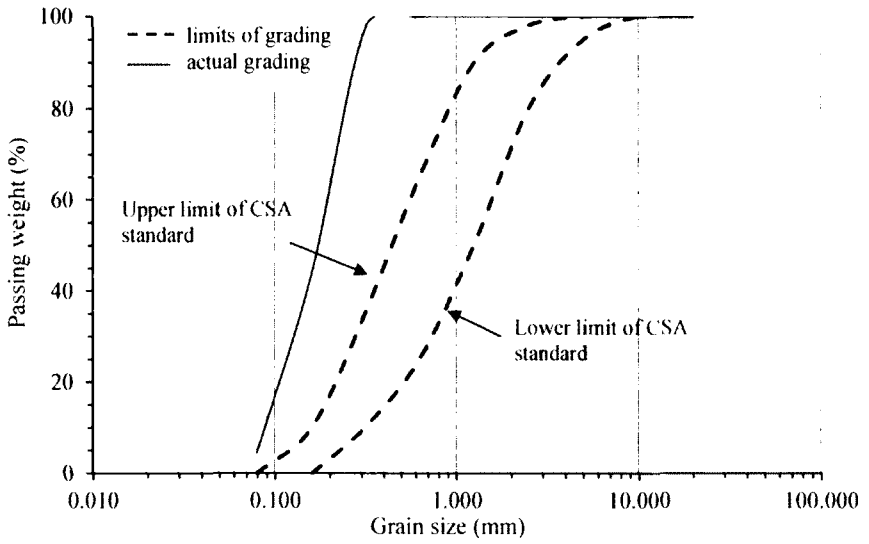


***Figure A.7:*** *Granular distribution of dune sand (from the Arabic Gulf) used in phase 2 of the concrete scale.*

***Table A.4:*** *Physical analysis of GU Cement.*

| Physical analysis of GU Cement | |
|---|---|
| Fineness retained on 45μm | 20.40% |
| Compressive strength at 7-days | 31.3 MPa |
| Compressive strength at 28-days | 41.4 MPa |
| Autodave Expansion | 0.10% |
| Density | 3.14 gr/cm$^3$ |

***Table A.5:*** *Chemical analysis of Class C Fly ash.*

| Chemical analysis of Fly ash Class C | |
|---|---|
| Silicon dioxide ($Sio_2$) | 53.40% |
| Aluminium oxide ($Al2O_3$) | 23.10% |
| Sulphur Trioxyde ($SO_3$) | 3.40% |
| Iron Oxide ($Fe_2O_3$) | 0.10% |
| Calcium Oxide (CaO) | 10.00% |
| Magnesium Oxide (MgO) | 1.10% |
| Moisture content | 0.03% |
| Loss of ignition | 0.40% |
| Total Alkalies as Equiv $Na_2O$ | 3.24% |

**Table A.6:** *Physical analysis of Class C Fly ash.*

| Physical analysis of Fly ash Class C | |
|---|---|
| Fineness retained on 45μm | 16.70% |
| Strength Activity Index with Cement | |
| % of control at 7-days | 88% |
| % of control at 28-days | 96% |
| Water requirement, Percent of Control | 94.80% |
| Autodave Expansion | 0.07% |
| Density | 2.04 gr/cm$^3$ |

**Table A.7:** *Chemical analysis of Class F Fly ash.*

| Chemical analysis of Fly ash Class F | |
|---|---|
| Silicon dioxide ($Sio_2$) | 53.89% |
| Aluminium oxide ($Al2O_3$) | 20.97% |
| Sulphur Trioxyde ($SO_3$) | 1.36% |
| Iron Oxide ($Fe_2O_3$) | 10.15% |
| Calcium Oxide (CaO) | 2.93% |
| Moisture content | 0.05% |
| Loss of ignition | 1.72% |
| Total Alkalies as Equiv $Na_2O$ | 4.31% |

**Table A.8:** *Physical analysis of Class F Fly ash.*

| Physical analysis of Fly ash Class F | |
|---|---|
| Fineness retained on 45μm | 9.90% |
| Strength Activity Index with Cement | |
| % of control at 7-days | 95.20% |
| % of control at 28-days | 109.70% |
| Water requirement, Percent of Control | 94.80% |
| Autodave Expansion | -0.02% |
| Density | 2.53 gr/cm$^3$ |

**Table A.9:** *Chemical analysis of Silica fume.*

| Chemical analysis of Silica fume | |
|---|---|
| Silicon dioxide ($Sio_2$) | 93.00% max. |
| Aluminium oxide ($Al2O_3$) | 0.40% max. |
| Sulphur Trioxyde ($SO_3$) | 0.40% max. |
| Iron Oxide ($Fe_2O_3$) | 0.8 % max. |
| Calcium Oxide (CaO) | 0.60% max. |
| Magnesium Oxide (MgO) | 0.60% max. |
| Sodium Oxide ($Na_2O$) | 0.20% max. |
| Potassium Oxyde ($K_2O$) | 1.20% max. |
| Carbon (Cfree) | 2.00% max. |
| PAF | 3.5% max. |

***Table A.10:*** *Physical analysis of Silica fume.*

| Physical analysis of Silica fume | |
|---|---|
| Fineness retained on 45μm | 0.0-5.0 % |
| Density | 2.2 gr/cm$^3$ |

***Table A.11:*** *Physical analysis of Slag.*

| Physical analysis of Slag | |
|---|---|
| Fineness retained on 45μm | 0.90% |
| Compressive strength | |
| at 7-days | 31.6 MPa |
| at 28-days | 39.2 MPa |
| Density | 2.99 gr/cm$^3$ |

# Appendix B

# Test Results

*Table B.1: Mix designs and fresh properties of the tested mortars.*

| Mixture | Sand | Cement | Slag | Silica | Fly ash C | Fly ash F | Added water | SP | Mini slump | | V-funnel | |
|---|---|---|---|---|---|---|---|---|---|---|---|---|
| | | | | | | | | | 15min | 80min | 25min | 85min |
| | kg/m$^3$ | kg/m$^3$ | kg/m$^3$ | kg/m$^3$ | kg/m$^3$ | kg/m$^3$ | kg/m$^3$ | kg/m$^3$ | mm | mm | sec. | sec. |
| Reference mixture | 1402.1 | 790.2 | - | - | - | - | 216.0 | 7.01 | 235 | 220 | 15 | 16 |
| 20% slag | 1396.8 | 631.4 | 157.9 | - | - | - | 217.2 | 5.06 | 230 | 170 | 33.6 | 49.2 |
| 25% slag | 1395.4 | 591.8 | 197.3 | - | - | - | 217.9 | 4.03 | 230 | 150 | 25.2 | 63 |
| 30% slag | 1394.1 | 552.2 | 236.7 | - | - | - | 217.7 | 4.29 | 234 | 200 | 26.1 | 20.5 |
| 40% slag | 1391.5 | 473.1 | 315.4 | - | - | - | 217.8 | 3.90 | 233 | 160 | 31.4 | 45.3 |
| 15% Fly ash C | 1332.0 | 652 | - | - | 115.0 | - | 215.0 | 4.6 | 227.5 | 182.5 | 16.7 | 15.6 |
| 20% Fly ash C | 1318.0 | 612 | - | - | 153.0 | - | 214.0 | 3.8 | 230.0 | 175.0 | 11.9 | 16 |
| 25% Fly ash C | 1304.0 | 572 | - | - | 191.0 | - | 214.0 | 3.1 | 227.5 | 160.0 | 18.7 | 14 |
| 30% Fly ash C | 1291.0 | 532 | - | - | 228.0 | - | 213.0 | 2.7 | 225.0 | 192.5 | 17.2 | 15.3 |
| 15% Fly ash F | 1348.0 | 654 | - | - | - | 115.0 | 215.0 | 5.6 | 230.0 | 200.0 | 12.6 | 14.4 |
| 20% Fly ash F | 1339.0 | 615 | - | - | - | 154.0 | 215.0 | 4.8 | 225.0 | 170.0 | 12.3 | 19.3 |
| 25% Fly ash F | 1331.0 | 575 | - | - | - | 192.0 | 215.0 | 4.6 | 227.5 | 175.0 | 18.6 | 22.2 |
| 6% silica+20 % Fly ash C | 1340.3 | 577.3 | - | 46.8 | 156.0 | 156.0 | 213.6 | 6.36 | 230 | 200 | 14 | 15.5 |
| 6% silica+25 % Fly ash C | 1328.5 | 536.9 | - | 46.7 | 194.5 | 194.5 | 212.7 | 6.88 | 235 | 235 | 11 | 11 |
| 6% silica+30 % Fly ash C | 1316.6 | 496.8 | - | 46.6 | 232.9 | 232.9 | 212.8 | 6.10 | 235 | 235 | 13.5 | 14.5 |
| 6% silica+10 % Fly ash F | 1371.1 | 659.5 | - | 47.1 | 78.5 | 78.5 | 215.0 | 6.49 | 225 | 21 | 14.6 | 18 |
| 6% silica+15 % Fly ash F | 1362.5 | 619.1 | - | 47.0 | 117.6 | 117.6 | 215.5 | 5.19 | 225 | 215 | 11.1 | 19 |
| 6% silica+20 % Fly ash F | 1353.8 | 578.9 | - | 46.9 | 156.5 | 156.5 | 214.9 | 5.45 | 225 | 195 | 16.1 | 19.2 |
| 25% Fly ash C+4 % silica | 1332.9 | 553.0 | - | 31.2 | 194.7 | 194.7 | 213.1 | 6.62 | 235 | 235 | 12.7 | 14 |
| 25% Fly ash C+8 % silica | 1324.1 | 520.9 | - | 62.2 | 194.4 | 194.4 | 212.5 | 6.88 | 235 | 235 | 10.5 | 12.5 |
| 15% Fly ash F+4 % silica | 1366.9 | 635.4 | - | 31.4 | 117.7 | 117.7 | 213.8 | 7.79 | 225 | 195 | 20 | 21.5 |
| 15% Fly ash F+8 % silica | 1358.0 | 602.9 | - | 62.6 | 117.4 | 117.4 | 212.7 | 8.70 | 225 | 205 | 16.5 | 19 |
| 2% silica | 1397.6 | 773.6 | - | 15.8 | - | - | 215.7 | 7.14 | 230 | 180 | 23.3 | 29 |
| 4% silica | 1393.0 | 757.1 | - | 31.5 | - | - | 215.3 | 7.40 | 230 | 205 | 16.2 | 23.1 |
| 5% silica | 1390.8 | 748.9 | - | 39.4 | - | - | 216.4 | 5.84 | 230 | 160 | 25 | 27 |
| 6% silica | 1388.5 | 740.7 | - | 47.3 | - | - | 214.9 | 7.66 | 235 | 230 | 13 | 16.2 |
| 8% silica | 1384.0 | 724.2 | - | 63.0 | - | - | 213.6 | 9.09 | 235 | 215 | 16.1 | 22.2 |
| 8% silica.rep.* | 1384.0 | 724.2 | - | 63.0 | - | - | 214.6 | 7.79 | 230 | 205 | 12.23 | 14.7 |
| 10% silica | 1379.5 | 707.8 | - | 78.6 | - | - | 214.4 | 7.66 | 235 | 1955 | 20.1 | 24.4 |
| 15% silica | 1368.3 | 667.0 | - | 117.7 | - | - | 212.2 | 10.00 | 225 | 215 | 13.2 | 15.5 |
| 6% silica - 0.22 *w/cm* | 1490.1 | 756.3 | - | 48.3 | - | - | 155.2 | 29.10 | 225 | 195 | 66 | 15 |
| 6% silica - 0.25 *w/cm* | 1438.8 | 748.4 | - | 47.8 | - | - | 188.8 | 13.60 | 225 | 195 | 40 | 16 |
| 6 % silica - 0.28 *w/cm* | 1388.5 | 740.7 | - | 47.3 | - | - | 213.4 | 9.61 | 235 | 220 | 13.2 | 15.5 |
| Paste volume = 300 l/m$^3$ | 1461.0 | 667.0 | - | 43.0 | - | - | 199.0 | 14.8 | 225.0 | 210.0 | 33.2 | 35.0 |
| Paste volume = 367 l/m$^3$ | 1264.0 | 782.0 | - | 50.0 | - | - | 233.0 | 9.7 | 225.0 | 218.0 | 15.9 | 16.4 |
| Paste volume = 400 l/m$^3$ | 1171.0 | 836.0 | - | 53.0 | - | - | 249.0 | 10.3 | 235.0 | 233.0 | 10.6 | 11.2 |

* All subsequent mixtures were prepared with sand 2, while precedent mixtures were prepared with sand 1.

***Table B.2:*** *Compressive strength of the tested mortars.*

| Mixture | 28-days | 56-days |
|---|---|---|
| | MPa | MPa |
| Reference mixture | 87 | 92 |
| 20% slag | - | - |
| 25% slag | 82 | 90 |
| 30% slag | - | - |
| 40% slag | 80 | 90 |
| 15% Fly ash C | 86 | - |
| 20% Fly ash C | 82 | - |
| 25% Fly ash C | 79 | - |
| 30% Fly ash C | 78 | - |
| 15% Fly ash F | 89 | - |
| 20% Fly ash F | 88 | - |
| 25% Fly ash F | 81 | - |
| 6% silica+20 % Fly ash C | 86 | 94 |
| 6% silica+25 % Fly ash C | 82 | 89 |
| 6% silica+30 % Fly ash C | 76 | 93 |
| 6% silica+10 % Fly ash F | 93 | 97 |
| 6% silica+15 % Fly ash F | 94 | 101 |
| 6% silica+20 % Fly ash F | 89 | 93 |
| 25% Fly ach C+4 % silica | 84 | 85 |
| 25% Fly ach C+8 % silica | 86 | 100 |
| 15% Fly ash F+4 % silica | 86 | 92 |
| 15% Fly ash F+8 % silica | 83 | 89 |
| 2% silica | 98 | 107 |
| 4% silica | 96 | 100 |
| 5% silica | 98 | 101 |
| 6% silica | 104 | 107 |
| 8% silica.rep.* | 86 | 93 |
| 10% silica | 107 | 114 |
| 15% silica | 103 | 107 |
| 6% silica - 0.22 *w/cm* | 91 | - |
| 6% silica - 0.25 *w/cm* | 88 | - |
| 6 % silica - 0.28 *w/cm* | - | - |
| Paste volume = 300 l/m$^3$ | 95 | - |
| Paste volume = 367 l/m$^3$ | 92 | - |
| Paste volume = 400 l/m$^3$ | 92 | - |

* All subsequent mixtures were prepared with sand 2, while the precedent mixtures were prepared with sand 1.

*Table B.3: Mix designs and compositions of the mixtures (prepared with local Canadian materials) in phase 1.*

| Mixture | Binder | | | | Paste | Sand | Aggregate | | Cement GU | Fly Ash C | Silica fume | Water | HRWRA |
|---|---|---|---|---|---|---|---|---|---|---|---|---|---|
| | GU | FAC | SF | kg/m$^3$ | l/m$^3$ | kg/m$_3$ | kg/m$_3$ | D max (mm) | kg/m$^3$ | kg/m$^3$ | kg/m$^3$ | l/m$^3$ | l/m$^3$ |
| HWC1 | 69% | 25% | 6% | 575 | 375 | 803 | 830 | 5-14 | 396.8 | 143.8 | 34.5 | 161.0 | 2.00 |
| HWC2 | 69% | 25% | 6% | 535 | 350 | 838 | 866 | 5-14 | 369.2 | 133.8 | 32.1 | 149.8 | 2.06 |
| HWC3 | 69% | 25% | 6% | 575 | 375 | 803 | 830 | 5-14 | 396.8 | 143.8 | 34.5 | 161.0 | 1.91 |
| HWC4 | 69% | 25% | 6% | 575 | 375 | 803 | 830 | 5-14 | 396.8 | 143.8 | 34.5 | 161.0 | 2.06 |
| SCC1 | 69% | 25% | 6% | 575 | 375 | 867 | 764 | 5-14 | 396.8 | 143.8 | 34.5 | 161.0 | 2.55 |
| SCC2 | 69% | 25% | 6% | 575 | 375 | 867 | 764 | 5-14 | 396.8 | 143.8 | 34.5 | 161.0 | 2.74 |
| SCC3-b | 69% | 25% | 6% | 575 | 375 | 867 | 764 | 5-14 | 396.8 | 143.8 | 34.5 | 161.0 | 3.06 |
| SCC4-b | 69% | 25% | 6% | 575 | 375 | 867 | 764 | 5-14 | 396.8 | 143.8 | 34.5 | 161.0 | 3.35 |
| SCC5 | 69% | 25% | 6% | 537 | 350 | 902 | 795 | 5-14 | 370.5 | 134.3 | 32.2 | 150.4 | 3.15 |
| SCC6 | 69% | 25% | 6% | 615 | 400 | 830 | 731 | 5-14 | 424.4 | 153.8 | 36.9 | 172.2 | 3.21 |
| SCC7 | 94% | 0% | 6% | 575 | 350 | 902 | 794 | 5-14 | 540.5 | 0.0 | 34.5 | 161.0 | 4.64 |
| SCC8 | 94% | 0% | 6% | 618 | 375 | 865 | 762 | 5-14 | 580.9 | 0.0 | 37.1 | 173.0 | 4.88 |
| SCC10 | 67% | 25% | 8% | 600 | 391 | 842 | 741 | 5-14 | 402.0 | 150.0 | 48.0 | 168.0 | 3.20 |
| SCC11 | 67% | 25% | 8% | 600 | 391 | 836 | 746 | 5-10 | 402.0 | 150.0 | 48.0 | 168.0 | 3.25 |
| CVC1 | 69% | 25% | 6% | 539 | 350 | 768 | 932 | 5-14 | 371.9 | 134.8 | 32.3 | 150.9 | 1.63 |
| CVC2 | 69% | 25% | 6% | 575 | 375 | 739 | 897 | 5-14 | 396.8 | 143.8 | 34.5 | 161.0 | 1.67 |
| SCC4H30-b | 69% | 25% | 6% | 575 | 375 | 867 | 764 | 5-14 | 396.8 | 143.8 | 34.5 | 161.0 | 3.59 |
| SCC12H30 | 67% | 25% | 8% | 600 | 391 | 836 | 746 | 5-10 | 402.0 | 150.0 | 48.0 | 168.0 | 3.62 |
| SCC13H35 | 67% | 25% | 8% | 600 | 391 | 836 | 746 | 5-10 | 402.0 | 150.0 | 48.0 | 168.0 | 3.73 |
| HWC4H30 | 69% | 25% | 6% | 575 | 375 | 803 | 830 | 5-14 | 396.8 | 143.8 | 34.5 | 161.0 | 2.20 |
| SCC8H30 | 94% | 0% | 6% | 618 | 375 | 865 | 762 | 5-14 | 580.9 | 0.0 | 37.1 | 173.0 | 4.88 |
| SCC4H30 | 69% | 25% | 6% | 575 | 375 | 867 | 764 | 5-14 | 396.8 | 143.8 | 34.5 | 161.0 | 3.44 |
| SCC3 | 69% | 25% | 6% | 575 | 375 | 867 | 764 | 5-14 | 396.8 | 143.8 | 34.5 | 161.0 | 2.87 |
| SCC4 | 69% | 25% | 6% | 575 | 375 | 867 | 764 | 5-14 | 396.8 | 143.8 | 34.5 | 161.0 | 3.19 |

*All mixtures were prepared with sand 2

*Table B.4: Fresh properties of the mixtures (prepared with local Canadian materials) in phase 1.*

| Mixture | Fresh properties | | | | | | | | | | | | | |
|---|---|---|---|---|---|---|---|---|---|---|---|---|---|---|
| | Density (kg/m³) | | | | L-Box (vibration of 5 sec for HWC) | | | | | | | | Sieve stability | |
| | 0:15 | | 1:45 | | 0:15 | | | | 1:45 | | | | 0:15 | 1:45 |
| (hr) | test | real | test | real | T-70 | H | h | h/H | T70 | H | h | h/H | | |
| HWC1 | 16310 | 2330 | 16140 | 2306 | 4.75 | 490 | 80 | 64% | - | 490 | 110 | 36% | - | - |
| HWC2 | 16423 | 2346 | 16432 | 2347 | 8.7 | 510 | 65 | 94% | - | - | 150 | 0% | - | - |
| HWC3 | 16182 | 2312 | 16241 | 2320 | - | 505 | 64 | 91% | - | 495 | 45 | 100% | - | - |
| HWC4 | 16315 | 2331 | 16275 | 2325 | 4.1 | 515 | 65 | 100% | 10.4 | 515 | 65 | 100% | - | - |
| SCC1 | 16360 | 2337 | 16376 | 2339 | 5 | 500 | 65 | 85% | 3.9 | 490 | 75 | 68% | - | - |
| SCC2 | 16404 | 2343 | 16522 | 2360 | 3.7 | 495 | 65 | 81% | 5.6 | 495 | 70 | 76% | - | - |
| SCC3-b | 16780 | 2397 | 16580 | 2369 | 3.3 | 505 | 64 | 91% | 5.3 | 510 | 70 | 89% | 9.1% | 8.0% |
| SCC4-b | 16659 | 2380 | 16855 | 2408 | 3.3 | 510 | 64 | 96% | 2.8 | 505 | 65 | 89% | 10.0% | 9.9% |
| SCC5 | - | - | - | - | 6.1 | 515 | 70 | 94% | 6.5 | 495 | 75 | 71% | 7.9% | 4.4% |
| SCC6 | 16423 | 2346 | 16357 | 2337 | 3.9 | 505 | 65 | 89% | 4.1 | 500 | 70 | 80% | 11.9% | 10.1% |
| SCC7 | 17014 | 2431 | 16978 | 2425 | 6.8 | 500 | 65 | 85% | 7.3 | - | - | - | 5.5% | 3.6% |
| SCC8 | 16982 | 2426 | 17008 | 2430 | 5.5 | 505 | 65 | 89% | 5.3 | 500 | 70 | 80% | 5.5% | 5.9% |
| SCC10 | 16536 | 2362 | 16532 | 2362 | 2.5 | 510 | 65 | 94% | 2 | 500 | 65 | 85% | 15.6% | 12.1% |
| SCC11 | 16630 | 2376 | 16705 | 2386 | 1.7 | 510 | 63 | 97% | 1.7 | 505 | 65 | 89% | 12.0% | 10.6% |
| CVC1 | 16656 | 2379 | - | - | - | - | - | - | - | - | - | - | - | - |
| CVC2 | 16451 | 2350 | 16591 | 2370 | - | - | - | - | - | - | - | - | - | - |
| SCC4H30-b | 16587 | 2370 | 16728 | 2390 | 4.1 | 502 | 66 | 86% | 3.9 | 505 | 67 | 87% | 11.5% | 10.0% |
| SCC12H30 | 16544 | 2363 | 16667 | 2381 | 2.3 | 510 | 65 | 94% | 3.2 | 497 | 63 | 84% | 9.6% | 8.7% |
| SCC13H35 | 16605 | 2372 | 16620 | 2374 | 2.4 | 505 | 60 | 95% | 2.5 | 505 | 64 | 91% | 10.3% | 8.9% |
| HWC4H30 | 16722 | 2389 | 16608 | 2373 | 4.8 | 510 | 65 | 94% | - | 460 | 105 | 32% | - | - |
| SCC8H30 | 16865 | 2409 | 17061 | 2437 | 3.4 | 505 | 65 | 89% | 6 | 495 | 70 | 76% | 7.4% | 7.5% |
| SCC4H30 | 16582 | 2369 | 16615 | 2374 | 3.0 | 507 | 60 | 97% | 3.7 | 495 | 64 | 82% | 11.7% | 8.0% |
| SCC3 | 16487 | 2355 | 16523 | 2360 | 3.1 | 505 | 62 | 93% | 5.1 | 500 | 70 | 80% | - | - |
| SCC4 | 16565 | 2366 | 16610 | 2373 | 4.1 | 510 | 65 | 94% | 4.6 | 505 | 68 | 86% | 10.1% | 11.4% |

*Table B.5: (continued) Fresh properties of the mixtures (prepared with local Canadian materials) in phase 1.*

| Mixture | Fresh properties | | | | | | | | | | | | | |
|---|---|---|---|---|---|---|---|---|---|---|---|---|---|---|
| | Density (kg/m³) | | | | L-Box (vibration of 5 sec for HWC) | | | | | | | | Sieve stability | |
| | 0:15 | | 1:45 | | 0:15 | | | | 1:45 | | | | 0:15 | 1:45 |
| (hr) | test | real | test | real | T-70 | H | h | h/H | T70 | H | h | h/H | | |
| HWC1 | 16310 | 2330 | 16140 | 2306 | 4.75 | 490 | 80 | 64% | - | 490 | 110 | 36% | - | - |
| HWC2 | 16423 | 2346 | 16432 | 2347 | 8.7 | 510 | 65 | 94% | - | - | 150 | 0% | - | - |
| HWC3 | 16182 | 2312 | 16241 | 2320 | - | 505 | 64 | 91% | - | 495 | 45 | 100% | - | - |
| HWC4 | 16315 | 2331 | 16275 | 2325 | 4.1 | 515 | 65 | 100% | 10.4 | 515 | 65 | 100% | - | - |
| SCC1 | 16360 | 2337 | 16376 | 2339 | 5 | 500 | 65 | 85% | 3.9 | 490 | 75 | 68% | - | - |
| SCC2 | 16404 | 2343 | 16522 | 2360 | 3.7 | 495 | 65 | 81% | 5.6 | 495 | 70 | 76% | - | - |
| SCC3-b | 16780 | 2397 | 16580 | 2369 | 3.3 | 505 | 64 | 91% | 5.3 | 510 | 70 | 89% | 9.1% | 8.0% |
| SCC4-b | 16659 | 2380 | 16855 | 2408 | 3.3 | 510 | 64 | 96% | 2.8 | 505 | 65 | 89% | 10.0% | 9.9% |
| SCC5 | - | - | - | - | 6.1 | 515 | 70 | 94% | 6.5 | 495 | 75 | 71% | 7.9% | 4.4% |
| SCC6 | 16423 | 2346 | 16357 | 2337 | 3.9 | 505 | 65 | 89% | 4.1 | 500 | 70 | 80% | 11.9% | 10.1% |
| SCC7 | 17014 | 2431 | 16978 | 2425 | 6.8 | 500 | 65 | 85% | 7.3 | - | - | - | 5.5% | 3.6% |
| SCC8 | 16982 | 2426 | 17008 | 2430 | 5.5 | 505 | 65 | 89% | 5.3 | 500 | 70 | 80% | 5.5% | 5.9% |
| SCC10 | 16536 | 2362 | 16532 | 2362 | 2.5 | 510 | 65 | 94% | 2 | 500 | 65 | 85% | 15.6% | 12.1% |
| SCC11 | 16630 | 2376 | 16705 | 2386 | 1.7 | 510 | 63 | 97% | 1.7 | 505 | 65 | 89% | 12.0% | 10.6% |
| CVC1 | 16656 | 2379 | - | - | - | - | - | - | - | - | - | - | - | - |
| CVC2 | 16451 | 2350 | 16591 | 2370 | - | - | - | - | - | - | - | - | - | - |
| SCC4H30-b | 16587 | 2370 | 16728 | 2390 | 4.1 | 502 | 66 | 86% | 3.9 | 505 | 67 | 87% | 11.5% | 10.0% |
| SCC12H30 | 16544 | 2363 | 16667 | 2381 | 2.3 | 510 | 65 | 94% | 3.2 | 497 | 63 | 84% | 9.6% | 8.7% |
| SCC13H35 | 16605 | 2372 | 16620 | 2374 | 2.4 | 505 | 60 | 95% | 2.5 | 505 | 64 | 91% | 10.3% | 8.9% |
| HWC4H30 | 16722 | 2389 | 16608 | 2373 | 4.8 | 510 | 65 | 94% | - | 460 | 105 | 32% | - | - |
| SCC8H30 | 16865 | 2409 | 17061 | 2437 | 3.4 | 505 | 65 | 89% | 6 | 495 | 70 | 76% | 7.4% | 7.5% |
| SCC4H30 | 16582 | 2369 | 16615 | 2374 | 3.0 | 507 | 60 | 97% | 3.7 | 495 | 64 | 82% | 11.7% | 8.0% |
| SCC3 | 16487 | 2355 | 16523 | 2360 | 3.1 | 505 | 62 | 93% | 5.1 | 500 | 70 | 80% | - | - |
| SCC4 | 16565 | 2366 | 16610 | 2373 | 4.1 | 510 | 65 | 94% | 4.6 | 505 | 68 | 86% | 10.1% | 11.4% |

*Table B.6: Rheological and tribological properties of the mixtures (prepared with local Canadian materials) in phase 1.*

| Mixture | Rheological and tribological properties | | | | | | | | | | | | | | | | | | | |
|---|---|---|---|---|---|---|---|---|---|---|---|---|---|---|---|---|---|---|---|---|
| | Viscosity (Pa s) | | | | Yield stress (Pa) | | | | $Itrib_{II}$ (Pa s/m) | | | | $Itrib_{co}$ (Pa s/m) | | | | $Itrib_{tot}$ (Pa s/m) | | | |
| (hr) | 0:30 | 1:00 | 1:30 | 2:00 | 0:30 | 1:00 | 1:30 | 2:00 | 0:30 | 1:00 | 1:30 | 2:00 | 0:30 | 1:00 | 1:30 | 2:00 | 0:30 | 1:00 | 1:30 | 2:00 |
| HWC1 | 93.6 | 104.0 | 88.9 | 74 | 235.3 | 322.3 | 330 | 380 | 2197 | 2025 | 2194 | 2424 | 8582 | - | - | - | 1801 | 1838 | 1921 | 2086 |
| HWC2 | 81.3 | 89.9 | 109 | 106 | 173 | 262.3 | 372 | 480 | 2769 | 2590 | 2203 | 2208 | 5190 | 7840 | - | - | 1850 | 2004 | 1998 | 2094 |
| HWC3 | 62.3 | 79.5 | 75.5 | 83.6 | 323.3 | 350.9 | 409 | 519 | 1993 | 1904 | 2097 | 1977 | - | - | - | - | 1744 | 1744 | 1925 | 1933 |
| HWC4 | 93.8 | - | 63.6 | 85.5 | 135.9 | - | 129 | 209 | 2311 | - | 3162 | 2185 | 5718 | - | 3634 | 6937 | 1681 | 1687 | 1732 | 1701 |
| SCC1 | 66.0 | 81.6 | 73.2 | 89.5 | 44.6 | 73.8 | 81.2 | 104 | 2602 | 2434 | 2118 | 2019 | 3044 | 4032 | 3824 | 5013 | 1411 | 1536 | 1384 | 1458 |
| SCC2 | 79.2 | 83.0 | 78.7 | 82.9 | 19.6 | 36.7 | 41.6 | 60 | 2579 | 2361 | 2325 | 2415 | 3544 | 3792 | 3627 | 4005 | 1496 | 1458 | 1424 | 1518 |
| SCC3-b | 61.8 | 57.2 | 66.4 | 71.7 | 5.7 | 7.0 | 6.9 | 13.4 | 2660 | 2904 | 2567 | 2762 | 2740 | 2536 | 2944 | 3186 | 1358 | 1359 | 1373 | 1481 |
| SCC4-b | 72.7 | 72.5 | 77.7 | 81.2 | - | - | - | - | 2660 | 2904 | 2567 | 2762 | 2740 | 2536 | 2944 | 3186 | 1358 | 1359 | 1373 | 1481 |
| SCC5 | 81.3 | 92.6 | 73.7 | 85.9 | 13.2 | 36.9 | 52.1 | 66.1 | 3214 | 2491 | 2929 | 2599 | 3613 | 4287 | 3470 | 4212 | 1706 | 1585 | 1602 | 1625 |
| SCC6 | 58.4 | 67.9 | 64.8 | 68.9 | - | 6.2 | 15.2 | 27 | 3409 | 3062 | 2783 | 3132 | 2589 | 3010 | 2887 | 3102 | 1478 | 1519 | 1421 | 1561 |
| SCC7 | 94.7 | 83.6 | 96 | 98 | 12.1 | 26.6 | 23.2 | 35.2 | 3075 | 3992 | 3369 | 3042 | 4204 | 3751 | 4289 | 4454 | 1779 | 1945 | 1893 | 1816 |
| SCC8 | 66.3 | 69.7 | 70.8 | 68.5 | 15.7 | 11.9 | 23.1 | 36.8 | 3300 | 3233 | 3065 | 3278 | 2949 | 3093 | 3188 | 3138 | 1564 | 1587 | 1573 | 1618 |
| SCC10 | 48.2 | 61.3 | 51.2 | 45.5 | 9.5 | 13.3 | 16.6 | 18.3 | 2503 | 1941 | 2327 | 2327 | 2139 | 2734 | 2297 | 2043 | 1154 | 1138 | 1163 | 1096 |
| SCC11 | 39.7 | 46.0 | 42.4 | 37.7 | 9.8 | 7.8 | 15.4 | 13.3 | 1916 | 1820 | 1950 | 2341 | 1772 | 2042 | 1896 | 1683 | 921 | 967 | 966 | 982 |
| CVC1 | 114.5 | 32.1 | - | - | 884.8 | - | - | - | 2140 | 2233 | - | - | - | - | - | - | - | - | - | - |
| CVC2 | 80.3 | 76.0 | 77.3 | 74 | 394.5 | 492.9 | 541 | 678 | 2007 | 1962 | 2149 | 2122 | - | - | - | - | - | - | - | - |
| SCC4H30-b | 73.9 | 85.3 | 69.4 | 64.3 | -11.9 | -13.9 | 3.9 | 9.6 | - | - | - | - | - | - | - | - | - | - | - | - |
| SCC12H30 | 42.4 | 83.6 | 39.2 | 42.4 | 9.2 | 26.6 | 17.7 | 16.7 | - | - | - | - | - | - | - | - | - | - | - | - |
| SCC13H35 | 78.8 | - | 75.8 | 80.3 | 130.5 | - | 217 | 270 | - | - | - | - | - | - | - | - | - | - | - | - |
| HWC4H30 | 88.8 | 87.8 | 82.4 | 74 | 5.4 | - | 26.8 | 45 | - | - | - | - | - | - | - | - | - | - | - | - |
| SCC8H30 | 85.9 | 94.2 | 80.2 | 74.0 | 5.4 | 25.7 | 26.8 | 43.3 | - | - | - | - | - | - | - | - | - | - | - | - |
| SCC4H30 | 52.2 | 56.4 | 52.1 | - | 4.1 | 5.4 | 8.4 | - | - | - | - | - | - | - | - | - | - | - | - | - |

***Table B.7:*** *Compressive strength of the mixtures (prepared with local Canadian materials) in phase 1.*

| Mixture | Compressive strength (MPa) | | | |
|---|---|---|---|---|
| | 1-day | 7-days | 28-days | 56-days |
| HWC1 | 15.3 | 58.1 | 74.9 | 81.3 |
| HWC2 | 32.6 | 59.3 | 79.2 | 81.2 |
| HWC3 | 28.7 | 51.3 | 69.7 | 70.3 |
| HWC4 | 23.0 | 54.6 | 69.4 | 79.7 |
| SCC1 | 29.5 | 52.8 | 72.3 | 82.1 |
| SCC2 | 29.3 | 43.2 | 73.3 | 70.9 |
| SCC3 | 29.0 | 58.6 | 66.9 | 77.6 |
| SCC5 | 34.3 | 54.4 | 74.5 | 84.8 |
| SCC6 | 29.7 | 67.7 | 81.4 | 83.1 |
| SCC4 | 24.6 | 59.9 | 82.3 | 89.6 |
| SCC7 | 39.7 | 73.2 | 93.0 | 91.6 |
| SCC8 | 35.6 | 77.8 | 89.2 | 97.4 |
| SCC10 | 27.2 | 59.0 | 78.2 | 87.0 |
| SCC11 | 32.0 | 62.2 | 82.4 | 91.0 |
| SCC3BIS | 28.8 | 62.6 | 79.8 | 86.2 |
| SCC12H30 | 33.7 | 63.1 | 80.5 | 89.9 |
| SCC13H35 | 37.1 | 59.7 | 82.9 | 88.9 |
| HWC4H30 | 39.2 | 58.2 | 79.7 | 86.5 |
| SCC8H30 | 36.0 | 72.0 | 89.3 | - |
| SCC4H30 | 34.4 | 58.8 | 77.9 | 87.5 |

*Table B.8: Mix designs of the concrete mixtures (prepared with the Arabic Gulf materials) in phase 2.*

| Mixture | Binder | | | | Paste | S/A | Sand | | Aggregate | | Cement GU | Fly ash C | Silica fume | w/cm |
|---|---|---|---|---|---|---|---|---|---|---|---|---|---|---|
| | GU | FAC | SF | kg/m$^3$ | l/m$^3$ | S/A | Crushed | Dune | 10mm | 20 | kg/m$^3$ | kg/m$^3$ | kg/m$^3$ | 0.28 |
| SCC21GM | 69% | 25% | 6% | 575 | 375 | 0.59 | 45.0% | 14.0% | 20% | 21% | 396.8 | 143.8 | 34.5 | 0.28 |
| SCC22GM | 69% | 25% | 6% | 575 | 375 | 0.59 | 49.0% | 10.0% | 20% | 21% | 396.8 | 143.8 | 34.5 | 0.28 |
| SCC23GM | 69% | 25% | 6% | 575 | 375 | 0.59 | 53.0% | 6.0% | 20% | 21% | 396.8 | 143.8 | 34.5 | 0.28 |
| SCC26GM | 69% | 25% | 6% | 575 | 375 | 0.59 | 45.0% | 14.0% | 26.5% | 14.5% | 396.8 | 143.8 | 34.5 | 0.28 |
| SCC27GM | 69% | 25% | 6% | 575 | 375 | 0.59 | 45.0% | 14.0% | 32.5% | 8.5% | 396.8 | 143.8 | 34.5 | 0.28 |
| SCC28GM | 69% | 25% | 6% | 575 | 375 | 0.56 | 42.7% | 13.3% | 34.9% | 9.1% | 396.8 | 143.8 | 34.5 | 0.28 |
| SCC29GM | 69% | 25% | 6% | 575 | 375 | 0.53 | 40.4% | 12.6% | 37.3% | 9.7% | 396.8 | 143.8 | 34.5 | 0.28 |
| SCC30GM | 69% | 25% | 6% | 575 | 375 | 0.59 | 45.0% | 14.0% | 32.5% | 8.5% | 396.8 | 143.8 | 34.5 | 0.28 |
| SCC31GM | 69% | 25% | 6% | 575 | 375 | 0.59 | 45.0% | 14.0% | 32.5% | 8.5% | 396.8 | 143.8 | 34.5 | 0.28 |
| SCC32GM | 69% | 25% | 6% | 605 | 375 | 0.59 | 45.0% | 14.0% | 32.5% | 8.5% | 417.5 | 151.3 | 36.3 | 0.25 |
| SCC33GM | 69% | 25% | 6% | 636 | 375 | 0.59 | 45.0% | 14.0% | 32.5% | 8.5% | 438.8 | 159.0 | 38.2 | 0.22 |
| SCC34GM | 94% | 0% | 6% | 618 | 375 | 0.59 | 45.0% | 14.0% | 32.5% | 8.5% | 580.9 | 0.0 | 37.1 | 0.28 |
| SCC35GM | 94% | 0% | 6% | 650 | 375 | 0.59 | 45.0% | 14.0% | 32.5% | 8.5% | 611.0 | 0.0 | 39.0 | 0.25 |
| SCC37GM | 94% | 0% | 6% | 618 | 375 | 0.59 | 45.0% | 14.0% | 32.5% | 8.5% | 580.9 | 0.0 | 37.1 | 0.28 |
| SCC36GM | 94% | 0% | 6% | 686 | 375 | 0.59 | 45.0% | 14.0% | 32.5% | 8.5% | 644.8 | 0.0 | 41.2 | 0.22 |
| SCC38GM | 94% | 0% | 6% | 600 | 364 | 0.59 | 45.0% | 14.0% | 32.5% | 8.5% | 564.0 | 0.0 | 36.0 | 0.28 |

*Table B.9: Mix compositions of the mixtures (prepared with the Arabic Gulf materials) in phase 2.*

| Mixture | Mix compositions | | | | | | | | |
|---|---|---|---|---|---|---|---|---|---|
| | Sand | | Aggregate | | Cement GU | Fly ash C | Silica fume | Water | HRWRA |
| | Crushed kg/m$^3$ | Dune kg/m$^3$ | 10 mm kg/m$^3$ | 20 mm kg/m$^3$ | kg/m$^3$ | kg/m$^3$ | kg/m$^3$ | l/m$^3$ | l/m$^3$ |
| SCC21GM | 736.22 | 223.11 | 356.29 | 332.1 | 396.8 | 143.8 | 34.5 | 161.0 | 3.45 |
| SCC22GM | 801.66 | 159.36 | 332.06 | 356.3 | 396.8 | 143.8 | 34.5 | 161.0 | 3.73 |
| SCC23GM | 867.1 | 95.617 | 332.06 | 356.3 | 396.8 | 143.8 | 34.5 | 161.0 | 4.00 |
| SCC26GM | 736.22 | 223.11 | 439.97 | 246.0 | 396.8 | 143.8 | 34.5 | 161.0 | 3.36 |
| SCC27GM | 736.22 | 223.11 | 539.59 | 144.2 | 396.8 | 143.8 | 34.5 | 161.0 | 3.59 |
| SCC28GM | 698.59 | 211.95 | 579.44 | 154.4 | 396.8 | 143.8 | 34.5 | 161.0 | 3.36 |
| SCC29GM | 660.96 | 200.8 | 619.28 | 164.6 | 396.8 | 143.8 | 34.5 | 161.0 | 3.45 |
| SCC30GM | 736.22 | 223.11 | 539.59 | 144.2 | 396.8 | 143.8 | 34.5 | 161.0 | 3.36 |
| SCC31GM | 736.22 | 223.11 | 539.59 | 144.2 | 396.8 | 143.8 | 34.5 | 161.0 | 3.59 |
| SCC32GM | 734.42 | 222.56 | 538.27 | 143.9 | 417.5 | 151.3 | 36.3 | 151.3 | 4.86 |
| SCC33GM | 733.9 | 222.4 | 537.89 | 143.8 | 438.8 | 159.0 | 38.2 | 139.9 | 7.27 |
| SCC34GM | 734.25 | 222.51 | 538.15 | 143.8 | 580.9 | 0.0 | 37.1 | 173.0 | 4.59 |
| SCC35GM | 736.22 | 223.11 | 539.59 | 143.8 | 611.0 | 0.0 | 39.0 | 162.5 | 6.55 |
| SCC37GM | 734.42 | 222.56 | 538.27 | 143.9 | 580.9 | 0.0 | 37.1 | 173.0 | 3.91 |
| SCC36GM | 734.25 | 222.51 | 538.15 | 143.8 | 644.8 | 0.0 | 41.2 | 150.9 | 10.91 |
| SCC38GM | 747.52 | 226.53 | 547.87 | 146.4 | 564.0 | 0.0 | 36.0 | 168.0 | 4.77 |

*Table B.10: Fresh properties of the mixtures (prepared with the Arabic Gulf materials) in phase 2.*

| Mixture | Fresh properties | | | | | | | | | | | | | |
|---|---|---|---|---|---|---|---|---|---|---|---|---|---|---|
| | Slump-flow (mm) | | | | T-50 (sec) | | | | V-funnel | | | | Air content | |
| (hr) | 0:15 | 0:45 | 1:15 | 1:45 | 0:15 | 0:45 | 1:15 | 1:45 | 0:15 | 0:45 | 1:15 | 1:45 | 0:15 | 1:45 |
| SCC21GM | 720 | 675 | 680 | 680 | 3.4 | 3.6 | 3.7 | 4.2 | 9 | 11.7 | 11.8 | 11.6 | 1.8% | 2.8% |
| SCC22GM | 710 | 725 | 705 | 690 | 4 | 3.9 | 3.8 | 4.1 | 10.5 | 10.4 | 10.5 | 12 | 1.8% | 2.4% |
| SCC23GM | 725 | 715 | 710 | 700 | 3.1 | 2.8 | 3.9 | 3.6 | 9.1 | 10.1 | 10.1 | 13.1 | 1.3% | 1.6% |
| SCC26GM | 730 | 695 | 670 | 700 | - | 4 | 4.2 | 3.9 | 7.6 | 9.5 | 9.8 | 10.6 | 1.9% | 2.6% |
| SCC27GM | 745 | 725 | 710 | 710 | 3.1 | 3.9 | 3.9 | 4.4 | 8.3 | 8.6 | 8.9 | 9.6 | 2.0% | 2.3% |
| SCC28GM | 715 | 710 | 710 | 700 | 3.6 | 3.5 | 3.2 | - | 10.2 | 9.9 | 10.5 | 10.4 | 2.2% | 2.7% |
| SCC29GM | 720 | 685 | 700 | 695 | 2.9 | 4 | 3.6 | 3.5 | 10.2 | 12 | 12.3 | 12.2 | 1.7% | 3.4% |
| SCC30GM | 720 | 700 | 710 | 685 | 2.7 | 2.9 | 2.9 | 3.2 | 7.9 | 8.6 | 8.7 | 8.3 | 2.3% | 2.4% |
| SCC31GM | 725 | 700 | 700 | 685 | 2.8 | 2.8 | 3.2 | 3.2 | 8.9 | 8.6 | 9 | 9 | 2.3% | 2.4% |
| SCC32GM | 750 | 740 | 765 | 735 | 3 | 4.5 | 3.9 | 5 | 12.7 | 14.7 | 13.3 | 15 | 1.5% | 1.1% |
| SCC33GM | 765 | 770 | 760 | 790 | - | 6.4 | 5.9 | 5.3 | 28.7 | 24 | 23 | 18.4 | 1.5% | 0.9% |
| SCC34GM | 710 | 645 | 650 | 605 | 2.7 | 3.8 | 3.7 | 5 | 7.8 | 10.3 | 11.1 | 14.5 | 1.9% | - |
| SCC35GM | 715 | 680 | 675 | 670 | 4.9 | 6.5 | 5.6 | 5.9 | 13.9 | 18.2 | 17.1 | 18.4 | 2.1% | 1.8% |
| SCC37GM | 705-3.2% | 710-4% | 685-6.2% | 695-7.5% | 3.1 | 2.7 | 2.5 | 1.9 | 8.4 | 9.2 | 7.4 | 5.7 | 2.3-4% | 6.2-7.5% |
| SCC36GM | 710 | 715-55min | 700-95min | - | 18 | 12.7-55min | 11.9-95min | - | 66 | 55-55min | 28-95min | - | 1.7% | 1.4% |
| SCC38GM | 725 | 700 | 700 | 695 | 2.9 | 3.7 | 3 | 3.9 | 9.2 | 10.9 | 10.5 | 12.7 | 1.4% | 1.7% |

**Table B.11:** *(cont'd)Fresh properties of the mixtures (prepared with the Arabic Gulf materials) in phase 2.*

| Mixture | Fresh properties | | | | | | | | | | | | | |
|---|---|---|---|---|---|---|---|---|---|---|---|---|---|---|
| | Density (kg/m$^3$) | | | | L-Box | | | | | | | | Sieve stability | |
| | (hr) 0:15 | | 1:45 | | 0:15 | | | | 1:45 | | | | 0:15 | 1:45 |
| | test | real | test | real | T-70 | H | h | h/H | T-70 | H | h | h/H | Seg. | Seg. |
| SCC21GM | 16765 | 2395 | 16916 | 2417 | 4.1 | 503 | 60 | 93% | 6 | 486 | 67 | 73% | 9% | 7.1% |
| SCC22GM | 16833 | 2405 | 16881 | 2412 | 3.2 | 508 | 60 | 98% | 3.5 | 503 | 62 | 91% | 9.5% | 7.7% |
| SCC23GM | 16778 | 2397 | 17056 | 2437 | 2.75 | 506 | 65 | 90% | 5.1 | 482 | 70 | 68% | 10.6% | 6.4% |
| SCC26GM | 16821 | 2403 | 16834 | 2405 | 2.9 | 503 | 61 | 92% | 3.5 | 499 | 65 | 84% | 10.8% | 6.2% |
| SCC27GM | 16846 | 2407 | 16848 | 2407 | 3 | 503 | 65 | 88% | 4.1 | 505 | 64 | 91% | 9.3% | 8.4% |
| SCC28GM | 16803 | 2400 | 16768 | 2395 | 2.9 | 510 | 64 | 96% | 3.1 | 505 | 68 | 86% | 6.2% | 6.2% |
| SCC29GM | 16800 | 2400 | 16872 | 2410 | 3.7 | 505 | 65 | 89% | 2.8 | 495 | 67 | 79% | 8.5% | 7.9% |
| SCC30GM | 16660 | 2380 | 16829 | 2404 | 2.6 | 502 | 67 | 85% | 2.9 | 500 | 66 | 84% | 10% | 7.9% |
| SCC31GM | 16726 | 2389 | 16821 | 2403 | 4.3 | 499 | 67 | 82% | 3.1 | 500 | 64 | 86% | 9.9% | 8.5% |
| SCC32GM | 16923 | 2418 | 17151 | 2450 | 4.8 | 505 | 63 | 92% | 6 | 504 | 66 | 88% | 10.8% | 10.7% |
| SCC33GM | 16942 | 2420 | 17380 | 2483 | 2.9 | 507 | 62 | 95% | 10.2 | 509 | 67 | 91% | 11.3% | 11.9% |
| SCC34GM | 17253 | 2465 | 17332 | 2476 | 3.7 | 496 | 67 | 80% | 6.2 | 480 | 77 | 61% | 7% | 4.9% |
| SCC35GM | 17379 | 2483 | 17349 | 2478 | 5.4 | 502 | 65 | 87% | 6.8 | 497 | 69 | 79% | 8.3% | 7.2% |
| SCC37GM | 17214 | 2459 | - | - | 2.6 | 500 | 63 | 87% | - | - | - | - | 8.6% | - |
| SCC36GM | 17370 | 2481 | 17500 | 2500 | 36 | 504 | 63 | 91% | 13.2 | 504 | 69 | 84% | 5% | 9.6% |
| SCC38GM | 17254 | 2465 | 17361 | 2480 | 3.3 | 504 | 62 | 92% | 5.1 | 499 | 68 | 81% | 7.9% | 6.5% |

*Table B.12: Rheogical properties of the mixtures (prepared with the Arabic Gulf materials) in phase 2.*

| Mixture | Rheological properties | | | | | | | | | | | |
|---|---|---|---|---|---|---|---|---|---|---|---|---|
| | Viscosity (Pa s) | | | | Yield stress (Pa) | | | | Diff. Viscosity (Pa s) | | | |
| (hr) | 0:30 | 1:00 | 1:30 | 2:00 | 0:30 | 1:00 | 1:30 | 2:00 | 0:30 | 1:00 | 1:30 | 2:00 |
| SCC21GM | 76.0 | 87.8 | 88.3 | 91.4 | 0.1 | 7.6 | 23.0 | 64.3 | 79.3 | 90.5 | 85.2 | 96.9 |
| SCC22GM | 82.7 | 84.8 | 75.8 | 84.4 | - | 4.3 | 10.4 | 28.6 | 86 | 85.4 | 77.5 | 82.2 |
| SCC23GM | 66.5 | 70.7 | 70.2 | 78.9 | - | - | 6.6 | 7.3 | 69.8 | 73.3 | 70.4 | 81.7 |
| SCC26GM | 67.2 | 75.1 | 75.8 | 79.3 | 7.4 | 17.0 | 22.0 | 17.6 | 69.9 | 75.2 | 77.6 | 81.0 |
| SCC27GM | 61.9 | 69.2 | 70.4 | 71.5 | 2.5 | 3.2 | 5.1 | 9.0 | 65.8 | 71.3 | 72.4 | 72.8 |
| SCC28GM | 64.5 | 62.7 | 63.4 | 61.4 | 3.9 | 9.3 | 9.8 | 18.4 | 66.6 | 64.1 | 64.8 | 61.4 |
| SCC29GM | 65.9 | 76.8 | 73.2 | 74.3 | 1.2 | 9.2 | 14.6 | 14.3 | 69.2 | 78.3 | 73.7 | 76.7 |
| SCC30GM | 56.5 | 57.0 | 53.7 | 52.1 | 2.0 | 6.7 | 11.5 | 12.1 | 59 | 59.5 | 54.6 | 53.1 |
| SCC31GM | 59.3 | 57.9 | 53.1 | 54.4 | - | 6.5 | 8.9 | 12.1 | 62.5 | 59.5 | 53.7 | 54.9 |
| SCC32GM | 117.8 | 112.8 | 123.2 | 128.1 | - | - | - | - | 132.9 | 121.2 | 131.9 | 136.3 |
| SCC33GM | 318.7 | 208.0 | 241.7 | 215.0 | - | 34.4 | - | 30.2 | 320 | 230 | 259 | 233 |
| SCC34GM | 56.2 | 56.7 | 62.3 | 74.0 | 21.8 | 30.9 | 36.7 | 66.3 | 57.8 | 56.8 | 61.8 | 71.3 |
| SCC35GM | 128.0 | 128.9 | 124.1 | 110.3 | - | 6.3 | 10.2 | 15.7 | 135.3 | 133.2 | 128.2 | 113.3 |
| SCC37GM | 45.4 | 40.7 | 33.1 | 30.6 | 14.7 | 21.0 | 27.8 | 36.0 | 47 | 40.7 | 31.5 | 28.1 |
| SCC36GM | 481.8 | 331.1 | 313.3 | - | 160.9 | - | - | - | 329.4 | 326.7 | 331.4 | - |
| SCC38GM | 57.4 | 59.2 | 58.0 | 55.5 | 1.1 | 4.4 | 7.2 | 13.0 | 60.6 | 61.2 | 58.9 | 55.7 |

*Table B.13: Tribological properties of the mixtures (prepared with the Arabic Gulf materials) in phase 2.*

| Mixture | Tribological properties | | | | | | | | | | | |
|---|---|---|---|---|---|---|---|---|---|---|---|---|
| | $Itrib_{II}$ (Pa s/m) | | | | $Itr_{co}$ (Pa s/m) | | | | $Itrib_{tot}$ (Pa s/m) | | | |
| (hr) | 0:30 | 1:00 | 1:30 | 2:00 | 0:30 | 1:00 | 1:30 | 2:00 | 0:30 | 1:00 | 1:30 | 2:00 |
| SCC21GM | 2580 | 2649 | 2373 | 3108 | 3367 | 3892.4 | 3966.04 | 4332 | 1465 | 1580 | 1493 | 1833 |
| SCC22GM | 2588 | 2393 | 2343 | 2339 | 3667 | 3759.8 | 3363.76 | 3821 | 1521 | 1468 | 1387 | 1457 |
| SCC23GM | 1971 | 1985 | 2210 | 2412 | 2946 | 3135.3 | 3112.66 | 3499 | 1186 | 1222 | 1300 | 1434 |
| SCC26GM | 2491 | 2265 | 2346 | 2411 | 2978 | 3341 | 3390.63 | 3537 | 1360 | 1353 | 1389 | 1436 |
| SCC27GM | 2824 | 2521 | 2477 | 2615 | 2742 | 3065.9 | 3118.95 | 3173 | 1395 | 1387 | 1382 | 1437 |
| SCC28GM | 3252 | 2942 | 3016 | 2679 | 2952 | 2841.8 | 2871.38 | 2720 | 1598 | 1484 | 1525 | 1372 |
| SCC29GM | 3162 | 3230 | 3684 | 3231 | 2952 | 2841.8 | 2871.38 | 2722 | 1565 | 1551 | 1716 | 1548 |
| SCC30GM | 2389 | 2195 | 2360 | 2239 | 2504 | 2526.9 | 2383.41 | 2315 | 1227 | 1177 | 1190 | 1141 |
| SCC31GM | 2469 | 2401 | 2190 | 2578 | 2629 | 2568.8 | 2354.16 | 2418 | 1277 | 1245 | 1137 | 1250 |
| SCC32GM | 3702 | 3799 | 3378 | 3941 | 5224 | 5001.5 | 5462.59 | 5679 | 2177 | 2170 | 2095 | 2338 |
| SCC33GM | 5044 | 6060 | - | - | 14129 | 9361 | - | - | 3727 | 3708 | - | - |
| SCC34GM | 2944 | 2649 | 2350 | 2381 | 2527 | 2575.7 | 2859.12 | 3614 | 1372 | 1320 | 1303 | 1459 |
| SCC35GM | 4841 | 4107 | 4209 | 4368 | 5674 | 5713.3 | 5499.45 | 4891 | 2616 | 2394 | 2389 | 2312 |
| SCC37GM | 2320 | 2169 | 2237 | 1976 | 2089 | 1828 | 1452.57 | 1346 | 1101 | 995 | 883 | 808 |
| SCC36GM | 4904 | 5583 | 5537 | - | 23781 | 14676 | 13889 | - | 4076 | 4048 | 3961 | - |
| SCC38GM | 2941 | 2713 | 2508 | 2918 | 2545 | 2626.4 | 2571.1 | 2468 | 1371 | 1341 | 1274 | 1346 |

***Table B.14:*** *Compressive strength and Chloride penetration of the mixtures (prepared with the Arabic Gulf materials) in phase 2.*

| Mixture | 28-days fc (MPa) | 56-days fc (MPa) | 56-days Ec (GPa) | 56-days flexural (MPa) | 56-days Chloride test (Coulombs) |
|---|---|---|---|---|---|
| SCC21GM | 90.6 | 99.5 | - | - | - |
| SCC22GM | 88.2 | 96.0 | - | - | - |
| SCC23GM | 96.7 | 102.6 | - | - | - |
| SCC26GM | 93.9 | 101.1 | - | - | - |
| SCC27GM | 91.8 | 98.4 | - | - | - |
| SCC28GM | 88.5 | 96.1 | - | - | - |
| SCC29GM | 88.4 | 96.4 | - | - | - |
| SCC30GM | 90.6 | 97.6 | 52.3 | 10.9 | 105 |
| SCC31GM | 88.7 | 92.6 | - | - | - |
| SCC32GM | 105.6 | 110.0 | 54.6 | 12.5 | 73 |
| SCC33GM | 111.8 | 121.7 | 58.0 | 13.2 | 57 |
| SCC33GM | 101.8 | 103.5 | 53.0 | 11.5 | 140 |
| SCC34GM | 101.8 | 103.5 | 53.0 | 11.5 | 140 |
| SCC35GM | 109.1 | 113.2 | 54.8 | 11.2 | 116 |
| SCC36GM | 119.6 | 122.5 | 55.6 | 12.1 | 159 |
| SCC37GM | 92.9 | 95.2 | - | - | - |
| SCC38GM | 101.6 | 105.4 | 55.1 | 9.5 | 84 |

*Table B.15: Mix designs of the pumped mixtures.*

| Mixture | GU | GU+8%SF | FAC | SF | Aggregate | | w/cm | S/A | Paste |
|---|---|---|---|---|---|---|---|---|---|
| | | | | | 10 mm | 20 mm | | | l/m$^3$ |
| CVC1 | *NA* | *NA* | *NA* | *NA* | *NA* | *NA* | *NA* | *NA* | *NA* |
| CVC2 | *NA* | *NA* | *NA* | *NA* | *NA* | *NA* | *NA* | *NA* | *NA* |
| CVC3 | *NA* | *NA* | *NA* | *NA* | *NA* | *NA* | *NA* | *NA* | *NA* |
| SCC1 | - | 92% | 0% | 8% | 80.0% | 20.0% | 0.29 | 0.53 | 382.34 |
| SCC2 | - | 92% | 0% | 8% | 80.0% | 20.0% | 0.29 | 0.53 | 382.59 |
| SCC3 | - | 92% | 0% | 8% | 80.0% | 20.0% | 0.29 | 0.53 | 382.46 |
| SCC4 | - | 67% | 25% | 8% | 80.0% | 20.0% | 0.29 | 0.53 | 382.52 |
| SCC5 | - | 92% | 0% | 8% | 80.0% | 20.0% | 0.29 | 0.53 | 378.88 |
| SCC6 | 75% | - | 25% | 8% | 80.0% | 20.0% | 0.29 | 0.53 | 378.05 |
| SCC7 | - | 92% | 0% | 8% | 80.0% | 20.0% | 0.29 | 0.53 | 382.87 |
| SCC8 | - | 92% | 0% | 8% | 80.0% | 20.0% | 0.25 | 0.53 | 383.12 |
| SCC9 | - | 92% | 0% | 8% | 80.0% | 20.0% | 0.34 | 0.53 | 378.43 |
| SCC10 | - | 92% | 0% | 8% | 80.0% | 20.0% | 0.29 | 0.53 | 382.46 |
| SCC11 | - | 92% | 0% | 8% | 80.0% | 20.0% | 0.29 | 0.53 | 407.54 |
| SCC12 | - | 92% | 0% | 8% | 80.0% | 20.0% | 0.29 | 0.53 | 358.44 |
| HWC1 | - | 92% | 0% | 8% | 80.0% | 20.0% | 0.30 | 0.50 | 359.85 |
| HWC2 | - | 92% | 0% | 8% | 80.0% | 20.0% | 0.30 | 0.50 | 362.08 |
| HWC3 | - | 92% | 0% | 8% | 80.0% | 20.0% | 0.30 | 0.50 | 383.10 |
| SCC13 | - | 92% | 0% | 8% | 80.0% | 20.0% | 0.30 | 0.53 | 382.82 |
| SCC14 | - | 92% | 0% | 8% | 80.0% | 20.0% | 0.29 | 0.53 | 381.08 |
| HWC4 | - | 92% | 0% | 8% | 80.0% | 20.0% | 0.25 | 0.50 | 385.18 |
| SCC15 | - | 92% | 0% | 8% | 80.0% | 20.0% | 0.29 | 0.53 | 382.71 |
| SCC16 | - | 92% | 0% | 8% | 80.0% | 20.0% | 0.29 | 0.50 | 382.71 |
| SCC17 | - | 92% | 0% | 8% | 80.0% | 20.0% | 0.29 | 0.47 | 382.52 |
| SCC18 | - | 92% | 0% | 8% | 68.0% | 32.0% | 0.29 | 0.52 | 383.12 |
| SCC19 | - | 92% | 0% | 8% | 68.0% | 32.0% | 0.22 | 0.52 | 389.29 |

*Table B.16: Mix compositions of the pumped mixtures.*

| Mixture | GU | GU+8%SF | FAC | Sand | Aggregate | | Water | HRW.1 | HRW.2 | VMA | AEA |
|---|---|---|---|---|---|---|---|---|---|---|---|
| | | | | | 10 mm | 20 mm | | | | | |
| | kg/m$^3$ | kg/m$^3$ | kg/m$^3$ | kg/m$^3$ | kg/m$^3$ | kg/m$^3$ | kg/m$^3$ | kg/m$^3$ | kg/m$^3$ | kg/m$^3$ | kg/m$^3$ |
| CVC1 | *N/A* | *N/A* | *N/A* | *N/A* | *N/A* | *N/A* | *N/A* | *N/A* | *N/A* | *N/A* | *N/A* |
| CVC2 | *N/A* | *N/A* | *N/A* | *N/A* | *N/A* | *N/A* | *N/A* | *N/A* | *N/A* | *N/A* | *N/A* |
| CVC3 | *N/A* | *N/A* | *N/A* | *N/A* | *N/A* | *N/A* | *N/A* | *N/A* | *N/A* | *N/A* | *N/A* |
| SCC1 | - | 600 | - | 850 | 603 | 151 | 169 | 15.0 | 1.40 | - | - |
| SCC2 | - | 600 | - | 850 | 603 | 151 | 169 | 15.0 | 1.67 | - | - |
| SCC3 | - | 600 | - | 850 | 603 | 151 | 169 | 15.0 | 1.53 | - | - |
| SCC4 | - | 600 | - | 850 | 603 | 151 | 169 | 15.0 | 1.60 | - | - |
| SCC5 | - | 435 | 144 | 850 | 603 | 151 | 165 | 10.0 | 0.50 | - | - |
| SCC6 | 442 | - | 146 | 850 | 603 | 151 | 167 | 9.0 | 0.00 | 1.0 | - |
| SCC7 | - | 600 | - | 850 | 603 | 151 | 169 | 15.0 | 1.97 | - | - |
| SCC8 | - | 646 | - | 850 | 603 | 151 | 149 | 20.0 | 2.40 | - | - |
| SCC9 | - | 560 | - | 850 | 603 | 151 | 186 | 8.0 | 0.15 | | - |
| SCC10 | - | 600 | - | 850 | 603 | 151 | 169 | 15 | 1.53 | - | - |
| SCC11 | - | 640 | - | 816 | 579 | 145 | 181 | 15 | 1.40 | - | - |
| SCC12 | - | 560 | - | 885 | 628 | 157 | 157 | 15 | 2.80 | - | - |
| HWC1 | - | 560 | - | 835 | 668 | 167 | 164 | 10.0 | 1.81 | - | - |
| HWC2 | - | 560 | - | 835 | 668 | 167 | 164 | 12.0 | 2.20 | - | - |
| HWC3 | - | 600 | - | 803 | 642 | 161 | 172 | 12.0 | 2.00 | - | - |
| SCC13 | - | 600 | - | 850 | 603 | 151 | 169 | 15 | 1.27 | - | 0.6667 |
| SCC14 | - | 600 | - | 850 | 603 | 151 | 169 | 15 | 0.00 | 0.053 | - |
| HWC4 | - | 647 | - | 803 | 642 | 161 | 154 | 18.9 | 0.00 | - | - |
| SCC15 | - | 600 | - | 850 | 603 | 151 | 169 | 15 | 1.80 | - | - |
| SCC16 | - | 600 | - | 803 | 642 | 161 | 169 | 15 | 1.80 | - | - |
| SCC17 | - | 600 | - | 754 | 680 | 170 | 169 | 15 | 1.60 | - | - |
| SCC18 | - | 600 | - | 850 | 527 | 248 | 169 | 15 | 2.23 | - | - |
| SCC19 | - | 682 | - | 850 | 527 | 248 | 137 | 25 | 4.13 | - | - |

*Table B.17: Fresh properties of the pumped mixtures.*

| Mixture | Fresh properties | | | | | | | | | | | | | | |
|---|---|---|---|---|---|---|---|---|---|---|---|---|---|---|---|
| | Slump/slump flow | | | | | | | | T-50 | | | | | | |
| | Ini.* | npl† | np2‡ | 1 | 2 | 3 | 4 | 5 | npl | np2 | 1 | 2 | 3 | 4 | 5 |
| CVC1 | *235* | *225* | *200* | *235* | *230* | *225* | *205* | *185* | - | - | - | - | - | - | - |
| CVC2 | *215* | *245* | *235* | *220* | *210* | *185* | *115* | - | - | - | - | - | - | - | - |
| CVC3 | *180* | *150* | *115* | *160* | *135* | *90* | *55* | - | - | - | - | - | - | - | - |
| SCC1 | 675 | 705 | 645 | 710 | 680 | 720 | 685 | 655 | 2.9 | 4.6 | 2.4 | 3.3 | 2.7 | 2.9 | 2.8 |
| SCC2 | 815 | 780 | 760 | 725 | 735 | 710 | 545 | 310 | 2.9 | 2.6 | 2.1 | 2.0 | 2.4 | 3.6 | - |
| SCC3 | 680 | 735 | 685 | 725 | 690 | 610 | 470 | - | 2.1 | 2.85 | 1.5 | 1.5 | 1.8 | - | - |
| SCC4 | 680 | 685 | 655 | 675 | 635 | 670 | 635 | 640 | 3.6 | 4.6 | 1.7 | 3.0 | 2.7 | 2.9 | 2.9 |
| SCC5 | 750 | 770 | 795 | 730 | 775 | 820 | 870 | 885 | 1.7 | 2.6 | 1.6 | 0.8 | 1.8 | 0.9 | 0.8 |
| SCC6 | 690 | 145 | - | 775 | - | - | - | - | - | - | 2.8 | - | - | - | - |
| SCC7 | 615 | 620 | 610 | 600 | 565 | 565 | 560 | | 4.5 | 5.5 | 4.8 | 3.5 | 6.3 | 4.7 | - |
| SCC8 | 690 | 670 | 640 | 645 | 675 | 680 | 665 | 665 | 3.9 | 6.6 | 4.2 | 3.5 | 4.3 | 3.5 | 3.1 |
| SCC9 | 735 | 705 | 720 | 675 | 725 | 780 | 785 | - | 0.8 | 1.28 | 1.3 | 1.2 | 0.8 | 0.5 | - |
| SCC10 | 700 | 690 | 635 | 675 | 645 | 670 | 630 | - | 3.1 | 3.44 | 2.7 | 3.0 | 1.7 | 2.5 | - |
| SCC11 | 765 | 700 | 680 | 670 | 700 | 670 | 645 | 510 | 1.9 | 2.28 | 2.1 | 1.4 | 2.2 | 1.8 | 3.9 |
| SCC12 | 630 | 555 | 500 | 480 | 460 | 410 | *180* | - | 12.1 | - | - | - | - | - | - |
| HWC1 | 410 | 410 | 400 | 425 | 410 | 390 | *195* | - | - | - | - | - | - | - | - |
| HWC2 | 610 | 520 | 470 | 560 | 500 | 410 | 390 | - | - | - | - | - | - | - | - |
| HWC3 | 560 | 550 | 460 | 520 | 460 | 420 | 340 | 150 | - | - | - | - | - | - | - |
| SCC13 | 720 | 695 | 645 | 690 | 690 | 690 | 690 | 630 | 2.6 | 4.3 | 2.4 | 2.7 | 3.0 | 2.3 | 3.2 |
| SCC14 | 700 | 680 | 735 | 690 | 730 | 740 | 780 | - | 1.9 | 2.28 | 1.7 | 1.7 | 1.7 | 1.3 | - |
| HWC4 | 580 | 515 | 550 | 590 | 580 | 600 | 560 | 600 | - | - | - | - | - | - | - |
| SCC15 | 600 | 620 | 610 | 625 | 640 | 630 | 615 | 610 | 3.5 | 5 | 3.1 | 2.4 | 2.7 | 2.5 | 2.8 |
| SCC16 | 670 | 670 | 655 | 625 | 680 | 630 | 625 | 590 | 4.3 | 4.78 | 3.7 | 2.3 | 2.9 | 3.0 | 3.0 |
| SCC17 | 740 | 695 | 660 | 655 | 700 | 675 | 660 | 660 | 2.8 | 3.78 | 2.5 | 2.1 | 1.8 | 1.9 | 2.5 |
| SCC18 | 730 | 650 | 630 | 620 | 665 | 620 | 610 | 570 | 4.5 | 4.66 | 3.69 | 3.25 | 2.72 | 3.8 | 2.97 |
| SCC19 | 690 | 640 | 610 | 610 | 560 | 500 | 470 | 340 | 5.6 | 8.6 | 5.6 | 6.9 | 8.5 | - | - |

* Initial test at concrete arrival

† Non-pumped concrete after final HRWRA adjustment

‡ Non-pumped concrete at the end of pumping tests

*Table B.18: (cont'd) Fresh properties of the pumped mixtures.*

| Mixture | Fresh properties | | | | | | | | | | | | | |
|---|---|---|---|---|---|---|---|---|---|---|---|---|---|---|
| | Temperature (°C) | | | | | | | V-funnel | | | | | | |
| | np1 | np2 | 1 | 2 | 3 | 4 | 5 | np1 | np2 | 1 | 2 | 3 | 4 | 5 |
| CVC1 | *21.3* | *19.1* | *19.4* | *19.5* | *19.6* | *19.9* | *20.5* | - | - | - | - | - | - | - |
| CVC2 | *20.6* | *18.8* | *20.1* | *19.9* | *19.2* | *20.5* | - | - | - | - | - | - | - | - |
| CVC3 | *19.6* | *18.4* | *18.8* | *20.3* | *21.2* | *21.9* | - | - | - | - | - | - | - | - |
| SCC1 | 16.6 | 15.8 | 17.8 | 18.2 | 20.0 | 20.8 | 21.4 | 7.9 | 9.7 | 5.5 | 5.5 | 6.1 | 4.6 | 6.2 |
| SCC2 | 24.1 | 21.6 | 22.8 | 22.8 | 22.9 | 23.2 | 23.9 | 5.3 | 7.4 | 4.0 | 3.7 | 4.0 | 6.3 | - |
| SCC3 | 17.1 | 17.3 | 19.6 | 20.0 | 21.7 | 21.3 | - | 5.8 | 8.0 | 3.7 | 3.2 | 3.5 | 6 | - |
| SCC4 | 20.8 | 19.1 | 19.9 | 21.0 | 21.2 | 21.6 | 19.2 | 10 | 8.7 | 6.8 | 6.7 | 4.8 | 4.5 | 5.7 |
| SCC5 | 24.1 | 21.7 | 23.1 | 22.9 | 22.5 | 22.2 | 22.0 | 4.4 | 5.1 | 2.9 | 2.3 | 1.8 | 1.9 | 1.6 |
| SCC6 | 24.8 | - | - | - | - | - | - | 19.1 | - | 1.2 | - | - | - | - |
| SCC7 | 18.5 | 17.6 | 16.9 | 18.4 | 18.3 | 16.9 | - | 10 | 10.7 | 9.1 | 8.3 | 9.6 | 8.1 | - |
| SCC8 | 21.3 | 19.2 | 21.1 | 21.1 | 20.7 | 21.4 | 21.5 | 9.1 | 12.2 | 6.5 | 7.9 | 7.5 | 7.3 | 6.9 |
| SCC9 | 21.3 | 20.7 | 20.5 | 19.9 | 20.6 | 20.1 | - | 1.9 | 2.8 | 2.1 | 2.1 | 1.9 | 1.8 | - |
| SCC10 | 20.8 | 17.6 | 19.6 | 20.7 | 21.6 | 20.2 | - | 6.1 | 8.1 | 6.3 | 5.5 | 5 | 5.1 | - |
| SCC11 | 22.2 | 21.2 | 22.8 | 23.2 | 23.1 | 23.2 | 24.0 | 4.3 | 6.0 | 3.6 | 3.4 | 3.5 | 4.2 | 6.4 |
| SCC12 | 17.3 | 16.1 | 21.0 | 22.0 | 22.6 | 24.1 | - | 13.3 | 19.0 | 8 | 12.7 | 11.5 | - | - |
| HWC1 | 20.2 | 19.3 | 20.1 | 22.4 | 24.1 | 25.3 | - | 13 | 21.8 | 12.9 | 13.5 | 16 | - | - |
| HWC2 | 20.6 | 19.4 | 21.8 | 23.6 | 25.0 | 26.3 | - | 8.9 | 14.9 | 8.2 | 9.4 | 12.7 | 15.6 | - |
| HWC3 | 21.0 | 20.1 | 22.0 | 24.8 | 26.2 | 27.8 | 29.2 | 8.1 | 10.2 | 7.5 | 8 | 14.2 | 12 | - |
| SCC13 | 13.0 | 13.8 | 14.9 | 17.0 | 18.4 | 19.5 | 20.5 | 6.2 | 7.6 | 4.7 | 3.9 | 4.7 | 3.9 | 4.3 |
| SCC14 | 17.5 | 17.1 | 18.5 | 19.7 | 20.5 | 20.8 | - | 4.2 | 4.9 | 3 | 2.9 | 3 | 2.6 | - |
| HWC4 | 12.7 | 13.7 | 14.7 | 16.1 | 17.9 | 19.1 | 20.1 | 10.7 | 11.1 | 7.6 | 8.1 | 7.9 | 7.4 | 7.3 |
| SCC15 | 13.6 | 14.1 | 15.7 | 17.1 | 17.6 | 18.0 | 19.6 | 7 | 7.4 | 6.1 | 5.35 | 5.2 | 5.6 | 5.1 |
| SCC16 | 16.9 | 15.3 | 17.4 | 20.1 | 20.9 | 20.6 | 22.4 | 7.4 | 10.0 | 6.8 | 5.9 | 7 | 7 | 6.8 |
| SCC17 | 17.1 | 16.9 | 18.6 | 19.7 | 20.9 | 20.2 | 20.4 | 5.8 | 8.4 | 6 | 5.3 | 5.5 | 6.9 | 5.5 |
| SCC18 | 20.1 | 19.5 | 21.3 | 22.8 | 23.8 | 24 | 23.8 | 8.1 | 10.5 | 7.5 | 7.3 | 7.5 | 8.2 | 7.5 |
| SCC19 | 23 | 21.8 | 24.4 | 25.8 | 27.8 | 28.7 | 29.8 | 17.4 | 31.1 | 19.1 | 16.6 | 30.1 | 30.2 | - |

*Table B.19: (cont'd) Fresh properties of the pumped mixtures.*

| Mixture | Fresh properties | | | | | | | | | | | | | |
|---|---|---|---|---|---|---|---|---|---|---|---|---|---|---|
| | L-box | | | | | | | Air (%) | | | | | | |
| | npl | np2 | 1 | 2 | 3 | 4 | 5 | npl | np2 | 1 | 2 | 3 | 4 | 5 |
| CVC1 | - | - | - | - | - | - | - | 2.0 | 1.8 | 2.5 | 2.8 | 2.8 | 2.8 | 2.5 |
| CVC2 | - | - | - | - | - | - | - | 1.8 | 1.6 | 1.8 | 1.8 | 2.2 | 2.4 | - |
| CVC3 | - | - | - | - | - | - | - | 3.0 | 2.8 | 3.0 | 3.0 | 3.2 | 2.6 | - |
| SCC1 | 83% | 85% | 97% | 100% | 100% | 87% | 64% | 3.0 | 2.9 | 3.0 | 2.6 | 2.4 | 3.2 | 3.5 |
| SCC2 | 88% | 91% | 83% | 86% | 80% | 39% | 0% | 1.2 | 1.2 | 2.0 | 2.0 | 2.3 | 2.8 | 3.8 |
| SCC3 | 92% | 90% | 83% | - | 72% | 0% | - | 3.5 | 3.3 | 3.4 | 3.7 | 3.8 | 3.2 | - |
| SCC4 | 93% | 88% | 87% | 79% | 77% | 75% | 75% | 2.0 | 2.2 | 2.5 | 2.0 | 2.0 | 2.0 | 2.2 |
| SCC5 | 89% | 98% | 83% | 100% | 96% | 89% | 94% | 1.8 | 1.4 | 2.5 | 2.7 | 2.3 | 2.3 | 2.3 |
| SCC6 | - | - | 91% | - | - | - | - | 2.3 | - | 0.8 | - | - | - | - |
| SCC7 | 75% | 65% | 73% | 73% | 65% | 64% | - | 3.2 | 3.0 | 2.8 | 2.4 | 2.7 | 2.5 | - |
| SCC8 | 85% | 86% | 85% | 82% | 84% | 85% | 80% | 2.1 | 1.9 | 2.2 | 2.4 | 2.4 | 2.7 | 2.7 |
| SCC9 | 89% | 86% | 85% | 86% | 97% | 99% | - | 1.6 | 1.5 | 1.7 | 1.8 | 1.7 | 2.2 | - |
| SCC10 | 81% | 85% | 81% | 77% | 77% | 70% | - | 1.8 | 1.8 | 1.8 | 1.6 | 1.7 | 1.9 | - |
| SCC11 | 81% | 82% | 82% | 82% | 82% | 67% | 33% | 1.0 | 1.3 | 1.6 | 1.7 | 1.8 | 2.2 | 2.5 |
| SCC12 | 54% | 0% | 50% | 24% | 0% | 0% | - | 4.8 | 3.7 | 4.0 | 3.8 | 3.4 | 4.2 | - |
| HWC1 | - | - | - | - | - | - | - | 3.3 | 2.8 | 2.8 | 2.5 | 2.8 | 2.8 | - |
| HWC2 | - | - | - | - | - | - | - | 3.7 | 3.2 | 2.7 | 2.8 | 2.7 | 2.8 | - |
| HWC3 | - | - | - | - | - | - | - | 2.7 | 2.7 | 3.0 | 2.7 | 2.5 | 2.6 | 2.8 |
| SCC13 | 82% | 87% | 77% | 84% | 78% | 74% | 69% | 6.5 | 5.8 | 8.2 | 8.0 | 7.6 | 7.2 | 6.0 |
| SCC14 | 80% | 100% | 93% | 85% | 88% | 93% | - | 3.8 | 3.4 | 4.5 | 4.5 | 3.5 | 3.5 | - |
| HWC4 | - | - | - | - | - | - | - | 4.2 | 3.8 | 3.7 | 3.0 | 2.8 | 2.5 | 3.0 |
| SCC15 | 91% | 79% | 73% | 83% | 75% | 77% | 81% | 6.4 | 5.4 | 2.8 | 2.7 | 2.6 | 2.6 | 2.7 |
| SCC16 | 81% | 63% | 81% | 88% | 77% | 65% | 63% | 4.2 | 4.2 | 2.5 | 2.3 | 2.0 | 2.0 | 2.5 |
| SCC17 | 71% | 75% | 72% | 79% | 72% | 72% | 43% | 3.0 | 3 | 2.4 | 1.8 | 2.0 | 2.0 | 2.0 |
| SCC18 | 87% | 76% | 65% | 73% | 73% | 60% | 59% | 1.2 | 3 | 1.7 | 1.8 | 2 | 2.1 | 2.7 |
| SCC19 | 77% | 58% | 61% | 51% | 17% | 0% | - | 2.4 | 3.5 | 2.8 | 2.95 | 2.9 | 3.2 | 3.4 |

*Table B.20: (cont'd) Fresh properties of the pumped mixtures.*

| Mixture | Fresh properties | | | | | | | | | | | | | |
|---|---|---|---|---|---|---|---|---|---|---|---|---|---|---|
| | Density (kg/m$^3$) | | | | | | | Sieve stability | | | | | | |
| | np1 | np2 | 1 | 2 | 3 | 4 | 5 | np1 | np2 | 1 | 2 | 3 | 4 | 5 |
| CVC1 | 2413 | 2401 | 2390 | 2396 | 2380 | 2368 | 2368 | - | - | - | - | - | - | - |
| CVC2 | 2368 | 2394 | 2409 | 2388 | 2384 | 2392 | - | - | - | - | - | - | - | - |
| CVC3 | 2376 | 2373 | 2378 | 2373 | 2370 | 2411 | - | - | - | - | - | - | - | - |
| SCC1 | 2422 | 2422 | 2424.3 | 2434 | 2435 | 2401 | 2380 | 11% | 8% | 11% | 10% | 11% | 11% | 8% |
| SCC2 | 2449 | 2411 | 2404 | 2398 | 2423 | 2343 | 2306 | 11% | 13% | 13% | 11% | 11% | 1% | 0% |
| SCC3 | 2381 | 2392.4 | 2377 | 2370 | 2340 | 2384 | - | 15% | 12% | 12% | 12% | 8% | 1% | - |
| SCC4 | 2432 | 2423.1 | 2397 | 2438.4 | 2412 | 2442 | 2430 | 9% | 9% | 12% | 10% | 11% | 14% | 8% |
| SCC5 | 2381 | 2418 | 2359 | 2367 | 2348 | 2307 | 2372 | 13% | 18% | 25% | 39% | 39% | 37% | 24% |
| SCC6 | 2350 | - | 2412 | - | - | - | - | - | - | 17% | - | - | - | - |
| SCC7 | 2410 | 2435 | 2406.8 | 2444 | 2395 | 2465 | | 4% | 6% | 7% | 7% | 7% | 5% | - |
| SCC8 | 2430 | 2452 | 2451 | 2442 | 2371 | 2436 | 2424 | 12% | 8% | 10% | 10% | 13% | 17% | 11% |
| SCC9 | 2360 | 2373.4 | 2355 | 2350 | 2374 | 2387 | - | 13% | 12% | 12% | 16% | 19% | 27% | - |
| SCC10 | - | 2416.9 | - | 2255 | 2265 | 2357 | - | 8% | 10% | 3% | 9% | 11% | 11% | - |
| SCC11 | 2338 | 2342.9 | 2335 | 2348 | 2335 | 2327 | 2325 | 13% | 15% | 15% | 10% | 13% | 13% | 3% |
| SCC12 | 2315 | 2350.9 | 2343 | 2338 | 2354 | 2315 | - | 7% | - | 2% | - | - | - | - |
| HWC1 | 2360 | 630 | 2373 | 2391 | 2367 | 2381 | - | - | - | - | - | - | - | - |
| HWC2 | 2353 | 2364 | 2347 | 2374 | 2370 | 2369 | - | - | - | - | - | - | - | - |
| HWC3 | 2228 | 2370 | 2360 | 2364 | 2373 | 2359 | 2363 | - | - | - | - | - | - | - |
| SCC13 | 2258 | 2284.9 | 2215 | 256 | 2247 | 2258 | 2288 | 12% | 12% | 11% | 13% | 10% | 13% | 12% |
| SCC14 | 2296 | 2318.3 | 2282 | 2279 | 2308 | 2315 | - | 15% | 13% | 14% | 14% | 16% | 17% | - |
| HWC4 | 2322 | 2339 | 2340 | 2361 | 2362 | 2372 | 2359 | - | - | - | - | - | - | - |
| SCC15 | 2257 | 2292.3 | 2361 | 2345 | 2371 | 2357 | 2358 | 9% | 10% | 8% | 11% | 9% | 8% | 8% |
| SCC16 | 2316 | 2316.6 | 2346 | 2369 | 2386 | 2383 | 2365 | 10% | 9% | 10% | 7% | 9% | 5% | 12% |
| SCC17 | 2339 | 2347.4 | 2363 | 2366 | 2377 | 2373 | 2363 | 12% | 10% | 10% | 8% | 9% | 10% | 11% |
| SCC18 | 2369 | 2374 | 2414 | 2411 | 2407 | 2389 | 2391 | 11% | 6% | 6% | 8% | 6% | 8% | 5% |
| SCC19 | 2420 | 2426 | 2419 | 2420 | 2425 | 2398 | 2424 | - | - | - | 6% | - | - | - |

*Table B.21: Rheological properties of the pumped mixtures measured with the ICAR rheometer.*

| Mixture | Rheological properties measured with the ICAR | | | | | | | | | | | |
|---|---|---|---|---|---|---|---|---|---|---|---|---|
| | Viscosity (Pa s) | | | | | | Yield stress (Pa) | | | | | |
| | np-0 | 1 | 2 | 3 | 4 | 5 | np-0 | 1 | 2 | 3 | 4 | 5 |
| CVC1 | 4.3 | 4.3 | 2.5 | 2.5 | 1.0 | 0.3 | 328.1 | 426.4 | 461.5 | 642.2 | 793.9 | 859.6 |
| CVC2 | 4.0 | 1.4 | 7.3 | 4.0 | 6.0 | - | 327.9 | 542.9 | 522.1 | 800.3 | 1296.4 | - |
| CVC3 | 17.0 | 14.7 | 18.7 | 19.8 | 9.7 | - | 40.5 | 49.4 | 20.1 | 17.9 | 107.0 | - |
| SCC1 | 36.7 | 36.3 | 25.0 | 24.6 | 23.8 | 24.0 | 46.6 | 47.7 | 47.8 | 51.5 | 73.1 | 145.2 |
| SCC2 | 24.2 | 18.0 | 17.9 | 14.5 | 14.0 | 2.1 | 19.9 | 73.9 | 68.0 | 124.9 | 2653.0 | 3203.3 |
| SCC3 | 32.0 | 18.0 | 16.3 | 11.6 | 20.0 | 24.0 | 29.0 | 51.0 | 58.0 | 202.4 | 800.0 | 145.2 |
| SCC4 | 26.7 | 26.7 | 23.4 | 19.3 | 16.3 | 14.4 | 63.2 | 63.2 | 38.0 | 52.6 | 71.2 | 89.1 |
| SCC5 | 19.8 | - | 11.5 | 9.1 | - | 8.6 | 16.9 | - | 0.0 | 5.7 | - | 9.8 |
| SCC6 | 42.5 | 12.8 | 25.0 | 24.6 | 23.8 | 24.0 | 575.6 | 3.3 | 47.8 | 51.5 | 73.1 | 145.2 |
| SCC7 | 42.9 | 36.0 | 29.6 | 28.5 | 31.0 | 14.4 | 94.0 | 134.5 | 108.4 | 121.3 | 141.3 | 89.1 |
| SCC8 | 43.2 | 31.7 | 32.7 | 30.0 | 61.0 | 37.9 | 47.6 | 39.1 | 42.2 | 40.0 | 38.9 | 0.7 |
| SCC9 | 17.6 | 13.9 | 13.8 | 14.1 | 11.5 | 7.0 | 41.2 | 68.2 | 54.8 | 54.1 | 134.2 | 674.0 |
| SCC10 | 27.9 | 24.5 | 19.5 | 19.0 | 19.8 | 14.4 | 50.0 | 69.6 | 76.0 | 80.5 | 92.5 | 89.1 |
| SCC11 | 17.6 | 13.9 | 13.5 | 14.2 | 11.5 | 7.0 | 41.2 | 68.2 | 56.1 | 53.7 | 134.2 | 674.0 |
| SCC12 | 77.0 | 33.9 | 40.5 | 28.7 | 13.9 | 14.4 | 92.7 | 227.9 | 249.9 | 596.2 | 1540.8 | 89.1 |
| HWC1 | 58.1 | 42.4 | 37.5 | 30.5 | 19.5 | 14.4 | 170.1 | 255.8 | 296.1 | 378.3 | 898.7 | 89.1 |
| HWC2 | 51.5 | 36.5 | 30.3 | 23.4 | 20.2 | 14.4 | 85.9 | 119.2 | 210.0 | 337.1 | 466.5 | 89.1 |
| HWC3 | 47.6 | 22.8 | 17.8 | 19.6 | 15.4 | 3.4 | 87.2 | 144.2 | 253.9 | 374.3 | 392.9 | 2383.9 |
| SCC13 | 31.8 | 31.1 | 20.2 | 20.4 | 17.9 | 20.2 | 33.8 | 35.8 | 55.1 | 50.5 | 76.0 | 66.8 |
| SCC14 | 18.4 | 12.5 | 13.9 | 14.8 | 12.1 | 0.3 | 44.6 | 46.9 | 37.0 | 34.5 | 33.5 | 648.5 |
| HWC4 | 50.6 | 31.2 | 30.7 | 29.6 | 24.7 | 23.9 | 83.2 | 75.4 | 85.9 | 79.6 | 110.6 | 132.7 |
| SCC15 | 31.2 | 23.3 | 19.3 | 18.7 | 19.0 | 15.4 | 76.5 | 108.5 | 100.6 | 96.4 | 95.0 | 127.6 |
| SCC16 | 34.7 | 25.5 | 19.9 | 25.1 | 22.0 | 19.0 | 49.1 | 94.1 | 90.1 | 111.7 | 96.0 | 156.8 |
| SCC17 | 27.4 | 20.9 | 17.8 | 18.6 | 19.4 | 17.6 | 40.8 | 87.8 | 77.0 | 82.2 | 124.3 | 94.5 |
| SCC18 | 38.9 | 26.5 | 21.8 | 19.5 | 23.0 | 18.7 | 28.5 | 102.1 | 108.4 | 173.6 | 206.7 | 220.1 |
| SCC19 | 105.0 | 105.1 | 70.5 | 71.3 | 61.4 | 57.2 | 81.0 | 76.9 | 171.9 | 302.8 | 635.6 | 1159.6 |

***Table B.22:*** *Equivalent rheological properties of the pumped mixtures obtained with the ConTec rheometer.*

| Mixture | Equivalent rheological properties measured with the ConTec | | | | | | | | | | | | | |
|---|---|---|---|---|---|---|---|---|---|---|---|---|---|---|
| | Viscosity (Pa s) | | | | | | | Yield stress (Pa) | | | | | | |
| | np-0 | 1 | 2 | 3 | 4 | 5 | 6 | np-0 | 1 | 2 | 3 | 4 | 5 | 6 |
| CVC1 | 8.1 | 8.1 | 4.7 | 4.7 | 1.9 | 0.5 | 6.3 | 347.3 | 454.4 | 492.7 | 689.7 | 855.1 | 926.6 | 740.7 |
| CVC2 | 7.6 | 2.6 | 13.9 | 7.6 | 11.3 | - | 5.6 | 347.1 | 581.4 | 558.8 | 862.0 | 1402.8 | 0 | 484.8 |
| CVC3 | 32.4 | 27.9 | 35.5 | 37.6 | 18.5 | - | - | 33.9 | 43.5 | 11.6 | 9.2 | 106.3 | 0 | 0 |
| SCC1 | 69.7 | 69.0 | 47.5 | 46.7 | 45.2 | 45.6 | 90.6 | 40.5 | 41.7 | 41.8 | 45.8 | 69.4 | 148.0 | 30.4 |
| SCC2 | 46.0 | 34.2 | 33.9 | 27.5 | 26.6 | 3.9 | 77.9 | 11.4 | 70.2 | 63.8 | 125.8 | 2881.5 | 3481.3 | 9.1 |
| SCC3 | 60.8 | 34.2 | 30.9 | 22.0 | 38.0 | 45.6 | 75.1 | 21.3 | 45.3 | 52.9 | 210.3 | 861.7 | 148.0 | 13.8 |
| SCC4 | 50.7 | 50.7 | 44.6 | 36.6 | 30.9 | 27.4 | 104.6 | 58.6 | 58.6 | 31.1 | 47.0 | 67.3 | 86.8 | 32.6 |
| SCC5 | 37.6 | - | 21.8 | 17.3 | - | 16.3 | 32.4 | 8.1 | 0 | 0 | 0 | 0 | 0.4 | 20.4 |
| SCC6 | 80.8 | 24.3 | 47.5 | 46.7 | 45.2 | 45.6 | 90.6 | 617.1 | 0 | 41.8 | 45.8 | 69.4 | 148.0 | 30.4 |
| SCC7 | 81.6 | 68.5 | 56.1 | 54.2 | 58.9 | 27.4 | 109.3 | 92.1 | 136.3 | 107.9 | 121.9 | 143.7 | 86.8 | 71.2 |
| SCC8 | 82.2 | 60.3 | 62.1 | 57.0 | 115.9 | 72.0 | 104.6 | 41.6 | 32.3 | 35.6 | 33.3 | 32.1 | 0 | 32.6 |
| SCC9 | 33.5 | 26.5 | 26.2 | 26.7 | 21.8 | 13.3 | 57.0 | 34.5 | 64.0 | 49.4 | 48.7 | 136.0 | 724.3 | 21.1 |
| SCC10 | 52.9 | 46.5 | 37.1 | 36.0 | 37.6 | 27.4 | 77.1 | 44.2 | 65.5 | 72.5 | 77.5 | 90.5 | 86.8 | 52.3 |
| SCC11 | 33.5 | 26.5 | 25.7 | 26.9 | 21.8 | 13.3 | 57.0 | 34.5 | 64.0 | 50.9 | 48.2 | 136.0 | 724.3 | 21.1 |
| SCC12 | 146.3 | 64.4 | 76.9 | 54.6 | 26.5 | 27.4 | 183.9 | 90.8 | 238.1 | 262.1 | 639.5 | 1669.2 | 86.8 | 147.7 |
| HWC1 | 110.4 | 80.6 | 71.3 | 58.0 | 37.1 | 27.4 | 123.9 | 175.1 | 268.4 | 312.4 | 402.0 | 969.2 | 86.8 | 263.6 |
| HWC2 | 97.9 | 69.4 | 57.6 | 44.5 | 38.4 | 27.4 | 118.3 | 83.4 | 119.6 | 218.6 | 357.1 | 498.1 | 86.8 | 113.4 |
| HWC3 | 90.4 | 43.4 | 33.9 | 37.3 | 29.3 | 6.5 | 93.2 | 84.7 | 146.9 | 266.4 | 397.7 | 417.9 | 2588.1 | 204.4 |
| SCC13 | 60.4 | 59.2 | 38.4 | 38.8 | 33.9 | 38.4 | 76.0 | 26.6 | 28.7 | 49.7 | 44.7 | 72.5 | 62.5 | 43.4 |
| SCC14 | 35.0 | 23.7 | 26.3 | 28.1 | 23.1 | 0.5 | 43.1 | 38.3 | 40.8 | 30.0 | 27.2 | 26.2 | 696.5 | 19.6 |
| HWC4 | 96.1 | 59.3 | 58.3 | 56.3 | 46.9 | 45.4 | 107.6 | 80.4 | 71.9 | 83.4 | 76.5 | 110.2 | 134.3 | 68.8 |
| SCC15 | 59.3 | 44.2 | 36.7 | 35.5 | 36.1 | 29.2 | 72.3 | 73.1 | 107.9 | 99.3 | 94.8 | 93.2 | 128.8 | 80.2 |
| SCC16 | 66.0 | 48.4 | 37.8 | 47.7 | 41.8 | 36.2 | 100.6 | 43.2 | 92.3 | 87.9 | 111.4 | 94.3 | 160.6 | 54.7 |
| SCC17 | 52.1 | 39.7 | 33.8 | 35.4 | 36.9 | 33.4 | 72.7 | 34.2 | 85.4 | 73.6 | 79.3 | 125.2 | 92.7 | 37.8 |
| SCC18 | 73.9 | 50.3 | 41.4 | 37.0 | 43.7 | 35.5 | 90.7 | 20.7 | 101.0 | 107.8 | 178.9 | 214.9 | 229.6 | 84.9 |
| SCC19 | 199.4 | 199.7 | 133.9 | 135.4 | 116.7 | 108.6 | 294.5 | 77.9 | 73.5 | 177.0 | 319.8 | 682.5 | 1253.7 | 144.0 |

*Table B.23: Tribological properties of the pumped mixtures.*

| Mixture | Tribological properties | | | | | | | | | | | | | | | | | |
|---|---|---|---|---|---|---|---|---|---|---|---|---|---|---|---|---|---|---|
| | $Itrib_{II}$ (Pa s/m) | | | | | | $Itrib_{co}$ (Pa s/m) | | | | | | $Itrib_{tot}$ (Pa s/m) | | | | | |
| | np-0 | 1 | 2 | 3 | 4 | 5 | np-0 | 1 | 2 | 3 | 4 | 5 | np-0 | 1 | 2 | 3 | 4 | 5 |
| CVC1 | 510.4 | 462.7 | 491.8 | 525.7 | 636.1 | 657.7 | - | 3123.8 | - | - | - | - | 510.4 | 462.9 | 491.8 | 525.7 | 636.1 | 657.7 |
| CVC2 | 358.2 | 495.1 | 490.6 | 670.3 | 980.4 | 440.0 | - | 3322.6 | - | - | - | - | 358.2 | 497.1 | 490.6 | 670.3 | 980.4 | 440.0 |
| CVC3 | 2761.2 | 2175.1 | 1840.7 | 3223.5 | 1572.1 | - | 1463.6 | 5611.9 | 1574.4 | 1668.8 | 3546.6 | - | 981.1 | 834.7 | 872.8 | 1152.1 | 1099.5 | 1275.9 |
| SCC1 | 2915.4 | 1792.0 | 1666.3 | 1797.7 | 1559.9 | 7815.1 | 3090.3 | 7594.1 | 2113.5 | 2091.2 | 3644.2 | 2097.8 | 1500.9 | 1142.2 | 934.1 | 969.2 | 1094.2 | 1733.0 |
| SCC2 | 1354.7 | 2432.2 | 1317.4 | 2700.7 | 1232.0 | 25.8 | 2041.4 | 6410.5 | 1573.1 | 1294.0 | 3919.2 | - | 817.0 | 964.8 | 719.5 | 880.7 | 1006.6 | 1332.2 |
| SCC3 | 2777.8 | 2060.6 | 1568.7 | 3812.7 | 1229.1 | 3694.4 | 2718.5 | 5905.4 | 1468.0 | 1175.2 | - | 1757.4 | 1375.1 | 885.6 | 764.4 | 948.0 | 1463.7 | 1263.4 |
| SCC4 | 3487.7 | 1851.2 | 1083.9 | 1839.9 | 1060.7 | - | 2356.7 | 6929.7 | 2009.3 | 1682.4 | 3802.2 | 1263.6 | 1419.4 | 1038.5 | 704.2 | 879.5 | 829.9 | 1859.8 |
| SCC5 | 1056.0 | - | 406.4 | 573.4 | 364.6 | - | 1668.8 | - | 967.8 | 766.3 | 3546.6 | 724.2 | 649.2 | - | 286.6 | 328.3 | 330.7 | 929.6 |
| SCC6 | 3485.6 | 1614.9 | - | - | - | - | 3585.1 | 4529.1 | - | - | - | - | 1772.4 | 684.2 | - | - | - | - |
| SCC7 | 3138.8 | 2620.2 | 2933.9 | 3183.7 | 4975.5 | - | 3695.9 | 9815.1 | 2586.6 | 2534.8 | 3658.9 | 1053.4 | 1702.5 | 1471.5 | 1380.4 | 1417.0 | 2117.5 | 1166.4 |
| SCC8 | 3473.1 | 2325.7 | 2493.5 | 1983.2 | 1554.6 | 7593.8 | 3644.7 | 8294.8 | 2759.3 | 2526.9 | 3546.6 | 3191.1 | 1778.9 | 1248.3 | 1312.0 | 1112.5 | 1081.2 | 2248.2 |
| SCC9 | 479.4 | 548.0 | 356.2 | 255.0 | 504.2 | 108.6 | 1548.4 | 2633.6 | 1484.9 | 1765.6 | 4692.3 | - | 366.5 | 391.5 | 288.8 | 224.3 | 463.4 | 261.9 |
| SCC10 | 1889.3 | 1332.5 | 1265.2 | 1755.7 | 2320.8 | 3284.2 | 2356.1 | 5517.8 | 1717.4 | 1633.7 | 3628.7 | 1153.2 | 1051.9 | 830.8 | 735.6 | 855.8 | 1424.7 | 857.4 |
| SCC11 | 1625.5 | 1209.4 | 1317.4 | 1591.6 | 911.1 | - | 1501.5 | 4066.4 | 1148.7 | 1212.2 | 3636.3 | 631.7 | 783.0 | 616.6 | 615.6 | 690.2 | 729.6 | 1117.6 |
| SCC12 | 3053.1 | 5104.4 | 3279.1 | 5457.3 | 1756.9 | - | 6579.5 | - | 3916.8 | 3479.4 | - | 950.9 | 2088.3 | 1903.9 | 1814.4 | 2253.0 | 2354.7 | 2660.7 |
| HWC1 | 2881.4 | 2876.9 | 3158.6 | 3108.6 | 2506.7 | - | 5475.0 | - | 3849.2 | 5273.9 | 8935.3 | 975.0 | 1897.2 | 1893.2 | 1770.9 | 2074.5 | 2385.9 | 2283.5 |
| HWC2 | 2611.2 | 3057.2 | 3605.1 | 8801.3 | 2862.6 | - | 4486.2 | - | 2995.1 | 2193.9 | 5190.8 | 1034.6 | 1653.2 | 1600.9 | 1673.1 | 1787.7 | 2002.1 | 1946.9 |
| HWC3 | 2471.5 | 3208.4 | 4703.0 | 1918.1 | 2430.5 | - | 4220.0 | 8776.2 | 1959.5 | 3073.8 | 7479.3 | 224.7 | 1563.7 | 1320.2 | 1583.2 | 1233.9 | 2070.1 | 2024.6 |
| SCC13 | 2280.0 | 1253.0 | 1424.6 | 1140.0 | 656.8 | 5998.5 | 2683.3 | 5597.2 | 1746.2 | 1756.4 | 3739.3 | 1738.2 | 1234.3 | 843.3 | 785.0 | 691.9 | 559.4 | 1382.4 |
| SCC14 | 1139.9 | 726.7 | 579.4 | 554.6 | 926.2 | - | 1557.7 | 2881.4 | 1169.8 | 1287.8 | 3586.9 | 21.8 | 658.8 | 434.6 | 389.7 | 388.1 | 737.9 | 345.6 |
| HWC4 | 2666.9 | 2752.1 | 2007.8 | 1685.6 | 2078.6 | - | 4515.9 | 9033.3 | 2685.1 | 2623.8 | 3620.8 | 2063.0 | 1679.5 | 1355.5 | 1151.9 | 1026.6 | 1321.4 | 1906.3 |
| SCC15 | 1794.5 | 1889.4 | 2604.8 | 2690.8 | 1368.5 | - | 2809.7 | 6665.7 | 1688.1 | 1606.1 | 3637.9 | 1337.2 | 1101.6 | 1001.8 | 1029.1 | 1011.4 | 994.7 | 1480.3 |
| SCC16 | 2511.0 | 3341.6 | 2849.0 | 1755.0 | 1776.0 | 2382.5 | 2965.9 | 9005.4 | 1724.7 | 2485.2 | 3586.9 | 1762.1 | 1363.1 | 1357.1 | 1077.4 | 1045.6 | 1192.3 | 1737.3 |
| SCC17 | 2287.8 | 1512.4 | 1980.4 | 1799.2 | 1235.3 | 5329.0 | 2347.7 | 5569.3 | 1524.9 | 1595.6 | 3640.7 | 1523.0 | 1162.9 | 840.8 | 870.3 | 847.1 | 923.9 | 1371.5 |
| SCC18 | 2060.6 | 3209.6 | 2125.8 | 5060.9 | 1604.9 | - | 3362.6 | 8951.3 | 2000.5 | 1732.2 | 4109.0 | 1713.9 | 1281.5 | 1347.1 | 1047.6 | 1307.1 | 1169.1 | 1816.7 |
| SCC19 | 5559.2 | 4465.1 | 4030.7 | 7144.4 | - | 7976.4 | 8860.7 | - | 6048.5 | 6266.3 | 4038.7 | 5629.8 | 3417.2 | 2994.6 | 2420.6 | 3342.8 | 4202.6 | 3625.7 |

*Table B.24: Compressive strength of the pumped mixtures.*

| Mixture | Age (days) | Pumped concrete (MPa) | Non-pumped concrete (MPa) |
|---|---|---|---|
| CVC1 | 44 | 46.3 | 49.6 |
| CVC2 | 44 | - | 46.3 |
| CVC3 | 44 | 46.9 | 48.2 |
| SCC1 | 22 | 73.3 | 70.0 |
| SCC2 | 22 | 69.7 | 70.2 |
| SCC3 | 22 | 67.2 | 75.0 |
| SCC4 | 29 | 79.4 | 75.0 |
| SCC5 | 29 | 68.4 | 66.1 |
| SCC7 | 29 | 74.9 | 76.9 |
| SCC8 | 29 | - | 81.8 |
| SCC9 | 29 | - | 81.8 |
| SCC10 | 29 | 78.6 | 76.6 |
| SCC11 | 29 | 71.7 | 69.8 |
| SCC12 | 29 | 77.5 | 75.2 |
| HWC1 | 29 | 79.9 | 72.5 |
| HWC2 | 29 | 80.3 | 75.8 |
| HWC3 | 29 | 78.3 | 76.2 |
| HWC4 | 29 | 83.1 | 78.5 |
| SCC13 | 29 | 64.5 | 66.5 |
| SCC14 | 29 | 73.5 | 66.7 |
| SCC15 | 29 | 80.3 | 68.3 |
| SCC16 | 29 | 82.3 | 73.6 |
| SCC17 | 29 | 78.5 | 70.4 |
| SCC18 | 29 | 81.5 | 67.1 |
| SCC19 | 29 | 89.1 | 88.6 |

*Table B.25: Pumping pressure loss per meter for 4-in pipes at fixed discharge rates during the 5 pumping cycles.*

| Mixture | Pumping cycle 1 | | | | | Pumping cycle 2 | | | | | Pumping cycle 3 | | | | |
|---|---|---|---|---|---|---|---|---|---|---|---|---|---|---|---|
| | Discharge | | | | | Discharge | | | | | Discharge | | | | |
| | 1 | 2 | 3 | 4 | 5 | 1 | 2 | 3 | 4 | 5 | 1 | 2 | 3 | 4 | 5 |
| CVC1 | 7.60 | 11.50 | 15.41 | 19.31 | 23.21 | 7.05 | 11.64 | 16.24 | 20.83 | 25.42 | 8.95 | 14.65 | 20.36 | 26.06 | 31.76 |
| CVC2 | 6.86 | 11.62 | 16.38 | 21.14 | 25.89 | 9.70 | 14.22 | 18.74 | 23.27 | 27.79 | 9.99 | 15.68 | 21.36 | 27.05 | 32.73 |
| CVC3 | 14.46 | 22.28 | 30.10 | 37.91 | 45.73 | 18.27 | 26.48 | 34.69 | 42.90 | 51.10 | 22.29 | 31.69 | 41.10 | 50.51 | 59.91 |
| SCC1 | - | - | - | - | - | 24.89 | 51.85 | 78.80 | 105.75 | 132.71 | 20.74 | 43.28 | 65.83 | 88.37 | 110.91 |
| SCC2 | - | - | - | - | - | 8.62 | 21.15 | 33.68 | 46.21 | 58.75 | 7.91 | 19.87 | 31.82 | 43.77 | 55.72 |
| SCC3 | 15.14 | 28.87 | 42.61 | 56.35 | 70.09 | - | 26.00 | 40.34 | 54.69 | 69.03 | 12.41 | 25.31 | 38.21 | 51.11 | 64.02 |
| SCC4 | 20.88 | 43.51 | 66.13 | 88.75 | 111.37 | - | 38.73 | 58.95 | 79.16 | 99.38 | 16.00 | 32.15 | 48.30 | 64.46 | 80.61 |
| SCC5 | 4.82 | 17.57 | 30.31 | 43.06 | 55.80 | 3.53 | 15.56 | 27.60 | 39.63 | 51.66 | 4.41 | 13.67 | 22.94 | 32.20 | 41.46 |
| SCC6 | - | 33.63 | 48.40 | 63.16 | 77.93 | - | - | - | - | - | - | - | - | - | - |
| SCC7 | 42.26 | 81.63 | 120.99 | 160.36 | 199.72 | 41.77 | 78.97 | 116.17 | 153.37 | 190.57 | 39.88 | 75.71 | 111.54 | 147.37 | 183.20 |
| SCC8 | 40.04 | 80.97 | 121.89 | 162.82 | 203.74 | 36.97 | 72.97 | 108.98 | 144.98 | 180.98 | 33.91 | 70.19 | 106.48 | 142.76 | 179.05 |
| SCC9 | 5.15 | - | 26.61 | 37.34 | 48.07 | 5.57 | - | 22.89 | 31.55 | 40.21 | 5.49 | - | 23.18 | 32.03 | 40.88 |
| SCC10 | 25.27 | 47.97 | 70.67 | 93.38 | 116.08 | - | 43.90 | 63.68 | 83.45 | 103.23 | 23.33 | 41.58 | 59.84 | 78.10 | 96.36 |
| SCC11 | 17.84 | 34.26 | 50.68 | 67.10 | - | - | 32.31 | 47.56 | 62.80 | 78.05 | 16.23 | 30.28 | 44.32 | 58.37 | 72.41 |
| SCC12 | - | 79.03 | 117.95 | 156.87 | 195.78 | - | 85.06 | 125.64 | 166.22 | 206.80 | 45.86 | - | - | - | 204.96 |
| HWC1 | 54.47 | 100.65 | 146.84 | 193.03 | 239.21 | 54.35 | 100.85 | 147.36 | 193.87 | 240.38 | 53.22 | 94.65 | 136.08 | 177.50 | 218.93 |
| HWC2 | 47.53 | 90.56 | 133.58 | 176.60 | 219.62 | 47.02 | 87.94 | 128.86 | 169.78 | 210.70 | 46.45 | 83.81 | 121.17 | 158.53 | 195.89 |
| HWC3 | 37.34 | 71.49 | 105.63 | 139.77 | 173.92 | 35.92 | 68.94 | 101.95 | 134.97 | 167.98 | 35.24 | 63.94 | 92.64 | 121.34 | 150.04 |
| SCC13 | 26.70 | 54.36 | 82.03 | 109.69 | 137.35 | 22.58 | 44.37 | 66.17 | 87.97 | 109.77 | - | 41.43 | 61.58 | 81.74 | 101.90 |
| SCC14 | 15.74 | 28.55 | 41.35 | 54.16 | 66.97 | 13.43 | - | 35.83 | 47.03 | 58.23 | 11.92 | - | 33.68 | 44.57 | 55.45 |
| HWC4 | 40.51 | 73.20 | 105.89 | 138.58 | 171.27 | 32.65 | 61.76 | 90.87 | 119.98 | 149.09 | 29.36 | 53.39 | 77.42 | 101.45 | 125.48 |
| SCC15 | 17.83 | 37.56 | 57.29 | 77.02 | 96.75 | 15.83 | 35.81 | 55.79 | 75.77 | 95.75 | 16.55 | 34.61 | 52.67 | 70.73 | 88.79 |
| SCC16 | 27.90 | 56.11 | 84.32 | 112.54 | 140.75 | 25.70 | 50.84 | 75.98 | 101.12 | 126.26 | 25.30 | 49.50 | 73.70 | 97.91 | 122.11 |
| SCC17 | 22.28 | 44.61 | 66.94 | 89.27 | 111.60 | 22.30 | 43.24 | 64.18 | 85.12 | 106.06 | 21.03 | 41.10 | 61.16 | 81.23 | 101.30 |
| SCC18 | - | 74.06 | 110.11 | 146.16 | 182.20 | 31.54 | 60.64 | 89.74 | 118.85 | 147.95 | - | - | 85.33 | 113.14 | 140.95 |
| SCC19 | - | - | - | - | - | 84.10 | 167.52 | 250.95 | 334.37 | - | 78.78 | 153.76 | 228.74 | 303.72 | 378.71 |

***Table B.26:*** *(cont'd) Pumping pressure loss per meter for 4-in pipes at fixed discharge rates during the 5 pumping cycles.*

| Mixture | Pumping cycle 4 Discharge | | | | | Pumping cycle 5 Discharge | | | | |
|---|---|---|---|---|---|---|---|---|---|---|
| | 1 | 2 | 3 | 4 | 5 | 1 | 2 | 3 | 4 | 5 |
| CVC1 | 10.41 | 16.91 | 23.40 | 29.90 | 36.39 | 11.23 | 17.99 | 24.76 | - | - |
| CVC2 | 12.88 | 19.39 | 25.89 | 32.40 | 38.91 | 22.36 | 30.71 | 39.06 | 47.40 | 55.75 |
| CVC3 | - | - | - | - | - | - | - | - | - | - |
| SCC1 | 18.97 | 40.59 | 62.22 | 83.84 | 105.46 | 20.46 | 42.26 | 64.06 | 85.86 | 107.66 |
| SCC2 | - | 13.56 | 24.59 | 35.62 | 46.66 | - | - | 43.21 | 55.04 | - |
| SCC3 | 16.36 | 28.64 | 40.92 | 53.20 | 65.49 | - | - | - | - | - |
| SCC4 | - | 30.29 | 45.15 | 60.00 | 74.86 | 15.04 | 30.20 | 45.36 | 60.52 | 75.68 |
| SCC5 | 4.18 | 13.50 | 22.82 | 32.13 | 41.45 | 4.02 | 13.36 | 22.69 | 32.03 | 41.37 |
| SCC6 | - | - | - | - | - | - | - | - | - | - |
| SCC7 | - | - | 113.18 | 150.01 | 186.84 | - | - | - | - | - |
| SCC8 | - | - | - | - | - | 33.89 | 68.11 | 102.33 | 136.55 | 170.77 |
| SCC9 | 5.39 | 13.97 | 22.56 | 31.14 | 39.72 | - | - | - | - | - |
| SCC10 | - | 40.70 | 58.51 | 76.32 | 94.13 | - | - | - | - | - |
| SCC11 | - | 31.23 | 45.63 | 60.03 | 74.43 | - | - | 49.85 | - | - |
| SCC12 | - | - | - | - | - | - | - | - | - | - |
| HWC1 | 57.33 | 97.40 | 137.46 | 177.52 | 217.59 | - | - | - | - | - |
| HWC2 | 48.29 | 84.14 | 119.99 | 155.84 | 191.70 | - | - | - | - | - |
| HWC3 | 38.24 | 65.39 | 92.54 | 119.69 | 146.84 | 49.48 | 78.36 | 107.24 | 136.12 | 165.00 |
| SCC13 | 18.87 | 37.61 | 56.35 | 75.09 | 93.83 | 19.30 | 36.88 | 54.46 | 72.04 | 89.62 |
| SCC14 | 13.30 | 23.20 | 33.10 | 43.00 | 52.91 | - | - | - | - | - |
| HWC4 | 27.69 | 50.49 | 73.30 | 96.11 | 118.92 | 27.62 | 49.64 | 71.67 | 93.69 | 115.71 |
| SCC15 | 15.33 | 32.22 | 49.12 | 66.01 | 82.90 | 14.79 | 29.06 | 43.34 | 57.62 | 71.90 |
| SCC16 | 24.34 | 48.25 | 72.16 | 96.08 | 119.99 | 23.73 | 46.64 | 69.56 | 92.47 | 115.38 |
| SCC17 | 21.34 | 40.14 | 58.94 | 77.74 | 96.54 | 21.67 | 41.02 | 60.36 | - | 99.05 |
| SCC18 | 29.95 | 56.31 | 82.66 | 109.02 | 135.38 | - | - | 84.53 | 111.13 | 137.73 |
| SCC19 | - | - | - | - | - | - | - | - | 346.25 | - |

*Table B.27: Pumping pressure loss per meter for 5-in pipes at fixed discharge rates during the 5 pumping cycles.*

| Mixture | Pumping cycle 1 Discharge | | | | | Pumping cycle 2 Discharge | | | | | Pumping cycle 3 Discharge | | | | |
|---|---|---|---|---|---|---|---|---|---|---|---|---|---|---|---|
| | 1 | 2 | 3 | 4 | 5 | 1 | 2 | 3 | 4 | 5 | 1 | 2 | 3 | 4 | 5 |
| CVC1 | 3.80 | 7.23 | 10.65 | 14.07 | 17.50 | 4.27 | 6.98 | 9.70 | 12.41 | 15.13 | 5.16 | 8.07 | 10.98 | 13.89 | 16.79 |
| CVC2 | 4.29 | 6.08 | 7.87 | 9.66 | - | 2.48 | - | - | - | - | 3.09 | 6.34 | 9.59 | 12.85 | 16.10 |
| CVC3 | 5.48 | 9.67 | 13.86 | 18.05 | 22.24 | 8.22 | 12.68 | 17.14 | 21.60 | 26.05 | 8.30 | 13.25 | 18.20 | 23.14 | 28.09 |
| SCC1 | - | 22.09 | 33.86 | - | - | 10.62 | 22.90 | 35.18 | 47.46 | 59.74 | 8.76 | 18.17 | 27.57 | 36.97 | - |
| SCC2 | - | - | 18.57 | 26.90 | - | - | - | - | - | - | 6.08 | 9.95 | 13.81 | - | - |
| SCC3 | - | 14.87 | 25.38 | 35.89 | 46.40 | 4.64 | 10.83 | 17.03 | 23.23 | 29.42 | 6.62 | 12.94 | 19.26 | 25.58 | 31.90 |
| SCC4 | 10.22 | 25.46 | 40.71 | 55.95 | 71.19 | 11.89 | 23.29 | 34.69 | 46.09 | 57.49 | 9.80 | 20.54 | 31.27 | 42.00 | 52.74 |
| SCC5 | 4.58 | 11.36 | 18.14 | 24.91 | 31.69 | 4.21 | 9.97 | 15.73 | 21.49 | 27.26 | 3.86 | 8.75 | 13.64 | 18.52 | 23.41 |
| SCC6 | - | 17.47 | 24.67 | 31.87 | 39.06 | - | - | - | - | - | - | - | - | - | - |
| SCC7 | 18.30 | 34.76 | 51.21 | 67.67 | 84.13 | 16.94 | 33.12 | 49.30 | 65.48 | 81.66 | 16.77 | 31.13 | 45.50 | 59.86 | 74.22 |
| SCC8 | 15.78 | 31.09 | 46.40 | 61.71 | 77.02 | 14.12 | 27.20 | 40.29 | 53.37 | 66.46 | 13.34 | 26.57 | 39.79 | 53.01 | 66.24 |
| SCC9 | 3.90 | - | - | - | - | 4.15 | - | - | - | - | 3.53 | - | - | - | - |
| SCC10 | 13.19 | 26.55 | 39.90 | 53.26 | 66.62 | - | - | - | - | 63.78 | - | - | 35.02 | 46.35 | 57.68 |
| SCC11 | 8.97 | 17.06 | 25.15 | 33.24 | 41.33 | 8.69 | 16.91 | 25.13 | 33.35 | 41.56 | 7.78 | 15.07 | 22.36 | 29.65 | 36.94 |
| SCC12 | 20.88 | - | - | - | 98.68 | 21.76 | 41.84 | 61.92 | 82.00 | 102.09 | - | - | - | - | - |
| HWC1 | 24.81 | 52.32 | 79.83 | 107.34 | 134.85 | 25.71 | 50.06 | 74.42 | 98.78 | 123.14 | 21.04 | 45.47 | 69.90 | 94.33 | 118.76 |
| HWC2 | 14.77 | 35.00 | 55.22 | 75.45 | 95.67 | 15.06 | 35.46 | 55.86 | 76.25 | 96.65 | 13.69 | 32.09 | 50.50 | 68.91 | 87.32 |
| HWC3 | 10.59 | 24.43 | 38.28 | 52.13 | 65.98 | 10.21 | 24.39 | 38.57 | 52.75 | 66.94 | 10.17 | 20.93 | 31.69 | 42.45 | 53.21 |
| SCC13 | - | 20.70 | 33.83 | 46.96 | 60.10 | - | 16.18 | 29.42 | 42.66 | 55.90 | 8.41 | 17.11 | 25.80 | 34.50 | 43.20 |
| SCC14 | 4.19 | - | 13.92 | - | - | 4.08 | 10.23 | 16.39 | 22.54 | 28.69 | 5.93 | 9.66 | - | - | - |
| HWC4 | 15.84 | 31.86 | 47.88 | 63.90 | 79.92 | 11.49 | 24.52 | 37.54 | 50.56 | 63.59 | 10.82 | 23.11 | 35.39 | 47.67 | 59.95 |
| SCC15 | 12.11 | 25.92 | 39.72 | 53.52 | 67.33 | 10.90 | 22.62 | 34.33 | 46.04 | 57.76 | 9.94 | 19.86 | 29.77 | 39.69 | 49.60 |
| SCC16 | 14.99 | - | 46.75 | - | 78.50 | - | - | - | - | 64.30 | 13.52 | 25.58 | 37.64 | 49.70 | 61.76 |
| SCC17 | 10.89 | 22.02 | 33.15 | 44.28 | 55.40 | 11.00 | 21.58 | 32.16 | 42.75 | 53.33 | 10.20 | 19.20 | 28.20 | 37.20 | 46.21 |
| SCC18 | 14.90 | 31.21 | 47.52 | 63.83 | 80.13 | 12.11 | 24.11 | 36.11 | 48.11 | 60.12 | 11.55 | 22.68 | 33.80 | 44.93 | 56.06 |
| SCC19 | - | 77.88 | 120.28 | - | - | 36.83 | - | - | - | - | 37.23 | - | - | - | 186.12 |

***Table B.28:*** *(cont'd) Pumping pressure loss per meter for 5-in pipes at fixed discharge rates during the 5 pumping cycles.*

| Mixture | Pumping cycle 4 | | | | | Pumping cycle 5 | | | | |
|---|---|---|---|---|---|---|---|---|---|---|
| | Discharge | | | | | Discharge | | | | |
| | 1 | 2 | 3 | 4 | 5 | 1 | 2 | 3 | 4 | 5 |
| CVC1 | - | - | - | - | - | - | - | - | - | - |
| CVC2 | 4.30 | 8.24 | 12.17 | 16.11 | 20.05 | 1.60 | 8.08 | 14.57 | - | - |
| CVC3 | - | - | - | - | - | - | - | - | - | - |
| SCC1 | 9.16 | 18.47 | 27.79 | 37.10 | 46.42 | 9.24 | 19.79 | 30.35 | - | - |
| SCC2 | 6.81 | 13.38 | 19.95 | 26.52 | 33.10 | - | - | - | - | - |
| SCC3 | 8.56 | 15.03 | 21.49 | - | - | - | - | - | - | - |
| SCC4 | 10.31 | 19.16 | 28.01 | 36.86 | 45.71 | 10.05 | - | - | - | - |
| SCC5 | 3.80 | 8.31 | 12.81 | 17.32 | 21.83 | 3.67 | 8.25 | 12.84 | - | - |
| SCC6 | - | - | - | - | - | - | - | - | - | - |
| SCC7 | 15.72 | 30.71 | 45.70 | 60.68 | 75.67 | - | - | - | - | - |
| SCC8 | - | - | - | - | - | 13.70 | 26.39 | 39.08 | - | - |
| SCC9 | 3.26 | 6.33 | - | - | - | - | - | - | - | - |
| SCC10 | - | 24.21 | 34.80 | 45.38 | 55.97 | - | - | - | - | - |
| SCC11 | - | - | 24.81 | 32.50 | 40.19 | - | - | - | - | - |
| SCC12 | - | - | - | - | - | - | - | - | - | - |
| HWC1 | 21.70 | 44.99 | 68.27 | 91.56 | 114.84 | - | - | - | - | - |
| HWC2 | 15.85 | 34.69 | 53.53 | 72.36 | 91.20 | - | - | - | - | - |
| HWC3 | 12.00 | 21.96 | 31.93 | 41.89 | 51.85 | 16.11 | 27.96 | 39.82 | - | - |
| SCC13 | - | 13.93 | 23.87 | 33.80 | 43.74 | - | 15.06 | 24.54 | - | - |
| SCC14 | 5.24 | 9.29 | 13.33 | - | - | - | - | - | - | - |
| HWC4 | 10.93 | 21.75 | 32.58 | 43.41 | 54.24 | 10.90 | 21.91 | 32.92 | - | - |
| SCC15 | 10.61 | 20.30 | 29.98 | 39.67 | 49.35 | 10.15 | 19.08 | 28.02 | - | - |
| SCC16 | 12.27 | 22.34 | 32.42 | 42.50 | 52.58 | 10.03 | 21.95 | 33.87 | - | - |
| SCC17 | 10.53 | 19.05 | - | 36.08 | 44.60 | 10.63 | 18.85 | 27.06 | - | - |
| SCC18 | 12.25 | 22.59 | 32.94 | 43.28 | 53.62 | 12.21 | 22.33 | 32.45 | - | - |
| SCC19 | - | - | - | - | - | - | - | - | - | - |

# Appendix C

# Pumping tests

***Table C.1:*** *Pressure loss of CVC1 measured at different discharge rates in 4 in. and 5 in. pipes.*

**CVC1**

| Cycle 1 | | | | | |
|---|---|---|---|---|---|
| Pressure loss (sensors) | | Pressure loss (straing gauges) | | Calibrated discharge | |
| 4 in (kPa/m) | 5 in. (kPa/m) | 4 in (kPa/m) | 5 in (kPa/m) | File (l/s) | Stopwatch (l/s) |
| 17.18 | 12.05 | | 12.97 | 13.84 | - |
| 15.80 | 11.27 | | 11.98 | 12.68 | 14.03 |
| 15.09 | 10.31 | | 11.01 | 11.46 | 12.59 |
| 13.99 | 9.12 | | 9.99 | 10.17 | 11.28 |
| 12.35 | 8.13 | | 9.13 | 8.97 | 10.20 |
| 10.62 | 6.79 | | 7.48 | 7.35 | 9.00 |
| 9.45 | 5.71 | | 6.20 | 6.30 | 7.32 |
| 10.08 | 5.44 | | 5.63 | 6.08 | 6.29 |

| Cycle 2 | | | | | |
|---|---|---|---|---|---|
| Pressure loss (sensors) | | Pressure loss (straing gauges) | | Calibrated discharge | |
| 4 in (kPa/m) | 5 in (kPa/m) | 4 in. (kPa/m) | 5 in. (kPa/m) | File (l/s) | Stopwatch (l/s) |
| 16.75 | 12.48 | | 11.62 | 15.98 | 15.76 |
| 16.13 | 11.17 | | 13.19 | 14.92 | 14.95 |
| 17.42 | 10.88 | | 11.18 | 13.77 | 14.02 |
| 17.07 | 9.93 | | 10.59 | 12.69 | 12.67 |
| 16.01 | 9.14 | | 9.32 | 11.07 | 11.04 |
| 14.20 | 8.15 | | 8.36 | 9.81 | 9.77 |
| 10.89 | 6.43 | | 6.37 | 7.33 | 7.30 |
| 8.38 | 5.29 | | 5.41 | 5.62 | 5.66 |

| Cycle 3 | | | | | |
|---|---|---|---|---|---|
| Pressure loss (sensors) | | Pressure loss (straing gauges) | | Calibrated discharge | |
| 4 in. (kPa/m) | 5 in. (kPa/m) | 4 in. (kPa/m) | 5 in. (kPa/m) | File (l/s) | Stopwatch (l/s) |
| 25.86 | 13.68 | | 12.66 | 16.17 | 15.77 |
| 24.82 | 12.69 | | 12.56 | 14.92 | 14.59 |
| 22.22 | 12.75 | | 11.33 | 13.84 | 13.85 |
| 21.58 | 11.49 | | 10.21 | 12.13 | 12.23 |
| 18.54 | 10.05 | | 8.79 | 10.47 | 10.53 |
| 15.57 | 8.65 | | 7.72 | 8.73 | 8.74 |
| 12.80 | 7.03 | | 6.27 | 6.70 | 6.68 |
| 10.14 | 5.70 | | 5.04 | 5.08 | 5.03 |

| Cycle 4 | | | | | |
|---|---|---|---|---|---|
| Pressure loss (sensors) | | Pressure loss (straing gauges) | | Calibrated discharge | |
| 4 in. (kPa/m) | 5 in. (kPa/m) | 4 in. (kPa/m) | 5 in. (kPa/m) | File (l/s) | Stopwatch (l/s) |
| 28.99 | 15.79 | | 14.10 | 15.98 | 15.93 |
| 28.51 | 14.69 | | 13.86 | 14.97 | 14.97 |
| 27.06 | 14.05 | | 12.60 | 13.92 | 13.94 |
| 24.96 | 13.44 | | 11.78 | 12.81 | 12.79 |
| 22.78 | 12.30 | | 10.84 | 11.58 | 11.57 |
| 19.03 | 10.89 | | 9.35 | 9.43 | 9.37 |
| 15.32 | 8.69 | | 7.40 | 6.96 | 6.98 |
| 10.83 | 6.09 | | 4.86 | 4.37 | 4.36 |

| Cycle 5 | | | | | |
|---|---|---|---|---|---|
| Pressure loss (sensors) | | Pressure loss (straing gauges) | | Calibrated discharge | |
| 4 in. (kPa/m) | 5 in. (kPa/m) | 4 in (kPa/m) | 5 in. (kPa/m) | File (l/s) | Stopwatch (l/s) |
| 26.24 | 19.82 | | 13.66 | 14.88 | 14.79 |
| 28.83 | 18.67 | | 13.84 | 14.64 | 14.53 |
| 27.92 | 17.16 | | 13.38 | 13.55 | 13.67 |
| 25.96 | 16.20 | | 12.89 | 12.61 | 12.50 |
| 23.54 | 14.77 | | 11.91 | 11.12 | 11.17 |
| 18.57 | 12.48 | | 9.89 | 8.63 | 8.56 |
| 14.87 | 10.65 | | 8.41 | 6.60 | 6.72 |
| 11.78 | 5.80 | | 5.11 | 3.93 | 4.00 |

**Potentially wrong data**

**Non-trusted data**

***Table C.2:*** *Pressure loss of CVC2 measured at different discharge rates in 4 in. and 5 in. pipes.*

**CVC2**

| Cycle 1 | | | | | |
|---|---|---|---|---|---|
| Pressure loss (sensors) | | Pressure loss (straing gauges) | | Calibrated discharge | |
| 4 in. (kPa/m) | 5 in. (kPa/m) | 4 in. (kPa/m) | 5 in. (kPa/m) | File (l/s) | Stopwatch (l/s) |
| 25.23 | 10.59 | | | | |
| 24.05 | 9.87 | | | | |
| 19.84 | 10.05 | | | | |
| 20.49 | 10.09 | | | | |
| 17.94 | 9.08 | 19.48 | 9.69 | | |
| 15.44 | 7.57 | 16.40 | 9.50 | | |
| 12.11 | 5.84 | 12.29 | 7.71 | | |
| 10.28 | 5.29 | 10.68 | 6.50 | | |

| Cycle 2 | | | | | |
|---|---|---|---|---|---|
| Pressure loss (sensors) | | Pressure loss (straing gauges) | | Calibrated discharge | |
| 4 in. (kPa/m) | 5 in. (kPa/m) | 4 in (kPa/m) | 5 in (kPa/m) | File (l/s) | Stopwatch (l/s) |
| 25.75 | **13.17** | **26.92** | **15.34** | 18.055 | 18.18 |
| 23.35 | **11.45** | 23.50 | **11.57** | 16.711 | 16.73 |
| 21.22 | 8.80 | 20.62 | 9.50 | 14.819 | 14.85 |
| 21.23 | 8.79 | 19.54 | 9.40 | 13.840 | 13.74 |
| 18.87 | 7.68 | 16.85 | 8.31 | 12.083 | 12.10 |
| 18.83 | 7.14 | 14.24 | 7.85 | 10.507 | 10.53 |
| 13.92 | 5.59 | 11.62 | 5.31 | 7.462 | 7.46 |
| 10.47 | 4.81 | 9.04 | 4.79 | 5.786 | 5.77 |

| Cycle 3 | | | | | |
|---|---|---|---|---|---|
| Pressure loss (sensors) | | Pressure loss (straing gauges) | | Calibrated discharge | |
| 4 in. (kPa/m) | 5 in. (kPa/m) | 4 in. (kPa/m) | 5 in. (kPa/m) | File (l/s) | Stopwatch (l/s) |
| **29.16** | **16.66** | **28.42** | **13.45** | 16.80 | 16.67 |
| 27.92 | **15.20** | 26.88 | **13.45** | 16.11 | 16.14 |
| 26.32 | 13.69 | 26.39 | 12.54 | 15.40 | 15.39 |
| 24.64 | 12.60 | 24.83 | 11.99 | 14.22 | 14.25 |
| 22.40 | 10.80 | 22.34 | 11.18 | 12.82 | 12.84 |
| 19.27 | 8.95 | 18.81 | 9.61 | 10.61 | 10.63 |
| 15.66 | 6.84 | 14.32 | 7.49 | 7.52 | 7.50 |
| 11.17 | 4.95 | 10.40 | 5.61 | 4.70 | 4.70 |

| Cycle 4 | | | | | |
|---|---|---|---|---|---|
| Pressure loss (sensors) | | Pressure loss (straing gauges) | | Calibrated discharge | |
| 4 in. (kPa/m) | 5 in. (kPa/m) | 4 in. (kPa/m) | 5 in. (kPa/m) | File (l/s) | Stopwatch (l/s) |
| 33.54 | **20.06** | 37.23 | **16.14** | 16.80 | 16.90 |
| 31.57 | 17.00 | 35.01 | 14.97 | 15.55 | 15.35 |
| 29.21 | 15.16 | 31.97 | 14.22 | 14.15 | 14.22 |
| 26.40 | 13.00 | 28.79 | 13.03 | 12.52 | 12.57 |
| 24.73 | 11.07 | 24.80 | 11.66 | 10.44 | 10.42 |
| 18.04 | 8.22 | 18.26 | 9.07 | 7.32 | 7.34 |
| 12.69 | 5.58 | 12.09 | 6.14 | 4.10 | 4.10 |

| Cycle 5 | | | | | |
|---|---|---|---|---|---|
| Pressure loss (sensors) | | Pressure loss (straing gauges) | | Calibrated discharge | |
| 4 in. (kPa/m) | 5 in. (kPa/m) | 4 in. (kPa/m) | 5 in. (kPa/m) | File (l/s) | Stopwatch (l/s) |
| 52.20 | 24.79 | 56.33 | 24.10 | 18.30 | 18.56 |
| 44.51 | 18.81 | 47.13 | 17.82 | 14.61 | |

**Potential non-equilibrium**

**Potentially wrong data**

***Table C.3:*** *Pressure loss of CVC3 measured at different discharge rates in 4 in. and 5 in. pipes.*

**CVC3**

| Cycle 1 | | | | | |
|---|---|---|---|---|---|
| Pressure loss (sensors) | | Pressure loss (straing gauges) | | Calibrated discharge | |
| 4 in. (kPa/m) | 5 in. (kPa/m) | 4 in. (kPa/m) | 5 in. (kPa/m) | File (l/s) | Stopwatch (l/s) |
| | | | | 16.59 | 16.92 |
| 36.20 | 18.86 | 35.70 | 16.38 | 15.53 | 15.71 |
| 34.77 | 16.42 | 34.38 | 15.40 | 14.34 | 14.37 |
| 33.43 | 15.96 | 32.39 | 15.14 | 13.31 | 13.29 |
| 30.47 | 13.42 | 28.36 | 13.19 | 11.40 | 11.39 |
| 24.74 | 11.13 | 23.59 | 11.58 | 9.09 | 9.13 |
| 19.31 | 8.45 | 17.49 | 9.08 | 6.31 | 6.28 |
| 13.59 | 6.11 | 12.46 | 6.34 | 3.71 | 3.71 |

| Cycle 2 | | | | | |
|---|---|---|---|---|---|
| Pressure loss (sensors) | | Pressure loss (straing gauges) | | Calibrated discharge | |
| 4 in. (kPa/m) | 5 in (kPa/m) | 4 in (kPa/m) | 5 in (kPa/m) | File (l/s) | Stopwatch (l/s) |
| **44.01** | **25.82** | **46.56** | **18.93** | 16.69 | 16.85 |
| 41.95 | **22.27** | 43.49 | **19.05** | 15.53 | 15.45 |
| 38.77 | 20.60 | 41.34 | 18.20 | 14.52 | 14.57 |
| 37.87 | 18.44 | 38.23 | 16.94 | 13.38 | 13.40 |
| 34.55 | 16.26 | 34.38 | 15.74 | 11.61 | 11.57 |
| 28.26 | 13.20 | 27.27 | 13.36 | 8.66 | 8.66 |
| 22.20 | 10.26 | 21.07 | 10.54 | 5.82 | 5.86 |
| 15.66 | 7.35 | 14.96 | 7.70 | 3.01 | 2.99 |

| Cycle 3 | | | | | |
|---|---|---|---|---|---|
| Pressure loss (sensors) | | Pressure loss (straing gauges) | | Calibrated discharge | |
| 4 in. (kPa/m) | 5 in. (kPa/m) | 4 in. (kPa/m) | 5 in. (kPa/m) | File (l/s) | Stopwatch (l/s) |
| 51.66 | **27.46** | 55.91 | **21.72** | 16.90 | 16.86 |
| 49.64 | **23.59** | 52.33 | **21.63** | 15.90 | 15.94 |
| 47.83 | 21.75 | 50.75 | 20.65 | 15.00 | 14.94 |
| 44.18 | 19.51 | 45.30 | 18.82 | 13.11 | 13.16 |
| 42.45 | 18.05 | 42.25 | 17.78 | 11.89 | 11.79 |
| 37.26 | 16.02 | 37.46 | 16.69 | 10.01 | 10.04 |
| 28.99 | 11.85 | 27.73 | 12.75 | 6.77 | 6.74 |
| 19.57 | 7.31 | 17.71 | 7.93 | 3.35 | 3.35 |

| Cycle 4 | | | | | |
|---|---|---|---|---|---|
| Pressure loss (sensors) | | Pressure loss (straing gauges) | | Calibrated discharge | |
| 4 in. (kPa/m) | 5 in (kPa/m) | 4 in. (kPa/m) | 5 in. (kPa/m) | File (l/s) | Stopwatch (l/s) |
| 68.32 | **30.75** | 75.83 | **30.34** | 16.19 | 16.43 |
| 65.45 | **27.70** | 70.79 | **30.99** | 15.00 | 15.07 |
| 63.24 | 25.24 | 68.19 | 29.06 | 13.81 | 13.85 |
| 57.00 | 23.81 | 62.31 | 27.84 | 12.11 | 12.11 |
| 52.87 | 20.00 | 55.81 | 24.89 | 10.35 | 10.61 |
| 48.85 | 18.54 | 51.58 | 23.81 | 8.85 | 8.80 |
| 40.60 | 14.33 | 41.56 | 20.52 | 5.98 | 5.99 |
| 30.36 | 9.82 | 30.03 | 15.46 | 2.42 | 2.39 |

**Non-trusted data**

**Potentially wrong data**

**Measurements treatment for the 5 in.-pipes sensors was performed with the help of the strain gauges**

**Table C.4:** *Pressure loss of SCC1 measured at different discharge rates in 4 in. and 5 in. pipes.*

## SCC1

| Cycle 1 | | | | | |
|---|---|---|---|---|---|
| Pressure loss (sensors) | | Pressure loss (straing gauges) | | Calibrated discharge | |
| 4 in. (kPa/m) | 5 in. (kPa/m) | 4 in. (kPa/m) | 5 in. (kPa/m) | File (l/s) | Stopwatch (l/s) |
| **127.66** | **55.28** | **110.96** | **61.99** | 16.55 | 16.56 |
| **115.48** | **49.16** | **101.77** | **56.63** | 15.52 | 15.74 |
| **102.01** | 42.29 | **89.68** | 49.16 | 14.29 | 14.35 |
| 91.02 | 37.53 | 79.78 | 44.30 | 13.05 | 13.23 |
| 77.28 | 32.20 | 69.24 | 38.95 | 11.78 | 11.74 |
| 62.30 | 25.53 | 57.06 | 31.51 | 9.77 | 9.81 |
| 44.33 | 18.61 | 44.74 | 23.92 | 7.18 | 7.19 |
| 27.75 | 11.94 | 32.03 | 16.02 | 4.50 | 4.46 |
| 20.33 | 9.22 | 22.96 | 11.42 | 3.14 | 3.06 |

| Cycle 2 | | | | | |
|---|---|---|---|---|---|
| Pressure loss (sensors) | | Pressure loss (straing gauges) | | Calibrated discharge | |
| 4 in. (kPa/m) | 5 in. (kPa/m) | 4 in. (kPa/m) | 5 in. (kPa/m) | File (l/s) | Stopwatch (l/s) |
| 103.69 | 47.37 | 97.84 | 51.60 | 15.25 | 15.45 |
| 90.66 | 41.16 | 85.64 | 46.21 | 13.99 | 13.99 |
| 82.51 | 35.75 | 77.67 | 40.31 | 12.86 | 12.86 |
| 75.24 | 32.56 | 70.30 | 37.21 | 11.99 | 12.00 |
| 65.84 | 27.64 | 62.01 | 31.99 | 10.70 | 10.67 |
| 50.99 | 21.03 | 50.45 | 25.37 | 8.41 | 8.46 |
| 36.95 | 15.30 | 40.81 | 18.71 | 6.13 | 6.19 |
| 23.84 | 10.17 | 27.71 | 12.41 | 3.87 | 3.89 |
| 19.62 | 8.81 | 22.67 | 10.10 | 3.14 | 3.15 |

| Cycle 3 | | | | | |
|---|---|---|---|---|---|
| Pressure loss (sensors) | | Pressure loss (straing gauges) | | Calibrated discharge | |
| 4 in. (kPa/m) | 5 in. (kPa/m) | 4 in. (kPa/m) | 5 in. (kPa/m) | File (l/s) | Stopwatch (l/s) |
| **93.49** | **43.56** | 88.46 | 45.40 | 16.45 | 16.50 |
| 87.52 | 36.54 | 83.03 | 40.83 | 15.34 | 15.45 |
| 78.12 | 33.40 | 75.01 | 38.39 | 14.29 | 14.23 |
| 65.48 | 26.85 | 63.82 | 31.34 | 12.22 | 12.18 |
| 50.29 | 20.88 | 49.82 | 24.51 | 9.55 | 9.58 |
| 33.83 | 14.07 | 34.34 | 16.29 | 6.51 | 6.55 |
| 22.35 | 9.54 | 22.51 | 10.79 | 4.16 | 4.18 |
| 19.61 | 8.50 | 19.82 | 9.63 | 3.54 | 3.56 |

| Cycle 4 | | | | | |
|---|---|---|---|---|---|
| Pressure loss (sensors) | | Pressure loss (straing gauges) | | Calibrated discharge | |
| 4 in. (kPa/m) | 5 in. (kPa/m) | 4 in. (kPa/m) | 5 in. (kPa/m) | File (l/s) | Stopwatch (l/s) |
| **85.90** | **39.78** | **83.20** | **43.32** | 15.79 | 15.84 |
| 78.52 | 35.03 | 77.15 | 38.91 | 14.45 | 14.42 |
| 70.68 | 31.60 | 69.98 | 36.01 | 13.71 | 13.85 |
| 65.08 | 28.30 | 64.75 | 32.35 | 12.56 | 12.52 |
| 54.77 | 24.89 | 55.32 | 28.61 | 11.00 | 11.07 |
| 43.95 | 19.89 | 45.73 | 23.21 | 8.90 | 8.92 |
| 30.98 | 14.42 | 32.62 | 16.93 | 6.30 | 6.31 |
| 19.73 | 9.44 | 20.49 | 10.90 | 3.80 | 3.81 |

| Cycle 5 | | | | | |
|---|---|---|---|---|---|
| Pressure loss (sensors) | | Pressure loss (straing gauges) | | Calibrated discharge | |
| 4 in. (kPa/m) | 5 in. (kPa/m) | 4 in. (kPa/m) | 5 in. (kPa/m) | File (l/s) | Stopwatch (l/s) |
| **88.77** | **43.78** | **86.79** | **46.41** | 15.79 | 15.79 |
| 82.75 | 39.26 | 81.62 | 42.61 | 14.76 | 14.72 |
| 71.42 | 34.89 | 71.78 | 38.31 | 13.64 | 13.60 |
| 65.95 | 30.67 | 66.50 | 34.19 | 12.50 | 12.47 |
| 54.26 | 25.66 | 55.06 | 29.12 | 10.47 | 10.47 |
| 45.60 | 20.76 | 47.36 | 24.15 | 8.80 | 8.87 |
| 33.02 | 15.31 | 35.02 | 17.54 | 6.40 | 6.40 |
| 20.12 | 9.43 | 21.56 | 10.89 | 3.60 | 3.62 |

**Non-trusted data (something strange with SGs 2)**

**Potentially wrong data**

**Measurements treatment for the 5 in.-pipes sensors was performed with the help of the strain gauges**

***Table C.5:*** *Pressure loss of SCC2 measured at different discharge rates in 4 in. and 5 in. pipes.*

**SCC2**

| Cycle 1 | | | | | |
|---|---|---|---|---|---|
| Pressure loss (sensors) | | Pressure loss (straing gauges) | | Calibrated discharge | |
| 4 in. (kPa/m) | 5 in. (kPa/m) | 4 in. (kPa/m) | 5 in. (kPa/m) | File (l/s) | Stopwatch (l/s) |
| 88.91 | | 78.61 | | 17.95 | 17.70 |
| 74.24 | 28.12 | 69.09 | 27.92 | 17.07 | 16.86 |
| 59.10 | 23.21 | 57.42 | 25.14 | 15.48 | 15.43 |
| 50.74 | 21.20 | 52.42 | 23.81 | 14.09 | 14.06 |
| 41.79 | 17.89 | 45.52 | 20.13 | 12.67 | 12.63 |
| 32.35 | 14.04 | 37.52 | 15.85 | 10.47 | 10.47 |
| 21.30 | 9.67 | 26.27 | 10.64 | 7.37 | 7.37 |
| 16.13 | 7.76 | 20.69 | 8.20 | 5.74 | 5.73 |

| Cycle 2 | | | | | |
|---|---|---|---|---|---|
| Pressure loss (sensors) | | Pressure loss (straing gauges) | | Calibrated discharge | |
| 4 in. (kPa/m) | 5 in. (kPa/m) | 4 in. (kPa/m) | 5 in. (kPa/m) | File (l/s) | Stopwatch (l/s) |
| 68.97 | | 70.95 | | 17.95 | 18.15 |
| 59.05 | 28.49 | 62.57 | 27.97 | 16.89 | 17.40 |
| 49.28 | 23.08 | 54.42 | 25.09 | 15.32 | 15.35 |
| 43.26 | 20.32 | 48.89 | 22.61 | 14.35 | 14.42 |
| 35.90 | 16.53 | 42.11 | 18.12 | 12.52 | 12.47 |
| 27.31 | 12.85 | 33.55 | 14.41 | 10.23 | 10.17 |
| 19.52 | 9.45 | 24.95 | 10.49 | 7.55 | 7.56 |
| 15.30 | 7.77 | 19.75 | 8.61 | 5.98 | 5.97 |

| Cycle 3 | | | | | |
|---|---|---|---|---|---|
| Pressure loss (sensors) | | Pressure loss (straing gauges) | | Calibrated discharge | |
| 4 in. (kPa/m) | 5 in. (kPa/m) | 4 in. (kPa/m) | 5 in. (kPa/m) | File (l/s) | Stopwatch (l/s) |
| 57.88 | 24.25 | 61.31 | 32.07 | 17.75 | 17.97 |
| 54.31 | 20.75 | 58.39 | 23.99 | 17.17 | 16.98 |
| 46.00 | 19.01 | 51.56 | 24.06 | 15.48 | 15.93 |
| 41.02 | 16.23 | 46.88 | 19.96 | 14.15 | 14.75 |
| 34.97 | 14.97 | 41.33 | 17.47 | 12.67 | 13.04 |
| 28.41 | 13.30 | 34.77 | 14.42 | 11.22 | 11.18 |
| 20.57 | 10.53 | 26.29 | 10.93 | 8.31 | 8.42 |
| 14.59 | 7.71 | 19.28 | 7.66 | 5.97 | 5.96 |

| Cycle 4 | | | | | |
|---|---|---|---|---|---|
| Pressure loss (sensors) | | Pressure loss (straing gauges) | | Calibrated discharge | |
| 4 in. (kPa/m) | 5 in. (kPa/m) | 4 in. (kPa/m) | 5 in. (kPa/m) | File (l/s) | Stopwatch (l/s) |
| 67.72 | 32.44 | 68.02 | 39.21 | 17.55 | 17.22 |
| 53.73 | 25.73 | 58.70 | 25.49 | 16.11 | 16.11 |
| 47.43 | 24.77 | 52.78 | 23.77 | 15.25 | 15.14 |
| 40.21 | 21.72 | 46.36 | 19.98 | 13.90 | 14.04 |
| 35.39 | 19.04 | 41.15 | 17.37 | 12.32 | 12.33 |
| 28.27 | 16.33 | 34.31 | 14.01 | 10.23 | 10.25 |
| 21.09 | 12.73 | 26.46 | 10.96 | 7.50 | 7.49 |
| 14.80 | 9.80 | 19.04 | 7.91 | 4.93 | 4.91 |

| Cycle 5 | | | | | |
|---|---|---|---|---|---|
| Pressure loss (sensors) | | Pressure loss (straing gauges) | | Calibrated discharge | |
| 4 in. (kPa/m) | 5 in. (kPa/m) | 4 in. (kPa/m) | 5 in. (kPa/m) | File (l/s) | Stopwatch (l/s) |
| 80.52 | 41.38 | 79.19 | 41.70 | 17.75 | 17.70 |
| 66.25 | 30.23 | 67.44 | 31.55 | 16.36 | 16.21 |
| 55.22 | 26.75 | 59.93 | 28.96 | 15.18 | 15.15 |
| 49.29 | 23.85 | 54.03 | 25.83 | 13.84 | 13.84 |
| 44.44 | 21.62 | 49.37 | 23.75 | 12.42 | 12.44 |
| 37.10 | 18.04 | 42.31 | 20.25 | 10.27 | 10.29 |
| 29.45 | 14.91 | 35.27 | 16.50 | 7.36 | 7.40 |
| 20.16 | 10.94 | 25.96 | 12.06 | 4.07 | 4.05 |

**Potential non-equilibrium**

**Potentially wrong data**

**No discharge calibration available**

**Measurements treatment for the 5 in.-pipes sensors was performed with the help of the strain gauges**

***Table C.6:*** *Pressure loss of SCC3 measured at different discharge rates in 4 in. and 5 in. pipes.*

**SCC3**

| Cycle 1 | | | | | |
|---|---|---|---|---|---|
| Pressure loss (sensors) | | Pressure loss (straing gauges) | | Calibrated discharge | |
| 4 in (kPa/m) | 5 in. (kPa/m) | 4 in. (kPa/m) | 5 in. (kPa/m) | File (l/s) | Stopwatch (l/s) |
| 91.09 | | 91.34 | | 15.47 | 15.70 |
| 73.72 | 34.53 | 74.85 | 32.43 | 14.59 | 14.57 |
| 65.70 | 27.85 | 67.75 | 27.54 | 13.71 | 13.75 |
| 57.02 | 24.83 | 60.18 | 25.31 | 12.54 | 12.71 |
| 47.28 | 20.88 | 51.94 | 21.42 | 11.28 | 11.34 |
| 33.49 | 15.52 | 40.63 | 16.16 | 8.93 | 8.96 |
| 25.28 | 11.68 | 31.97 | 12.24 | 6.95 | 6.97 |
| 15.27 | 7.41 | 19.95 | 7.26 | 4.04 | 4.04 |

| Cycle 2 | | | | | |
|---|---|---|---|---|---|
| Pressure loss (sensors) | | Pressure loss (straing gauges) | | Calibrated discharge | |
| 4 in. (kPa/m) | 5 in. (kPa/m) | 4 in (kPa/m) | 5 in (kPa/m) | File (l/s) | Stopwatch (l/s) |
| 60.53 | 32.12 | 67.28 | | 14.82 | 14.82 |
| 52.51 | 24.45 | 59.55 | 23.77 | 13.97 | 13.96 |
| 45.74 | 21.23 | 52.93 | 20.96 | 12.80 | 12.91 |
| 39.83 | 18.46 | 47.40 | 18.52 | 11.58 | 11.66 |
| 34.16 | 15.90 | 41.55 | 16.47 | 10.41 | 10.41 |
| 26.25 | 12.39 | 33.83 | 12.82 | 8.32 | 8.30 |
| 18.82 | 9.38 | 25.00 | 9.81 | 6.12 | 6.11 |
| 14.56 | 7.47 | 19.48 | 6.91 | 4.57 | 4.55 |

| Cycle 3 | | | | | |
|---|---|---|---|---|---|
| Pressure loss (sensors) | | Pressure loss (straing gauges) | | Calibrated discharge | |
| 4 in. (kPa/m) | 5 in. (kPa/m) | 4 in. (kPa/m) | 5 in. (kPa/m) | File (l/s) | Stopwatch (l/s) |
| 58.53 | 30.17 | 64.91 | 23.84 | 15.29 | 15.40 |
| 51.42 | 25.87 | 58.04 | 21.86 | 14.50 | 14.64 |
| 45.51 | 22.33 | 52.36 | 19.20 | 13.49 | 13.67 |
| 39.46 | 19.30 | 46.50 | 16.84 | 12.11 | 12.24 |
| 32.60 | 16.07 | 39.71 | 14.33 | 10.32 | 10.32 |
| 26.32 | 13.61 | 33.23 | 12.43 | 8.67 | 8.73 |
| 20.83 | 10.71 | 26.78 | 9.88 | 6.72 | 6.74 |
| 14.45 | 7.80 | 19.06 | 7.20 | 4.38 | 4.37 |

| Cycle 4 | | | | | |
|---|---|---|---|---|---|
| Pressure loss (sensors) | | Pressure loss (straing gauges) | | Calibrated discharge | |
| 4 in. (kPa/m) | 5 in. (kPa/m) | 4 in. (kPa/m) | 5 in. (kPa/m) | File (l/s) | Stopwatch (l/s) |
| 60.07 | 30.83 | 65.66 | 23.49 | 14.71 | 14.71 |
| 52.29 | 26.24 | 58.05 | 21.02 | 13.86 | 13.90 |
| 45.10 | 22.67 | 51.37 | 18.69 | 12.73 | 12.78 |
| 40.54 | 19.97 | 47.01 | 16.72 | 11.60 | 11.75 |
| 34.95 | 17.50 | 41.05 | 15.06 | 10.19 | 10.19 |
| 27.84 | 14.22 | 34.15 | 12.37 | 7.95 | 7.94 |
| 20.94 | 11.13 | 26.92 | 9.99 | 5.66 | 5.69 |
| 14.81 | 8.42 | 19.57 | 7.69 | 3.27 | 3.26 |

**Potential non-equilibrium**

**Potential error**

**Measurements treatment of sensors of 5 in. was performed with the help of the strain gauges**

***Table C.7:*** *Pressure loss of SCC4 measured at different discharge rates in 4 in. and 5 in. pipes.*

**SCC4**

| Cycle 1 | | | | | |
|---|---|---|---|---|---|
| Pressure loss (sensors) | | Pressure loss (straing gauges) | | Calibrated discharge | |
| 4 in (kPa/m) | 5 in (kPa/m) | 4 in. (kPa/m) | 5 in. (kPa/m) | File (l/s) | Stopwatch (l/s) |
| 108.30 | 59.01 | 118.02 | | 15.18 | 15.19 |
| 92.31 | 52.57 | 97.23 | 50.64 | 14.24 | 14.23 |
| 81.32 | 46.89 | 82.04 | 46.46 | 13.48 | 13.32 |
| 69.14 | 39.95 | 69.65 | 40.61 | 12.11 | 12.21 |
| 59.80 | 34.39 | 59.74 | 35.19 | 11.03 | 11.02 |
| 48.12 | 27.91 | 47.22 | 29.10 | 9.14 | 9.20 |
| 33.31 | 19.20 | 31.78 | 20.69 | 6.44 | 6.47 |
| 20.96 | 11.30 | 19.41 | 12.93 | 3.72 | 3.71 |

| Cycle 2 | | | | | |
|---|---|---|---|---|---|
| Pressure loss (sensors) | | Pressure loss (straing gauges) | | Calibrated discharge | |
| 4 in. (kPa/m) | 5 in. (kPa/m) | 4 in. (kPa/m) | 5 in. (kPa/m) | File (l/s) | Stopwatch (l/s) |
| **74.54** | **40.94** | **75.85** | **44.45** | 13.93 | 13.80 |
| **63.14** | **38.80** | **65.06** | **42.09** | 12.99 | 12.91 |
| 56.08 | 33.03 | 57.39 | 36.03 | 11.88 | 11.91 |
| 49.47 | 30.09 | 50.61 | 32.93 | 10.65 | 10.68 |
| 38.73 | 24.19 | 39.13 | 26.38 | 8.56 | 8.56 |
| 27.15 | 16.76 | 25.85 | 17.84 | 5.69 | 5.67 |
| 16.40 | 9.89 | 15.26 | 10.30 | 3.06 | 3.07 |

| Cycle 3 | | | | | |
|---|---|---|---|---|---|
| Pressure loss (sensors) | | Pressure loss (straing gauges) | | Calibrated discharge | |
| 4 in (kPa/m) | 5 in. (kPa/m) | 4 in. (kPa/m) | 5 in. (kPa/m) | File (l/s) | Stopwatch (l/s) |
| **59.44** | **38.84** | **62.72** | **36.75** | 14.08 | 14.08 |
| 53.43 | 34.66 | 56.12 | 32.93 | 13.20 | 13.04 |
| 47.34 | 30.95 | 49.59 | 29.98 | 12.17 | 12.21 |
| 42.70 | 27.25 | 43.66 | 26.47 | 10.99 | 10.98 |
| 34.94 | 22.10 | 34.44 | 21.64 | 9.01 | 9.01 |
| 25.14 | 15.66 | 23.66 | 15.27 | 6.22 | 6.22 |
| 16.31 | 10.36 | 15.20 | 10.26 | 3.77 | 3.78 |

| Cycle 4 | | | | | |
|---|---|---|---|---|---|
| Pressure loss (sensors) | | Pressure loss (straing gauges) | | Calibrated discharge | |
| 4 in. (kPa/m) | 5 in. (kPa/m) | 4 in. (kPa/m) | 5 in. (kPa/m) | File (l/s) | Stopwatch (l/s) |
| **53.89** | **31.28** | **57.38** | **30.69** | 13.70 | 14.07 |
| **49.17** | 31.71 | **51.71** | 30.67 | 13.06 | 13.08 |
| 42.48 | 26.61 | 43.63 | 25.91 | 11.66 | 11.60 |
| 37.50 | 23.93 | 37.49 | 23.37 | 10.25 | 10.28 |
| 30.60 | 19.81 | 29.45 | 18.76 | 8.44 | 8.48 |
| 21.55 | 14.11 | 20.21 | 12.91 | 5.63 | 5.61 |
| 14.41 | 9.07 | 13.38 | 8.86 | 3.38 | 3.36 |

| Cycle 5 | | | | | |
|---|---|---|---|---|---|
| Pressure loss (sensors) | | Pressure loss (straing gauges) | | Calibrated discharge | |
| 4 in (kPa/m) | 5 in (kPa/m) | 4 in. (kPa/m) | 5 in. (kPa/m) | File (l/s) | Stopwatch (l/s) |
| 53.10 | **34.76** | **55.52** | **32.10** | 13.77 | 14.07 |
| 50.55 | 32.47 | 51.10 | 30.77 | 13.06 | 13.10 |
| 43.67 | 28.00 | 43.41 | 26.98 | 11.71 | 11.81 |
| 38.97 | 25.11 | 38.24 | 24.58 | 10.56 | 10.72 |
| 31.10 | 20.48 | 29.70 | 20.01 | 8.65 | 8.59 |
| 23.06 | 15.44 | 21.79 | 14.74 | 6.28 | 6.29 |
| 13.98 | 9.24 | 13.21 | 9.30 | 3.32 | 3.32 |

**Potential non-equilibrium**

**Non-trusted result**

**Measurements treatment for the 4 in.-pipes sensors was performed with the help of the strain gauges**

***Table C.8:*** *Pressure loss of SCC5 measured at different discharge rates in 4 in. and 5 in. pipes.*

**SCC5**

| Cycle 1 | | | | | |
|---|---|---|---|---|---|
| Pressure loss (sensors) | | Pressure loss (straing gauges) | | Calibrated discharge | |
| 4 in. (kPa/m) | 5 in. (kPa/m) | 4 in. (kPa/m) | 5 in. (kPa/m) | File (l/s) | Stopwatch (l/s) |
| **40.51** | **24.49** | **48.56** | **27.56** | 14.97 | 14.99 |
| 39.41 | 21.64 | 43.62 | 25.01 | 14.20 | 14.20 |
| **33.92** | **19.99** | **36.46** | **22.63** | 13.06 | 13.13 |
| 28.45 | 17.12 | 31.03 | 19.77 | 11.91 | 11.92 |
| 23.83 | 15.23 | 26.20 | 17.37 | 10.69 | 10.77 |
| 16.59 | 11.02 | 19.05 | 12.61 | 8.13 | 8.09 |
| 10.68 | 7.58 | 13.24 | 8.89 | 5.63 | 5.61 |
| 8.89 | 6.63 | 11.48 | 7.64 | 4.78 | 4.80 |

| Cycle 2 | | | | | |
|---|---|---|---|---|---|
| Pressure loss (sensors) | | Pressure loss (straing gauges) | | Calibrated discharge | |
| 4 in. (kPa/m) | 5 in. (kPa/m) | 4 in. (kPa/m) | 5 in. (kPa/m) | File (l/s) | Stopwatch (l/s) |
| **40.00** | **20.93** | **39.39** | **23.07** | 15.15 | 14.97 |
| 34.69 | 18.67 | 34.57 | 20.94 | 14.11 | 14.02 |
| 29.12 | 16.89 | 29.42 | 18.89 | 12.86 | 12.82 |
| 24.30 | 14.99 | 25.20 | 16.37 | 11.68 | 11.63 |
| 20.85 | 13.08 | 22.01 | 14.46 | 10.50 | 10.44 |
| 14.74 | 9.60 | 16.45 | 10.55 | 7.93 | 7.94 |
| 9.93 | 6.90 | 11.91 | 7.71 | 5.76 | 5.73 |
| 9.62 | 6.85 | 11.54 | 7.13 | 5.53 | 5.51 |

| Cycle 3 | | | | | |
|---|---|---|---|---|---|
| Pressure loss (sensors) | | Pressure loss (straing gauges) | | Calibrated discharge | |
| 4 in. (kPa/m) | 5 in. (kPa/m) | 4 in. (kPa/m) | 5 in. (kPa/m) | File (l/s) | Stopwatch (l/s) |
| **31.78** | **18.15** | **32.32** | **20.24** | 15.53 | 15.54 |
| 30.48 | 17.08 | 30.50 | 19.50 | 14.53 | 14.50 |
| 24.74 | 15.22 | 25.58 | 17.79 | 13.50 | 13.50 |
| 23.04 | 13.69 | 23.10 | 15.97 | 12.28 | 12.20 |
| 19.05 | 11.90 | 19.30 | 13.58 | 10.74 | 10.62 |
| 14.45 | 9.03 | 15.33 | 10.41 | 8.39 | 8.40 |
| 9.65 | 6.52 | 10.80 | 7.72 | 6.13 | 6.14 |
| 9.32 | 6.40 | 10.38 | 7.36 | 5.84 | 5.84 |

| Cycle 4 | | | | | |
|---|---|---|---|---|---|
| Pressure loss (sensors) | | Pressure loss (straing gauges) | | Calibrated discharge | |
| 4 in. (kPa/m) | 5 in. (kPa/m) | 4 in. (kPa/m) | 5 in. (kPa/m) | File (l/s) | Stopwatch (l/s) |
| **31.09** | **16.28** | **29.25** | **18.69** | 14.97 | 14.96 |
| 27.47 | 14.99 | 26.24 | 17.37 | 13.88 | 13.92 |
| 23.67 | 13.68 | 22.76 | 15.95 | 12.72 | 12.72 |
| 21.01 | 12.25 | 20.50 | 14.18 | 11.57 | 11.62 |
| 17.43 | 10.38 | 17.38 | 12.20 | 10.10 | 10.11 |
| 13.22 | 8.12 | 13.92 | 9.65 | 7.98 | 7.98 |
| 9.86 | 6.41 | 10.90 | 7.42 | 6.21 | 6.24 |
| 9.33 | 6.15 | 10.66 | 7.04 | 5.92 | 5.89 |

| Cycle 5 | | | | | |
|---|---|---|---|---|---|
| Pressure loss (sensors) | | Pressure loss (straing gauges) | | Calibrated discharge | |
| 4 in. (kPa/m) | 5 in. (kPa/m) | 4 in. (kPa/m) | 5 in. (kPa/m) | File (l/s) | Stopwatch (l/s) |
| **31.44** | **16.52** | **29.48** | **19.07** | 14.79 | 14.75 |
| **26.39** | **14.93** | **24.79** | **17.29** | 13.80 | 13.74 |
| 23.67 | 13.33 | 22.42 | 15.19 | 12.66 | 12.70 |
| 21.08 | 12.39 | 20.22 | 14.62 | 11.91 | 11.94 |
| 16.91 | 10.24 | 17.00 | 12.07 | 9.89 | 9.90 |
| 12.07 | 7.69 | 12.88 | 9.36 | 7.58 | 7.55 |
| 9.74 | 6.20 | 10.98 | 7.45 | 6.18 | 6.16 |
| 9.35 | 6.21 | 10.67 | 7.36 | 5.96 | 5.99 |

**Potential non-equilibrium**

**Measurements treatment for the 4 in.-pipes sensors was performed with the help of the strain gauges**

***Table C.9:*** *Pressure loss of SCC6 measured at different discharge rates in 4 in. and 5 in. pipes.*

**SCC6**

| Cycle 1 | | | | | |
|---|---|---|---|---|---|
| Pressure loss (sensors) | | Pressure loss (straing gauges) | | Calibrated discharge | |
| 4 in. (kPa/m) | 5 in. (kPa/m) | 4 in. (kPa/m) | 5 in. (kPa/m) | File (l/s) | Stopwatch (l/s) |
| 19.25 | 10.18 | 16.77 | 5.29 | | |
| 29.43 | 15.96 | 26.50 | 9.84 | | |
| 44.30 | 22.15 | 39.80 | 11.36 | | |
| 48.00 | 24.97 | 41.62 | 9.53 | | |
| 53.85 | 27.09 | 45.35 | 10.25 | | |

| Cycle 2 | | | | | |
|---|---|---|---|---|---|
| Pressure loss (sensors) | | Pressure loss (straing gauges) | | Calibrated discharge | |
| 4 in. (kPa/m) | 5 in. (kPa/m) | 4 in. (kPa/m) | 5 in. (kPa/m) | File (l/s) | Stopwatch (l/s) |
| 13.95 | 8.02 | 13.54 | 9.45 | | |
| 22.15 | 11.43 | 22.33 | 14.92 | | |
| 31.82 | 15.60 | 31.10 | 17.99 | | |
| 37.95 | 19.41 | 37.27 | 21.37 | | |
| 48.75 | 22.36 | 44.81 | 23.64 | | |

| Cycle 3 | | | | | |
|---|---|---|---|---|---|
| Pressure loss (sensors) | | Pressure loss (straing gauges) | | Calibrated discharge | |
| 4 in. (kPa/m) | 5 in. (kPa/m) | 4 in. (kPa/m) | 5 in. (kPa/m) | File (l/s) | Stopwatch (l/s) |
| 15.63 | 7.16 | 14.31 | 6.56 | | |
| 24.62 | 11.46 | 23.64 | 11.36 | | |
| 31.28 | 14.77 | 29.92 | 14.19 | | |
| 37.07 | 19.22 | 36.32 | 17.22 | | |
| 43.75 | 21.31 | 41.17 | 19.09 | | |

**Potential non-equilibrium**

**No discharge calibration available**

**Measurements treatment for the 4 in.-pipes sensors was performed with the help of the strain gauges**

***Table C.10:*** *Pressure loss of SCC7 measured at different discharge rates in 4 in. and 5 in. pipes.*

**SCC7**

| Cycle 1 | | | | | |
|---|---|---|---|---|---|
| Pressure loss (sensors) | | Pressure loss (straing gauges) | | Calibrated discharge | |
| 4 in (kPa/m) | 5 in (kPa/m) | 4 in. (kPa/m) | 5 in. (kPa/m) | File (l/s) | Stopwatch (l/s) |
| 121.44 | 51.48 | 121.44 | 48.04 | 11.99 | 11.99 |
| 89.35 | 37.71 | 89.35 | 29.69 | 8.82 | 8.79 |
| 70.33 | 30.12 | 70.33 | 20.57 | 6.94 | 6.92 |
| 44.27 | 19.43 | 44.27 | 12.97 | 4.17 | 4.13 |
| 24.82 | 10.81 | 24.82 | 8.70 | 2.20 | 2.21 |

| Cycle 2 | | | | | |
|---|---|---|---|---|---|
| Pressure loss (sensors) | | Pressure loss (straing gauges) | | Calibrated discharge | |
| 4 in (kPa/m) | 5 in (kPa/m) | 4 in. (kPa/m) | 5 in (kPa/m) | File (l/s) | Stopwatch (l/s) |
| 113.71 | 47.27 | 113.71 | 46.28 | 11.23 | 11.25 |
| 99.41 | 40.86 | 99.41 | 38.00 | 9.88 | 9.88 |
| 83.55 | 35.21 | 83.55 | 31.27 | 8.42 | 8.41 |
| 65.38 | 26.66 | 65.38 | 23.88 | 6.56 | 6.55 |
| 35.28 | 13.32 | 35.28 | 12.34 | 3.25 | 3.24 |
| 22.15 | 9.23 | 22.15 | 8.01 | 1.93 | 1.93 |

| Cycle 3 | | | | | |
|---|---|---|---|---|---|
| Pressure loss (sensors) | | Pressure loss (straing gauges) | | Calibrated discharge | |
| 4 in. (kPa/m) | 5 in. (kPa/m) | 4 in. (kPa/m) | 5 in. (kPa/m) | File (l/s) | Stopwatch (l/s) |
| **112.68** | **46.52** | **112.68** | **44.39** | 11.88 | 11.87 |
| 101.25 | 41.35 | 101.25 | 39.19 | 10.84 | 10.77 |
| 84.23 | 34.72 | 84.23 | 30.78 | 8.94 | 8.97 |
| 63.42 | 26.06 | 63.42 | 22.28 | 6.67 | 6.66 |
| 33.48 | 13.95 | 33.48 | 11.63 | 3.26 | 3.26 |
| 21.47 | 9.65 | 21.47 | 7.99 | 1.95 | 1.94 |

| Cycle 4 | | | | | |
|---|---|---|---|---|---|
| Pressure loss (sensors) | | Pressure loss (straing gauges) | | Calibrated discharge | |
| 4 in. (kPa/m) | 5 in (kPa/m) | 4 in. (kPa/m) | 5 in. (kPa/m) | File (l/s) | Stopwatch (l/s) |
| 109.86 | 45.77 | 109.86 | 45.58 | 11.49 | 11.49 |
| 96.62 | 39.34 | 96.62 | 38.57 | 10.30 | 10.32 |
| 79.34 | 30.63 | 79.34 | 30.12 | 8.36 | 8.37 |
| 60.72 | 22.48 | 60.72 | 22.58 | 6.38 | 6.39 |
| 27.04 | 10.61 | 27.04 | 10.91 | 2.67 | 2.66 |
| 19.75 | 9.06 | 19.75 | 7.97 | 1.76 | 1.76 |

**Potential non-equilibrium**

**Measurements treatment for the 4 in.-pipes sensors was performed with the help of the strain gauges**

***Table C.11:*** *Pressure loss of SCC8 measured at different discharge rates in 4 in. and 5 in. pipes.*

## SCC8

| Cycle 1 | | | | | |
|---|---|---|---|---|---|
| Pressure loss (sensors) | | Pressure loss (straing gauges) | | Calibrated discharge | |
| 4 in. (kPa/m) | 5 in. (kPa/m) | 4 in. (kPa/m) | 5 in. (kPa/m) | File (l/s) | Stopwatch (l/s) |
| **122.18** | **47.05** | **122.18** | **50.00** | 11.44 | 11.42 |
| 104.51 | 40.15 | 104.51 | 41.70 | 10.17 | 10.21 |
| 85.29 | 32.65 | 85.29 | 32.86 | 8.52 | 8.49 |
| 63.58 | 24.12 | 63.58 | 23.31 | 6.39 | 6.39 |
| 31.73 | 12.91 | 31.73 | 12.16 | 3.23 | 3.23 |
| 21.14 | 8.73 | 21.14 | 8.36 | 2.06 | 2.07 |

| Cycle 2 | | | | | |
|---|---|---|---|---|---|
| Pressure loss (sensors) | | Pressure loss (straing gauges) | | Calibrated discharge | |
| 4 in. (kPa/m) | 5 in. (kPa/m) | 4 in. (kPa/m) | 5 in. (kPa/m) | File (l/s) | Stopwatch (l/s) |
| **110.94** | **41.70** | **110.94** | **44.61** | 11.28 | 11.31 |
| **95.28** | **36.06** | **95.28** | **37.53** | 10.17 | 10.14 |
| 74.14 | 27.69 | 74.14 | 27.28 | 8.09 | 8.13 |
| 52.23 | 19.54 | 52.23 | 18.51 | 5.75 | 5.78 |
| 24.74 | 9.78 | 24.74 | 9.43 | 2.69 | 2.69 |
| 22.24 | 8.71 | 22.24 | 8.36 | 2.29 | 2.29 |

| Cycle 3 | | | | | |
|---|---|---|---|---|---|
| Pressure loss (sensors) | | Pressure loss (straing gauges) | | Calibrated discharge | |
| 4 in. (kPa/m) | 5 in. (kPa/m) | 4 in. (kPa/m) | 5 in. (kPa/m) | File (l/s) | Stopwatch (l/s) |
| 108.60 | 40.51 | 108.60 | 40.66 | 12.04 | 12.09 |
| 94.32 | 35.77 | 94.32 | 34.65 | 10.70 | 10.76 |
| 73.05 | 27.18 | 73.05 | 24.63 | 8.49 | 8.56 |
| 52.37 | 19.90 | 52.37 | 17.17 | 6.16 | 6.18 |
| 28.79 | 11.84 | 28.79 | 10.07 | 3.48 | 3.48 |
| 21.57 | 8.73 | 21.57 | 7.80 | 2.46 | 2.46 |

| Cycle 4 | | | | | |
|---|---|---|---|---|---|
| Pressure loss (sensors) | | Pressure loss (straing gauges) | | Calibrated discharge | |
| 4 in. (kPa/m) | 5 in. (kPa/m) | 4 in. (kPa/m) | 5 in. (kPa/m) | File (l/s) | Stopwatch (l/s) |
| 97.88 | 36.65 | 97.88 | 38.22 | 11.23 | 11.15 |
| 85.43 | 32.49 | 85.43 | 33.58 | 10.13 | 10.29 |
| 69.36 | 25.85 | 69.36 | 25.60 | 8.31 | 8.34 |
| 47.86 | 17.96 | 47.86 | 17.27 | 5.82 | 5.83 |
| 26.04 | 10.29 | 26.04 | 9.68 | 3.14 | 3.14 |
| 20.96 | 8.56 | 20.96 | 7.95 | 2.41 | 2.57 |

| Cycle 5 | | | | | |
|---|---|---|---|---|---|
| Pressure loss (sensors) | | Pressure loss (straing gauges) | | Calibrated discharge | |
| 4 in. (kPa/m) | 5 in. (kPa/m) | 4 in. (kPa/m) | 5 in. (kPa/m) | File (l/s) | Stopwatch (l/s) |
| 97.20 | 37.09 | 97.20 | 39.59 | 11.13 | 11.17 |
| 84.73 | 32.89 | 84.73 | 35.00 | 10.09 | 10.21 |
| 67.29 | 25.90 | 67.29 | 26.42 | 8.07 | 8.08 |
| 45.90 | 17.89 | 45.90 | 17.59 | 5.51 | 5.49 |
| 23.31 | 9.87 | 23.31 | 9.46 | 2.76 | 2.76 |
| 20.35 | 8.79 | 20.35 | 8.35 | 2.28 | 2.28 |

**Potential non-equilibrium**

**Pressure sensors measurements in 4 in.-pipes was obtained with the help of the straing gauges**

***Table C.12:*** *Pressure loss of SCC9 measured at different discharge rates in 4 in. and 5 in. pipes.*

**SCC9**

| Cycle 1 | | | | | |
|---|---|---|---|---|---|
| Pressure loss (sensors) | | Pressure loss (straing gauges) | | Calibrated discharge | |
| 4 in (kPa/m) | 5 in (kPa/m) | 4 in. (kPa/m) | 5 in. (kPa/m) | File (l/s) | Stopwatch (l/s) |
| **39.98** | 16.40 | **39.98** | 14.69 | 16.29 | 16.26 |
| **35.63** | 15.40 | **35.63** | 14.36 | 15.30 | 15.35 |
| **31.62** | 13.68 | **31.62** | 12.63 | 14.08 | 14.03 |
| **26.81** | 11.95 | **26.81** | 10.85 | 12.43 | 12.47 |
| **22.62** | 10.43 | **22.62** | 9.26 | 11.04 | 11.04 |
| 16.90 | 8.35 | 16.90 | 7.44 | 8.70 | 8.70 |
| 11.83 | 6.45 | 11.83 | 5.76 | 6.36 | 6.36 |
| 10.80 | 5.74 | 10.80 | 5.06 | 5.57 | 5.60 |

| Cycle 2 | | | | | |
|---|---|---|---|---|---|
| Pressure loss (sensors) | | Pressure loss (straing gauges) | | Calibrated discharge | |
| 4 in. (kPa/m) | 5 in. (kPa/m) | 4 in (kPa/m) | 5 in. (kPa/m) | File (l/s) | Stopwatch (l/s) |
| **34.77** | 14.59 | **34.77** | | 15.88 | 15.90 |
| **30.74** | 13.21 | **30.74** | 13.36 | 14.76 | 15.00 |
| 27.40 | 11.92 | 27.40 | 11.75 | 13.77 | 13.71 |
| 23.10 | 10.54 | 23.10 | 10.17 | 12.18 | 12.15 |
| 19.00 | 9.16 | 19.00 | 8.63 | 10.54 | 10.55 |
| 14.60 | 7.53 | 14.60 | 6.76 | 8.37 | 8.39 |
| 10.78 | 6.14 | 10.78 | 5.52 | 6.36 | 6.37 |
| 10.47 | 5.69 | 10.47 | 5.42 | 6.01 | 6.00 |

| Cycle 3 | | | | | |
|---|---|---|---|---|---|
| Pressure loss (sensors) | | Pressure loss (straing gauges) | | Calibrated discharge | |
| 4 in (kPa/m) | 5 in. (kPa/m) | 4 in. (kPa/m) | 5 in. (kPa/m) | File (l/s) | Stopwatch (l/s) |
| 33.64 | 13.63 | 33.64 | | 16.08 | 16.18 |
| 30.12 | 12.31 | 30.12 | 11.37 | 15.11 | 15.21 |
| 27.37 | 11.33 | 27.37 | 10.43 | 14.08 | 14.18 |
| 23.22 | 10.04 | 23.22 | 9.26 | 12.43 | 12.49 |
| 19.57 | 8.78 | 19.57 | 8.24 | 10.83 | 10.82 |
| 15.41 | 7.21 | 15.41 | 6.98 | 8.67 | 8.63 |
| 11.56 | 5.63 | 11.56 | 5.44 | 6.52 | 6.50 |
| 11.24 | 5.48 | 11.24 | 5.28 | 6.24 | 6.28 |

| Cycle 4 | | | | | |
|---|---|---|---|---|---|
| Pressure loss (sensors) | | Pressure loss (straing gauges) | | Calibrated discharge | |
| 4 in. (kPa/m) | 5 in. (kPa/m) | 4 in. (kPa/m) | 5 in (kPa/m) | File (l/s) | Stopwatch (l/s) |
| 31.85 | 12.90 | 31.85 | 11.57 | 15.88 | 15.81 |
| 28.57 | 11.60 | 28.57 | 10.47 | 14.76 | 14.79 |
| 25.53 | 10.30 | 25.53 | 9.77 | 13.54 | 13.47 |
| 21.40 | 8.77 | 21.40 | 8.52 | 11.81 | 11.84 |
| 18.72 | 8.00 | 18.72 | 8.03 | 10.54 | 10.49 |
| 14.15 | 6.55 | 14.15 | 6.49 | 8.21 | 8.19 |
| 11.09 | 5.36 | 11.09 | 5.54 | 6.44 | 6.43 |
| 10.52 | 5.04 | 10.52 | 5.41 | 6.14 | 6.09 |

**Potential non-equilibrium**

**Non-trusted data**

**Measurements treatment for the 4 in.-pipes sensors was performed with the help of the strain gauges**

***Table C.13:*** *Pressure loss of SCC10 measured at different discharge rates in 4 in. and 5 in. pipes.*

## SCC10

| Cycle 1 | | | |
|---|---|---|---|
| Pressure loss (straing gauges) | | Calibrated discharge | |
| 4 in. (kPa/m) | 5 in. (kPa/m) | File (l/s) | Stopwatch (l/s) |
| - | - | - | - |
| - | - | - | - |
| - | - | - | - |
| 67.89 | 38.49 | 11.42 | 11.52 |
| 56.08 | 31.03 | 9.42 | 9.42 |
| 43.05 | 23.84 | 7.31 | 7.33 |
| 26.50 | 13.44 | 4.19 | 4.19 |
| 16.06 | 8.12 | 2.32 | 2.31 |

| Cycle 2 | | | |
|---|---|---|---|
| Pressure loss (straing gauges) | | Calibrated discharge | |
| 4 in. (kPa/m) | 5 in. (kPa/m) | File (l/s) | Stopwatch (l/s) |
| 77.39 | 44.74 | 14.89 | 14.77 |
| 72.54 | 40.94 | 13.77 | 13.67 |
| 65.81 | 35.59 | 12.46 | 12.32 |
| 59.28 | 32.53 | 11.05 | 11.03 |
| 48.87 | 25.81 | 8.89 | 8.89 |
| 37.77 | 20.13 | 6.74 | 6.76 |
| 23.26 | 12.09 | 3.82 | 3.82 |
| 11.05 | 6.13 | 1.44 | 1.42 |

| Cycle 3 | | | |
|---|---|---|---|
| Pressure loss (straing gauges) | | Calibrated discharge | |
| 4 in. (kPa/m) | 5 in. (kPa/m) | File (l/s) | Stopwatch (l/s) |
| 75.78 | 44.85 | 15.47 | 15.28 |
| 71.43 | 43.41 | 14.50 | 14.50 |
| 64.83 | 38.59 | 13.31 | 13.44 |
| 59.79 | 34.22 | 12.02 | 12.02 |
| 49.11 | 27.56 | 9.49 | 9.53 |
| 39.00 | 21.30 | 7.33 | 7.31 |
| 24.63 | 12.79 | 4.25 | 4.26 |
| 11.53 | 6.20 | 1.53 | 1.52 |

| Cycle 4 | | | |
|---|---|---|---|
| Pressure loss (straing gauges) | | Calibrated discharge | |
| 4 in. (kPa/m) | 5 in. (kPa/m) | File (l/s) | Stopwatch (l/s) |
| 72.74 | 43.28 | 14.89 | 14.87 |
| 65.33 | 39.11 | 13.70 | 13.63 |
| 60.95 | 35.91 | 12.69 | 12.59 |
| 54.90 | 32.57 | 11.32 | 11.32 |
| 44.16 | 26.44 | 8.72 | 8.72 |
| 32.88 | 19.33 | 6.17 | 6.18 |
| 20.56 | 12.74 | 3.43 | 3.43 |
| 10.92 | 6.21 | 1.35 | 1.35 |

***Table C.14:*** *Pressure loss of SCC11 measured at different discharge rates in 4 in. and 5 in. pipes.*

## SCC11

| Cycle 1 | | | |
|---|---|---|---|
| Pressure loss (straing gauges) | | Calibrated discharge | |
| 4 in. (kPa/m) | 5 in. (kPa/m) | File (l/s) | Stopwatch (l/s) |
| **65.42** | **35.11** | 14.32 | 14.51 |
| **58.23** | **30.76** | 13.44 | 13.64 |
| 51.87 | 25.83 | 12.01 | 12.04 |
| 45.53 | 22.66 | 10.80 | 10.82 |
| 37.32 | 18.69 | 8.97 | 8.85 |
| 27.64 | 13.31 | 6.53 | 6.50 |
| 13.71 | 6.98 | 3.00 | 3.00 |
| 7.61 | 4.11 | 1.36 | 1.36 |

| Cycle 2 | | | |
|---|---|---|---|
| Pressure loss (straing gauges) | | Calibrated discharge | |
| 4 in. (kPa/m) | 5 in. (kPa/m) | File (l/s) | Stopwatch (l/s) |
| **62.03** | **32.87** | 14.64 | 14.62 |
| **55.64** | 29.88 | 13.65 | 13.60 |
| 49.68 | 25.36 | 12.41 | 12.42 |
| 43.99 | 22.96 | 11.13 | 11.04 |
| 34.11 | 17.40 | 8.54 | 8.56 |
| 24.17 | 12.35 | 5.97 | 5.97 |
| 10.43 | 5.18 | 2.28 | 2.28 |
| 7.63 | 4.01 | 1.41 | 1.41 |

| Cycle 3 | | | |
|---|---|---|---|
| Pressure loss (straing gauges) | | Calibrated discharge | |
| 4 in. (kPa/m) | 5 in. (kPa/m) | File (l/s) | Stopwatch (l/s) |
| **55.78** | **27.89** | 14.24 | 14.35 |
| **51.70** | 25.98 | 13.30 | 13.53 |
| **45.68** | 22.19 | 12.12 | 12.13 |
| 40.85 | 19.49 | 10.94 | 10.95 |
| 33.28 | 16.84 | 8.91 | 8.88 |
| 24.10 | 11.51 | 6.28 | 6.27 |
| 15.01 | 6.99 | 3.71 | 3.72 |
| 7.25 | 3.62 | 1.37 | 1.37 |

| Cycle 4 | | | |
|---|---|---|---|
| Pressure loss (straing gauges) | | Calibrated discharge | |
| 4 in. (kPa/m) | 5 in. (kPa/m) | File (l/s) | Stopwatch (l/s) |
| **56.85** | **31.35** | 14.09 | 14.01 |
| **50.18** | **28.47** | 12.78 | 12.74 |
| 44.75 | 24.48 | 11.63 | 11.49 |
| 39.59 | 21.72 | 10.36 | 10.33 |
| 31.20 | 16.81 | 8.05 | 8.05 |
| 21.71 | 11.84 | 5.47 | 5.46 |
| 12.72 | 7.24 | 2.91 | 2.91 |
| 7.58 | 4.68 | 1.30 | 1.30 |

| Cycle 5 | | | |
|---|---|---|---|
| Pressure loss (straing gauges) | | Calibrated discharge | |
| 4 in. (kPa/m) | 5 in. (kPa/m) | File (l/s) | Stopwatch (l/s) |
| **62.60** | **34.58** | 13.94 | 14.01 |
| **54.22** | 31.96 | 12.65 | 12.59 |
| 48.32 | 27.74 | 11.42 | 11.44 |
| 43.06 | 24.56 | 10.24 | 10.30 |
| 36.99 | 20.34 | 8.60 | 8.61 |
| 28.45 | 15.59 | 6.31 | 6.33 |
| 16.17 | 8.77 | 2.99 | 3.00 |
| 10.41 | 5.66 | 1.24 | 1.24 |

**Potential non-equilibrium**

***Table C.15:*** *Pressure loss of SCC12 measured at different discharge rates in 4 in. and 5 in. pipes.*

## SCC12

| Cycle 1 | | | |
|---|---|---|---|
| Pressure loss (straing gauges) | | Calibrated discharge | |
| 4 in. (kPa/m) | 5 in. (kPa/m) | File (l/s) | Stopwatch (l/s) |
| **137.49** | **63.08** | 12.63 | 12.61 |
| **121.24** | **57.47** | 11.75 | 11.93 |
| 96.87 | 46.50 | 9.68 | 9.64 |
| 65.55 | 31.67 | 6.75 | 6.75 |
| 40.22 | 19.95 | 4.21 | 4.21 |
| 16.79 | 8.70 | 1.43 | 1.43 |

| Cycle 2 | | | |
|---|---|---|---|
| Pressure loss (straing gauges) | | Calibrated discharge | |
| 4 in. (kPa/m) | 5 in. (kPa/m) | File (l/s) | Stopwatch (l/s) |
| **124.46** | **60.55** | 11.50 | 11.50 |
| 111.76 | 53.33 | 10.32 | 10.29 |
| 89.82 | 45.03 | 8.73 | 8.66 |
| 61.68 | 29.71 | 5.88 | 5.90 |
| 30.91 | 15.39 | 2.70 | 2.70 |
| 19.46 | 9.35 | 1.36 | 1.37 |

| Cycle 3 | | | |
|---|---|---|---|
| Pressure loss (straing gauges) | | Calibrated discharge | |
| 4 in. (kPa/m) | 5 in. (kPa/m) | File (l/s) | Stopwatch (l/s) |
| 131.07 | 62.36 | 12.29 | 12.22 |
| 115.61 | 56.14 | 11.00 | 11.15 |
| 89.07 | 43.53 | 8.62 | 8.59 |
| 67.62 | 33.39 | 6.41 | 6.45 |
| 39.49 | 20.36 | 3.39 | 3.38 |
| 21.69 | 10.86 | 1.33 | 1.34 |

| Cycle 4 | | | |
|---|---|---|---|
| Pressure loss (straing gauges) | | Calibrated discharge | |
| 4 in. (kPa/m) | 5 in. (kPa/m) | File (l/s) | Stopwatch (l/s) |
| **145.05** | **68.95** | 12.23 | 12.24 |
| 125.17 | 60.48 | 10.36 | 10.40 |
| 99.44 | 49.92 | 8.46 | 8.50 |
| 74.01 | 36.93 | 5.77 | 5.77 |
| 40.56 | 20.94 | 2.45 | 2.45 |
| 29.34 | 15.24 | 1.34 | 1.34 |

**Potential non-equilibrium**

***Table C.16:*** *Pressure loss of HWC1 measured at different discharge rates in 4 in. and 5 in. pipes.*

## HWC1

| Cycle 1 | | | |
|---|---|---|---|
| Pressure loss (straing gauges) | | Calibrated discharge | |
| 4 in. (kPa/m) | 5 in. (kPa/m) | File (l/s) | Stopwatch (l/s) |
| **161.00** | **83.84** | 12.58 | 12.58 |
| **140.75** | 74.24 | 11.06 | 11.05 |
| 115.02 | 60.21 | 9.20 | 9.18 |
| 85.13 | 42.78 | 6.70 | 6.72 |
| 45.58 | 18.69 | 3.26 | 3.27 |
| 24.63 | 7.97 | 1.38 | 1.35 |

| Cycle 2 | | | |
|---|---|---|---|
| Pressure loss (straing gauges) | | Calibrated discharge | |
| 4 in. (kPa/m) | 5 in. (kPa/m) | File (l/s) | Stopwatch (l/s) |
| 143.27 | 73.23 | 11.40 | 11.31 |
| 122.27 | 59.91 | 9.94 | 9.94 |
| 100.00 | 49.85 | 8.12 | 8.12 |
| 72.77 | 35.62 | 5.70 | 5.69 |
| 37.94 | 16.67 | 2.55 | 2.55 |
| 24.79 | 10.59 | 1.35 | 1.35 |

| Cycle 3 | | | |
|---|---|---|---|
| Pressure loss (straing gauges) | | Calibrated discharge | |
| 4 in. (kPa/m) | 5 in. (kPa/m) | File (l/s) | Stopwatch (l/s) |
| 154.64 | 81.41 | 13.68 | 13.59 |
| 140.19 | 74.15 | 12.41 | 12.44 |
| 126.02 | 64.80 | 11.11 | 11.10 |
| 105.43 | 48.61 | 9.11 | 9.13 |
| 76.97 | 33.18 | 6.29 | 6.29 |
| 43.67 | 14.78 | 3.04 | 3.03 |
| 25.90 | 7.41 | 1.35 | 1.35 |

| Cycle 4 | | | |
|---|---|---|---|
| Pressure loss (straing gauges) | | Calibrated discharge | |
| 4 in. (kPa/m) | 5 in. (kPa/m) | File (l/s) | Stopwatch (l/s) |
| 149.70 | 74.68 | 13.02 | 13.05 |
| 131.89 | 66.78 | 11.65 | 11.59 |
| 117.55 | 55.69 | 10.13 | 10.09 |
| 104.86 | 49.39 | 8.74 | 8.75 |
| 75.73 | 32.09 | 5.71 | 5.72 |
| 45.21 | 14.69 | 2.72 | 2.71 |
| 29.57 | 5.76 | 1.32 | 1.32 |

**Potential non-equilibrium**

*Table C.17: Pressure loss of HWC2 measured at different discharge rates in 4 in. and 5 in. pipes.*

## HWC2

| Cycle 1 | | | |
|---|---|---|---|
| Pressure loss (straing gauges) | | Calibrated discharge | |
| 4 in. (kPa/m) | 5 in. (kPa/m) | File (l/s) | Stopwatch (l/s) |
| **161.43** | **72.93** | 13.74 | 13.66 |
| **135.61** | **57.93** | 11.81 | 11.79 |
| 118.79 | 48.89 | 10.43 | 10.55 |
| 98.81 | 39.34 | 8.89 | 8.88 |
| 66.21 | 21.97 | 5.92 | 5.94 |
| 33.18 | 6.62 | 2.68 | 2.68 |
| 20.41 | 3.93 | 1.36 | 1.36 |

| Cycle 2 | | | |
|---|---|---|---|
| Pressure loss (straing gauges) | | Calibrated discharge | |
| 4 in. (kPa/m) | 5 in. (kPa/m) | File (l/s) | Stopwatch (l/s) |
| **148.62** | **68.30** | 13.53 | 13.45 |
| 130.88 | 57.82 | 11.92 | 11.88 |
| 109.90 | 47.01 | 10.23 | 10.27 |
| 92.88 | 36.57 | 8.66 | 8.67 |
| 67.56 | 24.43 | 6.19 | 6.18 |
| 33.33 | 7.14 | 2.65 | 2.65 |
| 21.71 | 4.20 | 1.36 | 1.36 |

| Cycle 3 | | | |
|---|---|---|---|
| Pressure loss (straing gauges) | | Calibrated discharge | |
| 4 in. (kPa/m) | 5 in. (kPa/m) | File (l/s) | Stopwatch (l/s) |
| **140.50** | **63.76** | 14.02 | 13.88 |
| 125.31 | 53.18 | 12.30 | 12.30 |
| 110.95 | 46.61 | 10.99 | 11.01 |
| 92.29 | 34.77 | 8.99 | 8.99 |
| 61.96 | 20.39 | 5.69 | 5.70 |
| 36.23 | 7.14 | 2.92 | 2.92 |
| 22.29 | 3.96 | 1.35 | 1.35 |

| Cycle 4 | | | |
|---|---|---|---|
| Pressure loss (straing gauges) | | Calibrated discharge | |
| 4 in. (kPa/m) | 5 in. (kPa/m) | File (l/s) | Stopwatch (l/s) |
| **139.58** | **63.47** | 13.88 | 13.88 |
| **122.49** | 55.43 | 12.02 | 12.04 |
| 105.58 | 45.51 | 10.39 | 10.37 |
| 88.95 | 35.49 | 8.50 | 8.52 |
| 69.21 | 26.46 | 6.39 | 6.38 |
| 34.57 | 7.87 | 2.46 | 2.47 |
| 24.85 | 5.08 | 1.37 | 1.38 |

**Potential non-equilibrium**

*Table C.18: Pressure loss of HWC3 measured at different discharge rates in 4 in. and 5 in. pipes.*

## HWC3

| Cycle 1 | | | |
|---|---|---|---|
| Pressure loss (straing gauges) | | Calibrated discharge | |
| 4 in. (kPa/m) | 5 in. (kPa/m) | File (l/s) | Stopwatch (l/s) |
| **141.53** | **57.18** | 14.13 | 14.06 |
| **125.41** | **49.84** | 13.02 | 13.01 |
| **109.38** | **41.69** | 11.81 | 11.91 |
| 91.99 | 34.16 | 10.17 | 10.25 |
| 72.57 | 25.21 | 8.24 | 8.23 |
| 52.99 | 13.92 | 6.09 | 6.08 |
| 26.79 | 5.92 | 2.80 | 2.80 |
| 16.46 | 3.76 | 1.38 | 1.38 |

| Cycle 2 | | | |
|---|---|---|---|
| Pressure loss (straing gauges) | | Calibrated discharge | |
| 4 in. (kPa/m) | 5 in. (kPa/m) | File (l/s) | Stopwatch (l/s) |
| 124.73 | 48.67 | 14.06 | 14.07 |
| 111.28 | 43.73 | 13.09 | 13.04 |
| 98.05 | 37.13 | 11.76 | 11.75 |
| 85.05 | 31.94 | 10.37 | 10.31 |
| 67.31 | 22.18 | 8.20 | 8.25 |
| 50.20 | 12.94 | 5.90 | 5.89 |
| 28.31 | 7.12 | 2.94 | 2.94 |
| 16.80 | 4.41 | 1.35 | 1.34 |

| Cycle 3 | | | |
|---|---|---|---|
| Pressure loss (straing gauges) | | Calibrated discharge | |
| 4 in. (kPa/m) | 5 in. (kPa/m) | File (l/s) | Stopwatch (l/s) |
| **109.97** | **40.85** | 13.98 | 13.96 |
| 102.14 | 36.66 | 12.96 | 13.04 |
| 91.89 | 32.58 | 12.02 | 12.06 |
| 81.00 | 26.93 | 10.49 | 10.51 |
| 63.64 | 18.58 | 8.19 | 8.20 |
| 48.48 | 12.78 | 5.90 | 5.91 |
| 28.14 | 7.91 | 2.98 | 2.98 |
| 16.94 | 5.28 | 1.31 | 1.31 |

| Cycle 4 | | | |
|---|---|---|---|
| Pressure loss (straing gauges) | | Calibrated discharge | |
| 4 in. (kPa/m) | 5 in. (kPa/m) | File (l/s) | Stopwatch (l/s) |
| **114.24** | **41.16** | 14.28 | 14.17 |
| **101.33** | **38.57** | 13.09 | 13.10 |
| 91.85 | 32.34 | 11.76 | 11.71 |
| 83.11 | 29.46 | 10.71 | 10.69 |
| 69.10 | 22.44 | 8.65 | 8.64 |
| 52.80 | 15.23 | 6.10 | 6.10 |
| 28.53 | 8.64 | 2.56 | 2.56 |
| 20.14 | 6.50 | 1.32 | 1.32 |

| Cycle 5 | | | |
|---|---|---|---|
| Pressure loss (straing gauges) | | Calibrated discharge | |
| 4 in. (kPa/m) | 5 in. (kPa/m) | File (l/s) | Stopwatch (l/s) |
| 124.95 | 46.81 | 14.13 | 14.08 |
| 111.93 | 44.38 | 12.96 | 12.96 |
| 104.47 | 37.84 | 11.76 | 11.78 |
| 96.19 | 35.35 | 10.58 | 10.57 |
| 80.69 | 27.31 | 8.30 | 8.29 |
| 66.29 | 21.45 | 6.01 | 6.01 |
| 41.64 | 12.80 | 2.73 | 2.72 |
| 27.55 | 8.79 | 1.25 | 1.25 |

**Potential non-equilibrium**

*Table C.19: Pressure loss of HWC4 measured at different discharge rates in 4 in. and 5 in. pipes.*

## HWC4

| Cycle 1 | | | |
|---|---|---|---|
| Pressure loss (straing gauges) | | Calibrated discharge | |
| 4 in. (kPa/m) | 5 in. (kPa/m) | File (l/s) | Stopwatch (l/s) |
| 124.49 | 48.25 | 12.11 | 12.13 |
| 100.70 | 43.13 | 10.51 | 10.50 |
| 80.61 | 34.55 | 8.83 | 8.83 |
| 59.09 | 24.48 | 6.38 | 6.38 |
| 37.06 | 13.63 | 3.57 | 3.59 |
| 20.31 | 6.71 | 1.50 | 1.50 |

| Cycle 2 | | | |
|---|---|---|---|
| Pressure loss (straing gauges) | | Calibrated discharge | |
| 4 in. (kPa/m) | 5 in. (kPa/m) | File (l/s) | Stopwatch (l/s) |
| 124.85 | 50.36 | 15.14 | 15.26 |
| 110.72 | 44.16 | 14.03 | 14.08 |
| 97.19 | 39.81 | 12.69 | 12.79 |
| 84.02 | 34.89 | 11.48 | 11.44 |
| 67.66 | 27.21 | 9.44 | 9.43 |
| 52.69 | 19.73 | 7.12 | 7.18 |
| 33.00 | 11.04 | 3.89 | 3.91 |
| 17.25 | 5.68 | 1.51 | 1.51 |

| Cycle 3 | | | |
|---|---|---|---|
| Pressure loss (straing gauges) | | Calibrated discharge | |
| 4 in. (kPa/m) | 5 in. (kPa/m) | File (l/s) | Stopwatch (l/s) |
| 106.80 | 48.28 | 15.40 | 15.54 |
| 92.49 | 41.54 | 13.81 | 13.65 |
| 80.83 | 36.52 | 12.63 | 12.60 |
| 69.72 | 30.93 | 11.04 | 11.05 |
| 55.97 | 24.55 | 8.98 | 8.98 |
| 45.24 | 18.10 | 6.86 | 6.86 |
| 25.75 | 8.90 | 3.21 | 3.21 |
| 17.78 | 5.92 | 1.81 | 1.80 |

| Cycle 4 | | | |
|---|---|---|---|
| Pressure loss (straing gauges) | | Calibrated discharge | |
| 4 in. (kPa/m) | 5 in. (kPa/m) | File (l/s) | Stopwatch (l/s) |
| 91.31 | 40.37 | 14.17 | 14.15 |
| 80.54 | 36.72 | 13.13 | 13.08 |
| 71.23 | 31.70 | 11.94 | 12.01 |
| 61.97 | 27.52 | 10.64 | 10.65 |
| 51.75 | 22.21 | 8.79 | 8.80 |
| 40.27 | 16.72 | 6.47 | 6.45 |
| 22.85 | 8.45 | 2.91 | 2.90 |
| 14.48 | 4.83 | 1.29 | 1.29 |

| Cycle 5 | | | |
|---|---|---|---|
| Pressure loss (straing gauges) | | Calibrated discharge | |
| 4 in. (kPa/m) | 5 in. (kPa/m) | File (l/s) | Stopwatch (l/s) |
| 91.23 | 41.29 | 14.56 | 14.62 |
| 79.73 | 38.17 | 13.32 | 13.43 |
| 70.68 | 32.52 | 12.16 | 12.14 |
| 60.70 | 28.05 | 10.59 | 10.57 |
| 51.25 | 22.82 | 8.89 | 8.85 |
| 41.18 | 17.22 | 6.77 | 6.76 |
| 24.02 | 8.65 | 3.08 | 3.09 |
| 15.24 | 5.01 | 1.32 | 1.32 |

**Potential non-equilibrium**

***Table C.20:*** *Pressure loss of SCC13 measured at different discharge rates in 4 in. and 5 in. pipes.*

## SCC13

| Cycle 1 | | | |
|---|---|---|---|
| Pressure loss (straing gauges) | | Calibrated discharge | |
| 4 in. (kPa/m) | 5 in. (kPa/m) | File (l/s) | Stopwatch (l/s) |
| 104.62 | 41.68 | 13.98 | 13.80 |
| 94.61 | 39.47 | 13.28 | 13.43 |
| 80.35 | 32.45 | 11.78 | 11.82 |
| 70.46 | 28.50 | 10.68 | 10.71 |
| 57.30 | 22.12 | 8.71 | 8.66 |
| 41.48 | 16.40 | 6.35 | 6.26 |
| 21.66 | 8.20 | 3.20 | 3.20 |
| 12.14 | | 1.63 | 1.63 |

| Cycle 2 | | | |
|---|---|---|---|
| Pressure loss (straing gauges) | | Calibrated discharge | |
| 4 in. (kPa/m) | 5 in. (kPa/m) | File (l/s) | Stopwatch (l/s) |
| 84.79 | 34.83 | 13.84 | 13.76 |
| 73.62 | 31.82 | 12.75 | 12.75 |
| 65.18 | 28.11 | 11.68 | 11.69 |
| 58.09 | 25.01 | 10.50 | 10.52 |
| 45.90 | 17.44 | 8.45 | 8.44 |
| 32.60 | 11.97 | 5.92 | 5.92 |
| 19.42 | 6.30 | 3.43 | 3.42 |
| 11.11 | 4.38 | 1.79 | 1.74 |

| Cycle 3 | | | |
|---|---|---|---|
| Pressure loss (straing gauges) | | Calibrated discharge | |
| 4 in. (kPa/m) | 5 in. (kPa/m) | File (l/s) | Stopwatch (l/s) |
| 77.57 | 34.04 | 14.52 | 14.32 |
| 70.75 | 29.62 | 13.48 | 13.58 |
| 62.91 | 26.85 | 12.34 | 12.36 |
| 56.91 | 24.00 | 11.23 | 11.27 |
| 45.62 | 18.15 | 9.01 | 9.03 |
| 32.30 | 12.90 | 6.29 | 6.29 |
| 18.52 | 7.99 | 3.41 | 3.42 |
| 10.82 | 4.67 | 1.79 | 1.78 |

| Cycle 4 | | | |
|---|---|---|---|
| Pressure loss (straing gauges) | | Calibrated discharge | |
| 4 in. (kPa/m) | 5 in. (kPa/m) | File (l/s) | Stopwatch (l/s) |
| 69.66 | 29.29 | 14.13 | 14.16 |
| 62.25 | 28.14 | 13.28 | 13.28 |
| 57.33 | 23.86 | 12.46 | 12.43 |
| 50.80 | 21.49 | 11.13 | 11.17 |
| 41.29 | 16.50 | 9.14 | 9.13 |
| 30.69 | 10.96 | 6.65 | 6.66 |
| 17.79 | 5.34 | 3.66 | 3.66 |
| 9.91 | 2.50 | 1.85 | 1.85 |

| Cycle 5 | | | |
|---|---|---|---|
| Pressure loss (straing gauges) | | Calibrated discharge | |
| 4 in. (kPa/m) | 5 in. (kPa/m) | File (l/s) | Stopwatch (l/s) |
| 68.14 | 31.36 | 14.44 | 14.34 |
| 60.11 | 27.13 | 13.34 | 13.30 |
| 53.78 | 24.63 | 12.00 | 12.20 |
| 47.91 | 21.26 | 10.90 | 10.90 |
| 39.38 | 16.37 | 8.85 | 8.87 |
| 29.00 | 12.06 | 6.38 | 6.39 |
| 16.13 | 5.90 | 3.16 | 3.14 |
| 10.55 | 3.92 | 1.74 | 1.74 |

**Doubtful data**
**Unrealistic data**
**Potential non-equilibrium**

***Table C.21:*** *Pressure loss of SCC14 measured at different discharge rates in 4 in. and 5 in. pipes.*

## SCC14

| Cycle 1 | | | |
|---|---|---|---|
| Pressure loss (straing gauges) | | Calibrated discharge | |
| 4 in. (kPa/m) | 5 in. (kPa/m) | File (l/s) | Stopwatch (l/s) |
| 62.47 | 22.00 | 16.84 | 16.90 |
| 56.77 | 20.44 | 15.77 | 15.87 |
| 51.47 | 17.09 | 14.59 | 14.66 |
| 45.66 | 15.33 | 13.17 | 13.32 |
| 38.42 | 13.29 | 11.16 | 11.15 |
| 32.58 | 10.08 | 9.37 | 9.41 |
| 24.74 | 8.04 | 6.94 | 6.92 |
| 13.04 | | 3.02 | 3.03 |

| Cycle 2 | | | |
|---|---|---|---|
| Pressure loss (straing gauges) | | Calibrated discharge | |
| 4 in. (kPa/m) | 5 in. (kPa/m) | File (l/s) | Stopwatch (l/s) |
| 52.79 | 23.67 | 16.15 | 16.30 |
| 47.90 | 22.19 | 15.25 | 15.33 |
| 42.80 | 19.33 | 14.21 | 14.14 |
| 38.18 | 16.89 | 12.97 | 12.86 |
| 33.32 | 14.11 | 11.16 | 11.16 |
| 27.03 | 11.33 | 9.03 | 9.07 |
| 19.82 | 8.93 | 6.37 | 6.41 |
| 12.01 | | 3.31 | 3.30 |

| Cycle 3 | | | |
|---|---|---|---|
| Pressure loss (straing gauges) | | Calibrated discharge | |
| 4 in. (kPa/m) | 5 in. (kPa/m) | File (l/s) | Stopwatch (l/s) |
| 48.03 | | 16.44 | 16.51 |
| 43.75 | | 15.51 | 15.36 |
| 39.45 | | 14.44 | 14.89 |
| 35.00 | | 12.97 | 12.91 |
| 30.45 | | 11.21 | 11.31 |
| 25.17 | 10.64 | 9.23 | 9.20 |
| 18.97 | 8.59 | 6.52 | 6.50 |
| 11.18 | 5.10 | 3.27 | 3.26 |

| Cycle 4 | | | |
|---|---|---|---|
| Pressure loss (straing gauges) | | Calibrated discharge | |
| 4 in. (kPa/m) | 5 in. (kPa/m) | File (l/s) | Stopwatch (l/s) |
| 46.82 | 18.97 | 16.15 | 16.13 |
| 42.42 | 16.92 | 15.25 | 15.15 |
| 38.04 | 14.95 | 13.99 | 13.91 |
| 34.11 | 14.17 | 12.73 | 12.73 |
| 29.16 | 12.14 | 10.75 | 10.72 |
| 24.38 | 9.65 | 8.66 | 8.63 |
| 19.60 | 7.95 | 6.46 | 6.46 |
| 12.27 | | 3.35 | 3.33 |

**Doubtful data**

**Potential non-equilibrium**

***Table C.22:*** *Pressure loss of SCC15 measured at different discharge rates in 4 in. and 5 in. pipes.*

## SCC15

| Cycle 1 | | | |
|---|---|---|---|
| Pressure loss (straing gauges) | | Calibrated discharge | |
| 4 in. (kPa/m) | 5 in. (kPa/m) | File (l/s) | Stopwatch (l/s) |
| **91.60** | 56.50 | | |
| **81.04** | 51.52 | | |
| **71.96** | 46.67 | | |
| 61.74 | 40.09 | | |
| 46.46 | 31.19 | | |
| 34.10 | 24.48 | | |
| 20.13 | 14.32 | | |
| 10.10 | 6.76 | | |

| Cycle 2 | | | |
|---|---|---|---|
| Pressure loss (straing gauges) | | Calibrated discharge | |
| 4 in. (kPa/m) | 5 in. (kPa/m) | File (l/s) | Stopwatch (l/s) |
| 84.50 | 50.24 | | |
| 73.92 | 45.04 | | |
| 65.56 | 40.09 | | |
| 57.14 | 35.30 | | |
| 45.57 | 28.48 | | |
| 35.91 | 23.98 | | |
| 19.92 | 13.36 | | |
| 9.92 | 6.53 | | |

| Cycle 3 | | | |
|---|---|---|---|
| Pressure loss (straing gauges) | | Calibrated discharge | |
| 4 in. (kPa/m) | 5 in. (kPa/m) | File (l/s) | Stopwatch (l/s) |
| 77.52 | 42.63 | | |
| 68.08 | 39.19 | | |
| 61.52 | 33.77 | | |
| 54.01 | 30.34 | | |
| 44.87 | 26.07 | | |
| 31.41 | 19.10 | | |
| 18.04 | 10.53 | | |
| 10.19 | 5.97 | | |

| Cycle 4 | | | |
|---|---|---|---|
| Pressure loss (straing gauges) | | Calibrated discharge | |
| 4 in. (kPa/m) | 5 in. (kPa/m) | File (l/s) | Stopwatch (l/s) |
| 71.72 | 42.15 | | |
| 63.14 | 38.47 | | |
| 57.19 | 33.88 | | |
| 48.76 | 30.17 | | |
| 39.93 | 25.19 | | |
| 30.03 | 20.13 | | |
| 18.25 | 12.04 | | |
| 9.50 | 6.62 | | |

| Cycle 5 | | | |
|---|---|---|---|
| Pressure loss (straing gauges) | | Calibrated discharge | |
| 4 in. (kPa/m) | 5 in. (kPa/m) | File (l/s) | Stopwatch (l/s) |
| 65.93 | 40.16 | | |
| 55.66 | 36.42 | | |
| 50.96 | 32.64 | | |
| 43.21 | 28.68 | | |
| 36.61 | 25.28 | | |
| 29.99 | 20.18 | | |
| 19.60 | 12.39 | | |
| 9.86 | 6.58 | | |

**No discharge rate calibration available**
**Potential non-equilibrium**

***Table C.23:*** *Pressure loss of SCC16 measured at different discharge rates in 4 in. and 5 in. pipes.*

## SCC16

| Cycle 1 | | | |
|---|---|---|---|
| Pressure loss (straing gauges) | | Calibrated discharge | |
| 4 in. (kPa/m) | 5 in. (kPa/m) | File (l/s) | Stopwatch (l/s) |
| **118.41** | **61.96** | 14.64 | 14.65 |
| **104.71** | 55.86 | 13.52 | 13.49 |
| **91.08** | 48.30 | 12.38 | 12.42 |
| 80.08 | 42.13 | 11.16 | 11.15 |
| 64.50 | 33.91 | 9.34 | 9.39 |
| 48.43 | 25.77 | 7.11 | 7.14 |
| 24.83 | 13.94 | 3.61 | 3.61 |
| 12.95 | 7.47 | 1.73 | 1.74 |

| Cycle 2 | | | |
|---|---|---|---|
| Pressure loss (straing gauges) | | Calibrated discharge | |
| 4 in. (kPa/m) | 5 in. (kPa/m) | File (l/s) | Stopwatch (l/s) |
| **105.31** | **51.92** | 14.96 | 14.98 |
| **90.91** | **48.30** | 13.73 | 13.75 |
| 78.31 | 40.58 | 12.16 | 12.22 |
| 69.62 | 35.96 | 10.99 | 11.02 |
| 55.05 | 27.90 | 8.83 | 8.83 |
| 42.98 | 22.21 | 6.95 | 6.99 |
| 20.14 | 11.57 | 3.14 | 3.13 |
| 10.62 | 6.02 | 1.43 | 1.44 |

| Cycle 3 | | | |
|---|---|---|---|
| Pressure loss (straing gauges) | | Calibrated discharge | |
| 4 in. (kPa/m) | 5 in. (kPa/m) | File (l/s) | Stopwatch (l/s) |
| **87.76** | 44.97 | 14.25 | 14.18 |
| 81.12 | 41.31 | 12.93 | 12.93 |
| 74.83 | 38.73 | 12.21 | 12.26 |
| 67.11 | 34.14 | 11.03 | 11.08 |
| 56.37 | 28.17 | 9.34 | 9.37 |
| 41.24 | 20.55 | 6.69 | 6.71 |
| 19.70 | 11.21 | 3.12 | 3.11 |
| 10.30 | 6.46 | 1.37 | 1.37 |

| Cycle 4 | | | |
|---|---|---|---|
| Pressure loss (straing gauges) | | Calibrated discharge | |
| 4 in. (kPa/m) | 5 in. (kPa/m) | File (l/s) | Stopwatch (l/s) |
| 88.16 | 37.08 | 14.17 | 14.16 |
| 78.68 | 35.75 | 12.99 | 12.97 |
| 70.21 | 33.15 | 11.99 | 12.01 |
| 62.45 | 28.87 | 10.55 | 10.54 |
| 51.66 | 23.76 | 8.89 | 8.90 |
| 35.71 | 16.73 | 5.99 | 6.00 |
| 18.14 | 9.78 | 2.94 | 2.93 |
| 10.15 | 5.92 | 1.37 | 1.37 |

| Cycle 5 | | | |
|---|---|---|---|
| Pressure loss (straing gauges) | | Calibrated discharge | |
| 4 in. (kPa/m) | 5 in. (kPa/m) | File (l/s) | Stopwatch (l/s) |
| 87.80 | 45.71 | 14.56 | 14.52 |
| 74.95 | 37.79 | 12.87 | 12.81 |
| 66.41 | 31.55 | 11.72 | 11.71 |
| 58.85 | 26.48 | 10.50 | 10.52 |
| 47.80 | 20.37 | 8.53 | 8.51 |
| 34.03 | 14.25 | 5.96 | 5.94 |
| 18.07 | 7.72 | 2.92 | 2.92 |
| 10.46 | 4.88 | 1.35 | 1.35 |

**Potential non-equilibrium**

*Table C.24: Pressure loss of SCC17 measured at different discharge rates in 4 in. and 5 in. pipes.*

## SCC17

| Cycle 1 | | | |
|---|---|---|---|
| Pressure loss (straing gauges) | | Calibrated discharge | |
| 4 in. (kPa/m) | 5 in. (kPa/m) | File (l/s) | Stopwatch (l/s) |
| **88.84** | **44.12** | 14.18 | 14.20 |
| **78.14** | **40.14** | 13.00 | 12.99 |
| **68.02** | **35.28** | 11.95 | 11.91 |
| 60.86 | 30.41 | 10.73 | 10.78 |
| 48.63 | 24.00 | 8.83 | 8.90 |
| 34.62 | 16.51 | 6.37 | 6.38 |
| 15.88 | 7.73 | 2.90 | 2.90 |
| 9.39 | 4.70 | 1.55 | 1.55 |

| Cycle 2 | | | |
|---|---|---|---|
| Pressure loss (straing gauges) | | Calibrated discharge | |
| 4 in. (kPa/m) | 5 in. (kPa/m) | File (l/s) | Stopwatch (l/s) |
| **79.11** | 38.06 | 13.96 | 14.01 |
| **70.91** | 35.41 | 12.88 | 12.86 |
| 64.12 | 31.25 | 11.84 | 11.73 |
| 54.59 | 26.72 | 10.20 | 10.21 |
| 45.43 | 22.07 | 8.54 | 8.54 |
| 32.85 | 16.03 | 6.10 | 6.10 |
| 15.74 | 7.98 | 2.73 | 2.72 |
| 9.51 | 4.97 | 1.48 | 1.48 |

| Cycle 3 | | | |
|---|---|---|---|
| Pressure loss (straing gauges) | | Calibrated discharge | |
| 4 in. (kPa/m) | 5 in. (kPa/m) | File (l/s) | Stopwatch (l/s) |
| **77.88** | 35.44 | 14.89 | 14.91 |
| 71.88 | 32.15 | 13.60 | 13.59 |
| 63.55 | 29.31 | 12.63 | 12.75 |
| 55.76 | 25.33 | 11.09 | 11.09 |
| 44.54 | 21.11 | 8.96 | 8.95 |
| 31.03 | 15.12 | 6.26 | 6.26 |
| 15.43 | 7.46 | 2.78 | 2.77 |
| 9.76 | 5.11 | 1.53 | 1.53 |

| Cycle 4 | | | |
|---|---|---|---|
| Pressure loss (straing gauges) | | Calibrated discharge | |
| 4 in. (kPa/m) | 5 in. (kPa/m) | File (l/s) | Stopwatch (l/s) |
| **75.25** | **32.94** | 14.41 | 14.17 |
| **68.61** | 31.32 | 13.40 | 13.47 |
| 59.81 | 27.15 | 12.06 | 12.01 |
| 52.43 | 23.89 | 10.47 | 10.49 |
| 41.55 | 20.20 | 8.54 | 8.53 |
| 29.87 | 14.89 | 6.04 | 6.03 |
| 15.09 | 7.56 | 2.58 | 2.58 |
| 10.06 | 5.29 | 1.49 | 1.49 |

| Cycle 5 | | | |
|---|---|---|---|
| Pressure loss (straing gauges) | | Calibrated discharge | |
| 4 in. (kPa/m) | 5 in. (kPa/m) | File (l/s) | Stopwatch (l/s) |
| 76.15 | 32.28 | 14.56 | 14.58 |
| 65.67 | 30.17 | 13.07 | 13.10 |
| 58.49 | 26.35 | 11.89 | 11.89 |
| 52.20 | 24.00 | 10.64 | 10.60 |
| 40.99 | 19.37 | 8.43 | 8.43 |
| 27.82 | 13.59 | 5.45 | 5.46 |
| 13.43 | 6.90 | 2.11 | 2.10 |
| 10.85 | 5.54 | 1.46 | 1.46 |

**Potential non-equilibrium**

***Table C.25:*** *Pressure loss of SCC18 measured at different discharge rates in 4 in. and 5 in. pipes.*

## SCC18

| Cycle 1 | | | |
|---|---|---|---|
| Pressure loss (straing gauges) | | Calibrated discharge | |
| 4 in. (kPa/m) | 5 in. (kPa/m) | File (l/s) | Stopwatch (l/s) |
| **142.18** | **60.99** | 13.79 | 13.75 |
| **125.11** | **54.12** | 12.78 | 12.76 |
| **106.48** | 44.62 | 11.19 | 11.15 |
| 88.30 | 37.01 | 9.43 | 9.44 |
| 62.71 | 26.27 | 6.93 | 6.98 |
| 29.43 | 11.02 | 3.15 | 3.15 |
| 16.39 | 5.15 | 1.46 | 1.43 |

| Cycle 2 | | | |
|---|---|---|---|
| Pressure loss (straing gauges) | | Calibrated discharge | |
| 4 in. (kPa/m) | 5 in. (kPa/m) | File (l/s) | Stopwatch (l/s) |
| | | 13.72 | 13.79 |
| **95.25** | **39.63** | 12.36 | 12.31 |
| 79.99 | 32.41 | 10.47 | 10.44 |
| 64.04 | 25.43 | 8.55 | 8.56 |
| 48.43 | 18.65 | 6.53 | 6.52 |
| 24.22 | 9.00 | 3.06 | 3.06 |
| 13.65 | 5.00 | 1.38 | 1.38 |

| Cycle 3 | | | |
|---|---|---|---|
| Pressure loss (straing gauges) | | Calibrated discharge | |
| 4 in. (kPa/m) | 5 in. (kPa/m) | File (l/s) | Stopwatch (l/s) |
| 99.94 | | 13.72 | 13.70 |
| 88.97 | 36.01 | 12.54 | 12.57 |
| 76.76 | 30.70 | 10.95 | 10.89 |
| 67.09 | 27.02 | 9.57 | 9.56 |
| 45.87 | 17.62 | 6.56 | 6.57 |
| 26.97 | 10.23 | 3.60 | 3.60 |
| 13.97 | 5.35 | 1.49 | 1.49 |

| Cycle 4 | | | |
|---|---|---|---|
| Pressure loss (straing gauges) | | Calibrated discharge | |
| 4 in. (kPa/m) | 5 in. (kPa/m) | File (l/s) | Stopwatch (l/s) |
| 92.29 | 35.40 | 13.04 | 12.94 |
| 80.01 | 32.94 | 11.64 | 11.57 |
| 69.60 | 28.22 | 10.14 | 10.19 |
| 59.04 | 23.94 | 8.72 | 8.75 |
| 40.58 | 16.24 | 5.91 | 5.89 |
| 19.34 | 7.82 | 2.27 | 2.27 |
| 14.04 | 6.03 | 1.37 | 1.37 |

| Cycle 5 | | | |
|---|---|---|---|
| Pressure loss (straing gauges) | | Calibrated discharge | |
| 4 in. (kPa/m) | 5 in. (kPa/m) | File (l/s) | Stopwatch (l/s) |
| 93.58 | 35.49 | 12.97 | 12.96 |
| 81.87 | 31.90 | 11.59 | 11.53 |
| 72.37 | 27.43 | 10.34 | 10.32 |
| 58.03 | 22.50 | 8.27 | 8.29 |
| 44.43 | 17.72 | 6.27 | 6.28 |
| 22.57 | 8.81 | 2.60 | 2.60 |
| 15.29 | 5.85 | 1.35 | 1.35 |

**Potential non-equilibrium**
**Non-trusted results**

***Table C.26:*** *Pressure loss of SCC19 measured at different discharge rates in 4 in. and 5 in. pipes.*

## SCC19

| Cycle 1 | | | |
|---|---|---|---|
| Pressure loss (straing gauges) | | Calibrated discharge | |
| 4 in. (kPa/m) | 5 in. (kPa/m) | File (l/s) | Stopwatch (l/s) |
| 220.41 | 96.21 | 9.48 | 9.44 |
| 174.71 | 78.03 | 8.05 | 8.07 |
| 120.76 | 50.84 | 5.72 | 5.73 |
| 80.28 | 32.15 | 3.83 | 3.81 |
| 62.32 | 22.89 | 2.94 | 2.93 |
| 33.82 | 10.94 | 1.35 | 1.34 |

| Cycle 2 | | | |
|---|---|---|---|
| Pressure loss (straing gauges) | | Calibrated discharge | |
| 4 in. (kPa/m) | 5 in. (kPa/m) | File (l/s) | Stopwatch (l/s) |
| 209.37 | 94.82 | 9.73 | 9.72 |
| 167.43 | 79.05 | 8.12 | 8.13 |
| 106.69 | 47.77 | 5.35 | 5.36 |
| 77.52 | 33.77 | 3.86 | 3.86 |
| 51.79 | 20.90 | 2.42 | 2.43 |
| 34.29 | 12.85 | 1.36 | 1.35 |

| Cycle 3 | | | |
|---|---|---|---|
| Pressure loss (straing gauges) | | Calibrated discharge | |
| 4 in. (kPa/m) | 5 in. (kPa/m) | File (l/s) | Stopwatch (l/s) |
| 193.44 | 93.62 | 9.92 | 9.89 |
| 161.17 | 78.60 | 8.41 | 8.40 |
| 108.47 | 52.38 | 5.80 | 5.81 |
| 83.77 | 39.59 | 4.44 | 4.46 |
| 61.84 | 28.76 | 3.15 | 3.14 |
| 33.75 | 14.73 | 1.34 | 1.33 |

| Cycle 4 | | | |
|---|---|---|---|
| Pressure loss (straing gauges) | | Calibrated discharge | |
| 4 in. (kPa/m) | 5 in. (kPa/m) | File (l/s) | Stopwatch (l/s) |
| 201.65 | 96.11 | 9.70 | 9.67 |
| 157.90 | 80.93 | 7.95 | 7.96 |
| 113.07 | 56.07 | 5.72 | 5.73 |
| 78.23 | 38.79 | 3.82 | 3.82 |
| 60.55 | 29.39 | 2.76 | 2.77 |
| 37.36 | 16.97 | 1.30 | 1.29 |

| Cycle 5 | | | |
|---|---|---|---|
| Pressure loss (straing gauges) | | Calibrated discharge | |
| 4 in. (kPa/m) | 5 in. (kPa/m) | File (l/s) | Stopwatch (l/s) |
| 222.53 | 106.12 | 9.62 | 9.63 |
| 172.71 | 88.51 | 7.80 | 7.77 |
| 124.19 | 62.44 | 5.52 | 5.52 |
| 93.10 | 46.57 | 3.81 | 3.81 |
| 70.93 | 35.21 | 2.58 | 2.58 |
| 47.63 | 23.04 | 1.25 | 1.24 |